10
van der Waals Forces

Already the difficulties of avoiding a collision in a crowd are enough to tax the sagacity of even a well-educated Square; but if no one could calculate the Regularity of a single figure . . . all would be chaos and confusion, and the slightest panic would cause serious injuries.

From Abbott's *Flatland*

10.1 INTRODUCTION

10.1a What Are van der Waals Forces?

This chapter is concerned with one of the most important forces in surface and colloid chemistry, namely, *van der Waals forces* between atoms, molecules, or particles. These forces have their origin in the dipole or induced-dipole interactions at the atomic level and are therefore of extreme importance in almost all aspects of the study of materials. The strength of van der Waals forces increases in the case of interaction between macroscopic objects such as colloidal particles since typically each particle has a large number of atoms or molecules. We see in this chapter that there are three major types of van der Waals forces, and that one of these, known as the *dispersion force*, is always present (like the gravitational force). This fact implies that it is not always possible to ignore van der Waals forces in colloid science, although, as we see in Chapter 13 on colloid stability, there are methods one can use to minimize or override the influence of these forces in order to promote the stability of colloids against coagulation. For example, in Chapter 11 we see how ionic atmospheres near charged surfaces can override van der Waals attraction and prevent coagulation. This is discussed further in Chapter 13, in which we also see how polymer layers adsorbed (or grafted) on particles are often used to "mask out" the influence of van der Waals attraction.

Our objectives in this chapter are to look into the origin of van der Waals forces, see how they affect macroscopic behavior and properties of materials, and establish relations for scaling up the molecular-level forces to forces between macroscopic bodies.

10.1b Why Are van der Waals Forces Important?

One of the most important things to bear in mind in studying van der Waals forces is that this topic has ramifications that extend far beyond our discussion here. Van der Waals interactions, for example, contribute to the nonideality of gases and, closer to home, gas adsorption. We also see how these forces are related to surface tension, thereby connecting this material with the contents of Chapter 6 (see Vignette X below). These connections also imply that certain macroscopic properties and measurements can be used to determine the strength of van der Waals forces between macroscopic objects. We elaborate on these ideas through illustrative examples in this chapter.

VIGNETTE X WETTING AND SPREADING OF LIQUIDS: Stability of Thin Liquid Films

Why does a drop of pentane spread into a thin film when placed on a water surface, whereas a larger hydrocarbon such as dodecane breaks up into smaller droplets? This is not an academic question, as should be evident from the importance of wetting and contact angle phenomena that we discussed in Chapter 6. Why is it that we can produce relatively stable bubbles with a soap solution but not with pure water? Water droplets on an oily surface, dewdrops on a blade of grass, and soap bubbles or foams are so common in our daily life that they rarely engage our attention, but to a scientist they are a constant reminder of the ubiquitous van der Waals forces!

The very fact that the vapor phase of many substances can condense to form a liquid is a consequence of the existence of *attractive* van der Waals forces between atoms or molecules. An attractive intermolecular force is *not* needed for a gas to condense into a solid; solidification can occur purely as a result of "excluded-volume" interactions among the molecules at sufficiently large densities. The pressure in a fluid, the cohesion between materials, and the existence of surface energy or surface tension all result, partially or wholly, from van der Waals forces.

Let us return to the differing behavior of pentane and dodecane on water. The energy of a film (of thickness d) of substance 1 spread between a planar interface of materials 2 and 3 can be traced to the energies of interaction between 2 and 3 through 1. In macroscopic terms, under certain conditions (see Section 10.6a), this energy is proportional to $(-A/(12\pi d^2))$, where the proportionality constant is a material property known as the *Hamaker constant*, which, in this case, depends on certain physical properties of all the three materials. This energy is the *macroscopic* van der Waals energy and results from the cumulative effects of individual, *intermolecular* van der Waals energies summed over all the molecules of the macroscopic objects. It turns out that in the case of pentane, A can become negative (i.e., the van der Waals energy is positive and the force is repulsive) so that pentane spreads on the water's surface thereby separating the air (material 3) from water (material 2) to the extent permitted by other forces such as gravity. In the case of dodecane, however, the Hamaker constant is positive, the van der Waals force is attractive, and the film continues to thin and breaks up into small, lens-shaped droplets. The reason for the lens shape is discussed in Chapter 6.

Now we can understand what happens in the case of soap bubbles. As discussed in Chapter 7, the soap molecules spread on both air-water interfaces enclosing a film of water and provide the repulsion necessary to maintain a water film, similar to the case we discuss in Example 11.3. In the absence of soap molecules, the (attractive) air-air van der Waals forces through the water film rupture the film so that the bubbles are unstable.

Phenomena such as the ones described above are usually (and conveniently) described in terms of macroscopic properties such as surface tension, contact angle, and so on. This is what was done in Chapters 6 and 7. In the present chapter, we probe the *molecular* origin of van der Waals forces, go into some of the details of how they scale up in the case of macroscopic bodies, and illustrate their importance in molecular as well as macroscopic phenomena.

10.1c Focus of This Chapter

The focus of this chapter is to present a fairly comprehensive introduction to the van der Waals forces. In addition to giving an introduction to the origin of these forces, we also illustrate the prevalence of these forces through examples of their role in some of the common macroscopic phenomena that are not necessarily directly related to colloidal problems.

1. However, we begin with a classical example of van der Waals forces in colloid science, namely, their role in coagulation and colloid stability, in Section 10.2. This discussion also sets the stage for a more detailed discussion of colloid stability in Chapter 13.

2. Following this, we review briefly the so-called power law molecular interaction forces in Section 10.3 and develop the details of the different kinds of van der Waals forces in Section

10.4. Two illustrations of the implications of these forces to macroscopic behavior of materials are also provided here.

3. The van der Waals forces scale up from atomic distances to colloidal distances undiminished. How the molecular forces scale up in the case of large objects, expressions for such forces, definition of the Hamaker constant, and theories based on bulk material properties follow in Sections 10.5–10.7.

4. More often than not one deals with colloidal objects immersed in a liquid or other such media, and therefore interactions between similar or dissimilar materials in an arbitrary medium are of importance in colloid science. Moreover, it is very useful to relate such dissimilar interactions to those between identical particles in vacuum. In the last section (Section 10.8) we present what are known as "combining relations" for accomplishing this. The van der Waals forces between macroscopic objects are usually attractive, but under certain circumstances they (and, as a consequence, the Hamaker constant) can be negative, as noted in Vignette X. A brief discussion of this completes Section 10.8.

10.2 VAN DER WAALS FORCES AND THEIR IMPORTANCE IN COLLOID AND SURFACE CHEMISTRY

Almost all interfacial phenomena are influenced to various extents by forces that have their origin in atomic- and molecular-level interactions due to the induced or permanent polarities created in molecules by the electric fields of neighboring molecules or due to the instantaneous dipoles caused by the "positions" of the electrons around the nuclei. These forces consist of three major categories known as *Keesom* interactions (permanent dipole/permanent dipole interactions), *Debye* interactions (permanent dipole/induced dipole interactions), and *London* interactions (induced dipole/induced dipole interactions). The three are known collectively as the *van der Waals interactions* and play a major role in determining material properties and behavior important in colloid and surface chemistry. The purpose of the present chapter is to outline the basic ideas and equations behind these forces and to illustrate how they affect some of the material properties of interest to us.

Of the three forces mentioned above, the London force is always present (like the gravitational force) because it does not require the existence of permanent polarity or charge-induced polarity in the molecules. Even neutral atoms or molecules such as helium or hydrocarbons give rise to the London interaction. As a consequence, the London interaction plays a special role in colloid and surface chemistry. As mentioned above, it influences physical adsorption and surface tension; in addition, it is important in adhesion, wetting phenomena, structure of macromolecules such as proteins and other biological and nonbiological polymer molecules, and stability of foams and thin films. It also plays a very important part in determining the strengths of solids, properties of gases and liquids, heat of melting and vaporization of solids, and the like. We illustrate some of these using simple examples in subsequent sections.

Before we proceed to a molecular-level description of the van der Waals forces, it is useful to note a few other important points of information:

1. The van der Waals forces are always attractive (although, as we see in Section 10.8b, the London forces between two macroscopic bodies immersed in a medium can be repulsive, depending on the material properties).
2. They are relatively long ranged compared to other atomic- or molecular-level forces and can have an interval of influence ranging from about 0.2 nm to over 10 nm.
3. The London force is also often called the *dispersion force*. The word *dispersion* here has nothing to do with the role of the London force in colloidal dispersions, but is the result of the role this type of interaction force plays in the dispersion of light in the visible and ultraviolet wavelengths.
4. The dispersion force between two atoms, molecules, or large bodies is influenced by the presence of other nearby particles. Nevertheless, we consistently add pairwise interactions between the atoms in separate bodies as our procedure for scaling up

the interactions. This must be viewed as an approximation since perturbations by neighboring atoms limit the additivity of these forces.

More detailed and advanced information on these forces can be found in the book by Israelachvili (1991), which is devoted completely to intermolecular and surface forces. Here, we focus on the essential basic information and examples. Before we proceed to a physical explanation of these forces and the necessary equations, it is useful to explore the role played by the van der Waals forces in colloid stability since this theme reappears in our discussions of electrical double-layer forces in Chapter 11 and polymer-induced forces in Chapter 13.

10.2a Colloid Stability, van der Waals Attraction, and Potential Energy Curves

Colloid stability serves as a convenient example to illustrate the importance of the strength and range of van der Waals attraction between macroscopic bodies in a practical context and to introduce the idea of potential energy curves.

We introduced the concept of coagulation in Chapter 1, Section 1.4a, as that process by which two (or more) dispersed particles (primary or otherwise) cluster together to form an aggregate in which the individual units retain their identity but lose their kinetic independence. The fact that the primary particles are held together in these aggregates is evidence of the existence of attractive forces between the particles. The fact that some dispersions are stable with respect to the coagulation process is evidence that other forces that compete against attraction are also operative. In any specific system it is the relative magnitude of the attractive and repulsive forces between the particles that governs the coagulation behavior of the system.

Figure 10.1a is a schematic illustration of the kinds of interactions described above. The figure shows the potential energy of the interacting particles as a function of the distance of separation between them. It turns out that potential energy is a more useful quantity to deal with than force, although the force is given by the negative local slope of one of the curves in an illustration like Figure 10.1a. The figure shows two potential energy curves, one corresponding to attraction and the other to repulsion. By convention, the potential energy associated with repulsion is defined as positive, while the attraction is negative. The combination of repulsion and attraction allows us to speak of the "height" of energy "barriers" and the "depth" of energy minima.

An important aspect of Figure 10.1a is the fact that both the attraction and repulsion vary with the distance of separation between the bodies involved. Regardless of the specific shapes of the curves, both modes of interaction become weaker as the separation becomes larger. At sufficiently large distances the particles exert no influence on each other. The curves are deliberately interrupted at very small separations in view of the possibility of highly specific interactions at small separations. Our interest is in interactions of a more general type. In the schematic illustration shown, the two components vary in roughly the same way with distance, but this effective cancellation is only one of an assortment of possible attraction-repulsion combinations. One of our objectives in this section is to consider some of the combinations that are of interest.

The attractions of interest in colloid stability usually arise from the van der Waals forces, and we see below that they are scaled-up versions of the same intermolecular attractions discussed in the following section and that contribute to the nonideality and ultimately liquefaction of gases. In view of Figure 10.1a, we are interested in both the magnitude and the distance dependence of these attractive forces.

Our discussion of the repulsion between particles requires a more drawn out development. In Chapter 11 we consider the effects of ion atmosphere as the origin of repulsion. In Chapter 13, we discuss polymer-induced repulsive forces, which are often used to screen out the van der Waals forces. In these cases also, we are interested in both the magnitude and the distance dependence of these interactions.

Whether what we are discussing is attraction or repulsion, it is important to realize that the interaction between a pair of colloidal particles involves some fundamental physical

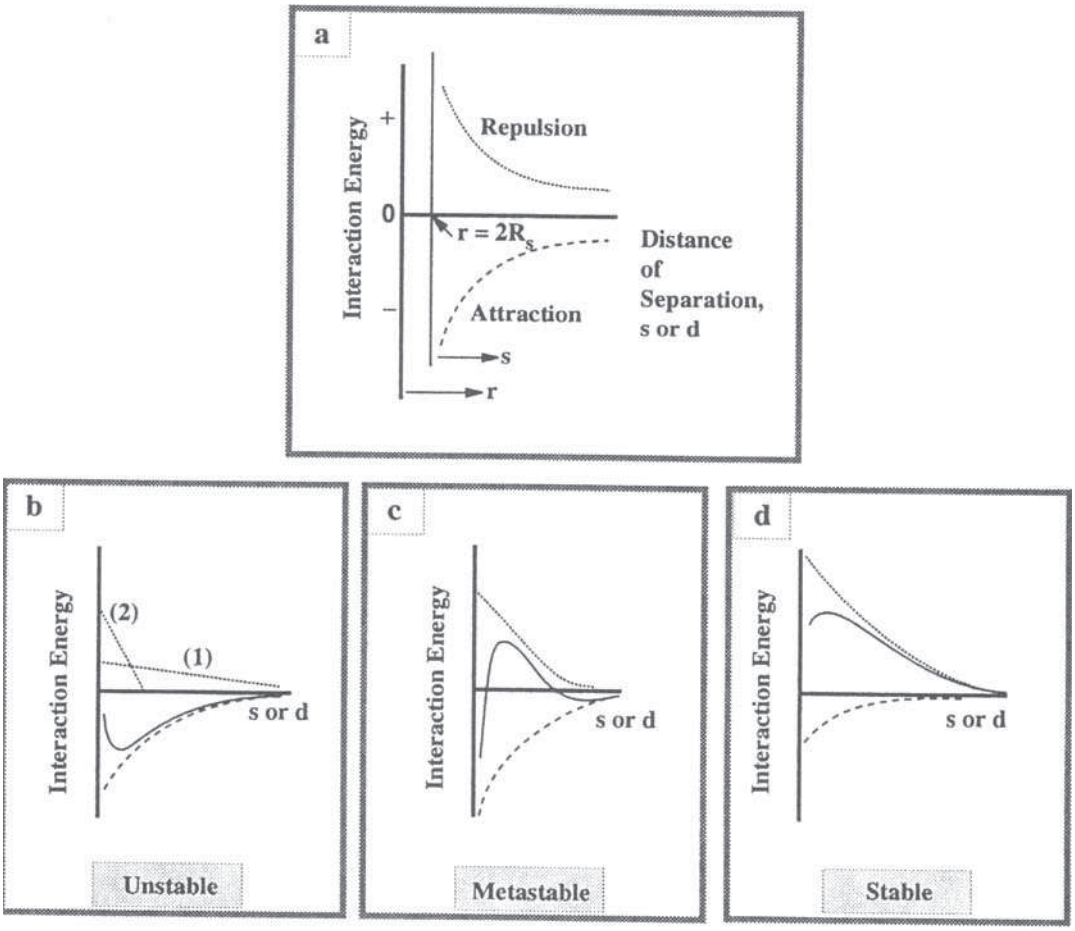


FIG. 10.1 Potential energy curves for the interaction of two colloidal particles, each of radius R_s. Negative values correspond to attraction and positive values to repulsion: (a) definition of variables; (b) repulsion less than attraction in magnitude and/or range; (c) repulsion and attraction comparable in magnitude and range; and (d) attraction less than repulsion.

phenomena and some geometrical considerations. The precise shapes of the curves in a plot like Figure 10.1a depend on both. For the quantitative interpretation of experimental results, it is important that both the physics and the geometry of the theory accurately (or at least approximately) describe the experimental system. From the point of view of pedagogy, however, we are more interested in physical phenomena than in particle geometry. For this reason we idealize dispersed particles as spheres and often discuss interactions between facing planar surfaces of bulk specimens of matter.

The axis representing the distance of separation in Figure 10.1a is defined in terms of the geometry of the interacting bodies. For spherical particles we define r as the variable that describes the separation of their centers. For spheres of (equal) radius R_s the separation of their surfaces along the line of centers is given by $(r - 2R_s)$, which we define as s. These are illustrated in Figure 10.1a. We define the distance of surface separation of two blocks of material by the symbol d.

The attraction and repulsion curves that describe the interaction of a pair of colloidal particles are usually not as evenly matched as those shown in Figure 10.1a. Next let us consider

some other possible combinations of interest. In Figures 10.1b–10.1d the individual attraction and repulsion curves are shown as dashed or dotted lines, and the resultant of the two is indicated by a solid line. It is the net interaction that governs the behavior, and the components have been adjusted to span an assortment of possible behaviors.

In Figure 10.1b the attraction is much stronger than the repulsion at large distances of separation. It is easy to imagine this occurring as a result of two different situations with respect to the repulsion component. The repulsion might be relatively small at all distances, as indicated by line 1 in Figure 10.1b, or it may drop off over a much shorter range of distance than the attraction, as shown by line 2. In either case the attraction dominates at the larger separations, and the particles can achieve a lower state of energy by maintaining the distance of separation corresponding to the potential energy minimum. Stated somewhat differently, it would take an energy corresponding to the depth of the minimum to disrupt an aggregate that had formed as a result of the particles adopting this equilibrium separation. If we identify the potential energy axis with free energy, it is apparent that the initial dispersed state is unstable with respect to the final aggregated state in this case.

In Figure 10.1d the relative magnitudes of attraction and repulsion are just the opposite of those in Figure 10.1b. In Figure 10.1d the repulsion dominates. In this case the separated particles are lower in energy than the aggregate, and stability with respect to coagulation is indicated.

Figure 10.1c is an intermediate situation in which attraction and repulsion each have regions of dominance. In this case there is a shallow minimum at large separations, a maximum at somewhat smaller separations, and a deep minimum at small separations. These minima are known as the *secondary* and *primary* minima, respectively, in the order cited. The actual depths of the minima and height of the maximum depend on the particulars of the components. Except for admitting the possibility of its existence, we shall not consider the secondary minimum any further. What is of particular interest to us is the fact that a minimum in energy results from coagulation in the primary minimum; however, access to that minimum first requires that an energy barrier be overcome. Such a system may be viewed as metastable, possessing a degree of *kinetic* stability even though it lacks thermodynamic stability. That is, coagulation is predicted, but it is expected to occur slowly. In this sense the barrier serves as an obstacle along the path to coagulation; its height is analogous to the activation energy in ordinary reaction chemistry. This last observation suggests that the kinetics of coagulation may offer some clue as to the height of the maximum in this intermediate situation.

Potential energy curves of the type shown in Figure 10.1 are thus seen to be useful constructs for understanding and describing coagulation phenomena. They also illustrate the role of the attractive van der Waals forces on the stability of colloids.

In the next section we consider the molecular origins of attractions between colloidal particles.

10.3 Molecular Interactions and Power Laws

To understand the origin of the attraction between colloidal particles, it is necessary to back off a bit and consider the interactions between individual molecules. Macroscopic interactions—as we shall call the interactions between colloids since these particles are large compared to atomic dimensions—are the summation of the pairwise interactions of the constituent molecules in the individual particles. Therefore we begin by examining the interactions between a pair of isolated molecules.

Our primary interest in this section is to discuss the functional form that relates potential energy to the distance of separation x for various types of interactions. For many interactions an inverse power dependence on the separation describes the potential energy. Several examples of this are shown in Table 10.1. The main point to be observed now is that the value of the exponent in the inverse power dependence on the separation differs widely for the various types of interactions. An immediate consequence of this is that the range of the interactions is quite different also.

TABLE 10.1 Partial List of Interactions Between Pairs of Isolated Ions and/or Molecules, with a Listing of Functions That Describe the Potential Energy Versus Separation, Along with Appropriate Proportionality Constants

Description	Φ	Definitions and restrictions*	Attributed to	Value of n in $\Phi \propto x^{-n}$
Ion 1–ion 2	$\frac{(ze)_1(ze)_2}{4\pi\varepsilon_0 x}$	z = valence, e = electron charge under vacuum—otherwise ε_r in denominator (sign depends on the z value)	Coulomb	1
Ion 1–permanent dipole 2	$\frac{(ze)_1\mu_2\cos\theta}{4\pi\varepsilon_0 x^2}$	μ = dipole moment, θ = angle between line of centers and axis of dipole; length of dipole small compared to x (sign depends on z and orientation)	Coulomb	2
Permanent dipole 1–permanent dipole 2	$\frac{(\text{const.})\mu_1\mu_2}{4\pi\varepsilon_0 x^3}$	Numerical constant (including sign) depends on orientation: const. = $\sqrt{2}$ for average overall orientations; const. = $+2$ for parallel and -2 for antiparallel alignment	Coulomb	3
Permanent dipole 1–induced dipole 2	$-\frac{(\alpha_{0,1}\mu_2^2 + \alpha_{0,2}\mu_1^2)}{(4\pi\varepsilon_0)^2 x^6}$	α_0 = polarizability (always negative)	Debye	6
Permanent dipole 1–permanent dipole 2	$-\frac{2}{3}\frac{\mu_1^2\mu_2^2}{(4\pi\varepsilon_0)^2 k_B T x^6}$	Free rotation of dipoles (always negative)	Keesom	6
Induced dipole 1–induced dipole 2	$-\frac{3h}{2}\frac{\nu_1\nu_2}{\nu_1+\nu_2}\frac{\alpha_{0,1}\alpha_{0,2}}{(4\pi\varepsilon_0)^2}\frac{1}{x^6}$	ν = characteristic vibrational frequency of electrons (always negative)	London	6
Induced dipole 1–induced dipole 2 (retarded)	$-\frac{23}{8\pi^2}hc\frac{\alpha_{0,1}\alpha_{0,2}}{(4\pi\varepsilon_0)^2 x^7}$	h = Planck's constant, c = speed of light; applies if $x > c/\nu$ (always negative)	Casimir and Polder	7
Repulsion	$+\frac{\xi}{x^{12}}$	Exponent in range 9 to 15; 12 mathematically convenient (always positive)		12

*The signs indicated are for the sign of Φ.

It is those functions with an inverse sixth-power dependence on the separation that are our main concern in this chapter. Those power laws with exponents greater or less than 6 are included in Table 10.1 mainly to emphasize the point that many types of interactions exist and that these are governed by different relationships. The interactions listed are by no means complete: Interactions of quadrupoles, octapoles, and so on might also be included, as well as those due to magnetic moments; however, all of these are less important than the interactions listed. Let us now examine Table 10.1 in greater detail.

The first three entries in Table 10.1 include Coulomb's law and two results that follow directly from it by treating stationary dipoles as a pair of charges and adding all pairwise interactions. What is important to note about these results is that the sign may be positive or negative—corresponding to repulsion or attraction—depending on the charge of ions, the orientation of the dipoles, or both.

By contrast, those results that involve an inverse sixth-power law are always negative; that is, attraction always results from interactions of the following types:

1. Permanent dipole/induced dipole interaction (*Debye equation*)
2. Permanent dipole/permanent dipole interaction (*Keesom equation*)
3. Induced dipole/induced dipole interaction (*London equation*)

The inverse seventh-power law is a special case of the induced dipole/induced dipole interaction that applies to the case of large separations; this is discussed in more detail in Section 10.5. As mentioned above, the three attractive interactions listed above are collectively known as van der Waals attraction. In Section 10.4 we discuss in greater detail the significance and the origin of the van der Waals attractions listed in Table 10.1. In the present section we are interested in only the exponent in the power law.

The last entry in Table 10.1 is the least well defined of those listed. This is of little importance to us, however, since our interest is in attraction, and the final entry in Table 10.1 always corresponds to repulsion. The reader may recall that so-called hard-sphere models for molecules involve a potential energy of repulsion that sets in and rises vertically when the distance of closest approach of the centers equals the diameter of the spheres. A more realistic potential energy function would have a finite (though steep) slope. An inverse power law with an exponent in the range 9 to 15 meets this requirement. For reasons of mathematical convenience, an inverse 12th-power dependence on the separation is frequently postulated for the repulsion between molecules.

In general, the combined effects of van der Waals attraction and interparticle repulsion at the molecular level may be represented by the equation

$$\Phi = \xi x^{-12} - \beta x^{-6} \tag{1}$$

in which the constant β has been used to represent the various constants in the Debye, Keesom, and London equations. Since the two terms on the right-hand side of Equation (1) correspond to opposing tendencies, the total potential energy function will display a minimum, the coordinates of which will describe an equilibrium situation. By differentiating Equation (1) with respect to x and setting the result equal to zero, the coordinates of the minimum can be evaluated. These are readily found to be

$$x_m = (2\xi/\beta)^{1/6} \tag{2}$$

and

$$\Phi_m = -(\beta/2)x_m^{-6} = -\xi x_m^{-12} \tag{3}$$

where the subscript reminds us that these are values at the minimum.

Equation (3) can be used to eliminate β and ξ from Equation (1) to obtain

$$\Phi = -\Phi_m[(x/x_m)^{-12} - 2(x/x_m)^{-6}] \tag{4}$$

Equations (1) and (4) or other variations of the 12-6 power law are often called the *Lennard-Jones potential.* The numerical values of the constants in the Lennard-Jones potential may be obtained from studies of the compressibility of condensed phases, the virial coefficients of gases, and by other methods. A summary of these methods and other expressions for the molecular interaction energy can be found in the book by Moelwyn-Hughes (1964).

Figure 10.2 is a plot of the Lennard-Jones function for methane, for which $\xi = 6.2 \cdot 10^{-134}$ J m^{12} and $\beta = 2.3 \cdot 10^{-77}$ J m^{6} ($x_m = 0.42$ nm and $\Phi_m = 2.1 \cdot 10^{-21}$ J).

Curves of this sort occur in many places in physical chemistry, and it is important to realize that they are the result of two contributions: a very short-range repulsion and a relatively long-range attraction. It is the latter with which we are primarily concerned, so we turn next to an examination of the origins of these inverse sixth-power attractions.

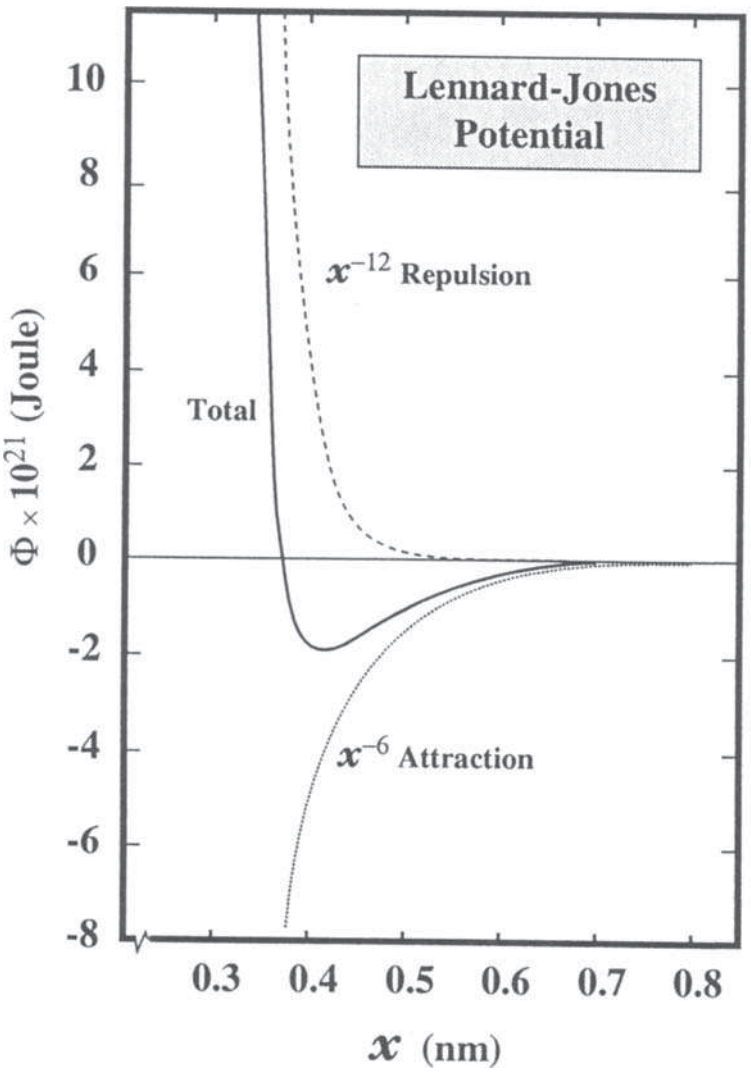


FIG. 10.2 Potential energy versus distance of separation for two methane molecules.

10.4 MOLECULAR ORIGINS AND THE MACROSCOPIC IMPLICATIONS OF VAN DER WAALS FORCES

In this section we outline the molecular origins of the Debye, Keesom, and London forces and discuss the strengths of these forces relative to each other. In addition, we also outline how macroscopic properties and behavior (such as the heat of vaporization of materials, nonideality of equations of state, and condensation of gases) can be traced to the influence of the above van der Waals forces and illustrate these through specific examples. Another example of the van der Waals forces, namely, the relation between the surface tension (or surface energy) of materials and the London force, is discussed in Section 10.7.

10.4a Molecular Origins of van der Waals Attractions

In Table 10.1 we saw that all random dipole-dipole interactions follow the inverse sixth-power law except the so-called *retarded* van der Waals attraction, which varies with the inverse seventh power of the separation. In this section we examine briefly the physical basis of the three different inverse sixth-power laws that describe intermolecular attractions. Space limitations prevent us from deriving the Debye, Keesom, and London expressions in detail. More complete derivations may be found in many physical chemistry textbooks, such as that by Moelwyn-Hughes (1964). The abbreviated discussion we present should be sufficient, however, to indicate the connection between these attractions and molecular parameters.

Interactions between dipoles, whether permanent or induced, are the result of the electric field produced by one dipole (subscript 1) acting on the second dipole (subscript 2). Therefore the first factor to consider in discussing such interactions is the field E produced by a dipole and measured a distance x from the dipole, with x large compared to the length of the dipole. Since we are dealing with the forces between charges, we must be attentive to the matter of units, as was the case in the similar discussion in Chapter 5, Section 5.2. The field has as units charge length $^{-2}$, but in SI this requires that we divide the charge by $4\pi\varepsilon_0 = 1.112 \cdot 10^{-10}$ J $^{-1}$ C^2 m $^{-1}$, in which case the field has the units N C $^{-1}$ (i.e., force per unit charge) or V m $^{-1}$ (i.e., potential gradient). The factor $4\pi\varepsilon_0$ is not required when cgs units are used; and, since the factor 4π may cancel, some of these relationships look different when written for other systems of units.

The field is a vector quantity and may be resolved into components as shown in Figure 10.3. We define θ to be the angle between the axis of the dipole and the line that connects the point under consideration with the center of the dipole and along which x is measured. The field may be resolved into the following components:

1. Parallel to the line of centers:

$$E_{\parallel} = -(2\mu_1/4\pi\varepsilon_0)x^{-3}\cos\theta \tag{5}$$

2. Perpendicular to the line of centers:

$$E_{\perp} = -(\mu_1/4\pi\varepsilon_0)x^{-3}\sin\theta \tag{6}$$

The total field is the square root of the sum of the squares of Equations (5) and (6), or

$$\begin{aligned} E &= -(\mu_1/4\pi\varepsilon_0)x^{-3}(\sin^2\theta + 4\cos^2\theta)^{1/2} \\ &= -(\mu_1/4\pi\varepsilon_0)x^{-3}(1 + 3\cos^2\theta)^{1/2} \end{aligned} \tag{7}$$

10.4a.1 Debye Interaction

Now let us consider the effect of such a field on a particle with no permanent dipole of its own. The field will induce a dipole in the second molecule; the magnitude of the induced dipole moment μ_2 is proportional to the field with the polarizability of the second molecule α_2 the proportionality constant (see Equation (5.11)):

$$\mu_2 = \alpha_2 E \tag{8}$$

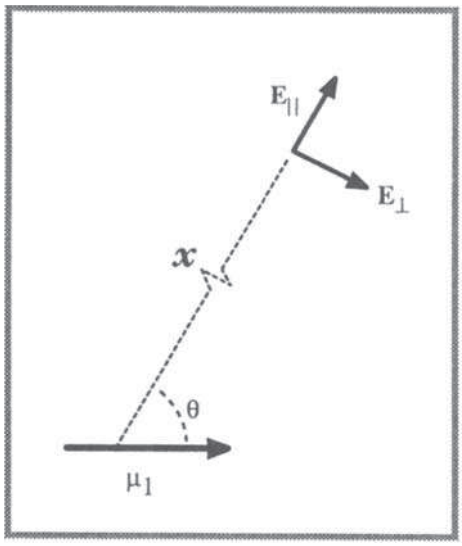


FIG. 10.3 The electric field a distance x from a dipole. The field is resolved into components parallel and perpendicular to the line of centers along which x is measured.

The potential energy of the second dipole due to this field is given by $-\mu_2 E$ or $-\alpha_2 E^2$. To this must be added the energy necessary to induce the dipole $(1/2)\alpha_2 E^2$ since the second is not a permanent dipole. Therefore the total potential energy Φ of the second dipole is

$$\Phi_2 = -(1/2)\alpha_2 E^2 \tag{9}$$

Substituting Equation (7) into this expression and averaging over all orientations yields

$$\Phi_2 = -[\alpha_2 \mu_1^2/(4\pi\varepsilon_0)^2]x^{-6} \tag{10}$$

The second dipole acts on the original dipole in a similar fashion, giving a second contribution to the interaction energy that is identical to Equation (10) except that the subscripts are interchanged. The total potential energy of attraction is the sum of these two contributions:

$$\Phi_D = -[(\alpha_2 \mu_1^2 + \alpha_1 \mu_2^2)/(4\pi\varepsilon_0)^2]x^{-6} \tag{11}$$

This is the *Debye equation* (subscript D) in Table 10.1 that describes the attraction between a permanent dipole and an induced dipole.

10.4a.2 Keesom Interaction

If this argument is applied to two *permanent* dipoles, the polarizability may be regarded as the sum of two contributions: one that is independent of the presence of the permanent dipole α_0 and a second that is the average effect of the rotation of the molecules in the electric field. The molar polarization P of a substance is given by

$$P = (N_A/3\varepsilon_0)[\alpha_0 + (\mu^2/3k_B T)] \tag{12}$$

The second term inside the brackets thus gives the average value of the orientation contribution to the polarizability. Note that the magnitude of the permanent dipole contribution is expressed relative to thermal energy (k_B is the Boltzmann constant) since increased thermal jostling tends to scramble the permanent dipoles. It is the second term in the brackets that is used in Equation (11) for the interaction of two permanent dipoles:

$$\Phi_K = -(2/3)\{\mu_1^2 \mu_2^2/[k_B T(4\pi\varepsilon_0)^2]\}x^{-6} \tag{13}$$

This is the *Keesom equation* (subscript K) from Table 10.1; it applies to the interaction of two permanent dipoles.

10.4a.3 London (Dispersion) Interaction

Finally, we turn our attention to the third contribution to van der Waals attraction, *London* (or *dispersion*) forces between a pair of induced dipoles. It will be noted that (at least) one permanent dipole is needed for the preceding sources of attraction to be operative. No such restriction is present for the London component. Therefore this latter quantity is present between molecules of all substances, whether or not they have a permanent dipole. These are the same forces that we considered in Chapter 6 when we discussed the Girifalco-Good-Fowkes equation.

The London equation for the attraction between a pair of induced dipoles is a quantum mechanical result that represents one of the contributions to the "bond" between a pair of particles. Like other quantum mechanical results, the interaction energy emerges as part of the solution to the Schrödinger equation. We dispense with a rigorous examination of the situation and consider only the physical model and the final results.

Figure 10.4 represents the situation we wish to consider. It represents two dipoles with length ℓ_i that is negligible compared to the distance between their centers. The dipoles are formed by the symmetrical vibration of electrons in the two particles. According to Table 10.1, the potential energy of two dipoles in this arrangement is $\pm 2\mu^2(4\pi\varepsilon_0)^{-1}x^{-3}$ or $\pm 2(e\ell_1)(e\ell_2)(4\pi\varepsilon_0)^{-1}x^{-3}$ since $\mu_i = e\ell_i$. In addition, each of the vibrating dipoles may be regarded as a harmonic oscillator for which the potential energy is given by

$$\Phi = (1/2)K\ell_i^2 \tag{14}$$

in which

$$K = (e^2/\alpha_0) \tag{15}$$

Combining these various energy contributions gives the following expression to be used as the potential energy of this system:

$$\Phi_I = (1/2)K\ell_1^2 \pm 2(e\ell_1)(e\ell_2)(4\pi\varepsilon_0)^{-1}x^{-3} + (1/2)K\ell_2^2 \tag{16}$$

When this net potential energy function is substituted into the one-dimensional Schrödinger equation and the suitable mathematical operations are carried out, the allowed energies E are found to be

$$E = [n_i + (1/2)]h\nu_i + [n_j + (1/2)]h\nu_j \tag{17}$$

in which

$$\nu_i = \nu\{1 - [2\alpha_0/(4\pi\varepsilon_0 x^3)]\}^{1/2} \tag{18}$$

and

$$\nu_j = \nu\{1 + [2\alpha_0/(4\pi\varepsilon_0 x^3)]\}^{1/2} \tag{19}$$

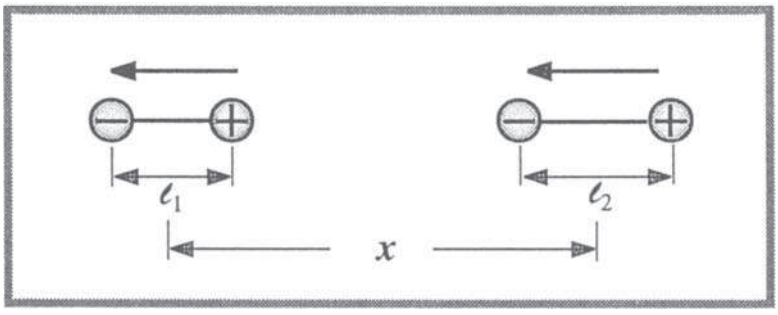


FIG. 10.4 A linear arrangement of two dipoles used to define the potential energy in the Schrödinger equation for the London interaction energy.

and the n_i and n_j are integers. Note that the terms in Equation (17) are formally identical to the energy of quantized harmonic oscillators of frequency ν_i and ν_j. In addition, we observe that ν_i and ν_j approach ν as $x \to \infty$. Thus ν is identified as the frequency of vibration for the system in the case in which the electrons vibrate independently.

The lowest energy for the two coupled oscillators is the situation in which $n_i = n_j = 0$, in which case Equation (17) becomes

$$E = (1/2)h(\nu_i + \nu_j) \tag{20}$$

On the other hand, the energy of two independent oscillators in their ground state is given by

$$E = 2[(1/2)h\nu] \tag{21}$$

The difference between Equations (20) and (21) gives the contribution of the interaction to the potential energy:

$$\Phi_L = (1/2)h[(\nu_i + \nu_j) - 2\nu] \tag{22}$$

This is one way of writing the London (subscript L) attraction between two induced dipoles.

If the expressions for ν_i and ν_j given by Equations (18) and (19) are substituted into Equation (22), the following result is obtained:

$$\Phi_L = (1/2)h\nu\left\{ \{1 - [2\alpha_0/(4\pi\varepsilon_0 x^3)]\}^{1/2} + \{1 + [2\alpha_0/(4\pi\varepsilon_0 x^3)]\}^{1/2} - 2 \right\} \tag{23}$$

Expanding the square roots by the binomial expansion (see Appendix A) and retaining no terms higher than second order yields

$$\Phi_L = -\frac{h\nu\alpha_0^2}{2(4\pi\varepsilon_0)^2} x^{-6} \tag{24}$$

Several modifications of Equation (24) are also important:

1. When the molecules are capable of vibration in all three dimensions, the numerical constant in Equation (24) becomes 4 rather than 2:

$$\Phi_L = -\frac{3h\nu\alpha_0^2}{4(4\pi\varepsilon_0)^2} x^{-6} \tag{25}$$

2. When unlike molecules are involved, their individual frequencies and polarizabilities are involved, and the expression equivalent to Equation (24) is

$$\Phi_L \approx -\frac{3}{2} h\left(\frac{\nu_1\nu_2}{\nu_1 + \nu_2}\right) \frac{\alpha_{0,1}\alpha_{0,2}}{(4\pi\varepsilon_0)^2} x^{-6} \tag{26}$$

   which is the result shown in Table 10.1. Note that this result becomes identical to the three-dimensional version of Equation (24) when the atoms are identical.

3. The quantity $h\nu$ in Equation (25) may be regarded as some energy that characterizes the system and is sometimes approximated by the *ionization energy* I:

$$\Phi_L \approx -\frac{3}{2}\left(\frac{I_1 I_2}{I_1 + I_2}\right) \frac{\alpha_{0,1}\alpha_{0,2}}{(4\pi\varepsilon_0)^2} x^{-6} \tag{27}$$

4. The frequency of a harmonic oscillator, the model for the two dipoles, equals $(1/2\pi)(K/m_e)^{1/2}$, where m_e is the mass of the electron. Substituting the value of K given by Equation (15) yields

$$\Phi_L = -\frac{3}{8}\left(\frac{he}{\pi}\right) \frac{\alpha_0^{3/2}}{m_e^{1/2}(4\pi\varepsilon_0)^2} x^{-6} \tag{28}$$

   for two identical molecules, since

$$\nu = \frac{1}{2\pi}\sqrt{\frac{e^2}{\alpha_0 m_e}} \tag{29}$$

Equations (25)–(28) are widely encountered expressions for the London attraction between two molecules.

In examining the Debye, Keesom, and London equations we see that (a) they share as a common feature an inverse sixth-power dependence on the separation and (b) the molecular parameters that describe the polarization of a molecule, polarizability and dipole moment, serve as proportionality factors in these expressions. For a full discussion of the experimental determination of α_0 and μ, a textbook of physical chemistry should be consulted (Atkins 1994). For our purposes, it is sufficient to note that the molar polarization of a substance can be related to its relative dielectric constant ε_r by

$$P = \frac{M}{\rho}\frac{\varepsilon_r - 1}{\varepsilon_r + 2} \tag{30}$$

where M and ρ are the molecular weight and density, respectively (Atkins 1994, Chapter 22).

Combining Equations (12) and (30) gives the general result

$$\frac{M}{\rho}\frac{\varepsilon_r - 1}{\varepsilon_r + 2} = \frac{N_A}{3\,\varepsilon_0}\left(\alpha_0 + \frac{\mu^2}{3k_BT}\right) \tag{31}$$

Thus studies of ε_r as a function of T may be analyzed to yield values of both α_0 and μ. For substances with no permanent dipole moment, $\mu = 0$ and $\varepsilon_r = n^2$, where n is the refractive index at long wavelengths. For such a system Equation (31) becomes

$$\frac{M}{\rho}\frac{n^2 - 1}{n^2 + 2} = \frac{N_A}{3\,\varepsilon_0}\alpha_0 \tag{32}$$

To use Equation (32) it is necessary to extrapolate to infinite wavelength (or zero frequency) to obtain the unperturbed polarizability since the electric field of the light also alters the molecule. Failure to carry out such an extrapolation introduces far less error, however, than is introduced by an approximation such as Equation (27).

10.4a.4 Relative Magnitudes of the Individual Contributions to van der Waals Interaction

In general, we may think of any molecule as possessing a dipole moment and a polarizability. This means that each of the three types of interaction may operate between any pair of molecules. Of course, in nonpolar molecules for which $\mu = 0$, two of the three sources of attraction make no contribution.

As we have already noted, all molecules display the dispersion component of attraction since all are polarizable and that is the only requirement for the London interaction. Not only is the dispersion component the most ubiquitous of the attractions, but it is also the most important in almost all cases. Only in the case of highly polar molecules such as water is the dipole-dipole interaction greater than the dispersion component. Likewise, the mixed interaction described by the Debye equation is generally the smallest of the three.

For a pair of identical molecules, Equations (11), (13), and (25) may be combined to give the *net* van der Waals attraction (subscript A) Φ_A:

$$\Phi_A = -\frac{1}{(4\,\pi\,\varepsilon_0)^2}\left(2\alpha_{0,1}\mu_1^2 + \frac{2\mu_1^4}{3\,k_BT} + \frac{3}{4}h\nu_1\alpha_{0,1}^2\right)x^{-6} = -\beta_{11}x^{-6} \tag{33}$$

The interaction parameter β_{11} is defined

$$\beta_{11} = \frac{1}{(4\,\pi\,\varepsilon_0)^2}\left(2\alpha_{0,1}\mu_1^2 + \frac{2\mu_1^4}{3\,k_BT} + \frac{3}{4}h\nu_1\alpha_{0,1}^2\right) \tag{34}$$

where the subscript 11 has been added to β as a reminder that this result applies to a pair of identical molecules.

We have gone through a rather complicated list of equations without looking at the magnitude of the various energy contributions. This is the subject of Example 10.1.

* * *

EXAMPLE 10.1 *Relative Magnitudes of van der Waals Forces and Relation to Heat of Vaporization.* The parameter β_{11} must have units energy length^6 in order to satisfy Equation (33). Verify these units as well as the dimensional consistency of each of the three terms in Equation (34). Taking $\mu = 1.0$ debye and $\alpha = 10^{-39}\ C^2\ m^2\ J^{-1}$, calculate the amount of energy needed to separate a pair of molecules from 0.3 nm to ∞. Scaled up by Avogadro's number, how does this energy compare with typical enthalpies of vaporization?

Solution: First, we examine the units of each of the terms in Equation (34). Example 5.1 makes it easy to analyze the units of terms containing α. That example shows that $(\alpha/4\pi\varepsilon_0)$ has units length^3. Polarizabilities are often tabulated as $(\alpha/4\pi\varepsilon_0)$, thereby having volume units.

The dipole moment has units of charge length, or C m in SI. The square of these units divided by the units of $(4\pi\varepsilon_0)$ therefore has units $C^2\ m^2/(C^2\ J^{-1}\ m^{-1})$ or $J\ m^3$.

The first term in Equation (34) involves the product of α and μ^2, each expressed in multiples of $(4\pi\varepsilon_0)$, and therefore has units $J\ m^6$ as required.

Since k_BT has units of energy, the second term in Equation (34) is seen to have units $(J\ m^3)^2/J = J\ m^6$.

Since $h\nu$ has units of energy, the third term has units $J\ (m^3)^2 = J\ m^6$. The debye is widely used as a unit of dipole moment. It is equal to 10^{-18} esu cm. To convert this to SI we write

$$1 \text{ debye} = 10^{-18} \text{ esu cm} \cdot (1 \text{ m}/100 \text{ cm}) \cdot (1.60 \cdot 10^{-19} \text{ C}/4.80 \cdot 10^{-10} \text{ esu})$$
$$= 3.336 \cdot 10^{-30} \text{ C m}$$

In Equation (34) the Debye term is given by

$$[2\alpha\mu^2/(4\pi\varepsilon_0)^2] = [2 \cdot (10^{-39})(3.34 \cdot 10^{-30})^2]/(1.11 \cdot 10^{-10})^2$$
$$= 1.81 \cdot 10^{-78}\ J\ m^6$$

and the Keesom term by

$$[(2/3)\mu^4/k_BT(4\pi\varepsilon_0)^2] = [2(3.34 \cdot 10^{-30})^4]/[3(1.38 \cdot 10^{-23})(293)(1.11 \cdot 10^{-10})^2]$$
$$= 1.67 \cdot 10^{-78}\ J\ m^6$$

To evaluate the London term we need the characteristic frequency ν. Using Equation (29), we obtain for this frequency

$$\nu = (1/2\pi)[(1.60 \cdot 10^{-19})^2/(10^{-39})(9.11 \cdot 10^{-31})]^{1/2}$$
$$= 8.44 \cdot 10^{14}$$

in terms of which the London energy is given by

$$[(3/4)h\nu\alpha^2/(4\pi\varepsilon_0)^2] = [3(6.63 \cdot 10^{-34})(8.44 \cdot 10^{14})(10^{-39})^2]/[4(1.11 \cdot 10^{-10})^2]$$
$$= 3.41 \cdot 10^{-77}\ J\ m^6$$

The sum of these three contributions gives the β_{11} value for this system $\beta_{11} = 3.76 \cdot 10^{-77}$ $J\ m^6$.

When the separation of the molecules is 0.3 nm, the energy is $3.76 \cdot 10^{-77}/(0.3 \cdot 10^{-9})^6 = 5.16 \cdot 10^{-20}$ J. When the distance of separation is infinity, the interaction energy is zero. Therefore scaling up $5.16 \cdot 10^{-20}$ J by Avogadro's number gives an estimate of the energy required to separate a mole of these molecules from a separation typical of a liquid to one that represents a gas: $(5.16 \cdot 10^{-20})(6.02 \cdot 10^{23}) = 31{,}000$ J. This final result is of the correct order of magnitude of heats of vaporization. ■

* * *

Dividing Equation (34) through by β_{11} gives the fractional contribution made to the total attraction by the Debye (D), Keesom (K), and London (L) components of potential energy:

$$f_D + f_K + f_L = 1 \tag{35}$$

Table 10.2 shows these fractions calculated for a variety of molecules. In virtually all cases except the highly polar water molecule, the London or dispersion component is the largest of the contributions to attraction. In the case of water, hydrogen bonding is also possible and contributes an additional strong interaction, so the role of dispersion is even less than shown in Table 10.2.

Before continuing with our development of van der Waals attraction, we examine how

TABLE 10.2 Percentage of the Debye, Keesom, and London Contributions to the van der Waals Attraction Between Various Molecules

Compound	μ (debye)	$\frac{\alpha}{4\pi\varepsilon_0} \times 10^{30}$ (m^3)	$\beta \times 10^{77}$ (J m^6)	Percentage contribution of Keesom (permanent-permanent)	Debye (permanent-induced)	London (induced-induced)
CCl_4	0.00	10.70	4.41	0.0	0.0	100.0
Ethanol	1.73	5.49	3.40	42.6	9.7	47.6
Thiophene	0.51	9.76	3.90	0.3	1.3	98.5
t-Butanol	1.67	9.46	5.46	23.1	9.7	67.2
Ethyl ether	1.30	9.57	4.51	10.2	7.1	82.7
Benzene	0.00	10.50	4.29	0.0	0.0	100.0
Chlorobenzene	1.58	13.00	7.57	13.3	8.6	78.1
Fluorobenzene	1.35	10.30	5.09	10.6	7.5	81.9
Phenol	1.55	11.60	6.48	14.5	8.6	76.9
Aniline	1.56	12.40	7.06	13.6	8.5	77.9
Toluene	0.43	11.80	5.16	0.1	0.9	99.0
Anisole	1.25	13.70	7.22	5.5	6.0	88.5
Diphenylamine	1.08	22.60	14.25	1.5	3.7	94.7
Water	1.82	1.44	2.10	84.8	4.5	10.5

Source: Dipole moments and polarizibilities from A. L. McClellan, *Tables of Experimental Dipole Moments*, W. H. Freeman, San Francisco, CA, 1963.

van der Waals forces at the atomic or molecular level influence the macroscopic properties of materials.

10.4b Macroscopic Implications

We have already seen from Example 10.1 that van der Waals forces play a major role in the heat of vaporization of liquids, and it is not surprising, in view of our discussion in Section 10.2 about colloid stability, that they also play a significant part in (or at least influence) a number of macroscopic phenomena such as adhesion, cohesion, self-assembly of surfactants, conformation of biological macromolecules, and formation of biological cells. We see below in this chapter (Section 10.7) some additional examples of the relation between van der Waals forces and macroscopic properties of materials and investigate how, as a consequence, measurements of macroscopic properties could be used to determine the Hamaker constant, a material property that represents the strength of van der Waals attraction (or repulsion; see Section 10.8b) between macroscopic bodies. In this section, we present one illustration of the macroscopic implications of van der Waals forces in thermodynamics, namely, the relation between the interaction forces discussed in the previous section and the *van der Waals equation of state*. In particular, our objective is to relate the molecular van der Waals parameter (e.g., β_{11} in Equation (33)) to the parameter a that appears in the van der Waals equation of state:

$$[p + (a/v^2)](v - b) = RT \tag{36}$$

where p is the pressure and v is the molar volume of the gas. Incidentally, van der Waals's proposal of the above equation, presented as part of his doctoral dissertation, pre-dates the development of what are now known as van der Waals forces. Interested readers may wish to consult his dissertation, which is now available as a book (van der Waals 1988).

Let us begin with a collection of N atoms of diameter σ in a volume V. We shall assume that the atoms are spherical and mutually impenetrable, that the interparticle energy of attraction between any two particles is given by $(-\beta_{11} r^{-6})$ for $r > \sigma$, with r the center-to-center

distance of separation between the two particles, and that the density (N/V) is sufficiently low that we can consider the total interatomic interaction energy as a sum of pair interactions (i.e., sum of interactions taken two atoms at a time). Given this information, our goal is to relate the parameters σ, β_{11}, N, and V to the van der Waals parameters a and b.

We first look into the "excluded-volume" effect, represented by the parameter b. Since the atoms are impenetrable, no atom can get closer than a distance σ from another. (Note that the location of each atom is represented by the location of the center of that atom.) This implies that each atom has a volume of $(4/3)\pi\sigma^3$ around its center that is not accessible to the center of any other atom; this volume is the excluded volume associated with each atom. (Figure 13.9 is an illustration of this situation for two colloidal particles of *different* radii.) The actual excluded volume per atom, b' (b, the excluded volume per mole, is equal to $N_A b'$, with N_A the Avogadro's number) is, however, smaller than $(4/3)\pi\sigma^3$ since the excluded volume of an atom as calculated above may overlap with that of other atoms. Therefore, to obtain an expression for b, we need to multiply the above value by N (since there are N atoms in the volume), take half of it since otherwise we will be "double counting" the excluded volumes, and divide by N to get excluded volume per atom, that is,

$$b' = (4/3)\pi\sigma^3 \cdot (N/2) \cdot (1/N) = (2/3)\pi\sigma^3 \tag{37}$$

Therefore, it follows that

$$b = (2/3)\pi\sigma^3 N_A \tag{38}$$

Now, we examine the effect of attraction. Each atom is surrounded by $(N - 1)$ atoms in the volume V. The number of atoms in a spherical shell of thickness dr at a distance r from any atom is $4\pi r^2(N/V)dr$. Therefore, the interaction energy u experienced by any atom is given by

$$u = \int_\sigma^S 4\pi \frac{N}{V}\left(-\frac{\beta_{11}}{r^6}\right) r^2\, dr = -\frac{4\pi N\beta_{11}}{V}\int_\sigma^S \frac{dr}{r^4} \tag{39}$$

where S is the radius of the container. The above equation can be integrated easily, and since S is usually very much larger than σ, the integration leads to

$$u = \frac{4\pi}{3}\frac{N}{V}\beta_{11}\left(\frac{1}{S^3} - \frac{1}{\sigma^3}\right) = -\frac{4\pi N\beta_{11}}{3\,V\sigma^3} \tag{40}$$

The total energy U for all the N atoms is then

$$U = -\frac{2\pi N^2\beta_{11}}{3\,V\sigma^3} \tag{41}$$

where we have again multiplied u by $(N/2)$ for the same reason as in the case of the expression for b.

Since pressure is equal to $-(\partial U/\partial V)_T$ and the deviation in pressure from ideality (i.e., from $pv = RT$) arising from the attractive forces in the van der Waals equation is equal to $(-a/v^2)$, we have

$$\left(\frac{\partial U}{\partial V}\right)_T = \frac{a}{v^2} = \frac{N^2 a}{N_A^2 V^2} \tag{42}$$

which we can combine with Equation (41) for U to obtain

$$a = \frac{2\pi N_A^2\beta_{11}}{3\,\sigma^3} \tag{43}$$

The above derivation shows that one can determine the van der Waals parameters a and b if σ (a measure of the size of the atom or molecules) and the van der Waals interaction energy parameter β_{11} are known. Alternatively, one can estimate β_{11} from known values of a and b. This is illustrated in Example 10.2.

* * *

EXAMPLE 10.2 *The Dispersion Force and Nonideality of Gases.* The nonideality of gases arises from the repulsive and attractive forces between atoms. As a consequence, the deviation of the properties of a gas from ideal gas behavior can be traced to the interatomic or intermolecular forces. Assume that methane follows the van der Waals equation of state at sufficiently low densities. It is known from experiments that (see Israelachvili 1991)

$$a = 2.28 \cdot 10^{-1}\ \mathrm{m^3\ J\ mol^{-2}} \qquad \text{and} \qquad b = 4.28 \cdot 10^{-5}\ \mathrm{m^3\ mol^{-1}}$$

Assume that the intermolecular attraction in this case is dominated by the London interaction, that is, $\Phi_L = -Cr^{-6}$, for which C is the London parameter (Equation (25)). Estimate the London constant from the equation-of-state data and compare it with the coefficient from Equation (25). The polarizability $[\alpha_0/(4\pi\varepsilon_0)]$ for CH_4 is $2.6 \cdot 10^{-30}\ \mathrm{m^3}$. The ionization energy I is $2.0185 \cdot 10^{-18}$ J (Israelachvili 1991, Chapter 6 and Table 6.1).

Solution: One can eliminate the molecular diameter σ from the equation for the parameter a using the equation for b to get C in terms of a and b:

$$C = 9abI/(4\pi^2 N_A{}^3)$$

Using $N_A = 6.022 \cdot 10^{23}\ \mathrm{mol^{-1}}$ and the given values of a and b, we get for C

$$C = 1.018 \cdot 10^{-77}\ \mathrm{J\ m^6} \qquad \text{(from the experimental } PV \text{ data)}$$

From Equation (27) for identical molecules, one has

$$\Phi_L = -(3/4)[\alpha_0/(4\pi\varepsilon_0)]^2 I r^{-6} = -Cr^{-6}$$

Therefore, the London constant C is given by

$$C = (3/4)[\alpha_0/(4\pi\varepsilon_0)]^2 I$$

From the given values of polarizability and ionization potential for CH_4, we have

$$C = 1.02 \cdot 10^{-77}\ \mathrm{J\ m^6} \qquad \text{(from the polarizability data)}$$

The two values agree remarkably well, showing the relation between the London force and the nonideality of the gas.

This example illustrates how equation-of-state data may be used to estimate the strength of van der Waals forces or vice versa. ■

* * *

In this section we have examined the three major contributions to what is generally called the van der Waals attraction between molecules. All three originate in dipole-dipole interactions of one sort or another. There are two consequences of this: (a) all show the same functional dependence on the intermolecular separation, and (b) all depend on the same family of molecular parameters, especially dipole moment and polarizability, which are fairly readily available for many simple substances. Many of the materials we encounter in colloid science are not simple, however. Hence we must be on the lookout for other measurable quantities that depend on van der Waals interactions. Example 10.2 introduces one such possibility. We see in Section 10.7 that some other difficulties arise with condensed systems that do not apply to gases.

In the next section we take a preliminary look at the way van der Waals attractions scale up for macroscopic (i.e., colloidal) bodies. This will leave us in a better position to look for other measurements from which to estimate the van der Waals parameters.

10.5 VAN DER WAALS FORCES BETWEEN LARGE PARTICLES AND OVER LARGE DISTANCES

The interaction between individual molecules obviously plays an important role in determining, for example, the nonideality of gas, as illustrated in Example 10.2. It is less clear how to apply this insight to dispersed particles in the colloidal size range. If atomic interactions are assumed to be additive, however, then the extension to macroscopic particles is not particularly difficult. Moreover, when dealing with objects larger than atomic dimensions, we also

have to consider interactions over appropriately large distances. In the case of the London attraction, forces over large distances show a more rapid decay than indicated by the inverse sixth-power equations derived in Section 10.4. This is known as (*electromagnetic*) *retardation*. We discuss these two important issues in this section before developing the equations for interactions between macroscopic bodies in Section 10.6.

10.5a Scaling van der Waals Interactions for Large Bodies

We begin by considering two spherical particles of the same composition and the same radius R_a. As Figure 10.5 shows, we consider two situations. In case (a) we consider spheres of radius R_a and in case (b) spheres of radius R_b. The two radii are related as follows:

$$R_b = fR_a \tag{44}$$

where f is a factor greater than unity.

Let us first focus on Figure 10.5a. Assume that every atom in sphere 1 attracts every atom in sphere 2 with an energy given by Equation (33). If $(\rho N_A/M)$ is the number of atoms per cubic centimeter in the material, then there are $(\rho N_A/M)dV_{1a}$ atoms in a volume element of sphere 1 and $(\rho N_A/M)dV_{2a}$ atoms in a volume element of sphere 2. The number of pairwise interactions between the two volume elements is $(1/2)\ (\rho N_A/M)^2\ dV_{1a}dV_{2a}$. The factor $(1/2)$ enters since each pair is counted twice. This number times the interaction per pair gives the increment in potential energy for the two interacting volume elements in case (a):

$$d\Phi_a = -\frac{1}{2}\left(\frac{\rho N_A}{M}\right)^2 \beta\, r_a^{-6}\, dV_{1a}\, dV_{2a} \tag{45}$$

By including additional geometrical considerations, the volume elements and their separation may be expressed in a common set of variables, and Equation (45) can be integrated over the volume of both spheres. Rather than complicate the issue by specific mathematical substitutions at this time, we indicate this procedure as follows:

$$\Phi_a = -\frac{1}{2}\left(\frac{\rho N_A}{M}\right)^2 \beta \int\int r_a^{-6}\, dV_{1a}\, dV_{2a} \tag{46}$$

Now let us turn our attention to Figure 10.5b. In this case the spheres are larger by a factor f as just noted. In addition to this, the distance between their centers is also assumed to

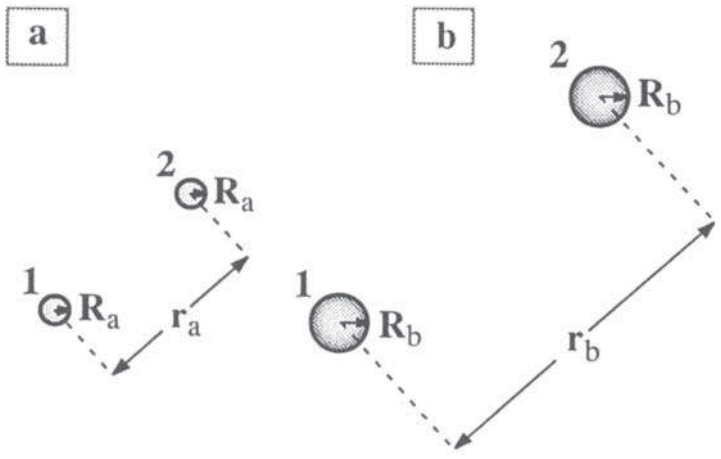


FIG. 10.5 Two spheres of equal radii separated by a distance r. All linear dimensions in (b) (i.e., R_b and r_b) are larger than those in (a) by a constant factor f.

be larger than that in case (a) by the factor f. If we let the separation of centers be represented by r, then

$$r_b = fr_a \tag{47}$$

Following the same procedure as used for case (a), we can evaluate the total interaction potential in case (b). It is given by

$$\Phi_b = -\frac{1}{2}\left(\frac{\rho N_A}{M}\right)^2 \beta \int\int r_b^{-6}\, dV_{1b}\, dV_{2b} \tag{48}$$

Since the linear scale in case (b) is larger by the factor f than that in case (a), Equation (48) can also be written

$$\Phi_b = -\frac{1}{2}\left(\frac{\rho N_A}{M}\right)^2 \beta \int\int (fr_a)^{-6}(f^3\, dV_{1a})(f^3\, dV_{2a}) \tag{49}$$

Note that the factor f cancels out of this expression entirely, so that

$$\Phi_a = \Phi_b \tag{50}$$

That is, the potential energy of attraction is identical in the two cases. This is an important result as far as the extension of molecular interactions to macroscopic spherical bodies is concerned. What it says is that two molecules, say, 0.3 nm in diameter and 1.0 nm apart, interact with exactly the same energy as two spheres of the same material that are 30.0 nm in diameter and 100 nm apart. Furthermore, an inspection of Equation (49) reveals that this is a direct consequence of the inverse sixth-power dependence of the energy on the separation. Therefore the conclusion applies equally to all three contributions to the van der Waals attraction. Precisely the same forces that are responsible for the association of individual gas molecules to form a condensed phase operate—over a suitably enlarged range—between colloidal particles and are responsible for their coagulation.

The analogy between the condensation of a gas and the coagulation of a dispersion is important. It points out that under certain circumstances the aggregation of the separated units is inevitable. However, there are also conditions under which the dispersed state is stable. We know from kinetic molecular theory that thermal energy—measured by k_BT per molecule or RT per mole—supplies a reference level against which all energies are judged to be large or small.

* * *

EXAMPLE 10.3 *The Strength of van der Waals Forces and the Structure of Materials.* It is interesting to ask why some substances such as very small, nonpolar argon and methane are gaseous at room temperature while substances made up of larger molecules (e.g., high molecular weight hydrocarbons) are liquids or solids. Consider argon as an example and show that the typical attractive energy of two argon atoms separated by a distance of about 0.38 nm is of the order of thermal energy (i.e., about k_BT) at room temperature. Discuss the implication of this order-of-magnitude estimation to the structure of a substance at room temperature. The quantity $[\alpha_0/(4\pi\varepsilon_0)]$ for argon is about $1.6 \cdot 10^{-30}$ m^3. The ionization energy I for Ar is roughly $2.5 \cdot 10^{-18}$ J.

Solution: Using Equation (27), with $I_1 = I_2 = I$, one observes that for two argon atoms separated by the given (typical) distance of separation the dispersion energy is approximately equal to

$$\begin{aligned}\Phi_L &= -(3/4)[\alpha_0/(4\pi\varepsilon_0)]^2\, I\, x^{-6} \\ &= -0.75 \cdot 2.56 \cdot 10^{-60} \cdot 2.5 \cdot 10^{-18} \cdot (0.38 \cdot 10^{-9})^{-6}\,\text{J} \\ &= -1.6 \cdot 10^{-21}\,\text{J}\end{aligned}$$

Since $k_B = 1.381 \cdot 10^{-23}$ J K^{-1}, at room temperature (say, $T = 290$ K), one has

$$\Phi_L = -1.6 \cdot 10^{-21} \approx -0.4\, k_BT$$

The above result implies that at room temperatures the attraction between two argon atoms is sufficiently weak relative to thermal energy (k_BT) that argon will remain as a gas rather than in

a condensed state (liquid or solid). In contrast, in the case of larger molecules, the attractive energies can be sufficiently high to make the material condense into a liquid or solid. Although the above estimate is crude, it explains the role of van der Waals forces on condensation.

This example illustrates how the London forces influence whether a material exists as a gas, a liquid, or a solid at a given temperature. ■

* * *

Thus, as illustrated in Example 10.3, a gas will condense if the energy of attraction between molecules is large compared to k_BT. Conversely, it remains dispersed if k_BT is larger. The same is true for colloidal particles also, at least if they are not too large. For larger particles externally applied energy—such as mechanical stirring—joins thermal energy in establishing a reference level of energy. In general, however, the height of the barriers or the depth of the minima in the potential energy curves we discussed in Section 10.2 are considered large or small relative to k_BT. The argument leading to Equation (50) shows that van der Waals attraction is as important for colloidal particles as it is for individual molecules.

In reaching this conclusion we have assumed that no time lag affects the field that establishes the attraction between the particles. We have also considered particles under vacuum so no intervening medium enters the picture. Each of these simplifying approximations has the effect of overestimating the van der Waals attraction between particles at large separations from one another and embedded in a medium. We consider presently the effect of a time lapse between the interaction of a field with two different particles; the effect of the medium is discussed in Section 10.8.

10.5b Electromagnetic Retardation of the London Force

The electric field responsible for the London attraction between molecules propagates itself with the speed of light between the particles. Thus, if a pair of molecules is widely separated, a time lag or a phase difference develops between vibrations at the two locations. The situation is analogous in many ways to the scattering of light by particles with dimensions that are large compared to the wavelength of the light (see Section 5.5). In the present situation we find that the importance of this time lag or retardation increases as the separation becomes comparable to the wavelength of the propagating field.

Equation (29) provides us with an expression for the frequency of the interaction. Therefore its wavelength is given by

$$n\lambda = \frac{c}{\nu} = 2\pi c\sqrt{\frac{\alpha_0 m_e}{e^2}} \tag{51}$$

where n is the refractive index. For typical values of n and α_0, λ is about 200 nm. As was the case with light scattering, separations less than about 1/20 of this distance may be considered "small compared to the wavelength." This means that at separations of about 10 nm or so the effects of retardation begin to enter the picture. Our reason for interest in this is the fact that the comparison of attraction and repulsion between colloidal particles is made at this distance in some cases.

We shall not present the detailed analysis of this complication. In essence, it involves the time-dependent Schrödinger equation rather than the time-independent equation that resulted in Equation (22). Casimir and Polder have investigated this situation. They found that for values of $r \gg \lambda$, the potential energy of attraction according to the modified London treatment is given by

$$\Phi_A = -\frac{23}{8\pi^2 (4\pi\varepsilon_0)^2}\frac{h c \alpha_0^2}{r^7} \tag{52}$$

This is the one entry in Table 10.1 that has not yet been discussed. Direct measurement of the force of attraction between macroscopic bodies reveals a crossover from an inverse sixth-power to an inverse seventh-power law at separations in the range 10 to 100 nm.

Equation (49) is particularly convenient to show the effects of retardation on the attrac-

tion between spherical particles at large separations. On correcting the potential function for retardation according to Equation (52), Equation (49) becomes

$$\Phi_b \propto \iint_{1 \text{ and } 2} (f r_a)^{-7} (f^3 dV_{1a})(f^3 dV_{2a}) = \frac{1}{f}\Phi_a \tag{53}$$

at large separations. This result shows that the scale factor f does *not* drop out of the expression in the case of the retarded van der Waals forces. Therefore the potential energy of the attraction decreases as the scale increases (i.e., as f increases).

In subsequent discussions we shall not consider the effect of retardation any further. Additional details are given by Israelachvili (1991), Israelachvili and Tabor (1973), and Sonntag and Strenge (1964).

The development that led to Equation (50) was conducted without any actual integrations being performed. In order to generate exact expressions for the van der Waals attraction between bodies of specific geometry, it is necessary to carry out these operations. This is discussed in the next section.

10.6 CALCULATING VAN DER WAALS FORCES BETWEEN MACROSCOPIC BODIES

The strategy for scaling up the van der Waals attraction to macroscopic bodies requires that all pairwise combinations of intermolecular attraction between the two bodies be summed. This has been done for several different geometries by Hamaker. We consider only one example of the calculations involved, namely, the case of blocks of material with planar surfaces. This example serves to illustrate the method and also provides a foundation for connecting van der Waals forces with surface tension, the subject of the next section.

10.6a Attraction Between Two Semi-Infinite Blocks

Figure 10.6a represents a molecule at O located a normal distance z from the surface of a bulk sample of the same material. The bulk portion is assumed to have a planar face but otherwise is of infinite extension. The molecule is located a distance x from all the molecules in the ring-shaped volume element shown in the figure. The volume of this ring is given by $dV = 2\pi y\, dy\, d\zeta$. Therefore the increment of interaction between the molecule and the block due to the molecules a distance x from the point O is given by

$$d\Phi = -(\rho N_A/M)\beta(2\pi y/x^6)dy\, d\zeta \tag{54}$$

We assume the ring is located a distance ζ inside the surface of the block; then

$$x^2 = (z + \zeta)^2 + y^2 \tag{55}$$

Combining Equations (54) and (55) gives

$$d\Phi = -(\rho N_A/M)\,\beta\, 2\pi[(z + \zeta)^2 + y^2]^{-3} y\, dy\, d\zeta \tag{56}$$

Equation (56) is now integrated over the volume of the block, that is, for $0 < y < \infty$ and $0 < \zeta < \infty$.

Integration over y yields

$$\int_0^\infty \frac{y dy}{[(z + \zeta)^2 + y^2]^3} = \frac{1}{2}\int_0^\infty \frac{du}{[(z + \zeta)^2 + u]^3} = -\frac{1}{2}\left\{\frac{1}{2[(z + \zeta)^2 + u]^2}\right\}_0^\infty = \frac{1}{4}\frac{1}{(z + \zeta)^4} \tag{57}$$

and integration over ζ yields

$$\frac{1}{4}\int_0^\infty \frac{d\zeta}{(z + \zeta)^4} = -\frac{1}{4}\left|\frac{1}{3(z + \zeta)^3}\right|_0^\infty = \frac{1}{12z^3} \tag{58}$$

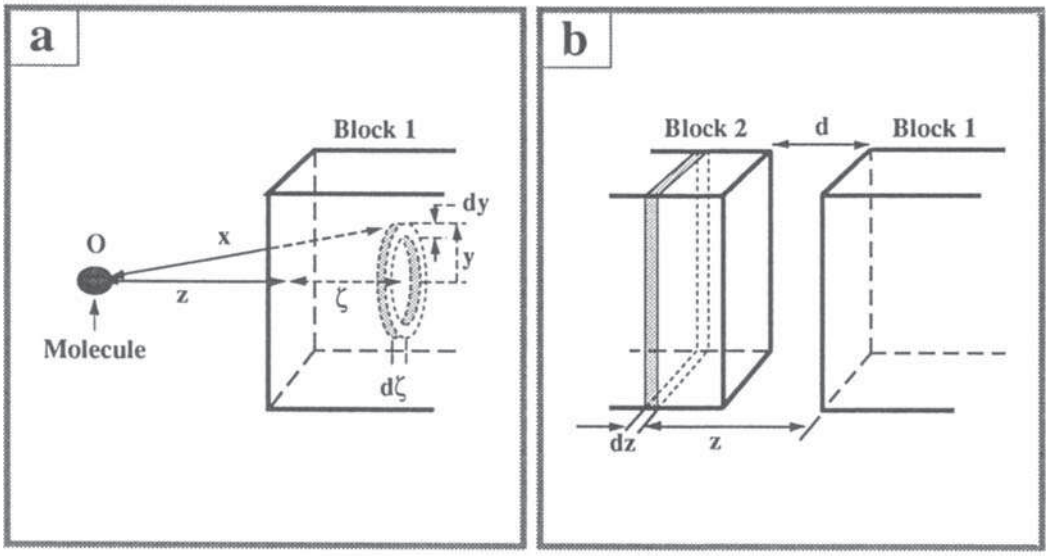


FIG. 10.6 Schematic illustration of interactions: (a) interaction between a molecule and a block of material; and (b) interaction between two blocks of material. (Redrawn with permission from P. C. Hiemenz, *J. Chem. Educ.*, **49**, 164 (1972).

Therefore the integration of Equation (56) over the block gives

$$\Phi = -(\rho N_A/M)\beta\pi/(6z^3) \tag{59}$$

Now suppose point O is located inside a second block of material as shown in Figure 10.6b. We recognize that all atoms in a slice of the second block a distance z from the first block will be attracted toward the second with an energy given by Equation (59). If we position a volume element of thickness dz at this location in the second block, we realize that it contains $(\rho N_A/M)$ molecules per unit area. This is $(\rho N_A/M)dz$ molecules; therefore the increment of attraction per unit area due to this slice is

$$d\Phi = -(\rho N_A/M)^2(\beta\pi/6)z^{-3}dz \tag{60}$$

Equation (60) may now be integrated over values of z between the distance of closest approach d and infinity. The result of this integration gives the potential energy of attraction per unit area between two blocks of infinite extension:

$$\Phi_A = -(\rho N_A/M)^2(\beta\pi/12)d^{-2} \tag{61}$$

where the subscript A has been appended to Φ to emphasize the fact that this energy is always attractive.

It is traditional to designate the cluster of constants $(\rho N_A/M)^2\pi^2\beta$ as the *Hamaker constant* A:

$$A = (\rho N_A\pi/M)^2\beta \tag{62}$$

With this change of notation. Equation (61) becomes

$$\Phi_A = -(A/12\pi)d^{-2} \tag{63}$$

The Hamaker constant has energy units since β has the units energy length^6 and the term in parentheses in Equation (62) has the units (volume^{-1})^2. The potential energy of attraction between blocks as calculated by Equation (63) is expressed per unit area of the facing surfaces. Note also that this attraction grows weaker as the distance increases. This is different from the

conclusion drawn for spheres in Equation (50). The scaling up of van der Waals forces, therefore, depends on the geometry of the bodies involved.

10.6b Magnitudes of Hamaker Constants

Although we have considered numerical values of β before, we have not encountered the Hamaker constant previously and hence have no feel for its magnitude. A particularly convenient form for an order of magnitude estimation of A is obtained by making the following stipulations:

1. Assume that the dispersion component is the dominant contributor to the attraction; therefore $\beta = (3/4)h\nu(\alpha/4\pi\varepsilon_0)^2$.
2. Recognize that $(\rho N_A/M)$ is the reciprocal of the volume per molecule, and that $(\alpha/4\pi\varepsilon_0)$ is typically about 10% the magnitude of atomic volume; therefore $A \approx (3/4)\pi^2 h\nu(0.1)^2$.
3. The quantity $h\nu$ is the same order of magnitude as the ionization potential, typically about 10^{-18} J.

Combining these results leads us to estimate the Hamaker constant to lie in the range 10^{-20} to 10^{-19} J. If we take the midpoint value of $5 \cdot 10^{-20}$ J for A, Equation (63) predicts that Φ_A equals 1.33 and $1.33 \cdot 10^{-2}$ mJ m^{-2} when d equals 1.0 and 10 nm, respectively. Table 10.3 presents Hamaker constants for some materials of practical interest. Values for many other materials and reviews of methods of calculating Hamaker constants are available in Gregory (1969) and Visser (1972).

10.6c van der Waals Interaction Energies for Other Geometries

The interaction of two infinite blocks separated at the surface by a distance d is one of the easiest possible situations to consider and therefore was chosen as the example to develop in detail. Bodies of different geometries have also been analyzed in much the same way that we have the blocks. The results of several such derivations are shown in Table 10.4. The expressions for Φ_A become more complicated for more complex geometrical situations, but considerable simplification results for spheres in which the separation is much less than the radius. The feature described by Equation (50) for interacting spheres is also evident in the results given in Table 10.4. It is most readily seen by examining the case of equal spheres separated by small distances. Note that both R, and d can be multiplied by any common factor without changing

TABLE 10.3 Hamaker Constants for Selected Materials

Material	$A \times 10^{20}$ Joules	Source
Acetone	4.2	Croucher and Hair
Alumina	15.4	Bargeman and van Voorst Vader
Gold	45.3	Bargeman and van Voorst Vader
Magnesia	10.5	Bargeman and van Voorst Vader
Metals	16–45	Visser
Natural rubber	8.58	Croucher and Hair
Polystyrene	7.8–9.8	Croucher and Hair ; Croucher
Silver	39.8	Bargeman and van Voorst Vader
Toluene	5.4	Croucher and Hair
Water	4.35	Bargeman and van Voorst Vader

Sources: D. Bargeman and F. van Voorst Vader, *J. Electroanal. Chem. Interfacial Electrochem.*, **37**, 45 (1972); Croucher and Hair 1977; Visser 1972; Croucher (1981).

TABLE 10.4 Potential Energy of Attraction Between Two Particles with the Indicated Geometries

Particles	Φ_A	Definitions/ Limitations
Two spheres	$-\frac{A}{6}\left[\frac{2R_1R_2}{f_1(R_1,R_2,d)} + \frac{2R_1R_2}{f_2(R_1,R_2,d)} + \ln\left(\frac{f_1(R_1,R_2,d)}{f_2(R_1,R_2,d)}\right)\right]$ $f_1(R_1,R_2,d) = d^2 + 2R_1d + 2R_2d$ $f_2(R_1,R_2,d) = d^2 + 2R_1d + 2R_2d + 4R_1R_2$	R_1,R_2 = radii; d = separation of surfaces along line of centers
Two spheres of equal radius	$-\frac{A}{6}\left[\frac{2R_s^2}{f_1(R_s,d)} + \frac{2R_s^2}{f_2(R_s,d)} + \ln\left(\frac{f_1(R_s,d)}{f_2(R_s,d)}\right)\right]$ $f_1(R_s,d) = d^2 + 4R_sd; f_2(R_s,d) = d^2 + 4R_sd + 4R_s^2$	$R_1 = R_2 = R_s$
Two spheres with equal radius	$-\frac{AR_s}{12d}$	$R_s >> d$
Two spheres of unequal radius	$-\frac{A R_1R_2}{6d(R_1 + R_2)}$	R_1 and $R_2 >> d$
Two plates of equal thickness	$-\frac{A}{12\pi}\left(\frac{1}{d^2} + \frac{1}{(d + 2\delta)^2} - \frac{2}{(d + \delta)^2}\right)$	δ = thickness of the plates; d = surface-to-surface distance
Identical blocks	$-\frac{A}{12\pi d^2}$	$\delta \to \infty$

the magnitude of the interaction energy. The expression for interacting plates of thickness δ in Table 10.4 is also seen to reduce to Equation (63) as $\delta \to \infty$.

10.7 THEORIES OF VAN DER WAALS FORCES BASED ON BULK PROPERTIES

Adding together molecular interactions to account for macroscopic attractions is undoubtedly an oversimplification. There are several things that this procedure overlooks that limit its validity. For example, even for two bodies under vacuum, those molecules nearer the surface screen the interactions of molecules buried more deeply in the material. Because of the inverse power dependence of the attraction, those molecules nearest the faces of the blocks make the predominant contribution to the interaction. If these molecules have permanent dipoles, they may experience orientation effects under the influence of the surface that are not described by the Debye and Keesom models. From a practical point of view, dipole moments and polarizabilities may not always be available for all substances of interest, as noted in Section 10.4. The possibility of surface heterogeneity confuses the choice of polarization parameters even further. Although we continue (for now) to assume a vacuum separates the bodies under consideration, the presence of an intervening medium can only aggravate all of the preceding points.

10.7a Dzyaloshinskii-Lifshitz-Pitaevskii Theory

For the above reasons a theory based entirely on measurable bulk properties rather than molecular parameters is a more powerful way of dealing with the interaction of macroscopic

bodies. Dzyaloshinskii, Lifshitz, and Pitaevskii (DLP) have developed such a macroscopic theory in a very general form from quantum field theory. Bulk dielectric properties of matter are the basis for this theory, so screening effects are built into the solution. Unfortunately, in its general form, the DLP theory is complicated and difficult to apply. An indication of this is found in the following expression for the Hamaker constant A_{213}—as it would be used in Equation (63)—for the interaction of blocks of material 2 and material 3 when the two are separated by material 1:

$$A_{213} = \frac{3}{8\pi^2} h \int_0^\infty \left[\frac{\varepsilon_2(i\xi) - \varepsilon_1(i\xi)}{\varepsilon_2(i\xi) + \varepsilon_1(i\xi)} \right] \left[\frac{\varepsilon_3(i\xi) - \varepsilon_1(i\xi)}{\varepsilon_3(i\xi) + \varepsilon_1(i\xi)} \right] d\xi \tag{64}$$

In this expression $\varepsilon(i\xi)$ is the dielectric "constant"—it is a function of frequency—along the imaginary frequency axis $i\xi$; it is measurable as the dissipative part of the spectrum of dielectric constant for any material. The latter is an experimentally determined function of frequency for each of the three components, and the complicated expression in Equation (64) is integrated over all frequencies.

Although very general, the difficulty in applying the DLP theory has limited its use and encouraged the development of various approximations and special cases. The only use we make of the DLP theory is to point out that the differences between the $\varepsilon(i\xi)$ values for the blocks and the medium appear in the numerator of Equation (64). If these dissipative components of dielectric constant matched at all frequencies for substances 1, 2, and 3, then the Hamaker constant would equal zero according to Equation (64). Although an exact match seems unlikely, this is the first indication we have had that an intervening medium might have a compensating effect on van der Waals attraction. This idea will be developed more fully in Section 10.8.

10.7b Semiclassical Approaches Based on Bulk Properties Such as Surface Tension

Because of the complexity of the DLP theory, several semiclassical treatments have been developed to simplify and extend its findings. One such extension is applicable to blocks of nonpolar materials at small separations and is of interest to us because of the possibility it offers for relating surface tension to intermolecular forces.

For now we consider the interaction of two identical blocks of material separated by their own equilibrium vapor. From the point of view of modifying the force of attraction, the vapor is assumed to have a negligible effect, behaving essentially like a vacuum. The facing planes become equilibrium surfaces characterized by an interfacial free energy γ.

Our starting point in this discussion is the resemblance between Figure 6.8a and Figure 10.6b. The former illustrates the work of cohesion and the latter the interaction between two blocks of material. Suppose we identify by d_0 the equilibrium spacing between molecules of a bulk sample of the material under consideration. Then the cohesion process represented by Figure 6.8a can be viewed as one in which two blocks of material are separated from $d = d_0$ to $d = \infty$. In terms of Equation (63),

$$\Delta\Phi = \Phi_\infty - \Phi_0 = (A/12\pi)\, d_0^{-2} \tag{65}$$

Equating this with the work of cohesion given by Equation (6.56), we obtain

$$2\gamma = (A/12\pi)\, d_0^{-2} \tag{66}$$

or

$$A = 24\pi\gamma d_0^2 \tag{67}$$

A system for which this model is apt to work best is a nonpolar material such as an alkane for which $\gamma \approx 25$ mJ m^{-2} as seen from Table 6.1. Using 0.2 nm for d_0, we calculate $A = 24\pi(0.025)(0.2 \cdot 10^{-9})^2 = 7.5 \cdot 10^{-20}$ J, which is very close to the value predicted for this quantity from molecular parameters in the last section.

The same logic that we used to obtain the Girifalco-Good-Fowkes equation in Section 6.10 suggests that the dispersion component of the surface tension γ^d may be better to use than γ itself when additional interactions besides London forces operate between the molecules. Also, it has been suggested that intermolecular spacing should be explicitly considered within the bulk phases, especially when the interaction at $d = d_0$ is evaluated. The Hamaker approach, after all, treats matter as continuous, and at small separations the graininess of matter can make a difference in the attraction. The latter has been incorporated into one model, which results in the expression

$$A = (4\pi/1.2)\gamma^d d_0^2 \tag{68}$$

where d_0 is the intermolecular spacing in the bulk material. The contention is that this is more suitable than Equation (67) for relating the Hamaker constant to surface tension for materials with interactions other than London forces. In addition to only a fraction of the full value of γ being used, the numerical coefficient in Equation (68) is only about one-seventh that in Equation (67). Both of these considerations reinforce the idea that Equation (67) gives an upper limit for A.

Equations (67) and (68) provide alternatives to Equations (34) and (62) for the evaluation of the Hamaker constant. Although the last approach uses macroscopic properties and hence avoids some of the objections cited at the beginning of the section, the practical problem of computation is not solved by substituting one set of inaccessible parameters (γ^d and d_0) for another (α and μ).

The primary objective of the present discussion is to show the intrinsic connection between surface tension and the van der Waals energy of attraction between macroscopic bodies. The connection not only provides computational options but also—and more importantly—unites two apparently separate phenomena and strengthens our confidence in the correctness of our understanding.

Table 10.5 shows a few numerical examples of how well this attempt at unification succeeds. Equations (28), (32), and (62) have been used to calculate values of the Hamaker constant from refractive index data at visible wavelengths. These values have then been used along with γ^d values from Chapter 6 to calculate d_0 values according to Equation (68). The resulting values of d_0 are seen to be physically reasonable. That such plausible values for d_0 are obtained is especially noteworthy in view of the approximations made in the calculations.

The applicability of this procedure receives a far more stringent test in the case of water and SiO_2 than for the hydrocarbons. London forces are assumed to be the only contributors to γ (i.e., $\gamma^d = \gamma$) for hydrocarbons. This is definitely not the case for quartz or water, so the d_0 values obtained for these substances are quite satisfactory.

TABLE 10.5 Calculations Intended to Show that Equations (67) and (68) Predict Values of the Hamaker Constant Compatible with Those Evaluated from Equations (28), (32), and (62)[a]

Compound	M (g mole^{-1})	ρ (g cm^{-3})	n	A(J)	γ^d (mJ m^{-2})	d_0 (nm)
Heptane	100.2	0.684	1.39	1.05×10^{-20}	20.3	0.22
Dodecane	170.3	0.749	1.42	9.49×10^{-21}	25.4	0.18
Eicosane	282.5	0.789	1.44	2.07×10^{-20}	29.0	0.26
SiO_2 (quartz)	60	2.650	1.54	4.14×10^{-20}	78.0	0.22
Polystyrene	(104)[b]	1.050	1.59	2.2×10^{-20}	41.0	0.23
Water	18	1.000	1.33	2.43×10^{-20}	21.3	0.33

[a]Equations (28), (32), and (62) are used to evaluate A, then A and γ^d values from Chapter 6 are used to evaluate d_0.
[b]Monomer.

10.7c Method Based on the Thermodynamics of Liquids

The Hamaker constants of nonpolar fluids and polymeric liquids can be obtained using an expression similar to Equation (67) in combination with the corresponding state theory of thermodynamics and an expression for interfacial energy based on statistical thermodynamics (Croucher 1981). This leads to a simple, but reasonably accurate and useful, relation for Hamaker constants for nonpolar fluids and polymeric liquids. We present in this section the basic details and an illustration of the use of the equation derived by Croucher.

An expression for the Hamaker constant analogous to Equation (67) had been proposed by Fowkes (1964) for the case when only dispersion forces determine the surface tension. The Fowkes equation

$$A = 6\pi d_0^2 \gamma \tag{69}$$

is somewhat difficult to use since the choice of d_0, the intermolecular distance, is not always clear because of the asymmetric shape of most molecules. The above equation can be rewritten as

$$A = 6a_m\gamma \tag{70}$$

where a_m is the surface area of a molecule. For spherical molecules, the area is well defined and the above equation reduces to Equation (67).

One can now substitute for the interfacial energy γ the following equation derived by Davis and Scriven (1976)

$$\gamma = (1/8)\rho^{-1/3}(\partial U/\partial V)_T \tag{71}$$

where ρ is the number density of the material and $(\partial U/\partial V)_T$ is the rate of change of the energy of the material with volume at constant temperature (i.e., the negative of internal pressure). This expression for γ can be used in combination with Equation (70) to obtain the Hamaker constant if the area a_m is known and if expressions or values for $(\partial U/\partial V)_T$ are available for any material for which the dispersion interaction determines γ. However, a simplified equation based on the above combination of equations and the corresponding state theory is possible (Croucher 1981; Croucher and Hair 1977), and one obtains

$$A = (3/4)\, k_B T[1 - (\xi\, V_r^{-1/3})]^{-1} \tag{72}$$

$$\text{with } \xi = (m/n)^{1/(n-m)} \tag{73}$$

where V_r is the reduced volume of the material and n and m are exponents of a power law potential similar to the one given in Equation (1). When $m = 6$ and $n = 12$, the intermolecular potential reduces to the Lennard-Jones potential mentioned in Section 10.3. Equation (72) is applicable to liquids (made up of simple molecules or polymers) in which dispersion forces dominate the attraction. It is not applicable to polar substances such as water or to glassy polymers.

The reduced volume V_r, which is needed for using Equation (72), can be determined from the relation

$$(\alpha T)^{-1} = -(m/3) + (n - m)[3(V_r^{(n-m)/3} - 1)]^{-1} + \xi[3(V_r^{1/3} - \xi)]^{-1} \tag{74}$$

where α is the coefficient of thermal expansion and *not* the polarizability. For the 6–∞ potential ($m = 6$, $n = \infty$), for which ξ is 1, Equation (74) becomes

$$V_r = \left(\frac{3 + 7\alpha T}{3 + 6\alpha T}\right)^3 \tag{75}$$

Equation (74) with $m = 6$ and $n = \infty$ has been tested for a range of α's by Croucher (1981) and leads to very good estimates for the Hamaker constant for a number of liquids. Moreover, the temperature dependence of the Hamaker constant is also accounted for explicitly. Example 10.4 illustrates the use of this procedure.

* * *

EXAMPLE 10.4 *Hamaker Constant of Liquid Polystyrene.* Estimate the Hamaker constant of liquid polystyrene at 298 K. The thermal expansion coefficient α for polystyrene at 298 K is approximately $5.7 \cdot 10^{-4}\ K^{-1}$. Compare your result with the experimentally obtained value of $A = 7.8 \cdot 10^{-20}$ J reported by Croucher (1981, Fig. 1).

Solution: From Equation (75), for $\alpha T = 5.7 \cdot 10^{-4} \cdot 298 \approx 0.17$, the reduced volume is given by

$$V_r = 1.132$$

One can obtain a good estimate for A using the above value of V_r and $\xi = 1$ from Equation (72). This leads to

$$A = (3/4) \cdot 1.38 \cdot 10^{-23} \cdot 298 \cdot [1 - (1/1.132)^{1/3}]^{-1}\ \text{J}$$
$$= 7.62 \cdot 10^{-20}\ \text{Joules} \quad \text{(from Croucher's equation)}$$
$$A = 7.8 \cdot 10^{-20}\ \text{Joules} \quad \text{(given experimental data)}$$

The estimate based on Croucher's equation is in excellent agreement with the reported result. ■

* * *

10.7d Direct Measurement of van der Waals Forces

It is extremely difficult to measure the Hamaker constant directly, although this has been the object of considerable research efforts. Direct evaluation, however, is complicated either by experimental difficulties or by uncertainties in the values of other variables that affect the observations. The direct measurement of van der Waals forces has been undertaken by literally measuring the force between macroscopic bodies as a function of their separation. The distances, of course, must be very small, so optical interference methods may be used to evaluate the separation. The force has been measured from the displacement of a sensitive spring (or from capacitance-type measurements).

A well-known example of this type of measurement is shown in Figure 10.7 for attractive van der Waals force between two mica surfaces. The result shown is obtained using the surface force apparatus developed originally in the early 1970s for interaction between two thin cylindrical surfaces (of radius R_c) at 90° to each other in vacuum. (This geometry mimics the interaction between two flat surfaces; see Israelachvili 1991. The surface force apparatus (see Chapter 1, Section 1.6c) has since gone through many refinements and can now be used for measuring interactions in electrolyte solutions and for tangential force measurements.)

It is evident from Figure 10.7 that the measurements are consistent with both unretarded and retarded attractive forces at appropriate separation distances. It has also been possible to verify directly the functional dependence on radii for the attraction between dissimilar spheres (see Table 10.4), to determine the retardation of van der Waals forces (see Table 10.1), and to evaluate the Hamaker constant for several solids, including quartz. Values in the range of $6 \cdot 10^{-20}$ to $7 \cdot 10^{-20}$ J have been found for quartz by this method. This is remarkably close to the value listed in Table 10.5 for SiO_2.

A more common situation than two bodies interacting across a vacuum is the case in which some medium intervenes between the interacting bodies. Before proceeding any further, then, let us examine the effect of this medium on particle interactions.

10.8 EFFECT OF THE MEDIUM ON THE VAN DER WAALS ATTRACTION

Until now we have considered the interaction between isolated molecules or macroscopic bodies when the particles are separated by a vacuum. Interactions in a vacuum is reasonable for molecules in the gas phase. However, for dispersions of one phase in another, the effect of the medium must be taken into account. Accounting for the effects of the medium leads to some useful combining relations for the Hamaker constant A_{ijk}, which is the Hamaker constant for interaction between i and k in medium j. In addition, situations may arise in which A_{ijk} is negative, that is, the interaction is repulsive. We review these in this section.

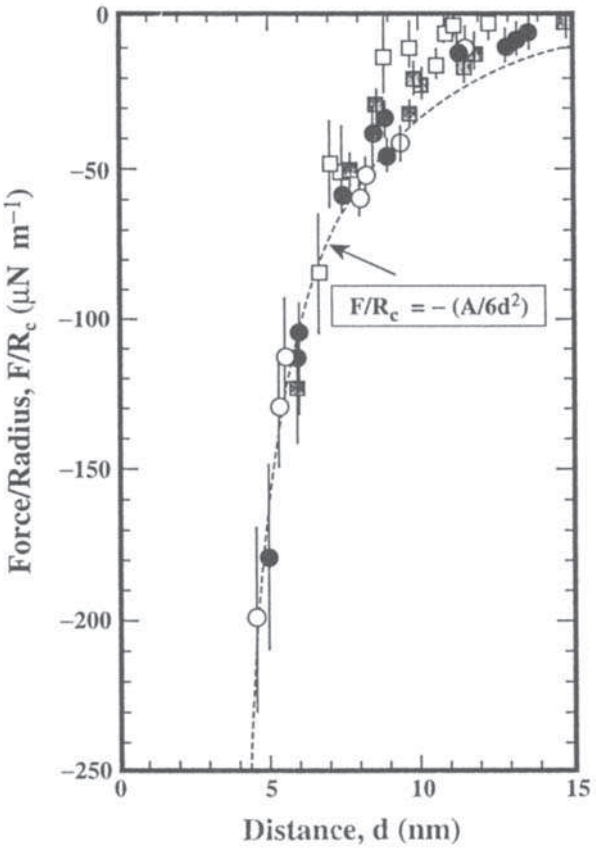


FIG. 10.7 Direct measurements of van der Waals dispersion forces. The measurements correspond to the force between two flat (mica) surfaces separated by a distance d. The line shown is the theoretical expression for unretarded van der Waals force. The figure shows that the unretarded expression describes the measurements sufficiently accurately for d about 6.5 nm or less. (Redrawn with permission of J. N. Israelachvili and G. E. Adams, *J. Chem. Soc., Faraday Trans. 1*, **78**, 975 (1978).)

10.8a Combining Relations for the Hamaker Constant

The easiest way to account for the effect of a medium is to consider the pseudochemical reaction illustrated in Figure 10.8a. The particles numbered 2 represent the dispersed phase, and those numbered 1 are the solvent. Note that both of the dispersed particles are of the same material in this reaction. In the initial condition, each dispersed particle and its satellite solvent particle comprise an independent kinetic unit. Figure 10.8a represents the process in which the two dispersed particles come together to form a doublet and the two solvent particles form a kinetically independent doublet.

The change in the potential energy that accompanies this process is given by

$$\Delta\Phi = \Phi_{11} + \Phi_{22} - 2\Phi_{12} \tag{76}$$

where the subscripts apply to the two types of particles. Each of the terms for Φ on the right-hand side of Equation (76) depends in the same way on the size and distance parameters and differs only in molecular parameters that are fully contained in the Hamaker constant. Therefore $\Delta\Phi$ follows the appropriate function for the interaction from Table 10.4 with the following value of the Hamaker constant:

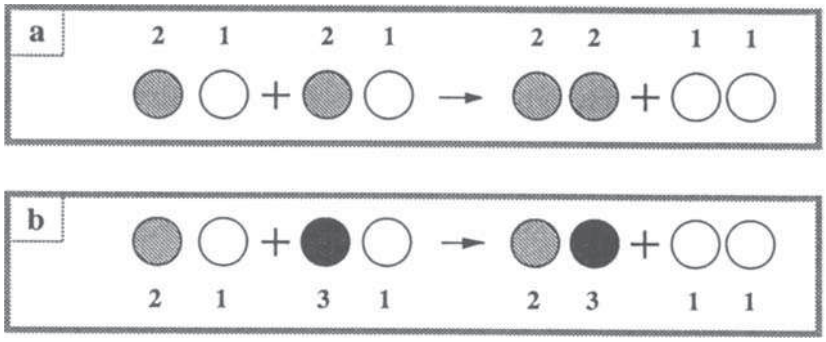


FIG. 10.8 The coagulation process as a pseudochemical reaction. The filled circles indicate particles of the dispersed phase and the open ones satellite particles of the solvent. In (a) the dispersed particles are chemically identical, and in (b) the dispersed particles are different substances.

$$A_{212} = A_{11} + A_{22} - 2A_{12} \tag{77}$$

The subscript 212 indicates two particles of type 2 separated by the medium of type 1.

An approximation that results in a useful simplification is

$$A_{12} \approx (A_{11}A_{22})^{1/2} \tag{78}$$

Equation (78) says that the interaction between dissimilar bodies is given by the geometrical mean of the homogeneous interactions for the two species considered separately. This geometrical *mixing rule* is widely used in solution theory to calculate heterogeneous interactions. We invoked this type of averaging procedure in Sections 3.4 and 6.10 when problems arose that required a 1-2 interaction to be expressed in terms of 1-1 and 2-2 interactions.

Combining Equations (77) and (78) leads to

$$A_{212} = (A_{11}^{1/2} - A_{22}^{1/2})^2 \tag{79}$$

This is the effective value of the Hamaker constant to be used in evaluating the attraction between (like) particles embedded in a medium. Equation (79) leads to three important generalizations about the value of A_{212}:

1. The effective Hamaker constant A_{212} is always positive, regardless of the relative magnitudes of A_{11} and A_{22}. Thus identical particles exert a net attraction on one another due to van der Waals forces in a medium as well as under vacuum.

2. Embedding particles in a medium generally diminishes the van der Waals attraction between them. Table 10.5 shows that the Hamaker constants for homogeneous interactions A_{ii} are generally of the same order of magnitude for different substances. Therefore the effective Hamaker constant—which depends on their difference according to Equation (79)—will be smaller than A_{ii} for either of the homogeneous interactions. For example, if A_{11} and A_{22} equal $8.1 \cdot 10^{-20}$ and $6.4 \cdot 10^{-20}$ J, then A_{212} is 10^{-21} J, almost two orders of magnitude less than the individual A_{ii} values.

3. For $A_{11} = A_{22}$, $A_{212} = 0$, and $\Phi_A = 0$, from the viewpoint of van der Waals forces, this condition corresponds to no net interaction between particles. By using experimental criteria to identify this state of affairs, it is possible to vary the medium in a disperse system until this condition is met and then use the surface tension of the medium (via Equation (67)) to evaluate A_{11} and, therefore A_{22}. Going further, Equation (67) can be applied again to estimate γ_{22} for the dispersed particles. This strategy implies that suitable values for d_0 are available.

Since van der Waals forces are responsible for the coagulation of lyophobic colloids, the mitigating influence of the continuous phase on the attraction between dispersed particles imparts a measure of stability to the system. This result was anticipated in our remarks about

the DLP theory in Section 10.7. An even more dramatic modification of van der Waals attraction results when three different substances are involved: dispersed particles of 2 and 3 separated by medium 1. Figure 10.8b shows the coagulation of the dispersed particles for this situation. By analogy with the coagulation of identical particles, we write the following:

1. For the change in potential energy,

$$\Delta\Phi = \Phi_{11} + \Phi_{23} - \Phi_{12} - \Phi_{13} \tag{80}$$

2. For the contribution of molecular properties,

$$A_{312} = A_{11} + A_{23} - A_{12} - A_{13} \tag{81}$$

3. With the A_{ij} values replaced by $(A_{ii}A_{jj})^{1/2}$

$$A_{312} = (A_{11}^{1/2}A_{11}^{1/2}) + (A_{22}^{1/2}A_{33}^{1/2}) - (A_{11}^{1/2}A_{22}^{1/2}) - (A_{11}^{1/2}A_{33}^{1/2}) \tag{82}$$

which factors to

$$A_{312} = (A_{33}^{1/2} - A_{11}^{1/2})(A_{22}^{1/2} - A_{11}^{1/2}) \tag{83}$$

10.8b Negative Hamaker Constants

What makes the result expressed in Equation (83) particularly interesting is that one of the factors in the equation can be positive and one negative, in which case the effective Hamaker constant itself becomes negative. A negative proportionality factor in an expression based on attraction makes the potential energy change positive. The pairwise attraction between bodies results in a net repulsion between dissimilar particles. Since the factors in Equation (83) must have different signs, all that is required for this condition of a negative effective Hamaker constant is that the A value for the continuous phase be intermediate between the Hamaker constants of the two types of dispersed particles: $A_{22} > A_{11} > A_{33}$ or $A_{33} > A_{11} > A_{22}$.

For each of the A terms in Equation (83) we may substitute the corresponding version of Equation (67). Strictly speaking, each material is characterized by its own intermolecular spacing, and this as well as its γ value should be used in Equation (67). In a number of systems that have been investigated, however, the observed range of d_0 values is quite narrow, suggesting that d_0 can be regarded as a constant, at least as a first approximation. For a variety of polymers a value of about 0.2 nm appears to be a reasonable estimate for d_0. With this (assumed constant) value factored out, Equation (83) becomes

$$A_{312} = 24\pi d_0^2(\gamma_3^{1/2} - \gamma_1^{1/2})(\gamma_2^{1/2} - \gamma_1^{1/2}) \tag{84}$$

With the assumed uniformity of d_0 values, Equation (84) shows that the coagulation of dissimilar particles becomes energetically unfavorable when the surface tension of the medium is intermediate between the surface tensions of the two kinds of dispersed units.

An interesting variation on this idea is the study of particle engulfment by an advancing solidification front. In such an experiment, solid particles are dispersed in an appropriate medium that is then allowed to solidify in a channel along which a suitable temperature gradient is maintained. The fate of the dispersed units is monitored microscopically as the solidification front advances. What is observed is that the dispersed particles are either engulfed by the solid or pushed along in the liquid by the advancing front. These observations can be interpreted in terms of the formalism we have developed by considering the solid and the dispersed units as interacting through a medium composed of the melt. The fact that the solid and the melt are chemically identical is immaterial since they are in different physical states.

If we designate the melt as component 1, the dispersed particles as 2, and the solid front as 3, then engulfment is equivalent to coagulation and occurs spontaneously when A_{312} is positive. In this case $\Delta\Phi$ as given by Equation (80) provides ΔG for the engulfment process and, since the Φ's themselves are negative, A_{312} must be positive for spontaneous engulfment. Conversely, rejection by the front requires a negative value for A_{312}. Again under the assump-

tion of the constancy of d_0, rejection is predicted so long as the surface tension of the melt is intermediate between the values of the solid and the dispersed particles. Example 10.5 considers an illustration of this kind of data.

* * *

EXAMPLE 10.5 *Particle Engulfment by An Advancing Solidification Front.* Experiments were conducted at 80°C in which the solidification front of naphthalene was observed to either engulf or reject dispersed particles of several solids. Table 10.6 lists the observed engulfment (E) or rejection (R) behavior for various systems as well as the surface tensions of the various substances. The surface tensions of solid and liquid naphthalene at 80°C are 26.4 and 32.8 mJ m^{-2}, respectively. Is the surface tension criterion cited above consistent with these observations? How might any inconsistencies be explained? Evaluate the product $(\gamma_3^{1/2} - \gamma_1^{1/2})(\gamma_2^{1/2} - \gamma_1^{1/2})$ for these systems.

Solution: The surface tension of liquid naphthalene (1) is greater than that of solid naphthalene (3). Therefore A_{312} is expected to be negative for all systems having γ values greater than γ_1. This is the case for the first six compounds listed in Table 10.6. Therefore these substances are expected to display rejection by the solidification front. This is indeed observed for five of the six cases. The case of nylon-6,12, which deviates from the predicted behavior, is best understood by examining the product $(\gamma_3^{1/2} - \gamma_1^{1/2})(\gamma_2^{1/2} - \gamma_1^{1/2})$. Values of this product for the various systems considered are listed in Table 10.6. The factor arising from the solid-liquid (3-1) naphthalene has the constant value -0.0186 for all cases, but differs when various solids are used as component 2. For nylon-6,12, the second factor becomes -0.0022, and the product of the two, $0.41 \cdot 10^{-4}$ mJ m^{-2}, is the smallest of all such products listed in the table. As the surface tension difference decreases, the sensitivity of the behavior to variations in d_0 increases. ■

* * *

It is apparent that a single dispersed phase could be investigated with an assortment of matrix materials having known properties. The engulfment-rejection behavior of these systems may then be used to establish bracketing values of γ and A for the dispersed phase.

Repulsive van der Waals forces occur in a number of practically important cases, such as for different types of polymers in organic solvents (van Oss et al. 1980) and for certain hydrocarbon films on water (as mentioned in Vignette X). For example, the use of repulsive van der Waals forces has been suggested as a way to dissociate antigen-antibody complexes by van Oss et al. (1979). A much more detailed and quantitative introduction to repulsive van der Waals forces may be found in Israelachvili (1991).

Although we have not stopped dealing with van der Waals attraction, we have come a long

TABLE 10.6 Results of Engulfment Experiments Involving Various Solids Dispersed in Naphthalene[a]

Dispersed particles	Observed behavior[b]	γ (mJ m^{-2})	$(\gamma_3^{1/2} - \gamma_1^{1/2})(\gamma_2^{1/2} - \gamma_1^{1/2}) \times 10^4$ (mJ m^{-2})
Acetal	R	41.9	−4.39
Nylon-6	R	41.7	−4.30
Nylon-6,6	R	40.8	−3.89
Nylon-12	R	38.4	−2.77
Nylon-6,10	R	36.0	−1.60
Nylon-6,12	R	32.0	+0.41
Polystyrene	E	27.6	+2.79
Teflon	E	15.5	+10.53
Siliconed glass	E	11.5	+13.75

Source: Data of A. W. Neumann, S. N. Omenyi, and C. J. van Oss, *Colloid Polym. Sci.*, **257**, 413 (1979).

[a]Data discussed in Example 10.5.

[b]E, engulfment; R, rejection.

way from our initial point of view. Without any help from a repulsive mode of interaction, we are able to account for situations in which the dispersed state of a system is energetically favored over the coagulated state. The dispersion medium clearly plays an important role in this, since the process involves breaking "bonds" between the dispersed particles and the medium and replacing them with new "bonds." Just as in a metathesis reaction between chemical compounds, it is the difference in the "bond strength" between the final and initial states that determines the net interaction. If the attraction between molecules can thus override itself, this may be helped along by other mechanisms based on actual repulsion between approaching surfaces. In Chapter 11 we consider the overlap of ion atmospheres as the basis for such a repulsion.

REVIEW QUESTIONS

1. What are the three *van der Waals forces*, and what is the molecular origin of each of them?
2. Which of these is usually the most dominant?
3. Why is the *London force* also referred to as the *dispersion force*?
4. It is claimed that the dispersion component of the van der Waals forces is always present regardless of the nature of the molecules. Why?
5. List at least three macroscopic material properties that result from, or are strongly influenced by, van der Waals forces, and explain the reasons physically.
6. When would you expect the dispersion force to be *repulsive*? Why?
7. What is the *Hamaker "constant"*? How is it related to molecular-level van der Waals forces?
8. List some reasons why it is desirable to relate Hamaker constants to measurable *macroscopic properties* instead of relying entirely on molecular parameters.
9. List a few methods that could be used to determine Hamaker constants of materials from relevant macroscopic properties.
10. Explain how Hamaker constants for interaction between identical materials in vacuum can be used to determine Hamaker constants for interaction between dissimilar materials immersed in an arbitrary medium.
11. Describe the conditions under which the Hamaker constant between two interacting colloidal particles is always positive. When can it be negative?
12. List a few macroscopic phenomena that can be traced to van der Waals forces.
13. What is the connection between surface energy of a material and the Hamaker constant of that material?

REFERENCES

General References (with Annotations)

Atkins, P. W., *Physical Chemistry*, 5th ed., W. H. Freeman, New York, 1994. (Undergraduate level. A good textbook on basic physical chemistry and a convenient reference on concepts such as dipole interactions, polarizability of materials and van der Waals equation of state.)

Gregory, J., *Adv. Colloid Interface Sci.*, **2**, 396 (1969). (A review article on van der Waals forces with tables of Hamaker constants for a number of materials.)

Israelachvili, J. N., *Intermolecular and Surface Forces*, 2d ed., Academic Press, New York, 1991. (Graduate and undergraduate levels. An excellent source for the relation between molecular-level van der Waals interactions and macroscopic properties and phenomena such as surface tension, cohesive energies of materials, adhesion, and wetting. Also discusses direct measurement of van der Waals forces using the surface force apparatus.)

Lyklema, J., *Fundamentals of Interface and Colloid Science: Volume I. Fundamentals*, Academic Press, London, 1991. (A graduate-level treatment of the topics discussed in this chapter.)

Mahanty, J., and Ninham, B. W., *Dispersion Forces*, Academic Press, New York, 1976. (An advanced monograph on dispersion forces. Discusses topics such as London and Lifshitz theories.)

Ross, S., and Morrison, I. D., *Colloidal Systems and Interfaces*, Wiley, New York, 1988. (Undergraduate level. A textbook on colloids with Hamaker constant data for more materials than given in this chapter.)

Verwey, E. J. W., and Overbeek, J. Th. G., *Theory of the Stability of Lyophobic Colloids*,

Elsevier, Amsterdam, Netherlands, 1948. (Graduate and undergraduate levels. The classic reference on colloid stability.)
Visser, J., *Adv. Colloid Interface Sci.*, **3**, 331 (1972). (A review article on van der Waals forces with tables of Hamaker constants for a number of materials.)

Other References

Croucher, M. D., *Colloid and Polymer Sci.*, **259**, 462 (1981).
Croucher, M. D., and Hair, M. L., *J. Phys. Chem.*, **81**, 1631 (1977).
Davis, H. T., and Scriven, L. E., *J. Phys. Chem.*, **80**, 2805 (1976).
Fowkes, F. M., *Ind. Eng. Chem.*, **56**, 40 (1964).
Israelachvili, J. N., and Tabor, D., Van der Waals Forces: Theory and Experiment. In *Progress in Surface and Membrane Science*, Vol. 7 (J. F. Danielli, M. D. Rosenberg, and D. A. Cadenhead, Eds.), Academic Press, New York, 1973.
Moelwyn-Hughes, E. A., *Physical Chemistry*, 2d ed., Macmillan, New York, 1964.
Sonntag, H., and Strenge, K., *Coagulation and Stability of Disperse Systems*, Halsted, New York, 1964.
Van der Waals, J. D., *On the Continuity of the Gaseous and Liquid States*, North-Holland, Amsterdam, Netherlands, 1988.
Van Oss, C. J., Absolom, D. R., Grossberg, A. L., and Neumann, A. W., *Immunological Communications*, **8**, 11 (1979).
Van Oss, C. J., Absolom, D. R., and Neumann, A. W., *Colloids and Surfaces*, **1**, 45 (1980).

PROBLEMS

1. The parameter β_{12} for heterogeneous (12) interactions plays a similar role as β_{11} (Equation (34)) does for homogeneous (11) interactions. Use entries from Table 10.1 to write an expression for β_{12}. If Debye interaction makes a negligible contribution to β_{12} and $\nu_1\nu_2/(\nu_1 + \nu_2) \simeq \frac{1}{2}(\nu_1\nu_2)^{1/2}$, show that

$$\beta_{12} = (f_{11L}\beta_{11})^{1/2}(f_{22L}\beta_{22})^{1/2} + (f_{11K}\beta_{11})^{1/2}(f_{22K}\beta_{22})^{1/2}$$

where the f terms are defined by Equation (35). If $f_{11L} = f_{22L}$ and $f_{11K} = f_{22K}$, show that this last result becomes

$$\beta_{12} \simeq (\beta_{11}\beta_{22})^{1/2}$$

Comment on the relevancy of this result to Equation (78). Criticize or defend the following proposition: The geometrical mixing rule does not require the absence of permanent dipoles, only that 11 and 22 interactions both consist of the same fraction of London and permanent dipole contributions. Specific interactions, such as hydrogen bonding, must also be absent in the 11, 22, and 12 systems.

2. Pressure is a manifestation of the kinetic energy of gas molecules. According to the van der Waals equation of state (see Eq. (36)), the pressure of 1 mole of gas must be increased by an amount a/v^2 due to intermolecular attractions that decrease the pressure from what it would be if ideal. Use the term a/v^2 as a general expression for the attraction between a pair of molecules and, based on this, reconstruct the argument leading to Equation (52).

3. A gas adsorption isotherm may be derived by comparing the adsorbed layer around a solid particle to a planetary atmosphere, with an equilibrium pressure p_0 at the surface. The change in free energy for a molecule going from the bulk pressure p to the surface is $k_BT \ln (p_0/p)$. Equating this with Equation (59), the potential energy of attraction responsible for the adsorption, gives

$$k_BT \ln\left(\frac{p_0}{p}\right) = \frac{\rho N_A}{M}\frac{\beta\pi}{6} z^{-3}$$

Since $z \propto V$, this may be written $\ln (p_0/p) = \text{const.}\ V^{-3}$, where V is the volume of gas adsorbed. A more general form of this isotherm, called the *Frenkel-Halsey-Hill (FHH) isotherm*, treats the power dependence of V as an unknown n and writes

$$\left(\frac{V}{V_m}\right)^n = \frac{K}{\ln (p_0/p)}$$

where V_m is the volume of gas at monolayer average.

Prepare a plot of the FHH isotherm using $n = 3$ and $K = 0.1$ and comment on the resemblance of this isotherm to actual gas adsorption isotherms as shown in Chapter 9.

4. The derivation of Equation (68) follows the same argument that leads to Equation (61), except that the blocks are assumed to be composed of stacks of matter of density ρ' in slices having a thickness δ and separated by a distance d. A molecule at O interacts with the ith slice in such a stack with an energy that is the analog of Equation (56):

$$-d\Phi_i = \frac{\rho' N_A \beta \delta}{M} \frac{2\pi y dy}{\{[z + i(d + \delta)]^2 + y\}^3}$$

Evaluate the attraction between the molecule and the ith layer by integrating this expression over all values of y between 0 and ∞. The assumption that $\rho'\delta = \rho(d + \delta)$ ensures that the blocks have the correct macroscopic density. If the separation between layers is the same as the separation of the surfaces of the blocks (i.e., $z = d$), then the equivalent of Equation (59) results from summing the Φ_i values for all i's between 0 and ∞ and taking the limit of $\delta \to 0$. Derive the analog of Equation (59) for matter with this hypothetical structure. Note that $\Sigma_i(1 + i)^{-4} = 1.082$. Equation (68) is obtained by assuming a similar structure for the second block and continuing along these lines.

5. Consider a body of water and a piece of styrofoam. Both are attracted by the earth because of gravity. However, when immersed in water, the styrofoam is effectively repelled by the earth due to the Archimedes principle. Use this analogy to explain the possibility of repulsive van der Waals forces between materials that, taken pairwise, experience only attractive forces.

6. Neumann et al.* have tabulated average values of experimentally determined Hamaker constants and then used surface tension data for the same systems to calculate d_0 values for the following materials:

Substance	$A_{22} \times 10^{20}$ (J)	γ (mJ m^{-2})
Polystyrene	8.47	33.0
Teflon	5.23	20.0
Nylon-6,6	12.05	46.0
Poly(methyl methacrylate)	8.83	39.0
n-Decane	5.13	23.9
Polyethylene	8.43	31.0
Poly(vinyl alcohol)	8.84	41.0
Poly(hexafluoropropylene)	5.20	17.0

Verify that the d_0 values thus calculated show a relatively narrow distribution around a mean value close to 0.2 nm. Criticize or defend the following proposition: As a mean center-to-center intermolecular spacing, this value is on the low side; as a back-calculated parameter, however, it probably compensates for deviations from the assumed geometry, breakdown of Equation (33) at short distances, or other shortcomings of the molecular additivity principle.

7. An extreme in sediment volume was used† as a criterion for the effective cancellation of interparticle attraction by the continuous phase. Nylon-6,6 dispersions consisting of 1.0 g of solid in 10 ml of *n*-propanol-thiodiethanol mixtures of various compositions were allowed to settle to sedimentation equilibrium. Listed here are the equilibrium sediment volumes, the volume/volume compositions, and the surface tensions of the media:

	n-Propanol-thiodiethanol (vol/vol)									
	20/20	60/40	45/55	35/65	25/75	20/80	15/85	10/90	7.5/92.5	5/95
V_{sed} (cm^3)	2.15	2.40	2.40	2.50	2.60	2.60	2.70	2.48	2.40	2.35
γ (mJ m^{-2})	26.20	28.70	30.90	33.60	36.20	38.20	39.60	40.70	44.00	47.10

*Neumann, A. W., Omenyi, S. N., and Van Oss, C. J., *Colloid Polym. Sci.*, **257**, 413 (1979).
†Neumann, A. W., Visser, J., Smith, R. P., Omenyi, S. N., Francis, D. W., Spelt, J. K., Vargha-Butler, E. B., Zingg, W., Van Oss, C. J., and Absolom, D. R., *Powder Technol.*, **37**, 229 (1984).

Plot the sediment volume versus the surface tension of the continuous phase for these dispersions. What is the apparent surface tension of the nylon-6,6? Briefly describe some precautions that must be observed in interpreting results such as these in terms of γ values for the dispersed solid.

8. African green monkey kidney cells (component 2) were cultured on suspensions of collagen-coated dextran particles (component 3). Harvesting such cells is traditionally accomplished by scraping, ultrasonication, or the use of chelating agents to disrupt cation bridging between surfaces 2 and 3. Van Oss et al.* reasoned that the cells might be eluted by lowering the surface tension of the suspending medium (component 1). What is the basis for this expectation? Dimethyl sulfoxide (DMSO) was incrementally added to cell-carrier particle dispersions in buffered aqueous solution. The surface tension of the eluting liquids and the percent yield of the harvested cells are tabulated:

Vol % DMSO	0.0	7.5	10.0	12.5	15.0	17.0	18.0	19.0
γ (mJ m^{-2})	73.0	67.0	65.0	63.6	62.1	61.2	60.7	60.3
Percent yield	8.4	15.1	16.5	35.6	42.3	59.3	66.7	80.1

For the solids γ_2 and γ_3 have been estimated to be 68.9 and 32 mJ m^{-2}, respectively. Is the observed behavior qualitatively consistent with expectations? Suggest some factors that might be responsible for any quantitative discrepancy.

*Van Oss, C. J., Charney, C. K., Absolom, D. R., and Flanagan, T. J., *BioTechniques,* 194 (Nov.–Dec. 1983).

11

The Electrical Double Layer and Double-Layer Interactions

Suppose that I had the power of passing through . . . things, so that I could penetrate my subjects, one after another, even to the number of a billion, verifying the size and distance of each by the sense of feeling.

From Abbott's *Flatland*

11.1 INTRODUCTION

11.1a What Is an Electrical Double Layer?

When ions are present in a system that contains an interface, there will be a variation in the ion density near that interface that is described by a profile like that shown in Figure 7.13. The boundary we identify as *the* surface defines the surface excess charge, as explained in Chapter 7. Suppose that it was possible to separate the two bulk phases at this boundary in the manner shown in Figure 6.8. Then, each of the separated phases would carry an equal and opposite charge. These two charged portions of the interfacial region are called the *electrical double layer*.

The purpose of this chapter is to introduce the basic ideas concerning electrical double layers and to develop equations for the distribution of charges and potentials in the double layers. We also develop expressions for the potential energies and forces that result from the overlap of double layers of different surfaces and the implication of these to colloid stability.

11.1b Why Are Electrostatic Effects Important?

Electrostatic and electrical double-layer forces play a very important role in a number of contexts in science and engineering. As we see in Chapter 13, the stability of a wide variety of colloids, ranging from food colloids, pharmaceutical dispersions, and paints, to colloidal contaminants in wastewater, is affected by surface charges on the particles. The filtration efficiency of submicron particles can be diminished considerably by electrical double-layer forces. As we point out in Chapter 13, coagulants are added to neutralize the electrostatic effects, to promote aggregation, and to enhance the ease of separation.

The electrostatic forces also play an important role in the conformation and structure of macromolecules such as polymers, polyelectrolytes, and proteins. The self-assembly of proteins from disks to virus is triggered by electrostatic interactions between neighboring subunits. In the case of polyelectrolytes (polymer molecules with charges) and charged colloids, transport behavior such as rheology is also affected significantly by charge effects, as we have already seen in Chapter 4.

Electrostatic and electrical double-layer interactions also create new opportunities in science and technology. We have already seen an example of this in a vignette in Chapter 1 on electrophoretic imaging devices, and another, on electrophotography, is described in the next

chapter. The very basis of electrokinetic phenomena and their implications and uses arise from electrical double-layer interactions.

As an additional example, Vignette XI draws attention to the role of electrostatic effects in molecular recognition and specificity in the biosciences.

VIGNETTE XI LIFE SCIENCES, BIOTECHNOLOGY, AND BIOMEDICAL ENGINEERING: Molecular Recognition and Specificity

Molecular recognition and specificity are the stuff of life. How are biological macromolecules able to recognize each other or recognize a membrane or a substrate and form specific associations? What do we need to know about the interplay between charged surface groups on interacting macromolecules such as proteins to design better drugs or to understand and modify enzyme catalysis? What determines the encounter between an influenza virus and its host site (a sialic acid residue) on a cell before the virus binds and enters the cell (by what is known as *endocytosis*)? These are the types of questions with answers that are central to the functioning of biological systems, design of drugs, development of artificial biomaterials, design of specific chromatographic techniques, and the like.

Although the answers to questions such as these depend on a complex array of factors ranging from the structure of the relevant molecules to their environment and the chemical activity of the medium containing the molecules, intermolecular (guest-host) interactions play a central role in determining the rate and the efficiency of the ultimate result. A major component of the many possible intermolecular forces is the electrostatic interaction, particularly because of the long-range nature of the Coulombic forces and the inevitable influence of the ionic atmospheres that surround the macromolecules and substrates.

The electrostatic interaction works in tandem with the diffusional (translational as well as rotational) motion of the macromolecules as the macromolecules find their way to their destination for that crucial first encounter. Moreover, the eventual mutual recognition of the guest and the host and the stability of the resulting binding depend on the changes in the free energy due to the encounter, contact, and binding. Such free energy changes can be sensitive to the details of the electrical double-layer contribution, and it is necessary to understand the electrostatic interactions between a target (i.e., a host such as a cell surface or an ion-exchange resin) and a guest (say, a protein) as a function of the ionic strength, separation distance, orientation, and details of the structure of the materials involved (e.g., both the guest and the host may have a mosaic of charged patches; see Figure 11.1). In many cases, a rather involved analysis of diffusional encounters (Brownian motion) in an ionic environment described by the nonlinear Poisson-Boltzmann equation may be necessary.

The purpose of the present chapter is to introduce some of the basic concepts essential for understanding electrostatic and electrical double-layer pheneomena that are important in problems such as the protein/ion-exchange surface pictured above. The scope of the chapter is of course considerably limited, and we restrict it to concepts such as the nature of surface charges in simple systems, the structure of the resulting electrical double layer, the derivation of the Poisson-Boltzmann equation for electrostatic potential distribution in the double layer and some of its approximate solutions, and the electrostatic interaction forces for simple geometric situations. Nonetheless, these concepts lay the foundation on which the edifice needed for more complicated problems is built.

11.1c Focus of This Chapter

This chapter focuses on some of the basic theories of electrical double layers near charged surfaces and develops the expressions for interaction energies when two electrical double layers overlap ("interact") with each other.

1. The first topic we discuss is the origin of the charge at certain surfaces through ion

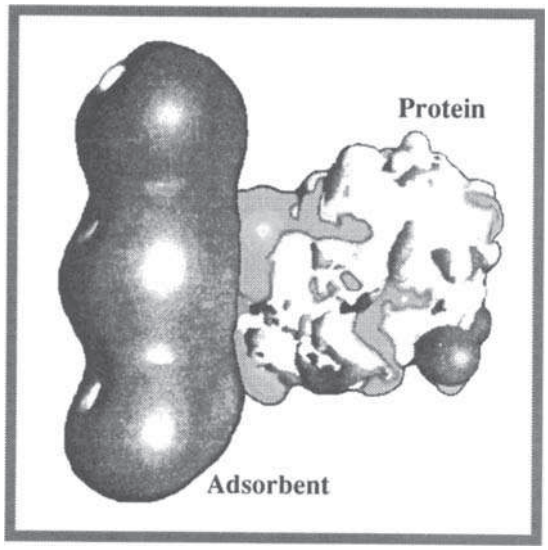


FIG. 11.1 Rat cytochrome b5 (a protein) in the apparent preferred chromatographic contact orientation with a simulated anion-exchange surface. Electrostatic equipotential surfaces are displayed for the protein and the ion-exchange surface according to the following scheme. The molecular surfaces of the protein and the resin are in an off-white color. The equipotential surfaces (on the protein as well as on the adsorbent) at a value of $+0.3\ k_BT/e$ ($+7.7$ mV) are represented by the dark regions. The equipotential surface on the protein at $-1.2\ k_BT/e$ (-30.8 mV) is in gray. (Reproduced with permission from D. J. Roush, D. S. Gill, and R. C. Willson, *Biophys. J.*, **66**, 1 (1994).)

adsorption (Section 11.2). A straightforward application of thermodynamics enables us to quantify this effect in terms of an electrical potential associated with the adsorbed ions.

2. After these phenomenological considerations, we turn our attention to various models for the distribution of charge near the surface, starting from the "capacitor model" in Section 11.3 and progressively refining it to more realistic approximations such as the Debye-Hückel model and Gouy-Chapman model (Sections 11.4–11.6). Although we examine several different models under several limiting conditions, most of the theoretical developments of this chapter will involve the following assumptions: (a) planar surfaces, (b) isolated surfaces, and (c) constant potential surfaces, examined specifically for (d) the variation of the potential with distance from the surface and (e) the effect of added electrolyte on the potential. However, expressions for spherical and cylindrical surfaces and for constant surface charge densities (rather than for constant surface potentials) are also summarized for some important cases.

3. To apply these ideas to coagulation phenomena, we must consider what happens to these distributions of potential when two similar surfaces approach one another (Section 11.7). To study coagulation phenomena, we need to compare the electrostatic effects of particle approach with the van der Waals effects discussed in the last chapter. This is done in terms of potential energy curves as discussed in Section 10.2. As we move through the chapter, our interest shifts from potential (volts) to potential energy (joules). It is important to keep track of the difference between the two as the development progresses.

4. Finally, a brief overview of the structure of the inner edge of the double layer (the so-called *Stern layer*), which accounts for the preferential adsorption of ions and the finite size of the ions, is presented in Section 11.8, along with a discussion of how the developments in previous sections can be modified to accommodate the variation in the surface potential because of the Stern layer.

11.2 SURFACE CHARGES AND ELECTRICAL DOUBLE LAYER: BACKGROUND

At the outset, we need to understand how a surface exposed to a liquid may acquire charges. This turns out to be important subsequently when we discuss the repulsive forces that appear as two charged surfaces approach each other. How the surface charge equilibrium (between the ions on the surface and those in solution) is established and how rapidly this is accomplished affect the magnitude of the forces. In addition, we also need to establish some basic concepts concerning the origin and the qualitative structure of the ionic atmosphere that develops in the vicinity of a charged surface exposed to a solution containing ions. This is our focus in this section.

11.2a Origin of Charges at a Surface

A surface immersed in a liquid can acquire charges in a number of ways. For example:

1. One of the common "charging" mechanisms is the preferential adsorption of an ion from a solution on an initially uncharged surface. An example of this mechanism is the binding of a Ca^{2+} ion on a zwitterionic (which implies that the surface group consists of surface dipoles but no net charge) head group of a lipid layer.
2. Another possible mechanism is the ionization or dissociation of a surface group (e.g., dissociation of a proton from a carboxylic group, namely, $-COOH \rightarrow -COO^- + H^+$, which leaves the surface with a negative charge).

The first of these is often the most common. Adsorption of Ag^+ and I^- on silver iodide particles is an example of this mechanism and is discussed in detail in the following section. Adsorption of H^+ and OH^- on insoluble oxides and adsorption of surfactants on mineral particles and air-water interfaces also fall under this category. Dissociation of surface groups is a common charging mechanism in the case of latex particles, which are frequently used in biomedical applications, as calibration standards in electron microscopy and as model particles in experiments on colloidal phenomena. In the case of clay minerals, one often encounters isomorphic substitution of ions (e.g., replacement of Si^{4+} ions in the crystalline mineral with other cations such as Al^{3+}, or replacement of Al^{3+} with Mg^{2+}). Accumulation of electrons is the main charge-inducing mechanism in the case of metal-solution interfaces. Table 11.1 presents a summary of these general charging mechanisms.

TABLE 11.1 Examples of Charging Mechanisms that Lead to Charges at an Interface[a]

	Nature of the interface	
	Air-Water Mercury-Water Oil-Water	Solid-Water
Preferential adsorption of ions	+	+
Dissociation of surface groups	−	+
Isomorphic substitution	−	+
Adsorption of polyelectrolytes	+	+
Accumulation of electrons	+	+

Source: J. Lyklema, Fundamentals of Electrical Double Layers in Colloidal Systems. In *Colloidal Dispersions* (J. Goodwin, Ed.), Royal Society of Chemistry, London, 1982, pp. 47–70.

[a]The signs in the table indicate the sign of the acquired charges.

In the following section we use the well-known and rather extensively studied silver iodide surface as a vehicle for introducing the basic concepts and terminology of charged surfaces and the nature of the ionic atmosphere that develops in the vicinity of such surfaces.

11.2b Reversible Electrodes: The Silver Iodide Electrode

To arrive at an understanding of the distribution of charge and potential near an interface, it is helpful to consider an electrode. A reversible electrode is one in which each of the phases contains a common ion that is free to cross the interface. The system Ag-AgI-aqueous solution is an example of a reversible electrode. A polarizable electrode, on the other hand, is impermeable to charge carriers, although charge may be brought to the surface by the application of an external potential. The system metallic Hg-aqueous solution is an example of a polarizable electrode; we discussed the relationship among the applied potential, the interfacial tension, and the adsorption of ions in Chapter 7, Section 7.11.

It is also convenient to divide ions into two categories: *potential determining* and *indifferent* ions. The terminology here is self-explanatory. For example, we can say that Ag^+ is potential determining for the Ag-Ag^+ electrode and that $NaNO_3$ is an indifferent electrolyte as far as this potential is concerned. This obviously neglects any effects of $NaNO_3$ on the activity of the Ag^+. Such an approximation increases in accuracy as the concentration of electrolyte decreases. We consistently neglect activity corrections in this chapter.

The solubility product constant for AgI is about $7.5 \cdot 10^{-17}$ at 25°C. This means that the equilibrium concentration of Ag^+ and I^- in a saturated solution of AgI in pure water equals about $8.7 \cdot 10^{-9}$ mole liter^{-1}. Electrokinetic experiments (Chapter 12) on AgI particles under these conditions reveal that the particles carry a negative charge in this case. Common ion sources such as $AgNO_3$ or KI may be added to the solution to vary the proportions of the Ag^+ and I^- ions in solution, subject to the condition that the ion product equals K_{sp}. When this is done, it is found that the AgI particles reverse charge at an Ag^+ concentration of about $3.0 \cdot 10^{-6}$ mole liter^{-1}. When the concentration of Ag^+ is greater than this, the particles are positively charged. For Ag^+ concentrations less than $3.0 \cdot 10^{-6}$ M, they are negatively charged.

One way of understanding these results is to consider the Ag^+ and I^- ions competing for adsorption sites on the surface. The tendency of both kinds of ions to adsorb at the AgI interface is not hard to understand. After all, the solid crystals would continue to grow if more ions were present. At the point of zero charge the two kinds of ions are adsorbed equally (in stoichiometric proportion). Negatively charged particles imply the adsorption of excess I^- ions, whereas positively charged particles imply excess Ag^+ adsorption. Since the zero point of charge and the saturation concentration in pure water do not coincide, we infer that the I^- ions have a greater affinity with the surface.

The Nernst equation provides us with a relationship that permits an electrical potential difference to be associated with a concentration difference. We adopt the convention that the potential at the AgI-solution interface is zero at the *zero point* (zp) of charge, a point at which the ion molarities will be symbolized c_{zp}. Our interest is to express the potential at the interface ψ_0 in terms of the concentration of ions in solution for conditions other than the zero point of charge. The Nernst equation gives

$$\psi_0 = (k_B T/e) \ln (c/c_{zp}) = (2.303\, RT/\mathcal{F}) \log (c/c_{zp}) \tag{1}$$

where $\mathcal{F}$ is the Faraday constant. We are accustomed to using the second form of Equation (1) in physical and analytical chemistry. The quantity $(2.303\, RT/\mathcal{F})$ has the familiar numerical value 0.05917 V at 25°C. Multiplying this by 10^3 and dividing by 2.303 gives 25.7 mV as the value of $(k_B T/e)$. We verify this result shortly, but this is a convenient way to relate a familiar numerical constant to the units most often used in surface and colloid chemistry.

Suppose we apply Equation (1) to AgI in "pure water" (i.e., no common ion source present). We use $c_{Ag} = 8.7 \cdot 10^{-9}$ and $c_{Ag,zp} = 3.0 \cdot 10^{-6}$ to calculate

$$\psi_0 = 25.7 \ln (8.7 \cdot 10^{-9}/3.0 \cdot 10^{-6}) = -150 \text{ mV} \tag{2}$$

Identical results would be obtained if the calculation had been based on I^- concentrations rather than Ag^+. As noted, the surface is negatively charged at this concentration since I^- is preferentially adsorbed.

In principle, part of the potential of any cell may be attributed to each interface; that is, if ψ_i is the potential drop associated with the ith interface, we can write for the total potential difference ψ_T

$$\psi_T = \psi_1 + \psi_2 + \ldots + \psi_i \tag{3}$$

Any electrochemical cell containing an Ag-AgI electrode automatically includes the AgI-solution interface and the potential associated with it. Generally speaking, we are not able to assign absolute numerical values to the various contributions in Equation (3). We can, however, design cells such that only one of the interfaces is sensitive to a particular ion. Clearly, Ag^+ and I^- are the potential-determining ions at the AgI-solution interface. If none of the other interfaces in the cell are appreciably affected by changes in the concentrations of these ions, then variations in the experimental cell potential ψ_T measure changes in ψ_0. This may be expressed

$$d\psi_T = d\psi_0 = (k_B T/e)(dc/c) \tag{4}$$

where c is the concentration of the potential-determining ion. This result is important because it shows how *changes* in ψ_0 can be measured even if ψ_0 itself is unknown. That is, to integrate Equation (4) back to an absolute value of ψ_0, an integration constant must be evaluated. According to our convention, this involves knowing the zero point of charge ($\psi_0 = 0$ at $c = c_{zp}$).

Although we have approached the potential ψ_0 from the perspective of electrodes, the discussion makes it clear that the potential given by Equation (1) applies to any AgI-aqueous solution interface, and not just to electrode surfaces. We may not always know the concentrations required to use Equation (1) numerically, but so long as the bulk concentration of potential-determining ions differs from c_{zp}, a potential difference exists at the surface. The ions of water itself are potential determining for many surfaces. These as well as added solutes or ions in equilibrium with the solid mean that surface potentials at (especially, but not exclusively) aqueous interfaces are the norm rather than something exceptional.

The potential at an interface can be related through the abundant relationships of thermodynamics to the concentration and adsorbability of ions, but thermodynamics provides no information as to how the potential varies as we move through a small distance perpendicular to the surface. This observation reminds us of Figure 7.13, in which the profile of the variation in some general property in the immediate vicinity of a surface is shown. Figure 11.2a is essentially the same drawing with the property under discussion specified as the potential.

The question we consider in the next few sections is this: How does the potential vary with distance across an interface? This question cannot be answered by thermodynamics alone, but it can be examined in terms of various models. We consider a succession of models for a planar surface between two phases. The models will become progressively more complex—and therefore realistic—as we proceed. As far as this presentation is concerned, models are proposed and modified in an intuitive way, rather than by critique of each in terms of experimental results.

11.3 THE CAPACITOR MODEL OF THE DOUBLE LAYER

Figure 11.2a shows schematically the situation in which the potential equals ψ_α at a position x_1, a small distance into the α phase, and equals ψ_β at x_2, a small distance into the β phase. One of our major goals in this chapter is to study the details of the potential variation between x_1 and x_2.

A vastly oversimplified model of how this potential variation might occur on a molecular scale (remember that the distance between x_1 and x_2 is of the order of molecular dimensions) is shown in Figure 11.2b. In this representation two smeared-out planes of charge are situated at

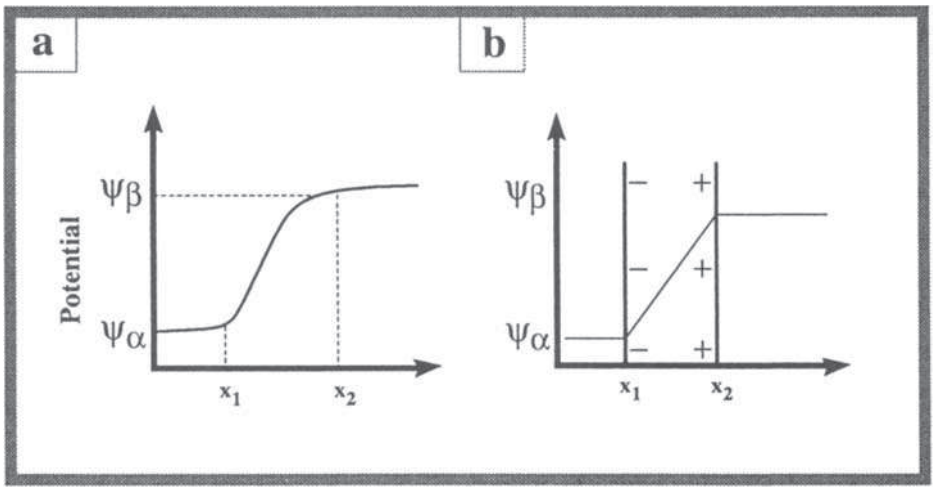


FIG. 11.2 The variation of electrochemical potential in the vicinity of the interface between two phases, α and β: (a) according to a schematic profile; and (b) according to the parallel plate capacitor model.

x_1 and x_2. Note that the model shown in Figure 11.2b resembles a parallel plate capacitor in which two charged conducting surfaces separated by a dielectric occur with a potential difference $\Delta\psi$ between them. Although this is certainly not a realistic picture of the actual distribution of charge at a solution interface, Figure 11.2b allows us to visualize a double layer of charge at an interface. Elsewhere in this book we have referred to the counterion atmosphere that adjoins a charged surface. Figure 11.2b represents this situation, and one of the layers may be regarded as a crude model of this ion atmosphere. This is the origin of the term *electrical double layer*, which is generally used to describe this physical situation, and we use this terminology from now on in preference to ion atmosphere.

Our interest in this chapter and in Chapter 12 is centered primarily on the part of the double layer that extends into the aqueous solution, which is the continuous phase in many important systems. There may be some interfaces between water and a second phase in which the charge on the nonaqueous phase is essentially concentrated on the surface plane. The rigid alignment of a second layer of counterions in the aqueous solution is implausible, however, because of thermal agitation, which tends to diffuse the ions throughout the solution. This leads to what is known as the *diffuse layer* (sometimes referred to as the *Gouy layer* or the Gouy-Chapman layer, in honor of G. Gouy and D. L. Chapman; see also Sections 11.4, 11.6, and 11.8). For now, the parallel plate capacitor model will get us started with the help of some basic relationships and units from elementary physics. The diffuse model of the double layer is discussed in other sections.

Coulomb's law is the basic point of departure. It may be written for the Coulombic force F_C as

$$F_C = (1/4\pi\varepsilon_0)(qq'/\varepsilon_r r^2) \tag{5}$$

to describe the force operating between two charges q and q' separated by a distance r. The factor ε_r is the dielectric constant of the medium, and the proportionality factor $(1/4\pi\varepsilon_0)$ implies that SI units are being used. Remember that ε_0 has the value $8.85 \cdot 10^{-12}$ C^2 J^{-1} m^{-1}, $4\pi\varepsilon_0 = 1.11 \cdot 10^{-10}$ C^2 J^{-1} m^{-1}, and $(1/4\pi\varepsilon_0) = 8.99 \cdot 10^9$ J m C^{-2}. This factor does not appear when cgs units are used. Appendix B contains some additional remarks about these two systems of units, which can be especially troublesome in electrical calculations.

Next let us consider the definition of the strength of an electric field E. The field E describes the force per unit charge in an electrically influenced environment,

$$E = F_C/q \tag{6}$$

Now suppose we bring two identical $+q$ charges toward one another to a distance of separation r. Combining Equations (5) and (6) enables us to calculate the field at that separation:

$$E = (1/4\pi\varepsilon_0)(q/\varepsilon_r r^2) \tag{7}$$

This is precisely the same as the force that a unit positive charge would experience at the same location. Since force is the negative gradient of the potential, Equation (7) also supplies a second definition of field:

$$E = -(d\psi/dx) \tag{8}$$

where ψ is the potential and x is the separation of the plates.

A fiction that helps us understand electric fields is the notion of lines of force. Suppose we imagine one line of force as emanating from each unit of positive charge. If the charge has a magnitude of $+q$, then there would be q lines of force produced by this particular charge.

A radial distance r from this central charge, the lines of force cut across a spherical surface of area $4\pi r^2$. If we divide the number of lines of force by the cross-sectional area, we obtain, in a vacuum,

$$(\text{Number of lines/area}) = q/4\pi r^2 = \varepsilon_0 E \tag{9}$$

Equation (9) shows that the field E and the number of lines per area are directly proportional, with ε_0 the factor of proportionality. In the presence of a dielectric, ε_r is inserted into Equation (9) to bring it into conformity with Equation (7). Now suppose we apply this idea to a parallel plate capacitor.

In the case of a capacitor—taken here as a prototype of a double layer—the charges are not isolated. Instead, the lines of force emanating from one charged surface terminate at an opposite charge on the other plate of the capacitor. Figure 11.3a represents such a situation when the plates are separated by a vacuum. Suppose a plate of area A carries q charges; then we define the charge density σ^* as

$$\sigma^* = q/A \tag{10}$$

Since a line of force is associated with each unit of charge, there are (q/A) lines of force crossing the evacuated gap between the two plates of the capacitor. As we have already seen,

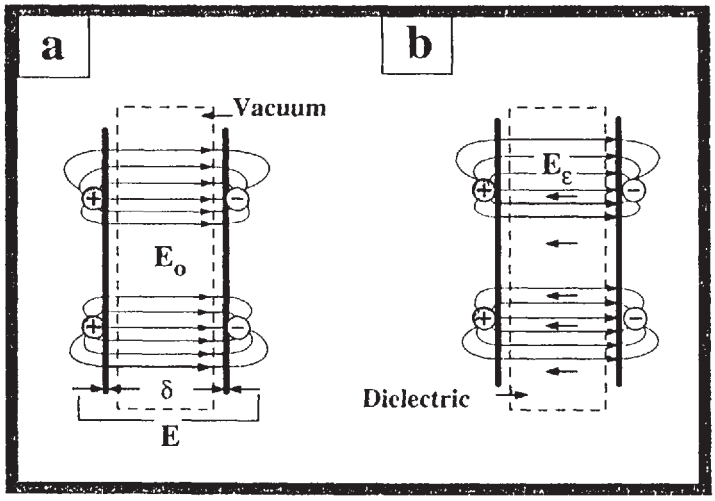


FIG. 11.3 The electric field in a parallel plate capacitor: (a) the dielectric is a vacuum; and (b) a material of dielectric constant ε_r is present.

the number of lines of force measures the field; therefore we write for a capacitor that contains a vacuum

$$E_0 = (q/\varepsilon_0 A) = (\sigma^*/\varepsilon_0) \tag{11}$$

If a substance with a relative dielectric constant ε_r is placed between the plates, the field will be less by this factor. This is because of the partially compensating field that is induced within the dielectric by dipole orientation, as suggested by Figure 11.3b. Therefore, in the presence of the dielectric, the field is given by

$$E_\varepsilon = (q/\varepsilon_r\varepsilon_0 A) = (\sigma^*/\varepsilon_r\varepsilon_0) \tag{12}$$

Next we ignore the directional (sign) aspect of the field and equate Equations (8) and (12) to obtain

$$(d\psi/dx) = (\Delta\psi/\delta) = (\sigma^*/\varepsilon_r\varepsilon_0) \tag{13}$$

where $\Delta\psi$ is the potential drop between plates separated by a distance δ. This equation relates the charge density, voltage difference, and distance of separation of the capacitor. Since this is the model we are using for the double layer, it is of interest to check whether Equation (13) agrees—at least qualitatively—with what we know about the double layer.

We saw in Chapter 7 that charged monolayers are likely to obey the two-dimensional ideal gas law, and we also saw that areas per molecule of 10 nm^2 or so were also required for this ideal law to apply. Hence we may estimate σ^* for a monovalent ion to be

$$\begin{aligned}\sigma^* &= (\text{ion}/10\ \text{nm}^2)(10^{18}\ \text{nm}^2/1\ \text{m}^2)(1.60\cdot10^{-19}\ \text{C/ion}) \\ &= 1.6\cdot10^{-2}\ \text{C m}^{-2}\end{aligned} \tag{14}$$

Taking the dielectric constant of water to be about 80, its bulk value, Equation (12) permits the field strength to be estimated:

$$\begin{aligned}E &= 1.6\cdot10^{-2}\ \text{C m}^{-2}/(80\cdot8.85\cdot10^{-12}\ \text{C}^2\ \text{J}^{-1}\ \text{m}^{-1}) \\ &= 2.26\cdot10^{7}\ \text{V m}^{-1}\end{aligned} \tag{15}$$

Even allowing for an order of magnitude error in this estimate, we see that there is an exceptionally strong field in the vicinity of a charged interface. In Section 12.8 we examine this in greater detail and consider whether we are justified in using bulk values for such parameters as the permittivity ε and the viscosity η within the double layer.

If we estimate the potential drop between the two phases, we may determine the distance over which the potential drop occurs from the value of E given by Equation (15). If we take the potential difference to be 0.10 V—an arbitrary but reasonable value—Equation (13) shows that the plate separation of an equivalent capacitor is

$$\delta = \Delta\psi/E = (0.10/2.26\cdot10^{7}) = 4.4\cdot10^{-9}\ \text{m} = 4.4\ \text{nm} \tag{16}$$

Considering the simplicity of the model and the arbitrariness of the numerical estimates made in this calculation, 4.4 nm seems like a reasonable estimate of the distance over which surface charge neutralization is accomplished.

Throughout this section we have examined the distribution of charge at an interface as if the charge were constrained to two planes. When one of the phases is an aqueous electrolyte solution, the inadequacy of this model is apparent. An immediate improvement of the model is anticipated if we allow for a diffuse double layer, that is, a situation in which the charge density varies with distance from the interface, as shown in Figure 11.4a. Alternatively, we might combine features from both the parallel plate distribution and the diffuse distribution to give a still more elaborate picture of the double layer, as shown in Figure 11.4b. We consider this last situation in Section 11.8. According to this picture, each part of the double layer is analyzed independently, and the effects combined according to the rule for adding capacitors in series:

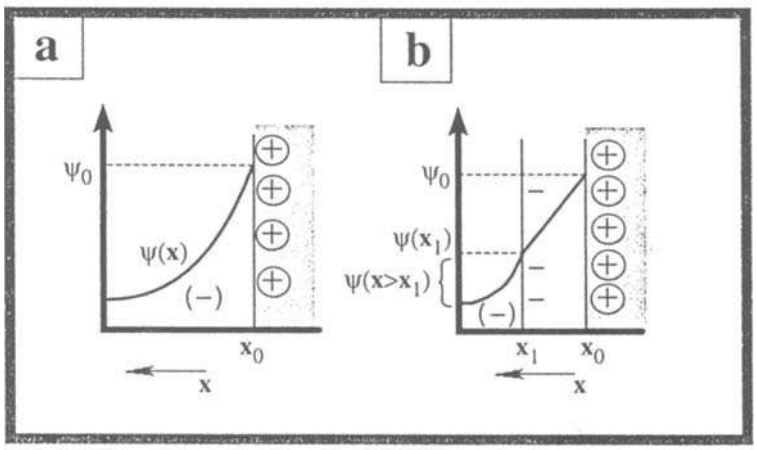


FIG. 11.4 Two models for the double layer: (a) a diffuse double layer; and (b) charge neutralization due partly to a parallel plate charge distribution and partly to a diffuse layer.

$$(1/C_T) = (1/C_1) + (1/C_2) + \ldots + (1/C_i) \tag{17}$$

where C_i is the capacitance of the ith element in series and C_T is the total capacitance.

11.4 THE DIFFUSE DOUBLE LAYER: THE DEBYE-HÜCKEL APPROXIMATION

In the preceding section we discussed the problem of the variation of potential with distance from an interface from the highly artificial perspective of a parallel plate capacitor. The variation of potential with distance from a charged surface of arbitrary shape is a classical electrostatic problem. The general problem is described by the *Poisson equation*,

$$(\partial^2\psi/\partial x^2) + (\partial^2\psi/\partial y^2) + (\partial^2\psi/\partial z^2) = -(\rho^*/\varepsilon) \tag{18}$$

or in terms of the Laplacian operator ∇^2,

$$\nabla^2\psi = -(\rho^*/\varepsilon) \tag{19}$$

where we define ε as the product $\varepsilon_r\varepsilon_0$ and thereby account for the effect of the medium. In these expressions, ρ^* is the charge density (i.e., C m^{-3}) in the system, a quantity that itself is a function of x, y, and z. The solution to this differential equation, therefore, is an expression for the potential that satisfies Equation (18) and also the boundary conditions of the specific problem. We adopt the convention of measuring all distances outward from the interface where the potential has the value ψ_0. As the distance from an isolated surface increases to infinity, the value of ψ approaches zero. The stipulation of an "isolated" surface means that we are concerned with only one interface at this time. In Section 11.7 we consider the case in which electrical double layers overlap.

11.4a Meaning of the Poisson Equation

The Poisson equation is a fundamental relationship of classical electrostatics and really need not be proved here. However, since we are using it as a starting point, it seems desirable to explore the meaning of this important equation to some extent.

Equation (7) describes the field a distance r from a charge $+q$. A basic law of electrostatics is that this field describes any distribution of charge that results in q units of positive charge being enclosed by a sphere of radius r. It is not critical that a single $+q$ charge be situated at

the center for this expression to apply. Suppose, therefore, we consider a portion of solution in which the charge is distributed with a uniform density ρ^*. In this case

$$q = (4/3)\pi r^3 \rho^* \tag{20}$$

and, from Equation (7),

$$E = r\rho^*/3\varepsilon \tag{21}$$

Next we multiply both sides of Equation (21) by r^2 and then differentiate with respect to r:

$$d(r^2E)/dr = r^2\rho^*/\varepsilon \tag{22}$$

In the present notation, Equation (8) becomes

$$E = -(d\psi/dr) \tag{23}$$

where the minus sign is included since ψ decreases as r increases.

Substituting this result into Equation (22) gives

$$\frac{1}{r^2}\frac{\partial}{\partial r}\left(r^2\frac{\partial\psi}{\partial r}\right) = -\frac{\rho^*}{\varepsilon} \tag{24}$$

Remember that the operator $\nabla^2\psi$ in Equation (19) transforms into the following form in spherical coordinates:

$$\nabla^2\psi = \frac{1}{r^2}\frac{\partial}{\partial r}\left(r^2\frac{\partial\psi}{\partial r}\right) + \frac{1}{r^2\sin\theta}\frac{\partial}{\partial\theta}\left(\sin\theta\frac{\partial\psi}{\partial\theta}\right) + \frac{1}{r^2\sin^2\theta}\left(\frac{\partial^2\psi}{\partial\phi^2}\right) \tag{25}$$

Thus the left-hand side of Equation (24) is seen to be identical to $\nabla^2\psi$ for the case (spherical symmetry) in which ψ is independent of θ and ϕ. Although this presentation does not constitute the most general proof of the Poisson equation, it does give it some plausibility.

There are many situations in which the spherically symmetrical case is specifically invoked, as in the Debye-Hückel theory of electrolyte nonideality, for example. We consider situations for which this is the case in Chapter 12. For now, however, we consider the potential distribution adjacent to a planar wall that carries a positive charge.

11.4b Potential Distribution Near Planar Surfaces

We define the direction perpendicular to the wall as the x direction and consider the wall as extending to infinity in the positive and negative y and z directions. In this case the operation $\nabla^2\psi$ becomes $(d\psi^2/dx^2)$, and Equation (18) is written

$$(d\psi^2/dx^2) = -\rho^*/\varepsilon \tag{26}$$

The next problem is to express the charge density as a function of the potential so the differential equation (26) can be solved for ψ. The procedure is to describe the ion concentrations in terms of the potential by means of a Boltzmann factor in which the work required to bring an ion from infinity to a position at which the potential ψ is given by $z_i e\psi$. The probability of finding an ion at this position is given by the Boltzmann factor, with this work appearing as the exponential of energy:

$$n_i/n_{i\infty} = \exp(-z_i e\psi/k_B T) \tag{27}$$

In this expression n_i is the number of ions of type i per unit volume near the surface, and $n_{i\infty}$ is the concentration far from the surface, that is, the bulk concentration. The valence number z_i is either a positive or negative integer.

The charge density is related to the ion concentrations as follows:

$$\rho^* = \sum_i z_i e\, n_i = \sum_i z_i e\, n_{i\infty} \exp\left(-z_i e\psi/k_B T\right) \tag{28}$$

Combining Equations (26) and (28) gives a result known as the *Poisson-Boltzmann equation*:

$$(d^2\psi/dx^2) = -(e/\varepsilon)\sum_i z_i n_{i\infty} \exp(-z_i e\psi/k_B T) \tag{29}$$

This same relationship is the starting point of the Debye-Hückel theory of electrolyte nonideality, except that the Debye-Hückel theory uses the value of $\nabla^2\psi$ required for spherical symmetry. It is interesting to note that Gouy (in 1910) and Chapman (in 1913) applied this relationship to the diffuse double layer a decade before the Debye-Hückel theory appeared.

The derivation of the Poisson equation implies that the potentials associated with various charges combine in an additive manner. The Boltzmann equation, on the other hand, involves an exponential relationship between the charges and the potential. In this way a fundamental inconsistency is introduced when Equations (26) and (28) are combined. Equation (29) does not have an explicit general solution anyhow and must be solved for certain limiting cases. These involve approximations that—at the same time—overcome the objection just stated.

We introduce the first of the Debye-Hückel approximations by considering only those situations for which $(z_i e\psi < k_B T)$. In this case the exponentials in Equation (28) may be expanded (see Appendix A) as a power series. If only first-order terms in $(z_i e\psi/k_B T)$ are retained, Equation (28) becomes

$$\rho^* = \sum_i z_i e n_{i\infty} [1 - (z_i e\psi/k_B T)] \tag{30}$$

Because of electroneutrality, two of the terms in Equation (30) cancel:

$$\sum_i z_i e n_{i\infty} = 0 \tag{31}$$

so that Equation (30) becomes

$$\rho^* = -\sum_i (z_i^2 n_{i\infty} e^2 \psi/k_B T) \tag{32}$$

In this approximation, the ion potentials are additive, so Equation (32) may be consistently substituted into Equation (26) to give

$$(d^2\psi/dx^2) = [(e^2/\varepsilon k_B T)\sum_i z_i^2 n_{i\infty}]\psi \tag{33}$$

The above equation is known as the *linearized* Poisson-Boltzmann equation since the assumption of low potentials made in reaching this result from Equation (29) has allowed us make the right-hand side of the equation linear in ψ. This assumption is also made in the Debye-Hückel theory and prompts us to call this model the Debye-Hückel approximation. Equation (33) has an explicit solution. Since potential is the quantity of special interest in Equation (33), let us evaluate the potential at 25°C for a monovalent ion that satisfies the condition $e\psi = k_B T$:

$$\psi = (k_B T/e) = (1.38\cdot 10^{-23})(298)/(1.60\cdot 10^{-19})$$
$$= 0.0257\ \text{V} = 25.7\ \text{mV} \tag{34}$$

Thus at 25°C potentials may be regarded as low or high, depending on whether they are less or more than about 25 mV. The factor $(e\psi/k_B T)$ appears often in double-layer calculations, so this conversion factor is worth remembering. The relationship of $(k_B T/e)$ to $(RT/\mathfrak{F})$ was noted in Section 11.2.

It is convenient to identify the cluster of constants in Equation (33) by the symbol κ^2, which is defined as follows:

$$\kappa^2 = [(e^2/\varepsilon k_B T)\sum_i z_i^2 n_{i\infty}] \tag{35}$$

With this change in notation, Equation (33) becomes simply

$$(d^2\psi/dx^2) = \kappa^2\psi \tag{36}$$

The above equation will have to be solved under the conditions that $\psi \to \psi_0$ as $x \to 0$ and $\psi \to 0$ as $x \to \infty$. The solution that satisfies these conditions is given by

$$\psi = \psi_0 \exp(-\kappa x) \tag{37}$$

In Section 11.5 we examine the implications of Equation (37) in detail.

11.4c Potential Distribution Around Spherical Surfaces

For studying the stability of colloidal particles in suspension (Chapter 13) or for determining the potential at the surface of particles (Chapter 12), one often needs expressions for potential distributions around small particles that have curved surfaces. Solving the Poisson-Boltzmann equation for curved geometries is not a simple matter, and one often needs elaborate numerical methods. The linearized Poisson-Boltzmann equation (i.e., the Poisson-Boltzmann equation in the Debye-Hückel approximation) can, however, be solved for spherical electrical double layers relatively easily (see Section 12.3a), and one obtains, in place of Equation (37),

$$\psi = \psi_0(R_s/r) \exp[-\kappa(r - R_s)] \tag{38}$$

where R_s is the radius of the spherical particle and r is the distance of any point in the double layer from the *center of the particle*. Notice that the above equation satisfies the required boundary conditions $\psi \to \psi_0$ as $r \to R_s$ and $\psi \to 0$ as $r \to \infty$. We return to this topic in Chapter 12 when we discuss motion of charged particles in electric fields.

11.4d Potential Distribution Around Cylindrical Surfaces

The solution of the linearized Poisson-Boltzmann equation around cylinders also requires numerical methods, although when cylindrical symmetry *and* the Debye-Hückel approximation are assumed the equation can be solved. The solution, however, requires advanced mathematical techniques and we will not discuss it here. It is nevertheless useful to note the form of the solution. The potential ψ for symmetrical electrolytes has been given by Dube (1943) and is written in terms of the charge density σ^* as

$$\psi = \sigma^* K_0(\kappa r)/[\varepsilon\kappa K_1(\kappa R_c)] \tag{39}$$

where r is the radial distance from the axis of the cylinder, R_c is the radius of the cylinder, and K_0 and K_1 are known as zero- and first-order modified Bessel functions of the second kind, respectively. A few values of these Bessel functions are tabulated in Table 11.2 and are useful for calculating electrophoretic mobilities (discussed in Chapter 12). A more detailed analysis of cylindrical double layers may be found in Hunter (1981).

TABLE 11.2 Bessel Functions $K_0(\kappa x)$ and $K_1(\kappa x)$ for Computing Potentials of Long Cylinders[a]

κx	$K_0(\kappa x)/[\kappa x K_1(\kappa x)]$	κx	$K_0(\kappa x)/[\kappa x K_1(\kappa x)]$
0.06	2.950	0.60	0.9942
0.08	2.675	1.00	0.7176
0.10	2.463	1.40	0.5426
0.14	2.151	2.00	0.4071
0.20	1.835	3.00	0.2872
0.40	1.275	4.00	0.2235

Source: H. A. Abramson, L. S. Moyer, and M. H. Gorin, *Electrophoresis of Proteins*, Reinhold, New York, 1942, p. 129.

[a]One may substitute either the radius of the cylinder R_c or the radial position r for the dummy variable x.

11.5 THE DEBYE-HÜCKEL APPROXIMATION: RESULTS

The Debye-Hückel approximation is strictly applicable only in the case of low potentials. Nevertheless, there are several reasons why the significance of Equation (37) should be fully appreciated:

1. It is simpler to understand than any of the modifications we consider subsequently.
2. It is a limiting result to which all equations that are more general must reduce in the limit of low potentials.
3. The effects of electrolyte concentration and valence in this approximation are qualitatively consistent with the results of more elaborate calculations.

11.5a Physical Significance of the Debye-Hückel Parameter κ

One of the most important quantities to emerge from the Debye-Hückel approximation is the parameter κ. This quantity appears throughout double-layer discussions and not merely at this level of approximation. Since the exponent κx in Equation (37) is dimensionless, κ must have units of reciprocal length. This means that κ^{-1} has units of length. This last quantity is often (imprecisely) called the "thickness" of the double layer. All distances within the double layer are judged large or small relative to this length. Note that the exponent κx may be written x/κ^{-1}, a form that emphasizes the notion that distances are measured relative to κ^{-1} in the double layer.

Since κ and κ^{-1} are such important quantities, we examine them in greater detail, first verifying their dimensions and then considering their numerical magnitude. Especially important is the dependence of κ and κ^{-1} on the concentration and valence of the electrolyte in solution.

It is an easy matter to verify that κ^2 as defined by Equation (35) does indeed have units of length^{-2}, or m^{-2} in SI. This is seen by writing the SI units for the various factors appearing in Equation (35) as follows:

$$\kappa^2 = (\mathrm{C})^2(\mathrm{m}^{-3})/(\mathrm{C}^2\mathrm{J}^{-1}\mathrm{m}^{-1})(\mathrm{J\,K}^{-1})\,(\mathrm{K}) = \mathrm{m}^{-2}$$

The parameter κ depends on concentration; accordingly, we must express it in practical concentration units. If n_i is expressed as the number of ions per cubic meter, then n_i is related to the molar concentration M_i of the ions and the Avogadro's number N_A by

$$n_i = 1000\, M_i N_A \tag{40}$$

since 1000 dm^3 = 1 m^3. Therefore Equation (35) yields

$$\kappa = [(1000\, e^2 N_A/\varepsilon k_B T) \sum_i z_i^2 M_i]^{1/2} \tag{41}$$

The summation in this expression is twice the ionic strength of the solution. We examine the numerical substitutions into Equation (41) in Example 11.1.

* * *

EXAMPLE 11.1 *Dependence of the Debye-Hückel Parameter κ on Temperature and Type of Electrolytes.* Evaluate the numerical factor in Equation (41) for aqueous solutions at 25°C. At this temperature $\varepsilon_r = 78.54$ for water. Calculate κ and κ^{-1} for 0.01 M solutions of 1 : 1, 2 : 1, and 3 : 1 electrolytes. Suggest how these values can be adapted to other temperatures (or media) without complete recalculation.

Solution: Recalling that $\varepsilon = \varepsilon_r\varepsilon_0$, we write

$$\kappa^2 = (1000)(1.60\cdot10^{-19})^2(6.02\cdot10^{23})(2I)/(78.54)(8.85\cdot10^{-12})(1.38\cdot10^{-23})(298)$$
$$= 2.32\cdot10^9(2I)^{1/2}\mathrm{m}^{-1}$$

and

$$\kappa^{-1} = 4.31 \cdot 10^{-10}(2I)^{-1/2}\ \text{m}$$

where I is the ionic strength. Note that, for a 1 : 1 electrolyte, the summation in Equation (41) gives $(2I)$. In general, for any symmetrical $(z:z)$ electrolyte, the ionic strength equals $z^2 M$ (or $I^{1/2} = |z| M^{1/2}$). Therefore in a 0.01 M solution of 1 : 1 electrolyte

$$\kappa = 3.29 \cdot 10^{8}\ \text{m}^{-1} \quad \text{and} \quad \kappa^{-1} = 3.04 \cdot 10^{-9}\ \text{m} = 3.04\ \text{nm}$$

For *asymmetrical* electrolytes the ionic strength is the same for, say, 1 : 2 as for 2 : 1 solutes; namely, 3 M as verified by substitution into the summation (and remembering the stoichiometry of the dissociation!). Therefore in a 0.01 M solution of 2 : 1 electrolyte

$$\kappa = 5.68 \cdot 10^{8}\ \text{m}^{-1} \quad \text{and} \quad \kappa^{-1} = 1.76 \cdot 10^{-9}\ \text{m} = 1.76\ \text{nm}$$

and in a 0.01 M solution of 3 : 1 electrolyte (I = 6 M)

$$\kappa = 8.04 \cdot 10^{8}\ \text{m}^{-1} \quad \text{and} \quad \kappa^{-1} = 1.24 \cdot 10^{-9}\ \text{m} = 1.24\ \text{nm}$$

It is easy enough to evaluate κ and κ^{-1} for different concentrations and valence types; it is more of a nuisance to recalculate these quantities at different temperatures and/or in different media. An easy way to do this using the expressions given is to factor out $\varepsilon_{r,298}$ and T = 298K and replace them with quantities pertinent to the problem at hand. For example, at 90°C, ε_r = 57.98 for water; therefore the value of κ at this temperature is given by

$$\begin{aligned}\kappa &= 2.32 \cdot 10^{9}[(78.54)(298)/(57.98)(363)]^{1/2}(2I)^{1/2} \\ &= 2.32 \cdot 10^{9}(1.05)(2I)^{1/2} \\ &= 2.45 \cdot 10^{9}(2I)^{1/2}\text{m}^{-1}\end{aligned}$$

■

* * *

Both κ and κ^{-1} are used extensively in this chapter and Chapters 12 and 13 (as well as in the sections on the rheology of charged dispersions in Chapter 4). Table 11.3 lists numerical values for these quantities and the pertinent equations for their calculation for aqueous solutions at 25°C. This table may be consulted as a source for κ and κ^{-1} values when these are required for exercises in these chapters.

Several things should be noted about Table 11.3:

1. The tabulated values of κ^{-1} multiplied by 10^9 give the double layer "thicknesses" in nanometers. For example, in a 0.01 M solution of a 1 : 1 electrolyte, κ^{-1} equals 3.04 nm.

TABLE 11.3 Values of κ and κ^{-1} for Several Values of Electrolyte Concentrations and Valences for Aqueous Solutions at 25°C

		Symmetrical electrolyte			Asymmetrical electrolyte	
		$\kappa\,(\text{m}^{-1}) = 3.29 \times 10^{9}\lvert z\rvert M^{1/2}$	$\kappa^{-1}\,(\text{m}) = 3.04 \times 10^{-10}\lvert z\rvert^{-1}M^{-1/2}$		$\kappa\,(\text{m}^{-1}) = 2.32 \times 10^{9}(\Sigma_i z_i^2 M_i)^{1/2}$	$\kappa^{-1}\,(\text{m}) = 4.30 \times 10^{-10}(\Sigma_i z_i^2 M_i)^{-1/2}$
Molarity	$z_+:z_-$			$z_+:z_-$		
0.001	1:1	1.04×10^{8}	9.61×10^{-9}	1:2, 2:1	1.80×10^{8}	5.56×10^{-9}
	2:2	2.08×10^{8}	4.81×10^{-9}	3:1, 1:3	2.54×10^{8}	3.93×10^{-9}
	3:3	3.12×10^{8}	3.20×10^{-9}	2:3, 3:2	4.02×10^{8}	2.49×10^{-9}
0.01	1:1	3.29×10^{8}	3.04×10^{-9}	1:2, 2:1	5.68×10^{8}	1.76×10^{-9}
	2:2	6.58×10^{8}	1.52×10^{-9}	1:3, 3:1	8.04×10^{8}	1.24×10^{-9}
	3:3	9.87×10^{8}	1.01×10^{-9}	2:3, 3:2	1.27×10^{9}	7.87×10^{-10}
0.1	1:1	1.04×10^{9}	9.61×10^{-10}	1:2, 2:1	1.80×10^{9}	5.56×10^{-10}
	2:2	2.08×10^{9}	4.81×10^{-10}	1:3, 3:1	2.54×10^{9}	3.93×10^{-10}
	3:3	3.12×10^{9}	3.20×10^{-10}	2:3, 3:2	4.02×10^{9}	2.49×10^{-10}

2. This "thickness" is about the same magnitude as the prediction based on the capacitor model (Equation (16)). The diffuse model is clearly superior, however, since it shows how the double layer "thickness" depends on the concentration and valence of the ions in the solution.
3. The "thickness" of the double layer varies inversely with z and inversely with $M^{1/2}$ for a symmetrical $z:z$ electrolyte. Therefore κ^{-1} equals 1.0 nm for a 0.01 M solution of a 3 : 3 electrolyte and is about 10 nm for a 0.001 M solution of a 1 : 1 electrolyte.

Figure 11.5 shows how the potential drops with distance from the surface according to Equation (37). The curves in this figure are drawn for two different variations in κ: in Figure 11.5a, a 1 : 1 electrolyte at 0.1, 0.01, and 0.001 M concentrations; and in Figure 11.5b, a 0.001 M solution of 1 : 1, 2 : 2, and 3 : 3 electrolytes. Again, it is important to recognize that the curves drop off more rapidly for either higher concentrations or higher valences of the electrolyte.

The curves in Figure 11.5 are marked at the x value that corresponds to κ^{-1}. Note that the potential has dropped to the value (ψ_0/e) at this point. Calling κ^{-1} the double layer "thickness" is clearly a misnomer. We see presently, however, that there is some logic underlying this terminology.

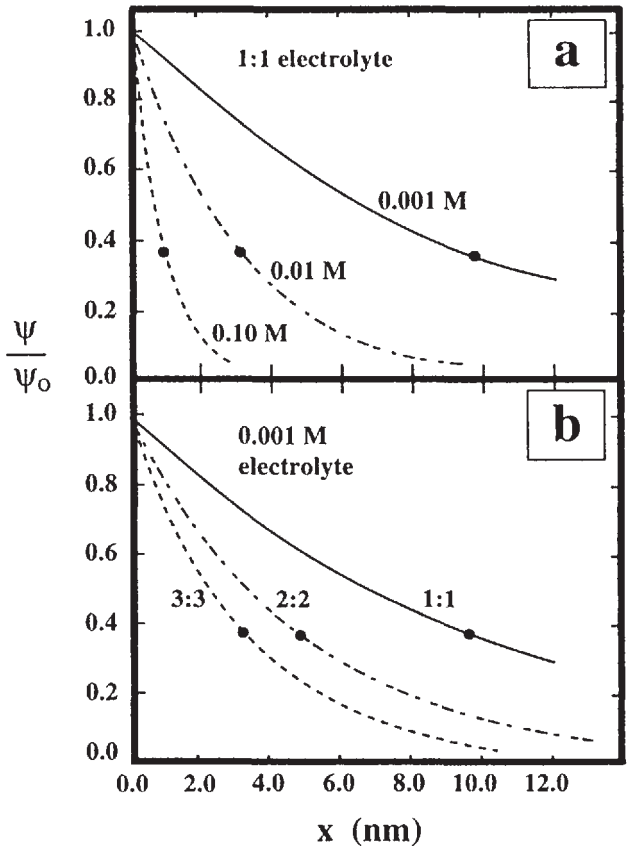


FIG. 11.5 Fraction of double-layer potential versus distance from a surface according to the Debye-Hückel approximation, Equation (37): (a) curves drawn for 1 : 1 electrolyte at three concentrations; and (b) curves drawn for 0.001 M symmetrical electrolytes of three different valence types.

11.5b Comparison Between the Capacitor and Diffuse Models

Although the potential is fundamentally a more important quantity than charge density, examining the charge density will enable us to compare the capacitor and diffuse models for the double layer.

The condition of electroneutrality at a charged interface requires that the density of charge at the two faces be equal. Note that this does not require the charges to be physically situated at the interface. When one of the phases contains a diffuse layer, the total charge contained in a volume element of solution of unit cross section and extending from the wall to infinity must contain the same amount of charge—although of opposite sign—as a unit area of wall contains. Stated in formula, this becomes

$$\sigma^* = -\int_0^\infty \rho^* dx \tag{42}$$

We now examine the implications of Equation (42) for the situation in which one of the adjoining phases contains the diffuse half of a double layer. Combining Equations (26) and (42) gives

$$\sigma^* = \varepsilon \int_0^\infty (d^2\psi/dx^2)dx \tag{43}$$

a result that is easily integrated to yield

$$\sigma^* = \varepsilon(d\psi/dx)\Big|_0^\infty \tag{44}$$

The quantity $d\psi/dx$ is zero at infinity, and we define its value at the wall by $(d\psi/dx)_0$; therefore Equation (44) becomes

$$\sigma^* = -\varepsilon(d\psi/dx)_0 \tag{45}$$

Equation (45) provides a relationship between the *surface charge density* and the slope of the potential at the surface. Next, we turn to Equation (37)—the Debye-Hückel approximation for ψ—to evaluate $(d\psi/dx)_0$. Differentiation leads to the value

$$(d\psi/dx)_0 = \lim_{x\to 0} [-\kappa\psi_0 \exp(-\kappa x)] = -\kappa\psi_0 \tag{46}$$

Substituting Equation (46) into Equation (45) gives

$$\sigma^* = \varepsilon\kappa\psi_0 \tag{47}$$

Rewriting Equation (47) in terms of κ^{-1}, the double-layer "thickness," yields

$$\sigma^* = \varepsilon(\psi_0/\kappa^{-1}) \tag{48}$$

Equation (48) is identical in form to Equation (13) for a parallel plate capacitor, with ψ_0 replacing $\Delta\psi$ and κ^{-1} replacing δ. This result shows that a diffuse double layer at low potentials behaves like a parallel plate capacitor in which the separation between the plates is given by κ^{-1}. This explains why κ^{-1} is called the double-layer thickness. It is important to remember, however, that the *actual* distribution of counterions in the vicinity of a charged wall is diffuse and approaches the unperturbed bulk value only at large distances from the surface.

Even allowing for the fact that the Debye-Hückel approximation applies only for low potentials, the above analysis reveals some features of the electrical double layer that are general and of great importance as far as stability with respect to coagulation of dispersions and electrokinetic phenomena are concerned. In summary, three specific items might be noted:

1. The distance (away from the wall) over which an electrostatic potential persists may be comparable to the dimensions of colloidal particles themselves.
2. The distance over which significant potentials exist decreases with increasing electrolyte concentration.
3. The range of electrostatic potentials decreases as the valence of the ions in solution increases.

The Debye-Hückel approximation to the diffuse double-layer problem produces a number of relatively simple equations that introduce a variety of double-layer topics as well as a number of qualitative generalizations. In order to extend the range of the quantitative relationships, however, it is necessary to return to the Poisson-Boltzmann equation and the unrestricted Gouy-Chapman theory, which we do in Section 11.6.

11.5c Relation Between the Surface Charge and Surface Potential for Spherical Double Layers

Before we proceed to the Gouy-Chapman theory of electrical double layers, it is worthwhile to note that relations similar to Equations (45) and (47) can also be derived for double layers surrounding spherical particles. The equation for surface charge density takes the form

$$\sigma^* = -\varepsilon(d\psi/dr)_{R_s} \tag{49}$$

where the subscript R_s implies that the slope $(d\psi/dr)$ is evaluated at the particle surface, that is, $r = R_s$. When the expression for ψ given in Equation (38) is substituted in this expression, one derives for the following equation

$$q = 4\pi R_s^2\sigma^* = 4\pi\varepsilon R_s(1 + \kappa R_s)\psi_0 \tag{50}$$

for the relation between the total charge q on the particle and the surface potential ψ_0.

11.5d Relation Between the Surface Charge and Surface Potential for Cylindrical Double Layers

In the case of cylindrical particles (of radius R_c), if one again assumes that the charge is smeared uniformly on the surface of the cylinders (including the flat circular ends), we can use Equation (39) to obtain

$$q = [2\pi\varepsilon\kappa R_c(2R_c + L)K_1(\kappa R_c)/K_0(\kappa R_c)]\psi_0 \tag{51}$$

where L is the length of the cylinder, and K_0 and K_1 are the Bessel functions listed in Table 11.2. Additional details are available in the references cited in Section 11.4d.

11.6 THE ELECTRICAL DOUBLE LAYER: GOUY-CHAPMAN THEORY

The theoretical inconsistencies inherent in the Poisson-Boltzmann equation were shown in Section 11.4 to vanish in the limit of very small potentials. It may also be shown that errors arising from this inconsistency will not be too serious under the conditions that prevail in many colloidal dispersions, even though the potential itself may no longer be small. Accordingly, we return to the Poisson-Boltzmann equation as it applies to a planar interface, Equation (29), to develop the Gouy-Chapman result without the limitations of the Debye-Hückel approximation.

If both sides of Equation (29) are multiplied by $2\,d\psi/dx$, we obtain

$$2(d\psi/dx)(d^2\psi/dx^2) = 2(d\psi/dx)\{-(e/\varepsilon)\sum_i z_i n_{i\infty}\exp(-z_i e\psi/k_B T)\} \tag{52}$$

The left-hand side of this equation is the derivative of $(d\psi/dx)^2$; therefore

$$(d\psi/dx)^2 = (2k_B T/\varepsilon)\sum_i n_{i\infty}\exp(-z_i e\psi/k_B T) + \text{const.} \tag{53}$$

The integration constant in this expression is easily evaluated if we define the potential in the solution at $x = \infty$ to be zero. At the same limit, $d\psi/dx$ also equals zero. In view of these conventions, Equation (53) becomes

$$(d\psi/dx)^2 = (2k_B T/\varepsilon)\sum_i n_{i\infty}[\exp(-z_i e\psi/k_B T) - 1] \tag{54}$$

This result may be integrated further if we restrict the electrolyte in solution to the symmetrical z : z type. In that case, Equation (54) can be written as

$$(d\psi/dx)^2 = (2k_BTn_\infty/\varepsilon)[\exp(-ze\psi/k_BT) + \exp(ze\psi/k_BT) - 2] \tag{55}$$

in which z is the absolute value of the valence number, the sign having been incorporated into the algebraic form. Note that in Equation (55) we have written $n_{i\infty}$ as simply n_∞ since we are considering symmetric (z : z) electrolytes. The bracketed term is readily seen to equal $[\exp(-ze\psi/2k_BT) - \exp(ze\psi/2k_BT)]^2$; therefore Equation (55) may be written as

$$(d\psi/dx)^2 = (2k_BTn_\infty/\varepsilon)[\exp(-ze\psi/2k_BT) - \exp(ze\psi/2k_BT)]^2 \tag{56}$$

Identifying $(ze\psi/k_BT)$ as y permits the simplification of notation to

$$\begin{aligned}(dy/dx) &= (2e^2z^2n_\infty/\varepsilon k_BT)^{1/2}[\exp(-y/2) - \exp(y/2)] \\ &= \kappa[\exp(-y/2) - \exp(y/2)]\end{aligned} \tag{57}$$

This last result may be written in an integrable form by defining u as $e^{y/2}$, in which case $dy = 2e^{-y/2}du$, and the following relationships hold:

$$\frac{dy}{e^{-y/2} - e^{y/2}} = \frac{2\,du}{e^{y/2}(e^{-y/2} - e^{y/2})} = \frac{2\,du}{1 - e^y} = \frac{2\,du}{1 - u^2} = \frac{du}{1 + u} + \frac{du}{1 - u} \tag{58}$$

Combining Equations (57) and (58) gives

$$\frac{du}{1 + u} + \frac{du}{1 - u} = \kappa\,dx \tag{59}$$

which is easily integrated to yield

$$\ln\left(\frac{1 + u}{1 - u}\right) = \kappa x + \text{const.} \tag{60}$$

The integration constant is evaluated from the fact that $\psi = \psi_0$, $y = y_0$, and $u = u_0$ at $x = 0$; therefore

$$\ln\left(\frac{(1 + u)(1 - u_0)}{(1 - u)(1 + u_0)}\right) = \kappa x \tag{61}$$

In terms of the physical variables, Equation (61) may be written

$$\begin{aligned}&\ln\{[\exp(ze\psi/2k_BT) + 1][\exp(ze\psi_0/2k_BT) - 1]/\{[\exp(ze\psi/2k_BT) - 1] \\ &\quad [\exp(ze\psi_0/2k_BT) + 1]\}\} = \kappa x\end{aligned} \tag{62}$$

Equation (62) describes the variation in potential with distance from the surface for a diffuse double layer without the simplifying assumption of low potentials. It is obviously far less easy to gain a "feeling" for this relationship than for the low-potential case. Anticipation of this fact is why so much attention was devoted to the Debye-Hückel approximation in the first place. Note that Equation (62) may be written

$$\begin{aligned}&[\exp(ze\psi/2k_BT) - 1]/[\exp(ze\psi/2k_BT) + 1] \\ &\quad = \{[\exp(ze\psi_0/2k_BT) - 1]/[\exp(ze\psi_0/2k_BT) + 1]\}\exp(-\kappa x)\end{aligned} \tag{63}$$

Equation (63) is the Gouy-Chapman expression for the variation of potential within the double layer. For simplicity, Equation (63) may be written

$$\Upsilon = \Upsilon_0 \exp(-\kappa x) \tag{64}$$

where Υ is defined by the relationship

$$\Upsilon = [\exp(ze\psi/2k_BT) - 1]/[\exp(ze\psi/2k_BT) + 1] \tag{65}$$

and Υ_0 is equal to Υ evaluated with $\psi = \psi_0$. Equation (64) shows that it is the ratio Υ that varies exponentially with x in the Gouy-Chapman theory rather than ψ, as is the case in the Debye-Hückel approximation. Some values of Υ_0 calculated for a variety of ψ_0 values are listed in Table 11.4.

As a check on the consistency of our mathematics, it is profitable to verify that Equation (63) reduces to Equation (37) in the limit of low potentials. Expanding the exponentials in Υ and truncating the series so that only one term survives in both the numerator and denominator results in the Debye-Hückel expression, Equation (37).

Another situation of interest in which Equation (63) simplifies considerably is the case of large values of x at which ψ has fallen to a small value regardless of its initial value. Under these conditions the exponentials of the left-hand side are expanded to give

$$ze\psi/4k_BT = \Upsilon_0 \exp(-\kappa x) \tag{66}$$

or

$$\psi = (4k_BT/ze)\,\Upsilon_0 \exp(-\kappa x) \tag{67}$$

For very large values of ψ_0, $\Upsilon_0 \to 1$. In this case, Equation (67) becomes

$$\psi = (4k_BT/ze) \exp(-\kappa x) \tag{68}$$

which shows that the potential in the outer (i.e., well removed from the wall) portion of the diffuse double layer is independent of the potential at the wall for larger potentials. In colloidal dispersions ($ze\psi_0/k_BT$) is generally greater than unity, but not too much greater. This means that approximations represented by Equations (37) and (67) will generally bracket the true potential-versus-distance curve given by Equation (63). The situation is shown graphically in Figure 11.6. In drawing these curves, we chose a value of ψ_0 equal to 77.1 mV and arbitrarily selected the electrolyte to be a 0.01 M solution of a 1 : 1 electrolyte for which κ^{-1} is 3.04 nm. Equation (68) is a poor approximation in this case because ψ_0 is not large enough. Values of the abscissa are readily converted into dimensionless variables that apply to any solution by dividing the x coordinate in nanometers by 3.04 nm.

We conclude this section by considering the expression for charge density, Equation (42), as it applies in the Gouy-Chapman model. As we saw in the preceding section, the charge density expression integrates to Equation (45) with no assumptions as to the nature of the potential function. Accordingly, we may combine Equations (45) and (56) to obtain

$$\sigma^* = \varepsilon(2k_BTn_\infty/\varepsilon)^{1/2}[\exp(ze\psi_0/2k_BT) - \exp(-ze\psi_0/2k_BT)] \tag{69}$$

TABLE 11.4 Variation of the Parameter Υ_0 with ψ_0 at 25°C

ψ_0 (mV)	Υ_0
260	0.9874
240	0.9814
220	0.9727
200	0.9600
180	0.9415
160	0.9149
140	0.8765
120	0.8230
100	0.7500
80	0.6528
60	0.5249
40	0.3711
20	0.1968

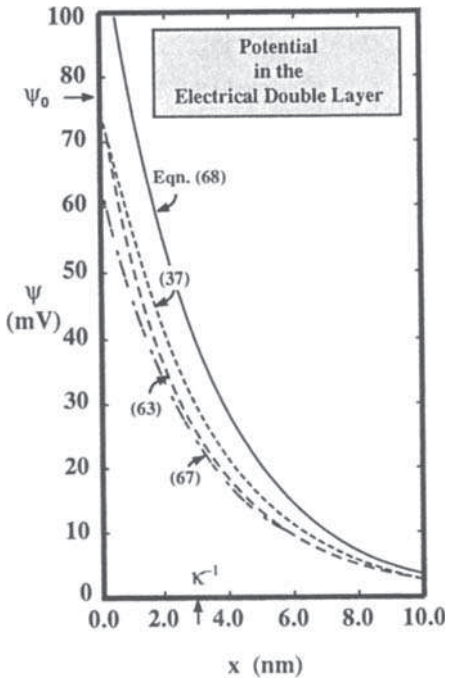


FIG. 11.6 Variation of the double-layer potential versus distance from the surface according to four expressions from this chapter. The figures are for $\psi_0 = 77.1$ mV and $\kappa = 3.29 \cdot 10^8\ m^{-1}$ (or 0.01 M solution of 1 : 1 electrolyte). Curves are drawn according to Equations (37), (63), (67), and (68).

Equation (69), known as the *Grahame equation*, describes the variation of charge density with potential at the surface with no limitations as to the value of the potential. Example 11.2 considers an application of this relationship.

* * *

EXAMPLE 11.2 *Relation Between Surface Charge Density and Surface Potential.* Show that for a 1 : 1 electrolyte in water at 25°C, Equation (69) can be rearranged to give

$$\psi_0 = 51.4 \sinh^{-1} [137/(\sigma^0 \sqrt{c})]$$

in which ψ_0 is expressed in millivolts, c is in moles per liter, and σ^0 is the area (in Å^2) per charge at the surface. Davies (1951) measured the potential across an air-aqueous NaCl interface that carried a monolayer of $C_{18}H_{37}N(CH_3)_3^+$. When the quaternary octadecyl-amine was at a pressure corresponding to $\sigma^0 = 85$ Å^2, the following potentials were measured at different concentrations of NaCl (data from Davies 1951):

E_{obs} (mV)	240	280	325	340	380
c_{NaCl} (M)	2.0	0.5	0.1	0.033	0.01

About 200 mV of these potential differences arises from dipole effects at the interface and should be subtracted from each value to give the double-layer contribution to the measured potentials. Compare these corrected values with the values of ψ_0 calculated by the equation given.

Solution: First recognize that $2 \sinh x = e^x - e^{-x}$; therefore Equation (69) can be written

$$\sigma^* = (8\varepsilon k_B T n_\infty)^{1/2} \sinh (ze\psi_0/2k_B T)$$

or

$$\sinh^{-1} [\sigma^* (8\varepsilon k_B T n_\infty)^{-1/2}] = ze\psi_0/2k_B T$$

For a 1 : 1 electrolyte, this yields

$$\psi_0 = (2k_BT/e) \sinh^{-1}[\sigma^*(8\varepsilon k_BTn_\infty)^{-1/2}]$$

To assure proper units, we assemble the following substitutions for this expression:

$$(2k_BT/e) = 2(1.38 \cdot 10^{-23})(298)/1.60 \cdot 10^{-19} = 0.0514 \text{ V} = 51.4 \text{ mV}$$

which gives the desired coefficient. Next we use Equation (40) to obtain n_∞; $n_\infty = (10^3)(6.02 \cdot 10^{23})c = 6.02 \cdot 10^{26}c$. With this the factor, $8\varepsilon k_BTn_\infty$ becomes

$$8(78.54)(8.85 \cdot 10^{-12})(1.38 \cdot 10^{-23})(298)(6.02 \cdot 10^{26}c) = 1.38 \cdot 10^{-2}c$$

Finally, σ^* is related to σ^0 as follows:

$$\sigma^* = 1.60 \cdot 10^{-19}/\sigma^0(10^{-10})^2 = 16/\sigma^0$$

From these components the argument of the sinh can be evaluated as $137/\sigma^0c^{1/2}$, which is the desired result.

By substituting the value of σ^0 into this expression and using the various NaCl concentrations given, ψ_0 values are readily calculated; these are to be compared with $E_{obs} - 200$. The following values are obtained:

ψ_0 (mV)	50.4	80.2	119.8	148.0	178.9
$(E_{obs} - 200)$ (mV)	40	80	125	140	180

The agreement between theory and experiment is seen to be quite satisfactory. ■

* * *

11.7 OVERLAPPING DOUBLE LAYERS AND INTERPARTICLE REPULSION

From the viewpoint of the stability of lyophobic colloids discussed in Chapter 13, this section (and the developments based on this in Chapter 13) is of central importance. In this section we examine the force per unit area—that is, the pressure—that operates on two charged surfaces as a result of the overlapping of their double layers. As we saw in Chapter 10, it is more convenient to compare attraction and repulsion between particles in terms of potential energy rather than force. Therefore we see how to express double-layer repulsion in terms of potential energy; this will be developed further in Chapter 13. As was the case with a single double layer, it is easier to treat overlapping double layers if the potential is low. Accordingly, the detailed derivation we consider will assume this condition. We generalize to the case of higher potentials below, but without presenting all the mathematical details of that situation. Following this, we show how the results obtained for interaction forces between flat surfaces can be used to obtain forces between curved double layers. Since the basic approach is more easily demonstrated for spherical surfaces, the results will be given for interaction between spherical particles only.

11.7a Repulsion Between Planar Double Layers

Figure 11.7 is a schematic representation of the situation with which we are concerned. It shows two plates of unspecified thickness; the planar faces of these plates are separated by a distance h. The plates are immersed in an infinite reservoir of electrolyte, the bulk concentration of which is n_∞. The potential at the surface of the plates is defined as ψ_0. It will be convenient to distinguish between the inner and outer regions of the solution. By the inner region, we refer to the region between the plates, and by the outer region we mean the region influenced by only one of the faces.

When the distance between the plates is large, the potential on both the inner and outer faces will drop with distance from the surface according to Equation (63) or one of its approximations. The profile of the potential drop in this case is shown by the solid curve in the outer region in Figure 11.7 and by the dashed line in the inner region. As the distance between the plates decreases, the potential from each of the inner faces begins to overlap in the inner region. Therefore the net potential in the inner region varies as the solid line in the figure for this region. The potential in the outer region is unaffected by the separation of the

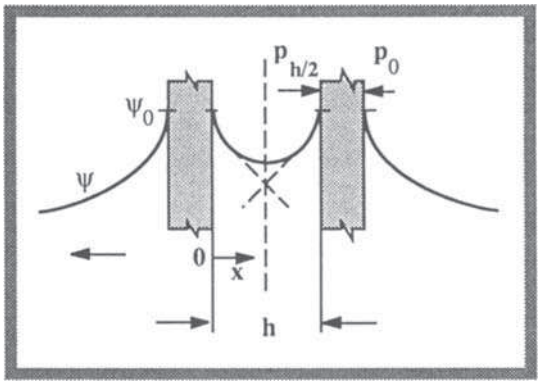


FIG. 11.7 Schematic representation of the overlap of two double layers when a pair of plates is brought to a surface separation h.

plates. Since we already know how to handle the potential in the outer region, our interest now focuses on the potential in the inner region in which double layer overlap occurs.

11.7a.1 Repulsive Force Between Interacting Surfaces

At equilibrium all forces on any volume element of a solution must balance. Suppose we apply this equilibrium criterion to a volume element of solution that lies in the plane parallel to the face of the plates in Figure 11.7 and lies a distance x from the face of one of these plates. Two kinds of force must operate on this volume element: osmotic pressure and electrostatic forces. According to Equations (4.25) and (4.27), the x component of the pressure force acting on the volume element (i.e., per unit volume) is given by

$$F_x = -dp/dx \tag{70}$$

The electrical force per unit volume is given by the product of the charge density times the field strength according to Equation (6):

$$F_{el} = -\rho^*(d\psi/dx) \tag{71}$$

Combining these results with the criterion for equilibrium leads to the expression

$$(dp/dx) + \rho^*(d\psi/dx) = 0 \tag{72}$$

When Equation (26) is substituted for ρ^*, this becomes

$$(dp/dx) - \varepsilon(d^2\psi/dx^2)(d\psi/dx) = 0 \tag{73}$$

Since

$$(d^2\psi/dx^2)(d\psi/dx) = (1/2)(d/dx)(d\psi/dx)^2$$

Equation (73) can be written

$$(d/dx)[p - (\varepsilon/2)(d\psi/dx)^2] = 0 \tag{74}$$

This result shows that the condition for equilibrium is equivalent to requiring that

$$[p - (\varepsilon/2)(d\psi/dx)^2] = \text{const.} \tag{75}$$

at all locations in the solution. Equation (75) shows that two influences—the pressure and the electric field—operate within the solution. The electric field contribution from $(d\psi/dx)^2$ is known as the *Maxwell pressure* (or, *Maxwell stress*). Equation (75) also shows that the difference between the two contributions is a constant that still remains to be evaluated. We are specifically interested in evaluating this constant in the inner region. We proceed in two steps: (i) first, we obtain p in terms of ψ, and (ii) then, we replace ψ as a function of the distance between the plates.

At this point, the symmetry of the situation shown in Figure 11.7 becomes helpful. We realize that ψ goes through a minimum at the midpoint position; that is, $d\psi/dx = 0$ at $x = h/2$. Thus the constant in Equation (75) equals the pressure at the midpoint $p_{h/2}$. The difference between the pressure and the field effect is equal to this quantity at all locations between the plates. Because of this constancy, the entire inner region is characterized by the parameters that apply at the midpoint. Therefore $\psi_{h/2}$ is the potential that governs the repulsion between the surfaces. Next, we write Equation (72) as

$$dp = -\rho^* d\psi \tag{76}$$

Now Equation (28) may be substituted for ρ^* for a $z:z$ electrolyte, giving

$$dp = -zen_\infty[\exp(-ze\psi/k_BT) - \exp(ze\psi/k_BT)]d\psi \tag{77}$$

Since $e^x - e^{-x} = 2\sinh x$, Equation (77) may also be written

$$dp = 2zen_\infty \sinh(ze\psi/k_BT)\, d\psi \tag{78}$$

Equation (78) is easily integrated between the following limits: $p = p_0$ (the outer reference pressure) at $\psi = 0$ and $p = p_{h/2}$ at $\psi = \psi_{h/2}$. Integration of Equation (78) gives

$$p_{h/2} - p_0 = 2k_BTn_\infty[\cosh(ze\psi_{h/2}/k_BT) - 1] = F_R \tag{79}$$

Equation (79) gives the excess pressure at $x = h/2$, and therefore the force per unit area with which the plates are pushed apart, F_R.

This analysis is one of several treatments of double-layer repulsion presented in Verwey and Overbeek's classic book cited at the end of this chapter. The reader will find the topics of this chapter developed in great detail in that source.

Although Equation (79) is correct, it is not particularly helpful. The problem is that F_R is expressed in terms of the potential at the midpoint, which is itself an unknown quantity. For the special case in which $h/2$ is relatively large, the approximation given by Equation (67) may be applied to the potential from each of the two approaching surfaces. The potential at the midpoint then becomes

$$\psi_{h/2} \approx \psi_1 + \psi_2 \approx 2(4k_BT\Upsilon_0/ze)\exp(-\kappa h/2) \tag{80}$$

according to this approximation. This approximation if often called the *superposition approximation* and is clearly admissible only when the surfaces are sufficiently far apart so that the overlap of the double layers is moderate. Since this result applies well away from the surface, the potential is low when Equation (80) holds. Therefore $\cosh(ze\psi_{h/2}/k_BT)$ in Equation (79) may be expanded as a power series (see Appendix A), with only the leading terms retained. This leads to the result

$$F_R \approx k_BTn_\infty(ze\psi_{h/2}/k_BT)^2 = k_BTn_\infty[8\Upsilon_0\exp(-\kappa h/2)]^2 \tag{81}$$

or

$$F_R \approx 64k_BTn_\infty\Upsilon_0^2\exp(-h/\kappa^{-1}) \tag{82}$$

An issue of considerable practical importance is how the force of repulsion described by Equation (79) and its approximation Equation (82) varies with the electrolyte content of a solution. Since κ varies with $n_\infty^{1/2}$, Equation (82) is of the form

$$F_R = C_1n_\infty\exp(-C_2n_\infty^{1/2}) \tag{83}$$

where C_1 is a constant and C_2 remains fixed for a given distance of separation h. The exponential factor is clearly the more sensitive involvement of n_∞ in Equation (83). Therefore this expression shows that the force of repulsion decreases with increasing electrolyte concentration between two surfaces compared at the same separation, at least at relatively large separation. The addition of indifferent electrolyte to an aqueous dispersion of a lyophobic colloid may induce the coagulation of that colloid. Equation (83) is therefore an important step toward understanding this behavior. One interesting system to which these ideas have been applied is

the case of liquid films. An aqueous soap bubble, for example, reaches an equilibrium thickness at which the various forces acting on it balance out. Such forces are readily enumerated:

1. Gas pressure tends to squeeze the two faces of the film together.
2. Van der Waals attraction between the two gas masses is transmitted across the liquid surface.
3. Amphipathic surfactant ions adsorb at the liquid surface—tails out—so counterions form diffuse double layers that can overlap in a manner resembling Figure 11.7.
4. The equilibrium thickness of most bubbles is so much less than the radius of curvature of the bubble that the air masses can be regarded as blocks with planar faces like those in our models. In research studies on such systems, the bubbles are allowed to equilibrate on frames that make their compliance with the model even better.

In Example 11.3 we discuss the results of such a study with soap bubbles.

* * *

EXAMPLE 11.3 *Influence of Electrostatic Repulsion on the Thickness of Soap Bubbles.* Lyklema and Mysels (1965) measured the equilibrium thickness of a soap bubble as 73.1 nm when the bubble was stabilized by $8.7 \cdot 10^{-4}$ M sodium dodecyl sulfate and the hydrostatic pressure on the surface of the film was 66 N m^{-2}. In this experiment the thickness satisfies the condition of equilibrium between the hydrostatic pressure and the force of repulsion between double layers on the adjacent faces of the film, as given by Equation (82). Assuming that the adsorption of dodecyl sulfate ions at the air-solution interface gives a very high value of ψ_0, calculate the equilibrium bubble thickness predicted by this model. Criticize or defend the following propositions: If an appreciable concentration of indifferent electrolyte is added to the soap solution, the calculation just given is no longer feasible because (a) Equation (82) ceases to be valid for F_R and (b) van der Waals attraction between the two air masses also promotes film thinning.

Solution: The strategy here is to neglect van der Waals forces and to solve Equation (82) for h when $F_R = 66$ N m^{-2}. If ψ_0 is large enough, $\Upsilon_0 = 1$; furthermore, by Equation (40), $n_\infty = 1000 MN_A = 5.24 \cdot 10^{23}$ liter^{-1}. Assuming the bulk concentration is undiminished by adsorption, we obtain $\kappa = 3.29 \cdot 10^9 \cdot M^{1/2} = 9.70 \cdot 10^7$ m^{-1}. Therefore $66 = 64(5.24 \cdot 10^{23})(1.38 \cdot 10^{-23})(298) \exp[-(9.70 \cdot 10^7)h]$, from which we find $h = 7.88 \cdot 10^{-8}$ m $= 78.8$ nm. Considering that this calculation is insensitive to the actual potential at the surface, the agreement between this quantity and the experimental film thickness is acceptable.

The quantity F_R continues to be valid in the presence of indifferent electrolyte as long as the electrolyte is a $z:z$ type of compound. As a matter of fact, added electrolyte helps meet the requirement that $\psi_{h/2}$ be low, which actually improves the applicability of Equation (82).

Adding electrolyte will cause the film to thin by shortening the range of the repulsive force. At smaller distances of separation the van der Waals attraction is definitely increased and should be added (as force area^{-2}) to the pressure before attempting this kind of calculation. Even without added electrolyte, the air masses attract each other; neglecting this is another possible source of discrepancy between theory and experiment in this example. ■

* * *

11.7a.2 Energy of Repulsion Between Planar Double Layers

We discuss the topic of colloid stability and the role of electrostatic repulsion in imparting stability to a dispersion in Chapter 13. In order to evaluate fully the effect of electric charge on the stability of a colloidal dispersion, it is necessary to compare the magnitude of the repulsion between particles with the magnitude of the attraction between them. The attraction is most readily described in terms of potential energy; therefore the repulsion should be expressed in this form as well. For the approximation we have just discussed, this is not particularly difficult to evaluate. Since potential energy is given by the force times the distance through which it operates, we may write

$$d\Phi_R = -F_R dh \tag{84}$$

In this expression, $d\Phi_R$ is the increment in potential energy arising from a change in the

separation. The minus sign arises from the fact that the potential energy decreases with increasing separation.

Substituting the approximation given by Equation (82) for F_R gives

$$d\Phi_R = -64k_BTn_\infty\Upsilon_0^2 \exp(-h/\kappa^{-1})dh \tag{85}$$

a result that is easily integrated by recalling that $\Phi_R = 0$, when $h = \infty$. Integration yields

$$\Phi_R = 64k_BTn_\infty\kappa^{-1}\Upsilon_0^2 \exp(-h/\kappa^{-1}) \tag{86}$$

This particular form is limited in applicability to situations in which the separation of the surfaces is large compared to κ^{-1} and ψ_0 is large so that $\Upsilon_0 \approx 1$. As we did with the force of repulsion, we may write Φ_R as

$$\Phi_R = C_3 n_\infty^{1/2} \exp(-C_2 n_\infty^{1/2}) \tag{87}$$

since κ varies with $n_\infty^{1/2}$. In Equation (87), C_2 is the same as the one in Equation (83), but C_3 is a different constant that is proportional to C_1. Again we see that at large separations the potential energy of repulsion decreases with increasing electrolyte concentration. The continued emphasis on large separations is formally imposed by the use of approximation represented by Equation (67) in the development of this result. There are practical reasons for interest in this limit also. As colloidal particles approach one another, it is the outermost portions of their double layers that first interact. The outcome of such an encounter, then, is influenced by the interaction between the particles at large separations.

The derivation of Equation (86) is possible only because relatively simple approximations are available that permit $\psi_{h/2}$ to be solved explicitly and generate an integrable expression for Φ_R. This is not generally the case, however, so the approach used to reach Equation (86) is not applicable to most situations. Verwey and Overbeek have found another method for evaluating Φ_R, but the mathematics are tedious by this approach, involving numerical integrations. The method consists of calculating the free energy difference between particles separated by a distance h and infinitely separated. The interested reader will find details of this method discussed by Verwey and Overbeek in their 1948 book. As far as we are concerned, it is sufficient to note the following conclusions from the general theory:

1. A potential energy of repulsion may extend appreciable distances from surfaces, but its range is compressed (i.e., reduced) by increasing the electrolyte content of the system.
2. The conditions under which approaching particles first influence one another are at large distances of separation, for which the approximate relationship given by Equation (86) holds.
3. The sensitivity of aqueous lyophobic colloids to electrolyte content is due to the dependence of interparticle repulsion on this concentration.

What makes these generalizations significant is their relation to the discussion of the potential energy of attraction as developed in the last chapter. Item 1 means that, at least under some conditions, double-layer repulsion competes with van der Waals attraction in both magnitude and range to govern particle interactions. Item 2, we shall see, is similar to the attitude we take in discussing steric stabilization in Section 13.7, namely, that the interactions the particles experience at their first encounter are the easiest to handle and may determine their subsequent behavior. Item 3 indicates that the location and shape of the repulsion curves in Figure 10.1 are governed by the electrolyte concentration in the system. There are two aspects to this last point. The concentration of the potential-determining ions determines the potential at the wall via Equation (1), and the indifferent electrolyte content determines κ^{-1}, which in turn measures the range over which Φ_R decays. As we discussed in Section 10.2, the net potential energy curve—the result of attractive and repulsive components—is a convenient way to analyze coagulation phenomena. In Chapter 13 we combine the various results from this chapter and Chapter 10 to arrive at a quantitative theory for electrostatic stabilization against coagulation. The resulting theory is generally called the *DLVO theory* after B. Derja-

guin, L. D. Landau, E. J. W. Verwey, and J. Th. G. Overbeek, who initially brought the diverse elements of this theory together.

11.7b Interaction Between Spherical Double Layers: The Derjaguin Approximation

As we mentioned in our discussion of the planar double layers, solving the Poisson-Boltzmann equation for the potential variation in curved double layers is complex and requires numerical solutions in the general case. One can see then that the same holds in the case of interacting double layers as well. In addition, the force of interaction between curved surfaces cannot be expressed in terms of the osmotic pressure at the midpoint of separation, as we did in Section 11.7a. This is because electrical stresses (i.e., the Maxwell stresses) arising from the derivative of ψ do not become zero as they did in the case of planar double-layer interaction (see Equation (75)). However, the solution we obtained for interacting planar double layers can be used in combination with what is known as the *Derjaguin approximation* to obtain the potential energy of interaction between two spherical particles. The basic geometric idea behind the Derjaguin approximation is that the surface of the spheres (or curved surfaces, in general) may be divided into a collection of small stepped surfaces of plane geometry. These infinitesimal planes will become ring-shaped flat plates in the case of spherical particles. The equations for plane geometry we developed above can then be used for determining the interactions between corresponding rings on the two spheres, and these can be integrated over all the rings. This is illustrated in Example 11.4.

* * *

EXAMPLE 11.4 *Interaction Between Spherical Particles: The Use of the Derjaguin Approximation.* Spherical particles can be approximated by a stack of circular rings with planar faces as shown in Figure 11.8. Use Equation (86) to describe the repulsion between rings separated by a distance z and derive an expression for the repulsion between the two spheres of equal radius R_s. Assume that the strongest interaction occurs along the line of centers and make any approximations consistent with this to obtain the final result.

Solution: Indexing the various tiers of rings by i, we note that the increment of the interaction due to the ith ring is $d\Phi_R = \Phi_i dA_i$, with the area of the ring $2\pi h_i dh$. We eliminate dh as follows: The separation of the ith ring z_i is related to the distance of closest approach by the formula $(1/2)(z_i - s) = [R_s - (R_s^2 - h^2)^{1/2}]$, in which the factor (1/2) arises because part of the effect occurs at each surface. Since R_s is a constant, this last result may be differentiated and rearranged to give $[R_s(1 - h^2/R_s^2)^{1/2}]dz = 2hdh$. This may be combined with the expression for

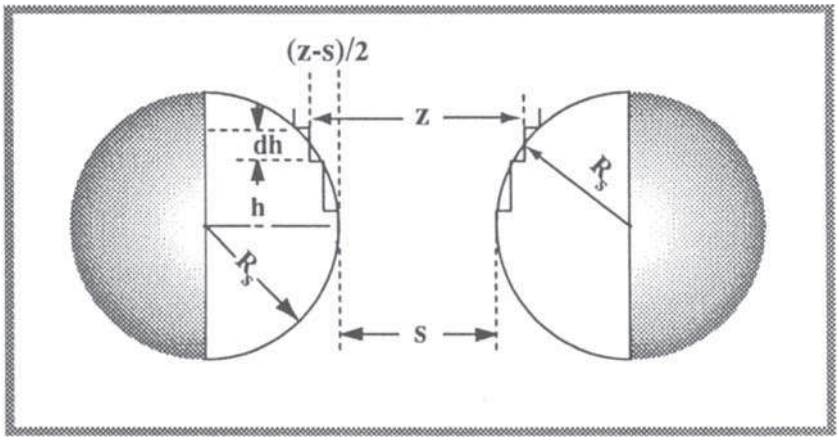


FIG. 11.8 Schematic illustration that shows how the repulsion between spheres may be calculated from the interaction between flat plates.

$d\Phi_R$ to yield $d\Phi_R = \pi R_s(1 - h^2/R_s^2)^{1/2}\Phi(z)dz$, where the functional notation has been added to Φ as a reminder that it is different for each ring. Substituting Equation (86) for $\Phi(z)$, we obtain

$$d\Phi_R = \pi R_s(1 - h^2/R_s^2)^{1/2}(64k_BTn_\infty\kappa^{-1}\Upsilon_0^2)\exp(-\kappa z)dz$$

If we further assume that $h^2/R_s^2 \ll 1$, this simplifies to

$$d\Phi_R = (64\pi R_s k_B T n_\infty \kappa^{-1}\Upsilon_0^2)\exp(-\kappa z)dz$$

The total potential energy of repulsion is given by integrating over all values of z. This is most readily done by assuming that z varies between s and infinity. This upper limit is justified because the potential function drops off exponentially with distance. Therefore large separations make a negligible contribution to the total. Integrating between these limits, we obtain

$$\Phi_R = (64\pi R_s k_B T n_\infty \kappa^{-2}\Upsilon_0^2)\exp(-\kappa s)$$

Under various circumstances, it may be justified to replace either the exponential or Υ_0 by their series approximations, thereby simplifying this result still further. ■

* * *

The Derjaguin approximation illustrated in the above example is suitable when $\kappa R^* > 10$, that is, when the radius of curvature of the surface, denoted by the radius R^*, is much larger than the thickness of the double layer, denoted by κ^{-1}. (Note that for a spherical particle $R^* = R_s$, the radius of the particle.) Other approaches are required for thick double layers, and Verwey and Overbeek (1948) have tabulated results for this case. The results can be approximated by the following expression when the Debye-Hückel approximation holds:

$$\Phi_R = (4\pi R_s^2 \varepsilon \psi_0^2)\exp(-\kappa s)/(s + 2R_s) \tag{88}$$

This expression, although seldom useful in the case of aqueous dispersions, is very useful in nonaqueous dispersions, for which the double layer is usually very thick.

11.7c Interaction Between Double Layers: Other Considerations

The above discussions illustrate that the interactions between overlapping electrical double layers depend on a number of considerations, such as the magnitude of the surface potential, the thickness of the double layer, and the type of electrolyte, among others. Moreover, the expressions that have been obtained here (and others that are available in the literature) depend on additional conditions that are determined by the approximations made in deriving the expressions.

In addition to all these, it is also important to keep in mind that the results depend also on what types of surface equilibrium conditions exist as the double layers interact. For example, when two charged surfaces approach each other, the overlap of the double layers will also affect the manner in which the charges on the surfaces adjust themselves to the changing local conditions. As the double layers overlap and get "compressed," the local ionic equilibrium at the surface may change, and this will clearly have an impact on the potential distribution and on the potential energy of interaction.

For example, if we assume for the moment that the surface ionic equilibrium is reestablished rapidly as the two surfaces approach each other, we can identify two limiting situations depending on the origin of the surface charges. If the surface charges are the result of adsorption of potential-determining ions, the surface potential will remain constant as the two surfaces approach each other. In this case, the surface charge densities will change. On the other hand, if the surface charges are the result of ionization, the charge densities will remain constant while the potentials readjust themselves. The results we have obtained in the previous sections are based on the former.

The differences between the above two limiting cases are not very significant when the separation distances are large, and one can get good qualitative and fairly quantitative estimates of interaction energies using the constant-potential condition. It is, however, important to know that differences exist, and that they may be important, depending on the types of surfaces involved. Overbeek (1952a, 1952b) provides additional discussions on this topic. Clearly, intermediate conditions (referred to as *charge regulation*) are also possible (and are more likely), although very little is known currently about dealing with such cases.

In addition to the above considerations, practical situations often demand that we consider *dissimilar* surfaces (i.e., the potentials or surface charges of the interacting surfaces may differ from each other). In the case of particles, one may also have different sizes. The method of deriving expressions for interaction energies in these cases does not involve any new fundamental concepts. In fact, the expressions we have derived for interactions between identical planar surfaces can be extended using simple graphical and geometrical arguments to interactions between dissimilar surfaces.

A good discussion of this may be found in Hunter (1987, Chapter 6). It is, however, helpful to list some expressions for interactions between dissimilar spherical particles since they are useful in studying heterocoagulation problems. Hogg et al. (1966) and Wiese and Healy (1970) have derived the following equations for spherical particles for low surface potentials and thin double layers:

$$\Phi_R^{\psi} = N_1\{N_2 f(s) + \ln[1 - \exp(2\kappa s)]\} \tag{89}$$

and

$$\Phi_R^{\sigma} = N_1\{N_2 f(s) - \ln[1 - \exp(2\kappa s)]\} \tag{90}$$

with

$$N_1 = \pi\varepsilon R_{s,1}R_{s,2}(\psi_{0,1}^2 + \psi_{0,2}^2)/(R_{s,1} + R_{s,2}) \tag{91}$$

$$N_2 = 2\psi_{0,1}\psi_{0,2}/(\psi_{0,1}^2 + \psi_{0,2}^2) \tag{92}$$

and

$$f(s) = \ln\left(\frac{1 + e^{-\kappa s}}{1 - e^{-\kappa s}}\right) \tag{93}$$

In the above equations, s is the shortest surface-to-surface separation distance, $R_{s,i}$ is the radius of the ith particle, $\psi_{0,i}$ is the corresponding surface potential, and the superscripts of Φ_R indicate whether the particles interact at constant potential (ψ) or constant surface charge (σ). These equations can be reduced to appropriate simpler forms when $R_{s,1} = R_{s,2}$ or $\psi_{0,1} = \psi_{0,2}$. In addition, interactions between a flat surface and a particle (needed, for example, when considering filtration or deposition problems) can also be obtained by taking one of the radii to infinity (plane).

11.8 "NOT-QUITE-INDIFFERENT" ELECTROLYTES: STERN ADSORPTION

At the beginning of this chapter we divided electrolytes into categories of potential determining and indifferent. We saw in Section 11.2 that the potential-determining ions are adsorbed at surfaces and determine the value of ψ_0 according to Equation (1). Throughout our discussion of the diffuse double layer, we have treated indifferent electrolytes as point charges with no chemical uniqueness except for their valence number. While this is a useful simplifying approximation, it underestimates the complexity of the "real world." The assumption that ions have no volume is acceptable for the bulk region of dilute solutions, but real ions cannot be drawn toward charged surfaces without crowding becoming a problem. At the inner edge of the diffuse part of the double layer some sort of saturation limit must be approached.

One way of handling this—according to O. Stern—is to divide the aqueous part of the double layer by a hypothetical boundary known as the *Stern surface*. The Stern surface is situated a distance δ from the actual surface. Figure 11.9 schematically illustrates the way this surface intersects the double layer potential and how it divides the charge density of the double layer.

The Stern surface is drawn through the ions that are assumed to be adsorbed on the charged wall. (This surface is also known as the *inner Helmholtz plane* [IHP], and the surface running parallel to the IHP, through the surface of shear (see Chapter 12) shown in Figure 11.9, is called the *outer Helmholtz plane* [OHP]. Notice that the diffuse part of the ionic cloud beyond the OHP is the diffuse double layer, which is also known as the *Gouy-Chapman*

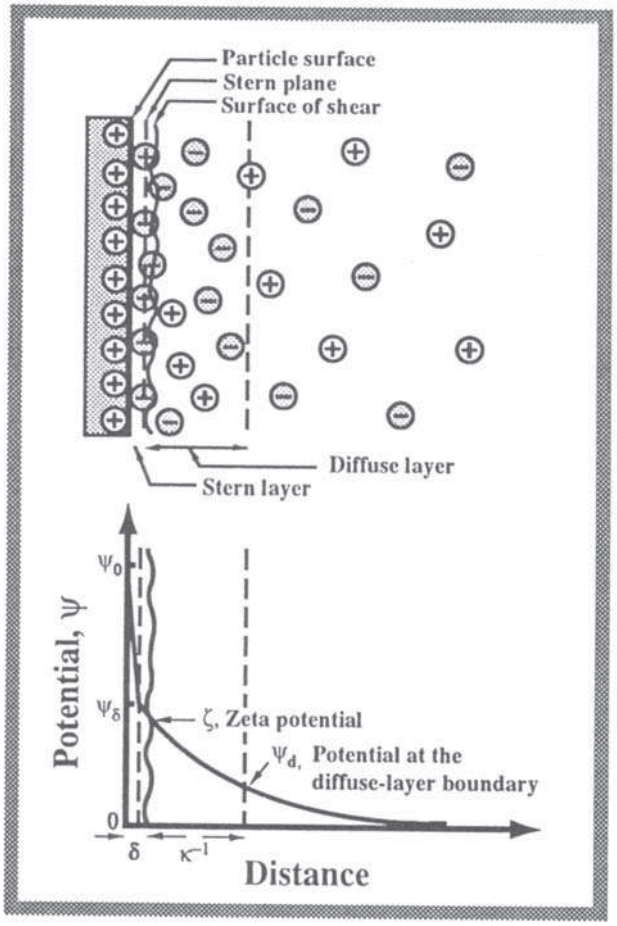


FIG. 11.9 Schematic illustration of the variation of potential with distance from a charged wall in the presence of a Stern layer. See Chapter 12 for discussion of surfaces of shear and zeta potential.

layer as mentioned in Section 11.3.) There are several consequences of assuming an adsorbed layer of ions at the surface:

1. An adsorption isotherm may be written for these ions that allows for surface saturation and thus introduces the idea of finite ionic size. The Langmuir isotherm (Equation (7.67)) is one expression that can be used for this purpose:

$$\theta = Kn_\infty/(1 + Kn_\infty) \tag{94}$$

   In this expression θ is the fraction of surface adsorption sites occupied, n_∞ is the concentration of the adsorbed ions in the solution, and K is a constant.

2. The constant in Equation (94) is easily shown to be proportional to a Boltzmann factor in which the exponential energy consists of two contributions: $ze\psi_\delta$, the electrical energy associated with the ion in the Stern layer, and ϕ, the specific chemical energy associated with the adsorption:

$$K \approx \exp\left[(ze\psi_\delta + \phi)/k_B T\right] \tag{95}$$

3. The Stern layer resembles the parallel plate capacitor model for the double layer. Therefore Equation (13) may be applied to this region:

$$(\psi_0 - \psi_\delta)/\delta = \sigma_\delta^*/\varepsilon_\delta \tag{96}$$

and ε_δ is the product of ε_0 and the relative dielectric constant that applies within the Stern layer.

4. The fraction of surface sites occupied equals the ratio $\sigma_\delta^*/\sigma_{\delta 0}^*$, where $\sigma_{\delta 0}^*$ is the charge density at surface saturation. Therefore, Equations (94) and (96) may be combined to give

$$(\psi_0 - \psi_\delta)/\delta = (1/\varepsilon_\delta)[\sigma_{\delta 0}^* Kn_\infty/(1 + Kn_\infty)] \tag{97}$$

This equation shows that the potential drop in the Stern layer increases with the concentration of the adsorbed ion and ultimately approaches a constant value when the surface is saturated.

Outside the Stern surface the double layer continues to be described by Equation (63) or one of its approximations. The only modifications of the analysis of the diffuse double layer required by the introduction of the Stern surface are that x be measured from δ rather than from the wall and that ψ_δ be used instead of ψ_0 as the potential at the inner boundary of the diffuse layer.

The Stern theory is difficult to apply quantitatively because several of the parameters it introduces into the picture of the double layer cannot be evaluated experimentally. For example, the dielectric constant of the water is probably considerably less in the Stern layer than it would be in bulk because the electric field is exceptionally high in this region. This effect is called *dielectric saturation* and has been measured for macroscopic systems, but it is difficult to know what value of ε_δ applies in the Stern layer. The constant K is also difficult to estimate quantitatively, principally because of the specific chemical interaction energy ϕ. Some calculations have been carried out, however, in which the various parameters in Equation (97) were systematically varied to examine the effect of these variations on the double layer. The following generalizations are based on these calculations:

1. As ϕ increases, K increases and the equilibrium amount adsorbed for any n_∞ value short of saturation also increases.
2. As the electrolyte concentration increases, increasing amounts of the potential drop occur in the Stern layer. This is true even if $\phi = 0$, which shows that specific chemical effects are not necessary for this result.
3. Values of ψ_δ that are much less than ψ_0 are possible in dilute solutions only if ϕ is relatively large.
4. The quantity ψ_δ varies only slightly with ϕ—although it is highly sensitive to n_∞—until ϕ is relatively large.

Values of the parameter ϕ may be experimentally evaluated for the mercury-water surface from electrocapillary studies. The displacement of the coordinates of the electrocapillary maxima in Figure 7.23 reflects differences in the intrinsic adsorbability of various ions. Electrocapillary studies reveal that the strength of specific adsorption at the mercury-water interface for some monovalent anions follows the order

$$I^- > SCN^- > Br^- > Cl^- > OH^- > F^-$$

whereas for some monovalent cations the order is

$$N(C_2H_5)_4^+ > N(CH_3)_4^+ > Tl^+ > Cs^+ > Na^+$$

In general, the specific adsorption of an ion is enhanced by larger size—and therefore larger polarizability—and lower hydration, which itself is a function of ion size. For example, among the ions just listed, the large I^- ion is the most strongly adsorbed, and the small but highly hydrated Na^+ ion is adsorbed least.

By allowing for surface saturation, the Stern theory overcomes the objection to the Gouy-Chapman theory of excessive surface concentrations. In so doing, however, it trades off one set of difficulties for another. In the Gouy-Chapman theory the functional dependence of ψ on x involves only the parameters κ and ψ_0. The former is known and the latter may be

evaluated—at least for some surfaces—by Equation (1) when the point of zero charge is known. The Stern modification of the double-layer picture introduces parameters that are not only difficult to estimate—such as δ and K (or ϕ)—but also specific characteristics of different ions. The generality of the Gouy-Chapman model is thus lost when the specific adsorption effects of the Stern theory are considered.

It is the outer portion of the double layer that interests us most as far as colloidal stability is concerned. The existence of a Stern layer does not invalidate the expressions for the diffuse part of the double layer. As a matter of fact, by lowering the potential at the inner boundary of the diffuse double layer, we enhance the validity of low-potential approximations. The only problem is that specific adsorption effects make it difficult to decide what value to use for ψ_δ.

In subsequent chapters it will be the potential in the diffuse double layer that concerns us. It can be described relative to its value at the inner limit of the diffuse double layer, which may be either the actual surface or the Stern surface. We continue to use the symbol ψ_0 for the potential at this inner limit. It should be remembered, however, that specific adsorption may make this quantity lower than the concentration of potential-determining ions in the solution would indicate. We see in Chapter 12 how the potential at some (unknown) location close to this inner limit can be measured. It is called the *zeta potential*.

REVIEW QUESTIONS

1. List some of the mechanisms by which a surface exposed to a liquid may acquire charges.
2. What is the *Helmholtz double layer*?
3. Explain the *Stern layer* and discuss its relation to the *inner Helmholtz plane*.
4. What is the *outer Helmholtz plane*?
5. What is the *diffuse layer*, and what is its relation to the *Gouy-Chapman theory* of electrical double layers?
6. Why is an electrical double layer called a "double layer"?
7. What is the physical significance of the *Poisson equation*?
8. What are the assumptions that are needed to obtain the *linearized Poisson-Boltzmann* (LPB) equation from the *Poisson-Boltzmann* equation, and under what conditions would you expect the LPB equation to be sufficiently accurate? What is the relation between the *Debye-Hückel approximation* and the LPB equation?
9. In what way does the Gouy-Chapman theory extend the Debye-Hückel approach?
10. Describe the physical significance of the Debye-Hückel parameter κ. How does it vary with the bulk concentration n_∞ for a 1 : 1 electrolyte? How does it vary with ionic charge for a constant bulk concentration?
11. What is the relation between the surface charge density and the potential in a double layer?
12. Why is there a repulsion between two surfaces with like charges in a liquid?
13. What is the so-called Derjaguin approximation?
14. Explain the difference between (electrical) potential and potential energy.
15. Why is it that the force of double-layer interactions for curved surfaces cannot be derived using osmotic pressure arguments as is done in the case of planar double layers?

REFERENCES

General References (with Annotations)

Crow, D. R., *Principles and Applications of Electrochemistry*, 4th ed., Blackie A and P, London, 1994. (Undergraduate level. An introduction to electrochemistry; requires only basic physical chemistry as prerequisite.)

Hunter, R. J., *Zeta Potentials in Colloid Science: Principles and Applications*, Academic Press, London, 1981. (Advanced level. The focus of this book is on the role of electrical double layers and zeta potential on electrophoresis and electroviscous effects. This volume presents some details on electrical double layers around nonspherical particles not discussed in the present book.)

Hunter, R. J., *Foundations of Colloid Science*, Vol. 1, Oxford University Press, Oxford, England, 1987. (Undergraduate level. Chapter 6 of this volume treats electrical double layers and

interactions. Some additional details on interactions between dissimilar electrical double layers are presented.)

Israelachvili, J. N., *Intermolecular and Surface Forces*, 2d ed., Academic Press, New York, 1991. (Graduate and undergraduate levels. The objective of this excellent reference is to relate atomic-and molecular-level interactions to surface forces. Chapter 12 discusses electrical double-layer forces and how they can be measured using the surface force apparatus (which we have described in Chapter 1).)

Kruyt, H. R. (Ed.), *Colloid Science, Vol. 1. Irreversible Systems*, Elsevier, Amsterdam, Netherlands, 1952. (A classic reference on colloids. Chapters 4 and 6 by Overbeek, cited below, discuss the electrochemistry of the double layer and double-layer interactions.)

Overbeek, J. Th. G., Electrochemistry of Double Layer. In *Colloid Science*, Vol. 1 (H. R. Kruyt, Ed.), Elsevier, Amsterdam, Netherlands, 1952a, pp. 115–193. (See the annotation under Kruyt 1952.)

Overbeek, J. Th. G., The Interaction Between Colloidal Particles. In *Colloid Science*, Vol. 1 (H. R. Kruyt, Ed.), Elsevier, Amsterdam, Netherlands, 1952b, pp. 245–277. (See the annotation under Kruyt 1952).

Verwey, E. J. W., and Overbeek, J. Th. G., *Theory of the Stability of Lyophobic Colloids*, Elsevier, Amsterdam, Netherlands, 1948. (Another classic reference, by two of the originators of the DLVO theory of colloidal interactions.)

Other References

Davies, J. T., *Proc. R. Soc.*, **208A**, 224 (1951).

Dube, G. P., *Indian J. Phys.*, **17**, 189 (1943).

Goodwin, J. W. (Ed.), *Colloidal Dispersions*, Royal Society of Chemistry, London, 1982.

Hogg, R., Healy, T. W., and Fuerstenau, D. W., *Trans. Faraday Soc.*, **62**, 1638 (1966).

Loeb, A. L., Overbeek, J. Th. G., and Wiersema, P. H., *The Electrical Double Layer Around a Spherical Colloid Particle*, Massachusetts Institute of Technology Press, Cambridge, MA, 1960.

Lyklema, J., and Mysels, K. J., *J. Am. Chem. Soc.*, **87**, 2539 (1965).

Wiese, G. R., and Healy, T. W., *Trans. Faraday Soc.*, **66**, 490 (1970).

PROBLEMS

1. Show that the one-dimensional Poisson equation for planar electrical double layers discussed in the text has the following analog in the case of spherically symmetric double layers:

$$\frac{1}{r^2}\frac{\partial}{\partial r}\left(r^2\frac{\partial\psi}{\partial r}\right) = -\frac{\rho^*}{\varepsilon}$$

   Obtain the corresponding Poisson-Boltzmann equation and the linearized version based on the Debye-Hückel approximation.

2. Solve the Poisson-Boltzmann equation for a spherically symmetric double layer surrounding a particle of radius R_s to obtain Equation (38) for the potential distribution in the double layer. Note that the required boundary conditions in this case are: $\psi = \psi_0$ at $r = R_s$, and $\psi \to 0$ as $r \to \infty$. (Hint: Transform $\psi(r)$ to a new function $y(r) = r\psi(r)$ before solving the LPB equation.)

3. Develop the equivalent of Equation (47) for the surface charge density of a spherical particle (i.e., the relation between σ^* and $(d\psi/dr)$ evaluated at the surface).

4. The viscosity of negatively charged colloidal agar (0.14% at 50°C) was studied with a variety of different electrolytes added.* The ratio of the specific viscosity ($\eta_{sp} = \eta/\eta_0 - 1$) in the presence of salt to η_{sp} without salt is given below for some of these salts at several concentrations:

*Kruyt, H. R., and deJong, H. G., *Kolloid Z.*, **100**, 250 (1922).

	$(\eta_{sp})_{salt}/(\eta_{sp})_{H_2O}$							
c (m Eq liter^{-1})	KCl	K_2SO_4	$K_4Fe(CN)_6$	$BaCl_2$	$SrCl_2$	$MgSO_4$	$La(NO_3)_3$	$Pt(en)_3(NO_3)_4$[a]
0.25	–	–	–	–	–	–	–	79.2
0.50	90.8	90.7	90.5	–	–	–	76.6	69.7
1.00	–	–	–	78.2	77.9	78.6	–	64.0
2.00	81.2	81.4	81.1	–	–	–	68.1	60.6
4.00	77.3	77.5	76.7	70.6	70.9	71.6	67.2	60.0

[a]en = ethylenediamine.

Discuss this electroviscous effect in terms of the concepts of this chapter and Chapter 4.

5. The deficiency of positive ions ($\Gamma_+ < 0$) adjacent to a positively charged planar surface may be evaluated as follows ($y = ze\psi/k_BT$):

$$\Gamma_+ \overset{(1)}{=} \int_0^\infty (c_0 - c_x)dx \overset{(2)}{=} \int_0^\infty (1 - e^{-y})dx \overset{(3)}{=} c_0 \int_0^\infty (1 - e^{-y})\frac{dx}{dy}dy \overset{(4)}{=} c_0 \int_{\psi_0}^0 \frac{(1 - e^{-y})dy}{dy/dx}$$

$$\overset{(5)}{=} \frac{c_0}{\kappa} \int_{\psi_0}^0 \frac{1 - e^{-y}}{e^{-y/2} - e^{y/2}}dy \overset{(6)}{=} -\frac{c_0}{\kappa} \int_{\psi_0}^0 e^{-y/2}dy \overset{(7)}{=} \frac{2c_0}{\kappa}\left|1 - \exp\left(\frac{ze\psi_0}{2k_BT}\right)\right|$$

Present the physical and/or mathematical justification for equalities (1)–(7) in this sequence. Show that the final result is equivalent, at high surface potentials, to emptying a region of thickness $2\kappa^{-1}$ of ions possessing the same charge as the wall.

6. If a soap film is sufficiently thin, its equilibrium thickness is the result of the double-layer repulsion, given by Equation (82), and van der Waals attraction, given by

$$F_A = \frac{\partial \Phi_A}{\partial d} = \frac{A}{6\pi}d^{-3}$$

according to Equation (10.63). These conditions are satisfied by certain films studied by Lyklema and Mysels,* who obtained the following results with 1 : 1 electrolyte:

Concentration (mole liter^{-1})	0.103	0.066	0.0197
Thickness of aqueous layer (Å)	91	94	153
Thickness of entire film (Å)	123	126	185

Use the thickness of the aqueous layer in Eq. (82) to calculate F_R per unit area (assume $\Upsilon_0 = 1$). By equating this quantity to F_A per unit area (just given) and using the total film thickness, estimate A for each of these data. Explain why two different values are used for d in this calculation.

7. Using the average value of A you determined in Problem 6, criticize or defend the proposition that van der Waals forces are negligible compared to hydrostatic forces when the hydrostatic forces equal 660 dyne cm^{-2} in a film for which the total thickness is 763 Å. Note that this is the assumption made in Example 11.3. Qualitatively reexamine the last question in light of the results of this problem.

8. Criticize or defend the following propositions: The DLVO theory should apply to particles dispersed in nonaqueous media once ε and A for the solvent have been included in the relevant expressions. Since ion concentrations are low in media with low dielectric constant, κ^{-1} will be very large for such systems. For a concentrated colloid the mean interparticle spacing may be less than κ^{-1}. In such a case it is more plausible to picture a particle approaching a "target" as traveling along a potential energy plateau rather than facing a potential energy barrier.

   Comment on the relevancy of these propositions to the observation† that a 15% (by volume) water-in-benzene emulsion stabilized by the calcium salt of didodecylsalicylic acid has a ψ_0 of ~130 mV, yet breaks immediately after preparation.

*Lyklema, J., and Mysels, K. J., *J. Am. Chem. Soc.*, **87**, 2539 (1965).

†Albers, W., and Overbeek, J. Th. G., *J. Colloid Sci.*, **14**, 501 (1959).

9. The interfacial tension at the electrocapillary maximum for several electrolytes in dimethylformamide (DMF) solutions has been measured as a function of the electrolyte concentration:*

	γ_{max} (dyne cm^{-1})		
log c	KI	LiCl	KSCN
0	354	366	370
−0.3	356	367	371
−1.0	361	369	373
−1.3	364	370	374

Use these results to estimate the relative adsorbabilities of the I^-, Cl^-, and SCN^- ions from DMF. How does the sequence of anion adsorbabilities compare with that from aqueous solution as given in Section 11.8? More comprehensive electrocapillary data suggest that SCN^- is more solvated in DMF than in water. Is this consistent with the adsorbability series just compared?

10. A negatively charged AgI dispersion was caused to coagulate by the addition of various electrolytes. The concentrations of several divalent metal nitrates needed to produce coagulation are as follows:†

Salt	$Mg(NO_3)_2$	$Ca(NO_3)_2$	$Sr(NO_3)_2$
$c \times 10^3$ (mole liter^{-1})	2.60	2.40	2.38
Salt	$Ba(NO_3)_2$	$Zn(NO_3)_2$	$Pb(NO_3)_2$
$c \times 10^3$ (mole liter^{-1})	2.26	2.50	2.43

That these different compounds produce the same effect at so nearly the same concentration argues that the principal cause of the effect is electrostatic. Use the average of these concentrations to calculate (a) the value of κ at which this system coagulates, (b) the force of repulsion (Equation (82)), and (c) the potential energy of repulsion (Equation (86)) when two planar surfaces are separated by a distance of 10 nm. For the purpose of calculation in parts (b) and (c), ψ_0 may be taken as 100 mV. Comment on the applicability of these equations to the physical system under consideration.

11. The slight differences in the concentrations of divalent cations required to flocculate the AgI sol of the preceding problem may be attributed to differences in the adsorbability of these cations at the AgI-solution interface. Use the data of Problem 10 to rank the cations with respect to their tendency to adsorb. Is there a correlation between adsorbability and ion size and/or hydration? List any references consulted for data concerning the last two quantities.

12. Once the significance of the midpoint between two parallel plates for the force between those plates is established, there are several ways of arriving at Equation (79). One argument is that the plates shown in Figure 11.7 function as a semipermeable membrane, sustaining a concentration difference between $x = h$ and the outer region of the solution. Use Equations (3.25) and (27) to show that the osmotic pressure across this "semipermeable membrane" is given by Equation (79).

*Bezuglyi, V. D., and Korshikov, L. A., *Electrokhimiya,* **3**, 390 (1967).

†Kruyt, H. R., and Klompe, M. A., *Kolloid Beihefte,* **54**, 484 (1942).

12

Electrophoresis and Other Electrokinetic Phenomena

There is a constant attraction to the South . . . yet the hampering effect of the southward attraction is quite sufficient to serve as a compass in most parts of our earth.

From Abbott's *Flatland*

12.1 INTRODUCTION

The word *electrokinetic* implies the combined effects of motion and electrical phenomena. Specifically, our interest in this chapter centers on those processes in which a relative velocity exists between two parts of the electrical double layer. This may arise from the migration of a particle relative to the continuous phase that surrounds it. Alternatively, it could be the solution phase that moves relative to stationary walls.

12.1a What Are Electrokinetic Phenomena?

There are four phenomena that are normally grouped under the term *electrokinetic phenomena*.

1. *Electrophoresis*: This refers to movement of a particle (and any material attached to the surface of the particle) relative to a stationary liquid under the influence of an applied electric field.
2. *Electroosmosis*: Here, the liquid (an electrolyte solution) moves past a charged surface (e.g., the surface of a capillary tube or through a porous plug) under the influence of an electric field. Thus, electroosmosis is the complement of electrophoresis. The pressure needed to balance the electroosmotic flow is known as *electroosmotic pressure*.
3. *Streaming potential*: This is a consequence of the electric field created when a liquid (an electrolyte) is forced to flow past a charged surface. The situation here is the opposite of electroosmosis.
4. *Sedimentation potential*: This is due to the electric field created by charged particles sedimenting in a liquid. This situation is the opposite of electrophoresis.

The first three electrokinetic processes are our concern in this chapter, with the emphasis on electrophoresis.

12.1b Why Study Electrokinetic Phenomena?

In each case the electrokinetic measurements can be interpreted to yield a quantity known as the *zeta* (ζ) *potential*. It is important to note that this is an experimentally determined potential measured in the double layer near the charged surface. Therefore it is the empirical equivalent

to the surface potentials discussed in the Chapter 11. We saw in Chapter 10 how the stability of a hydrophobic colloid depends on the relative magnitude of the potential energies of attraction and repulsion between a pair of particles approaching a collision with each other. Therefore the electrokinetic or ζ potential has a direct bearing on the material of the previous two chapters and the following one as far as the theory and practice of colloid stability are concerned.

In addition to the above, there are a number of phenomena or processes of practical utility that are based on principles of electrokinetic processes. We already saw in Chapter 1 the possibility of developing image displays based on electrophoretic motion (i.e., electrophoretic image displays, Vignette I.4). There are so-called liquid immersion development devices in which the image that needs to be copied is transferred onto a plate or paper as a pattern of charges so that the transferred image could be developed by exposing the plate or paper to a dispersion of appropriately charged dye particles (Lyne and Aspler 1982). The method is actually an *electrophoretic* development process and is highlighted further in Vignette XII. Electroosmosis, for instance, has also been used in a number of practical applications such as dewatering of soils for construction purposes and dewatering of waste sludges and may also be useful for controlling toxic leakage in waste sites through the injection of detoxifying agents (Probstein 1994). We list some more applications in Section 12.11.

VIGNETTE XII ELECTROKINETIC PHENOMENA IN MODERN TECHNOLOGY: Electrophotography

When one thinks of electrokinetic phenomena in the context of a first-level course on colloid and surface chemistry, the first thought that probably comes to mind is the use of such phenomena to measure zeta potentials and charges of colloidal species. But, as we have already seen in Chapter 1 and as we see later in this chapter, electrokinetic phenomena play a significant role in many other applications. We take a look at one such application here and see why the topics we consider in this chapter and in others are important in that context.

Using photoconductive insulating surfaces to produce latent electrostatic images was suggested by Carlson over 50 years ago (Carlson 1938, 1940). The image thus produced is developed using toner particles of colloidal size and is subsequently transferred to paper. This forms the basis of *xerography*, a "dry" copying technique. (A modification of this process in which paper with a photoconductive coating containing a ZnO binder is used directly is known as *electrofax*. It is seldom used today.)

There are a number of advantages for using *liquid-developing* processes instead of "dry" processes: (a) the possibility of high resolution using fine-grain suspensions, (b) minimizing "edge effect" (namely, the partially higher image density caused by stronger electric field in the edge regions of the latent image) through the control of the conductivity of the developer, and (c) the possibility of compact equipment design. The liquid-development process was first proposed by Metcalfe (1955, 1956) and seeks to develop the latent image by *electrophoretic* particle deposition from a colloidal dispersion. Theories of the liquid-development process rest on the electrophoretic mobility equations (e.g., Henry's equation) we derive in this chapter and are presented by Kurita (1961) and Ohyama et al. (1961), among others (see Kitahara and Watanabe 1984).

Let us focus here on *some* of the *general issues* that a colloid scientist should be concerned with in this context: (a) the toner must have stable polarity and stable charges on the particles and must be stable against settling; (b) the liquid must have low ion concentration and a low dielectric constant to avoid "electrical leakage" of the electrostatic image; and (c) color, concentration, and distribution of the pigment particles inside the toner particles must be such that the quality of the developed image is high. In order to guarantee these, information on physicochemical properties of the liquid developer (e.g., viscosity, dielectric constant, etc.), the mechanisms responsible for the charges on the toner particles, and the interaction forces responsible for stabilization (usually steric hindrance and polymer-mediated

forces arising from polymer additives) must be examined. These factors also determine the electrophoretic mobility of the particles and are, therefore, important since the electrophoretic mobility, in turn, determines the image density and the developing time (Kitahara and Watanabe 1984, Chapter 17).

12.1c Focus of This Chapter

The focus of this chapter is to present the basics of electrokinetic phenomena and to provide a working knowledge of the subject. Some classical and some novel applications of these phenomena are also summarized at the end of the chapter.

1. We begin with the definition of electrophoretic mobility, namely, the velocity of a charged particle per unit field strength (Section 12.2).
2. Our next task is to relate this mobility to the zeta potential. This requires a number of assumptions, and we focus on the most important of these. We derive the equations for thick electrical double layers (Section 12.3) and for thin double layers (Section 12.4) first and then examine how intermediate cases can be studied (Section 12.5).
3. Following this we derive the equation for electroosmotic flow and relate it to the zeta potential of the charged surface (Section 12.6). Section 12.7 focuses on the streaming potential and compares the zeta potentials obtained by the different methods.
4. Although the ζ potential is undoubtedly an important quantity in colloid chemistry, it is not totally free of ambiguity. The problem is this: It is not clear at what location within the double layer the potential is measured. The derivations of this chapter show that the ζ potential is the double-layer potential close to the surface, but the precise quantitative meaning of close cannot be defined. We examine this briefly in Section 12.8.
5. Following the above, we address some of the experimental aspects of electrophoresis. In this context, a few other forms of electrophoresis (e.g., moving boundary electrophoresis and zone electrophoresis) are described briefly. The last of these is used when separation of charged species, rather than the measurement of mobilities, is the item of interest (Section 12.9).
6. One of the applications of zeta potential measurements is in the determination of surface charges of colloids such as proteins. We look into this briefly in Section 12.10 and derive the equation connecting the surface charge to the zeta potential under some simplifying assumptions.
7. Finally, a number of examples of applications of electrokinetic phenomena are described briefly in Section 12.11.

Most textbooks on colloids usually devote no more than a chapter or two to electrokinetic phenomena since so many other topics also need to be covered for a balanced introduction to colloid and surface chemistry. A recent textbook (Masliyah 1994) focuses almost exclusively on electrokinetic phenomena and may be consulted for details not presented here.

12.2 MOBILITIES OF SMALL IONS AND MACROIONS IN ELECTRIC FIELDS: A COMPARISON

The fact that positive ions migrate toward the cathode and negative ions migrate toward the anode is so well known as to be virtually self-evident. It seems equally evident, therefore, that positively and negatively charged colloidal particles should display similar migrations. Indeed, this is the case. Because we are relatively familiar with the conductivity of simple electrolytes, we start our discussion of electrokinetic phenomena with a comparison of the mobilities of the particles in the small ion and macroion size domains.

12.2a Mobility of An Ion in An Electric Field

An isolated ion in an electric field experiences a force directed toward the oppositely charged electrode. This force is given by the product of the charge of the ion q times the electric field E:

$$F_{el} = qE \tag{1}$$

In SI units, E is expressed in volt meter^{-1} and q in coulombs, so F_{el} is correctly given in newtons, since C V = J = N m. The cgs unit system, which is widely encountered in older references, requires dividing the right-hand side of Equation (1) by a factor of about 300 since 299.8 V = 1.0 statvolt. Use of Equation (1) is limited to situations in which the electric field at the ion is due to the applied potential gradient only, undisturbed by the effects of other ions in the solution (i.e., infinite dilution).

An ion in an electric field thus experiences an acceleration toward the oppositely charged electrode. However, its velocity does not increase without limit. An opposing force due to the viscous resistance of the medium increases as the particle velocity increases:

$$F_{vis} = fv \tag{2}$$

where f is the *friction factor* (see Equation (2.2)). A stationary-state velocity is established quite rapidly in which these two forces are equal:

$$v = qE/f \tag{3}$$

The situation is thus very much like the sedimentation velocity discussed in Chapter 2 in which the gravitational forces on a particle are opposed by viscous resistance.

As a further development, we may tentatively substitute the value for f given by Stokes's law (Equation (2.8)) to obtain

$$v = qE/(6\pi\eta R_s) \tag{4}$$

where R_s is the radius of the particle, assumed to be a sphere by this substitution. The charge of a simple ion can be written as the product of its valence z times the electron charge e:

$$q = ze \tag{5}$$

Substitution of this result into Equation (4) yields

$$v = zeE/(6\pi\eta R_s) \tag{6}$$

The *velocity per unit field* is defined as the *mobility* u of the ion:

$$u = v/E \tag{7}$$

For simple ions mobilities are typically on the order of 10^{-8} m s^{-1}/V m^{-1} (m^2 V^{-1} s^{-1}). It is shown in physical chemistry (see, for example, Atkins 1994) that the mobility of an ion is directly proportional to its equivalent conductance λ_{i0}:

$$u_i = \lambda_{i0}/\mathfrak{F} \tag{8}$$

where $\mathfrak{F}$ is the *Faraday constant*. We have stipulated the conductance at infinite dilution (subscript 0) as a reminder that these relationships all refer to isolated ions. When ion mobilities are analyzed by Equation (6), quite reasonable values for the radii of the hydrated ions are obtained.

12.2b Electrophoretic Mobility of Macroions

The success and relative simplicity of conductivity as a method of study for small ions prompt us to extend these ideas to particles in the colloidal size range. For the purpose of our discussion here, we can treat a charged colloidal particle as an ion of large charge, hence the name *macroion*. However, we identify shortly some of the differences between such macroions and small ions with respect to their response to an applied electric field. For certain colloids the experimental aspects of studying mobilities are simpler than for small ions because of the

possibility of measuring the velocity of high-contrast particles by direct microscopic observation. If the velocity and the field responsible for the migration are known, the mobility of the colloid may be evaluated directly from Equation (7). When the term is applied to colloidal particles, the mobility is known specifically as the *electrophoretic mobility*. In this case the overall phenomenon is known as *electrophoresis*, and the specific experimental technique of direct microscopic observation of the electrophoretic mobility is called *microelectrophoresis*. This and other electrophoretic techniques are described in more detail in Section 12.9.

Although the electrophoretic mobility is—at least in some cases—a readily measured quantity, its interpretation is considerably more difficult for colloidal particles than for small ions. First, we realize that the charge carried by a colloidal particle is not a constant known quantity as is the case for simple ions. This prevents us from using Equation (6) to evaluate R_s, but suggests instead a method by which the charge might be determined. Suppose, for example, we substitute Equation (2.32) for f rather than use Stokes's law for this quantity. Then the electrophoretic mobility is given by

$$u = ze/(k_BT/D) = zeD/(k_BT) \tag{9}$$

It appears that the combination of electrophoresis and diffusion experiments would allow for the evaluation of the charge carried by the macroion. Again, the situation is reminiscent of the procedures described in Chapter 2 in which sedimentation and diffusion experiments were combined. However, this is only the beginning of the difficulty. The validity of Equation (9) is limited to the situation in which a charged particle is considered in isolation from other ions. A charged colloid will be surrounded by an electrical double layer, as we saw in Chapter 11. Thus the field at the particle is modified by the potential of the double layer; that is, the migrating unit is the charged colloidal particle along with its electrical double layer just as the same composite is the kinetic unit in coagulation.

Therefore this strategy for determining the charge of a colloid from electrophoresis measurements is invalid except for the rather special case of determining the conditions of zero charge for the colloid. We return to a discussion of this point in Section 12.10.

In Chapter 11 we discussed the structure of the double layer in terms of the potential at the surface. This background plus the realization that the ion atmosphere also contributes to the electrophoretic mobility of a colloid suggests that potential rather than charge is the more useful parameter to pursue. This is the topic of the following section. In discussing the migration of charged colloidal particles through a solution containing small ions, it is convenient to begin by distinguishing between two extremes of particle size. We saw in Chapter 11 that the parameter κ^{-1} (see Table 11.3) is a convenient way to characterize the "thickness" of the ion atmosphere near a surface. Distances are regarded as large or small relative to this quantity, as discussed in Section 4.8. For simplicity we restrict our consideration to spherical, nonconducting particles (of radius R_s) and begin by examining the two extremes of very small and very large particles. These designations acquire specific meaning when compared to κ^{-1}, taken as a standard length. Thus the two cases we consider first are those in which R_s/κ^{-1} (or simply κR_s) is either small or large.

Figure 12.1 shows schematically the shape of the flow streamlines around the particle in the two cases. The dashed line in the figure is displaced from the surface of the spherical particles by an amount κ^{-1}. In Figure 12.1a, R_s is small (compared to κ^{-1}) and the streamlines undergo negligible displacement. In Figure 12.1b, on the other hand, the streamlines follow the contours of the particle nearly tangentially. Since matter is conserved, a flow streamline that carries matter into a volume element must also carry matter out of that volume element. Charge is also conserved, so the same number of lines of force must enter and leave a volume element. Accordingly, the streamlines shown schematically in Figure 12.1 may also be regarded as describing the electric field in the neighborhood of small and large particles.

12.3 ZETA POTENTIAL: THICK ELECTRICAL DOUBLE LAYERS

We know from Chapter 11 that the potential drops gradually with distance from a charged surface, its range decreasing with increasing electrolyte content. Most of the expressions

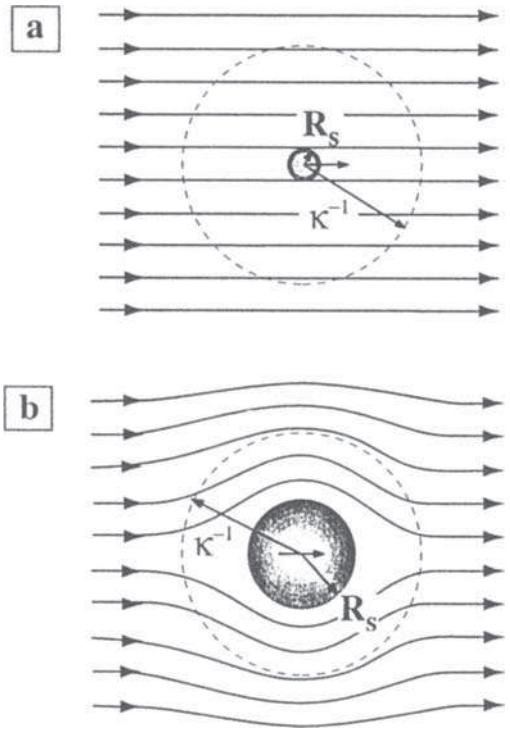


FIG. 12.1 Streamlines (which also represent the electric field) around spherical particles of radius R_s. The dashed lines are displaced from the surface of the spheres by the double-layer thickness κ^{-1}. In (a) κR_s is small; in (b) κR_s is large.

developed in Chapter 11, however, describe the situation adjacent to a planar wall. In the present context we need to know how the potential varies with distance from the surface of a sphere, as discussed briefly in Section 11.4c. We examine this a little closely before proceeding to discuss how the results are used for understanding motion of spherical colloidal particles in electric fields.

12.3a Potential Distribution Around a Spherical Particle

The Poisson equation (see Equation (11.18)) gives the fundamental differential equation for potential as a function of charge density. The Debye-Hückel approximation may be used to express the charge density as a function of potential as in Equation (11.28) if the potential is low. Combining Equations (11.24) and (11.32) gives

$$\frac{1}{r^2}\frac{d}{dr}\left(r^2\frac{d\psi}{dr}\right) = \frac{e^2}{\varepsilon k_B T}\left(\sum_i z_i^2 n_i\right)\psi = \kappa^2\psi \tag{10}$$

Remember that ε is equal to the product of ε_0 times ε_r with $\varepsilon_0 = 8.85 \cdot 10^{-12}\ C^2\ J^{-1}\ m^{-1}$; for water at 25°C, $\varepsilon_r = 78.54$. Because of its importance to the present material, we repeat the defining expression for κ as given originally by Equation (11.41):

$$\kappa = \left(\frac{1000\ e^2 N_A}{\varepsilon k_B T}\sum_i z_i^2 M_i\right)^{1/2} \tag{11}$$

or, in terms of ionic strength $I = (1/2)\Sigma_i z_i^2 M_i$,

$$\kappa = \left(\frac{2000\, e^2 N_A I}{\varepsilon k_B T} \right)^{1/2} \tag{12}$$

Remember that Table 11.3 contains some useful numerical values of κ at different concentrations of various electrolytes. Equation (10) is the basic relationship of the Debye-Hückel theory and may be integrated as follows. The variable x is introduced with the following definition:

$$x = r\psi \tag{13}$$

Thus Equation (10) may be written

$$\frac{d}{dr}\left(r^2 \frac{d\psi}{dr} \right) = \kappa^2 r x \tag{14}$$

Now let us consider the incorporation of Equation (13) into the left-hand side of Equation (14):

$$\frac{d\psi}{dr} = \frac{d(x/r)}{dr} = \frac{1}{r}\frac{dx}{dr} - \frac{x}{r^2} \tag{15}$$

and

$$\frac{d}{dr}\left(r^2 \frac{d\psi}{dr} \right) = \frac{d}{dr}\left(r \frac{dx}{dr} - x \right) = r \frac{d^2x}{dr^2} \tag{16}$$

Combining Equations (14) and (16) gives

$$d^2x/dr^2 = \kappa^2 x \tag{17}$$

for which a general solution is

$$x = A \exp(-\kappa r) + B \exp(\kappa r) \tag{18}$$

as may be readily verified by differentiation. Replacing x in this equation by its definition in Equation (13) gives

$$\psi = \frac{A \exp(-\kappa r)}{r} + \frac{B \exp(\kappa r)}{r} \tag{19}$$

Since $\psi \to 0$ as $r \to \infty$, it is apparent that $B = 0$.

To evaluate A we proceed as follows. In the limit of infinite dilution—that is, as $\kappa \to 0$—the potential around the charged particle is given by the expression for the potential of an isolated charge. Elementary physics gives this as

$$\psi = \frac{1}{4\pi\varepsilon}\frac{q}{r} \tag{20}$$

a distance r from a charge q. As $\kappa \to 0$, Equations (19) and (20) must converge; therefore A must equal $(q/4\pi\varepsilon)$. The general expression for potential around a spherical particle at low potential may be written as

$$\psi = \frac{q}{4\pi\varepsilon r} \exp(-\kappa r) \tag{21}$$

Notice that if we use the condition that $\psi = \psi_0$ at $r = R_s$ we will recover the result developed in Section 11.4c for a spherical particle of finite size (given by radius R_s).

As a reminder that the level of approximation in Equation (21) is the same as that of the Debye-Hückel limiting law, the following example continues from this last result to the Debye-Hückel expression for the mean ionic activity coefficient of an electrolyte solution.

* * *

EXAMPLE 12.1 *Debye-Hückel Expression for Ionic Activity Coefficients.* The Debye-Hückel limiting law attributes all of the nonideality of an electrolyte solution to electrostatic effects

associated with the diffuse double layer. As a way to isolate this effect, consider the hypothetical process of discharging an ion in a solution of concentration c_1 moving it to a solution of concentration c_2, and then recharging it in the new solution. The individual steps and general expressions for the associated free energy changes are listed below, with the subscripts 1 and 2 indicating the two concentration conditions:

$$q = ze \text{ at } c_1 \rightarrow q = 0 \text{ at } c_1 \qquad \Delta G = N_A \int_{ze}^{0} \psi_1 \, dq$$

$$q = 0 \text{ at } c_1 \rightarrow q = 0 \text{ at } c_2 \qquad \Delta G = RT \ln (c_2/c_1)$$

$$q = 0 \text{ at } c_2 \rightarrow q = ze \text{ at } c_2 \qquad \Delta G = N_A \int_{0}^{ze} \psi_2 \, dq$$

$$\text{Net: } q = ze \text{ at } c_1 \rightarrow q = ze \text{ at } c_2 \qquad \Delta G_{net} = RT \ln (a_2/a_1)$$

where a_i is the activity of component i and can be written as $a_i = \gamma_i c_i$ in terms of the *activity coefficient* γ_i. Derive the Debye-Hückel expression for the activity coefficient γ, assuming Equation (21) describes ψ and that solution 2 is dilute and solution 1 very dilute.

Solution: The activities in the expression for ΔG_{net} can be replaced by the product of concentrations and activity coefficients:

$$\Delta G_{net} = RT \ln (\gamma_2 c_2/\gamma_1 c_1) = RT \ln (\gamma_2/\gamma_1) + RT \ln (c_2/c_1)$$
$$= N_A \int_{ze}^{0} \psi_1 \, dq + RT \ln (c_2/c_1) + N_A \int_{0}^{ze} \psi_2 \, dq$$

Since solution 1 is very dilute, γ_1 can be set equal to unity, in which case

$$RT \ln \gamma_2 = N_A \int_{ze}^{0} \psi_1 \, dq + N_A \int_{0}^{ze} \psi_2 \, dq$$

The activity coefficient for (dilute) solution 2 is therefore obtained by evaluating the integrals based on Equation (21). Using a series approximation (see Appendix A) for the exponential in Equation (21) and retaining only the leading term for solution 1, where κ_1 (i.e., c_1) is very small, and the first two terms for solution 2, where κ_2 is small but larger than for 1, we obtain $\psi_1 = q/4\pi\varepsilon r$ and $\psi_2 = (q/4\pi\varepsilon r)(1 - \kappa_2 r)$. With these substitutions the integrals can be evaluated as follows:

$$RT \ln \gamma_2 = (N_A/4\pi\varepsilon r) \left(\int_{ze}^{0} q \, dq + \int_{0}^{ze} q \, dq - \kappa_2 r \int_{0}^{ze} q \, dq \right) = N_A \kappa_2 (ze)^2/8\pi\varepsilon$$

Substituting Equation (12) for κ yields

$$\ln \gamma_2 = -(N_A z^2 e^2/8\pi\varepsilon RT) (2000 e^2 N_A/\varepsilon k_B T)^{1/2} I^{1/2}$$

For aqueous solutions at 25°C this becomes $\log_{10} \gamma_2 = 0.0509 z^2 I^{1/2}$, or, with a bit more argumentation, $\log_{10} \gamma_\pm = -0.0509 z_+ z_- I^{1/2}$, which is the result sought. ■

* * *

12.3b Zeta Potential

Next, let us consider the application of Equation (21) to a particle migrating in an electric field. We recall from Chapter 4 that the layer of liquid immediately adjacent to a particle moves with the same velocity as the surface; that is, whatever the relative velocity between the particle and the fluid may be some distance from the surface, it is zero at the surface. What is not clear is the actual distance from the surface at which the relative motion sets in between the immobilized layer and the mobile fluid. This boundary is known as the *surface of shear*. Although the precise location of the surface of shear is not known, it is presumably within a couple of molecular diameters of the actual particle surface for smooth particles. Ideas about adsorption from solution (e.g., Section 7.7) in general and about the Stern layer (Section 11.8) in particular give a molecular interpretation to the stationary layer and lend plausibility to the statement about its thickness. What is most important here is the realization that the surface of shear occurs well within the double layer, probably at a location roughly equivalent to the Stern surface. Rather than identify the Stern surface as the surface of shear, we define the potential at the surface of shear to be the zeta potential ζ. It is probably fairly close to the

Stern potential ψ_δ in magnitude, and definitely less than the potential at the surface ψ_0. The relative values of these different potentials are shown in Figure 12.2.

Distances within the double layer are considered large or small, depending on their magnitude relative to κ^{-1}. Thus in dilute electrolyte solutions, in which κ^{-1} is large, the surface of shear—which is close to the particle surface even in absolute units—may be safely regarded as coinciding with the surface in units relative to the double-layer thickness. Therefore, in the case for which κ^{-1} is large (or κ small), Equation (21) becomes

$$\zeta = \frac{q}{4\pi\varepsilon R_s} \exp\ (-\kappa R_s) \tag{22}$$

where R_s is the actual radius of the particle.

Since this result applies only when κ is small, the exponential may be expanded (see Appendix A) to give

$$\zeta \approx \frac{q}{4\pi\varepsilon R_s} \frac{1}{\exp\ (\kappa R_s)} \approx \frac{q}{4\pi\varepsilon R_s} \frac{1}{(1 + \kappa R_s)} \tag{23}$$

This result may also be written

$$\zeta = \frac{q}{4\pi\varepsilon R_s} \frac{\kappa^{-1}}{R_s + \kappa^{-1}} \tag{24}$$

which is the same as

$$\zeta = \frac{q}{4\pi\varepsilon R_s} - \frac{q}{4\pi\varepsilon\ (R_s + \kappa^{-1})} \tag{25}$$

This last result is interesting because it may be interpreted as the sum of two superimposed potentials: one arising from a charge q on a surface of radius R_s and a second arising from a charge $-q$ on a sphere of radius $(R_s + \kappa^{-1})$. This is the net potential between two concentric spheres carrying equal but opposite charges and differing in radius by an amount κ^{-1}. Such a

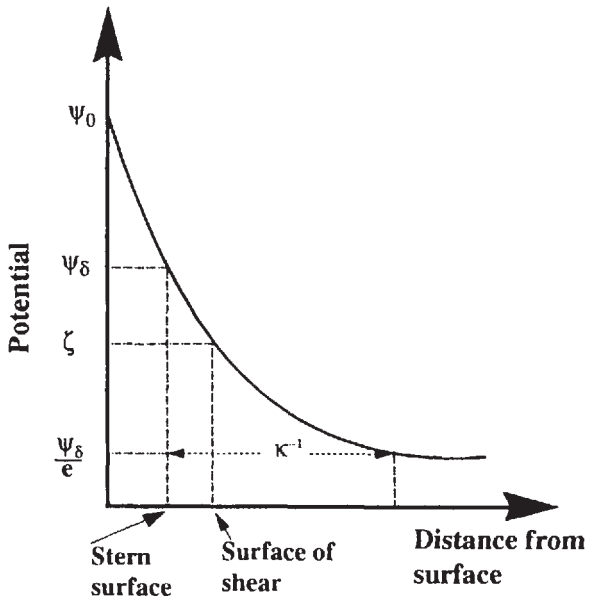


FIG. 12.2 The relative magnitudes of various double-layer potentials of interest.

situation corresponds to a concentric sphere capacitor. As in Chapter 11, we again see the double layer behaving as if it was a capacitor with a characteristic spacing κ^{-1}.

12.3c Electrophoretic Mobility and the Hückel Equation

Having explored the capacitor analogy, we no longer need to retain the second term in the series expansion of the exponential in Equation (23). For our present purposes it is sufficient to note that for small values of κR_s, Equation (22) becomes

$$\zeta = \frac{q}{4\pi\varepsilon R_s} \tag{26}$$

Solving this result for q and combining with Equations (5)–(7), we obtain

$$u = \frac{2\,\varepsilon\,\zeta}{3\,\eta} \tag{27}$$

The possible usefulness of this relationship—which is known as the *Hückel equation*—should not be overlooked. Throughout Chapter 11 we were concerned with the potential surrounding a charged particle. Equation (11.1) provides a way of evaluating the potential at the surface, ψ_0, in terms of the concentration of potential-determining ions. Owing to ion adsorption in the Stern layer, this may not be the appropriate value to use for the potential at the inner limit of the diffuse double layer. Although ζ is not necessarily identical to ψ_0, it is nevertheless a quantity of considerable interest.

More elaborate theory shows that Equation (27) is valid for spheres when κR_s is less than about 0.1. This imposes a rather severe restriction on the applicability of this result in aqueous systems since for $R_s = 10^{-8}$ m the corresponding concentration is about 10^{-5} M for a 1 : 1 electrolyte. In nonaqueous media, however, ion concentrations may be very low, and this result assumes increasing importance.

* * *

EXAMPLE 12.2 *Relation Between Electrophoretic Mobility and Zeta Potential.* In many references the Hückel equation is written $u = \varepsilon_r\zeta/6\pi\eta$. How do you account for the difference between this expression and Equation (27)? What is the ζ potential of a particle that displays a mobility of 10^{-4} cm^2 V^{-1} s^{-1} in water at 20°C for which $\eta = 0.010$ P and $\varepsilon_r = 80.4$, assuming the Hückel potential applies?

Solution: The discrepancy between the equation given here and Equation (27) arises from the fact that the equation above is written for cgs units whereas Equation (27) applies to SI. Remember that $\varepsilon = \varepsilon_r\varepsilon_0$ in Equation (27) and that the vacuum permittivity ε_0 usually appears with the factor 4π. When we combine Equations (6) and (26), the ratio $4\pi/6\pi$ reduces to 2/3. Many electrokinetic formulas differ by a factor 4π, depending on the system of units being used, and the reader is cautioned to be aware of this difference. The presence or absence of the vacuum permittivity in the equation is the key to the system being used, although this factor is sometimes hidden, as in the case of Equation (27).

Either system of units can be used to calculate ζ from the mobility given; in either case some unit conversion must be done on the mobility since the units given are a hybrid of SI and cgs units.

In SI the mobility is given by

$$10^{-4}\ \text{cm}^2\ \text{V}^{-1}\ \text{s}^{-1} \cdot (1\ \text{m}/100\ \text{cm})^2 = 10^{-8}\ \text{m}^2\ \text{V}^{-1}\ \text{s}^{-1}$$

Therefore

$$\zeta = [(10^{-8})\ (3)\ (0.010\ \text{P} \cdot 1\ \text{kg m}^{-1}\ \text{s}^{-1}/10\ \text{P})]/[2\ (80.4)\ (8.85 \cdot 10^{-12})]$$
$$= 2.11 \cdot 10^{-2}\ \text{V} = 21.1\ \text{mV}$$

In cgs, the mobility is given by

$$10^{-4}\ \text{cm s}^{-1}/\text{V cm}^{-1} \cdot 300\ \text{V/statV} = 3 \cdot 10^{-2}\ \text{cm}^2\ \text{statV}^{-1}\ \text{s}^{-1}$$

Therefore

$$\zeta = [6\pi(3 \cdot 10^{-2})(0.010)]/80.4 = 7.03 \cdot 10^{-5}\ \text{statV}$$

or

$$\zeta = 7.03 \cdot 10^{-5}\ \text{statV} \cdot 300\ \text{V/statV} = 2.11 \cdot 10^{-2}\ \text{V}$$

Note that the factor 300 V/statvolt enters the calculation twice if cgs units are used. ■

* * *

The next question to be considered is the relationship between u and ζ when κR_s is not small.

12.4 ZETA POTENTIAL: THIN ELECTRICAL DOUBLE LAYERS

In this section we consider the situation in which the thickness of the double layer is negligible compared to the radius of curvature of the surface. The derivation is not limited to any particle geometry as long as the radius of curvature R^* is large compared to κ^{-1}. This situation may be brought about by making κ^{-1} small (i.e., κ large), which is equivalent to dealing with relatively high concentrations of electrolyte or with flat or slightly curved surfaces. For our purposes it is convenient to consider a planar surface, but the results will apply equally to any case for which the product κR^* is large.

12.4a Helmholtz-Smoluchowski Equation for Electrophoretic Mobility

Suppose we consider a volume element of area A and thickness dx situated a distance x from a planar surface as shown in Figure 12.3. The viscous force on the face nearest the surface is given by

$$F_x = \eta A \left(\frac{dv}{dx}\right)_x \tag{28}$$

and the force exerted on the face farther from the surface is given by

$$F_{x+dx} = \eta A \left(\frac{dv}{dx}\right)_{x+dx} \tag{29}$$

In these equations v is the relative velocity between the particle and the surrounding medium. The difference between Equations (28) and (29) therefore equals the net viscous force on the volume element:

$$F_{vis} = \eta A \left[\left(\frac{dv}{dx}\right)_{x+dx} - \left(\frac{dv}{dx}\right)_x\right] \tag{30}$$

Equation (4.12) can be used to write Equation (30) as

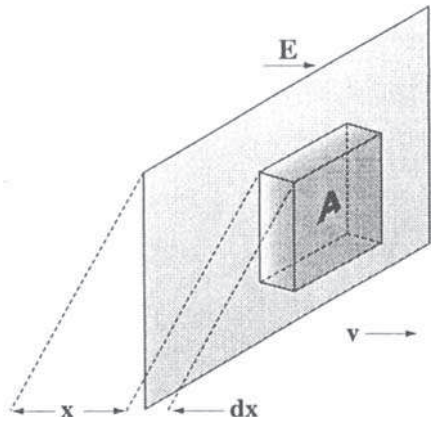


FIG. 12.3 Location of a volume element of solution adjacent to a planar wall.

$$F_{vis} = \eta A \frac{d^2v}{dx^2} dx \tag{31}$$

Under stationary-state conditions an equal and opposite force is exerted on the volume element by the electric field acting on the ions contained in the volume element. The force on the ions is given by the product of the field strength times the total charge. The latter equals the charge density ρ^* times the volume of the element; therefore

$$F_{el} = E\rho^* A\, dx \tag{32}$$

The Poisson equation for a planar surface (Equation (11.26)) may now be used as a substitution for ρ^* to yield

$$\rho^* = -\varepsilon \nabla^2\psi = -\varepsilon \frac{d^2\psi}{dx^2} \tag{33}$$

where the second result applies specifically to the region adjacent to the planar surface and where ψ is the potential at a distance x from the surface.

Setting Equations (31) and (32) equal to each other, substituting Equation (33), and simplifying leads to the equation

$$\eta \frac{d^2v}{dx^2} = -\varepsilon E \frac{d^2\psi}{dx^2} \tag{34}$$

With certain assumptions this result may be integrated twice to give the relation between v and ψ.

The integration of Equation (34) is carried out by assuming that both η and ε are constants in the vicinity of the surface. We return to a discussion of this assumption in Section 12.8. Making this assumption, we can write Equation (34) as

$$\frac{d}{dx}\left(\eta \frac{dv}{dx}\right) = -E \frac{d}{dx}\left(\varepsilon \frac{d\psi}{dx}\right) \tag{35}$$

In this form the first integration is readily found to give

$$\eta \frac{dv}{dx} = -E\varepsilon \frac{d\psi}{dx} + C_1 \tag{36}$$

The constant of integration C_1 is evaluated by noting that both dv/dx and $d\psi/dx$ must equal zero at large distances from the surface; therefore $C_1 = 0$.

The resulting expression is easily integrated again with the following limits: (a) at the surface of shear $\psi = \zeta$ and $v = 0$; (b) at the outside edge of the double layer $\psi = 0$ and v equals the observed velocity of particle migration. Therefore

$$\eta \int_v^0 dv = -E\varepsilon \int_0^\zeta d\psi \tag{37}$$

or

$$\eta v = \varepsilon E \zeta \tag{38}$$

In terms of electrophoretic mobility, Equation (38) can be written as

$$u = v/E = (\varepsilon\zeta)/\eta \tag{39}$$

Equation (39) is known as the *Helmholtz-Smoluchowski equation*. No assumptions are made in its derivation as to the actual structure of the double layer, only that the Poisson equation applies and that bulk values of η and ε apply within the double layer. It has been shown that this result is valid for values of κR^* larger than about 100 (i.e., $\kappa R_s > 100$ for spherical particles).

12.4b Hückel and Helmholtz-Smoluchowski Equations as Limiting Cases

We have now reached the position of having two expressions—Equations (27) and (39)—to describe the relationship between the mobility of a particle (an experimental quantity) and the zeta potential (a quantity of considerable theoretical interest). The situation may be summarized by noting that both the Hückel and the Helmholtz-Smoluchowski equations may be written as

$$u = C\frac{\varepsilon\zeta}{\eta} \tag{40}$$

where C is a constant with a numerical value that depends on the magnitude of κR_s. In the limit of both large and small values of κR_s, the value of C becomes independent of κR_s:

1. For $\kappa R_s < 0.1$

$$C = (2/3) \tag{41}$$

2. For $\kappa R_s > 100$

$$C = 1 \tag{42}$$

In view of the widely different pictures of the electric field surrounding the particles in the two extremes—as shown schematically in Figure 12.1—it is not surprising that different results are obtained in the two limits.

A major remaining problem is that many systems of interest in colloid chemistry do not correspond to either of these two limiting cases. The situation is summarized in Figure 12.4, which maps the particle radii R_s and 1 : 1 electrolyte concentrations that correspond to various κR_s values. Clearly, there is a significant domain of particle size and/or electrolyte concentration for which neither the Hückel nor the Helmholtz-Smoluchowski equations can be used to evaluate ζ from experimental mobility values. The relationship between ζ and u for intermediate values of κR_s is the topic of the following section.

12.5 ZETA POTENTIAL: GENERAL THEORY FOR SPHERICAL PARTICLES

It is apparent from the above sections that the understanding of electrophoretic mobility involves both the phenomena of fluid flow as discussed in Chapter 4 and the double-layer potential as discussed in Chapter 11. In both places we see that theoretical results are dependent on the geometry chosen to describe the boundary conditions of the system under consideration. This continues to be true in discussing electrophoresis, for which these two topics are combined. As was the case in Chapters 4 and 11, solutions to the various differential equations that arise are possible only for rather simple geometries, of which the sphere is preeminent.

12.5a General Formulation of Electrophoresis for Spherical Particles: Henry's Equation

The generalized electrophoresis problem has been solved for spherical and rod-shaped particles and, more approximately, for random coils. In this section we restrict our attention to spheres, although in the limit of large values of κR_s, the Helmholtz-Smoluchowski equation is obtained, a result that is independent of particle shape. In the general theory the conductivity of the particle is one of the parameters that must be considered. We discuss only the case of nonconducting spheres. It has been shown experimentally that mercury droplets for which κR_s is large follow Equation (39), even though—as conductors—the full theory predicts they should show zero mobility. The explanation of this anomaly is that the surface of the metallic drops becomes sufficiently polarized to block the passage of current through the particle. Thus even a metallic particle may behave as an insulator, thereby justifying our choice of the nonconducting particle as the model for consideration.

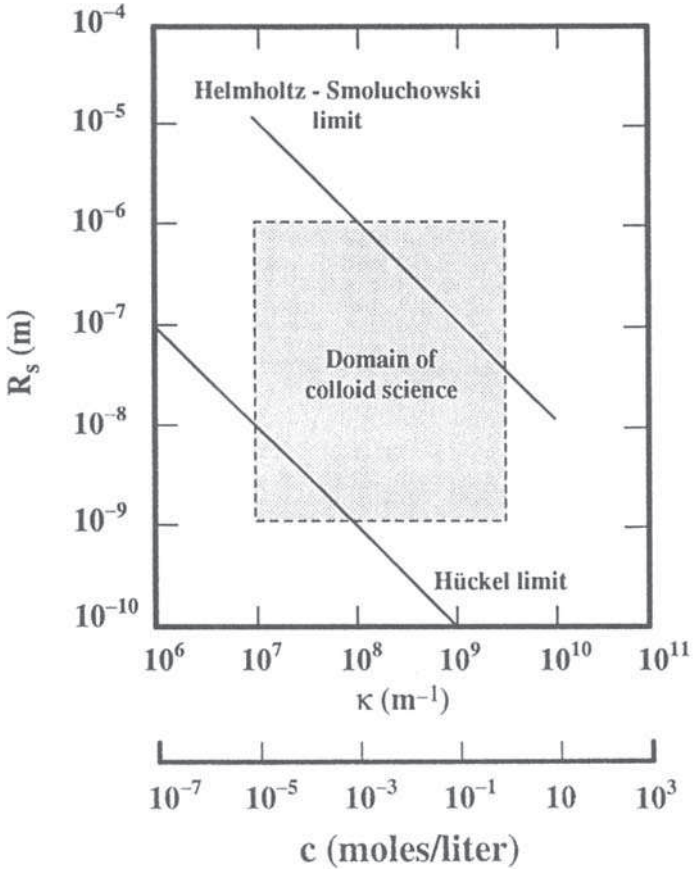


FIG. 12.4 The domain within which most investigations of aqueous colloidal systems lie in terms of particle radii and 1 : 1 electrolyte concentration. The diagonal lines indicate the limits of the Hückel and the Helmholtz-Smoluchowski equations. (Redrawn with permission from J. Th. G., Overbeek, Quantitative Interpretation of the Electrophoretic Velocity of Colloids. In *Advances in Colloid Science*, Vol. 3 (H. Mark and E. J. W. Verwey, Eds.), Wiley, New York, 1950.)

In addition, we consider only the case in which the colloid is present in small concentration so that colloid-colloid interactions can be ignored. We assume that the diffuse part of the double layer is adequately described by the Gouy-Chapman theory. Since the surface of shear more or less coincides with the Stern surface, it is the diffuse part of the double layer and not the Stern layer (where specific adsorption occurs) in which we are interested. Specific adsorption in the Stern layer may have a large effect on the zeta potential itself, but should be unimportant when it comes to establishing the connection between u and ζ. The Gouy-Chapman theory ignores the actual discreteness of electrical charges and is also subject to the objections against the Poisson-Boltzmann equation (see Section 11.4). An extensive body of research has been devoted either to circumventing these limitations or to estimating the approximation introduced by their use. Overbeek and Wiersma (1967) have rightly noted that it is rather futile to introduce one or two corrections to the theory while neglecting other approximations that are probably of the same magnitude. A safer procedure, they note, is to use the simpler theory, keeping in mind the semiquantitative nature of the result.

By assuming that the external field—deformed by the presence of the colloidal particle—and the field of the double layer are additive, D. C. Henry derived the following expression for mobility:

$$u = \frac{\varepsilon}{\eta}\left(\zeta + 5\,R_s^5 \int_\infty^{R_s} \frac{\psi}{r^6}\,dr - 2\,R_s^3 \int_\infty^{R_s} \frac{\psi}{r^4}\,dr\right) \tag{43}$$

where r is the radial distance from the center of the particle. To go beyond Equation (43), it is necessary to know ψ as a function of r. The resulting expressions are mathematically intractable unless a relatively simple expression is used for ψ. We may use the Debye-Hückel approximation given by Equation (19) for this, but the constant in that equation is best evaluated somewhat differently before proceeding.

We return to the solution of the Poisson-Boltzmann equation for a spherical particle, Equation (19), with $B = 0$:

$$\psi = \frac{A \exp(-\kappa r)}{r} \tag{44}$$

In the present development we evaluate A by recalling that $\psi = \zeta$ when $r = R_s$. Therefore

$$A = R_s \zeta \exp(\kappa R_s) \tag{45}$$

and Equation (44) becomes

$$\psi = \frac{R_s\,\zeta}{r} \exp[-\kappa(r - R_s)] \tag{46}$$

This equation, with ψ_0 instead of ζ, was given without proof as Equation (11.38) in Section 11.4c. Combining Equations (43) and (46) and integrating leads to the result

$$u = \frac{2\,\varepsilon\,\zeta}{3\,\eta} f(\alpha) \tag{47a}$$

where

$$f(\alpha) = \left(1 + \frac{1}{16}\alpha^2 - \frac{5}{48}\alpha^3 - \frac{1}{96}\alpha^4 - \frac{1}{96}\alpha^5 - \left[\frac{1}{8}\alpha^4 - \frac{1}{96}\alpha^6\right] \exp(\alpha) \int_\infty^\alpha \frac{e^{-t}}{t}\,dt\right) \quad \text{with} \quad \alpha = \kappa R_s < 1 \tag{47b}$$

For $\kappa R_s > 1$, the function $f(\alpha)$ becomes (see Hunter 1981)

$$f(\alpha) = \left(\frac{3}{2} - \frac{9}{2}\alpha^{-1} + \frac{75}{2}\alpha^{-2} - 330\,\alpha^{-3}\right) \tag{47c}$$

The above result (Equations (47a)-(47c)) is known as *Henry's equation*. Two specific assumptions underlying its derivation should be pointed out:

1. The ion atmosphere is undistorted by the external field.
2. The potential is low enough to justify writing $e\psi/k_BT < 1$, which is equivalent to requiring that $\psi < 25$ mV (Section 11.2b).

It should also be noted that in the limit of $\kappa R_s \to 0$, Equation (47a) reduces to the Hückel equation, and in the limit of $\kappa R_s \to \infty$, it reduces to the Helmholtz-Smoluchowski equation. Thus the general theory confirms the idea introduced in connection with the discussion of Figure 12.1, that the amount of distortion of the field surrounding the particles will be totally different in the case of large and small particles. The two values of C in Equation (40) are a direct consequence of this difference. Figure 12.5a shows how the constant C varies with κR_s (shown on a logarithmic scale) according to Henry's equation.

12.5b Effect of Double-Layer Relaxation

We noted above that many systems of interest in colloid chemistry involve intermediate values of κR_s, so Henry's equation fills an important gap. At the same time it explicitly introduces additional restrictions: (a) low potentials and (b) undistorted double layers. A topic of consid-

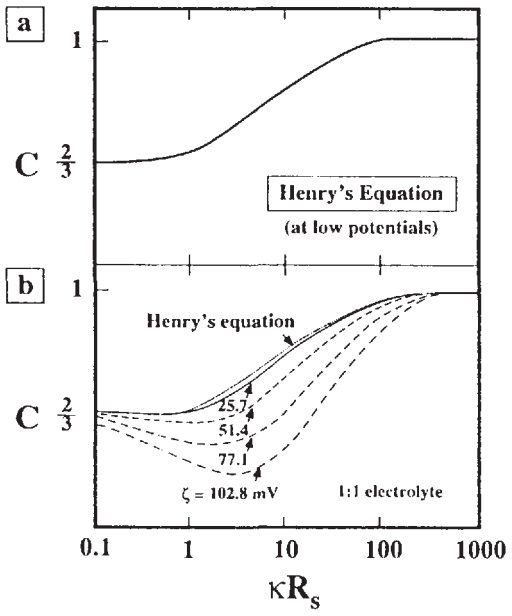


FIG. 12.5 Variation of the constant C (Equation (40)) with κR_s (log scale): (a) at low potentials according to Henry's equation; and (b) for various potentials. (Data from P. H. Wiersma, A. L. Loeb, and J. Th. G. Overbeek, *J. Colloid Interface Sci.*, **22**, 78 (1966); redrawn with permission from Shaw 1969.)

erable importance is the actual distortion of the double layer that accompanies particle migration. The consequences of this distortion—known as the *relaxation effect*—are known to be important in the conductivity of simple electrolytes. A remaining development, therefore, is to consider the relaxation effect in colloidal systems.

Because the charged particle and its ion atmosphere move in opposite directions, the center of positive charge and the center of negative charge do not coincide. If the external field is removed, this asymmetry disappears over a period of time known as the *relaxation time.* Therefore, in addition to the fact that the colloid and its atmosphere move countercurrent with respect to one another (which is called the *retardation effect*), there is a second inhibiting effect on the migration that arises from the tug exerted on the particle by its distorted atmosphere. Retardation and relaxation both originate with the double layer, then, but describe two different consequences of the ion atmosphere. The theories we have discussed until now have all correctly incorporated retardation, but relaxation effects have not been included in any of the models considered so far.

A number of workers have tackled the problem of relaxation. The use of computers has greatly assisted this area of research because of the complexity of the mathematics involved. Loeb et al. (1960) report the results of some numerical solutions to the mobility problem with relaxation specifically considered. Figure 12.5b summarizes some results from these studies for the case of a 1 : 1 electrolyte. The various curves correspond to values of zeta equaling 25.7, 51.4, 77.1, and 102.8 mV at 25°C. It will be noted that the restriction to low potentials no longer applies in the theory from which these curves were evaluated. It is evident from the figure that the relaxation effect is negligible when $\zeta < 25$ mV, regardless of the value of κR_s, and in the limit of both large and small values of κR_s, regardless of the value of ζ. That is, intermediate values of κR_s and large potentials correspond to the condition of maximum resistance to flow arising from relaxation.

A family of curves qualitatively similar in appearance to those shown in Figure 12.5b

results when C is plotted versus κR_s at constant ζ with the valence of the electrolyte taken as the variable parameter. In that case the relaxation effect is found to increase with the valence of the counterions. As the valence of those small ions that have the same charge as the macroion increases, the relaxation effect leads to a higher mobility (at constant ζ) than would be predicted from Henry's equation.

In this section we have considered the relationship between u and ζ under conditions of intermediate κR_s values, a wide range of ζ values, and a number of ionic valence possibilities. The relationship is seen to be quite complex, except in the Hückel and Helmholtz-Smoluchowski limits. When the particle size and electrolyte concentration conditions are such that one of these limits clearly applies, ζ can be evaluated unambiguously from experimental mobilities. The Helmholtz-Smoluchowski limit is independent of particle shape. The Hückel equation is equally free from ambiguity, although it does require spherical particles and—as already noted—the circumstances under which it holds are not especially useful for aqueous colloids. If a particle is of intermediate size with definite, known values of κ and R_s and with ζ known to be small, Henry's equation (or Figure 12.5a) could be used to evaluate ζ from mobility measurements. As the complexity (i.e., higher potentials, mixed electrolyte valences) of the system increases, however, the feasibility of evaluating ζ from experimental mobilities becomes increasingly tenuous. In these circumstances precise experimental results are best reported as mobilities, with the corresponding value of ζ only an approximation.

12.6 ELECTROOSMOSIS

In all the sections of this chapter until now we have focused attention on electrophoresis. We have seen that the potential at the surface of shear can be measured from electrophoretic mobility measurements, provided the system complies with the assumptions of a manageable model. One feature that has been conspicuously lacking from our discussions is any comparison between electrophoretically determined values of ζ and potential values determined by another method. The reasons for this are twofold:

1. Other techniques for measuring ζ are contingent on the same set of assumptions associated with electrophoresis and therefore do not constitute an independent determination.
2. Uncertainty as to the location within the double layer at which the shear surface is located makes it difficult to relate ζ to other double-layer potentials, such as ψ_0 as determined from knowledge of the concentration of potential-determining ions (see Equation (11.1)).

In this section we describe *electroosmosis* and in the following section the *streaming potential*. These two electrokinetic techniques also permit the evaluation of ζ, but are subject to objection 1. In Section 12.8 we examine in greater detail the location of the surface of shear, which is the essence of objection 2 above.

12.6a Difference Between Electroosmosis and Streaming Potential

Above we defined electrokinetic phenomena as arising from the relative motion of a charged surface and its associated double layer. In electrophoresis it is the dispersed phase that moves, with the continuous phase remaining (more or less) stationary. It is apparent that the required relative motion between a surface and its double layer could also be brought about by causing the electrolyte solution to flow past a stationary charged wall. The complements of electrophoresis are electroosmosis and streaming potential. These two measurements differ from each other as follows: (a) in *electroosmosis* it is an applied potential that induces the flow of solution, as illustrated in Figure 12.6; (b) in *streaming potential* the solution is made to flow by applying a pressure, and a potential is induced as a result. Cause and effect are thus interchanged in electroosmosis and streaming potential.

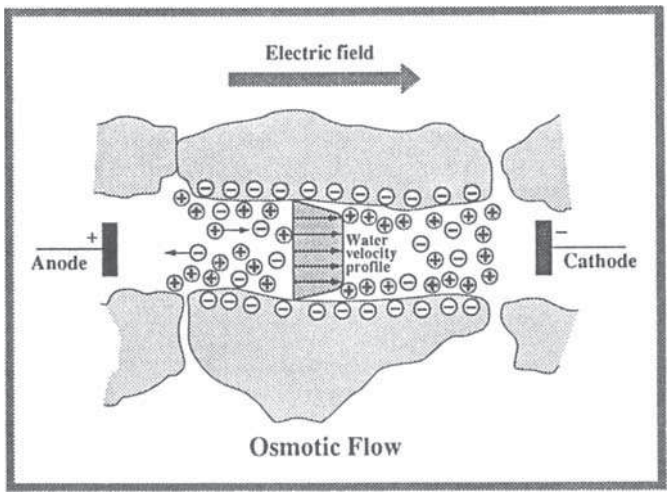


FIG. 12.6 Electroosmotic flow through a pore. If the fluid flow occurs as a result of applied pressure difference along the length of the pore, the resulting potential difference is known as the streaming potential. (Adapted with permission from Probstein 1994.)

12.6b Relating Electroosmotic Flow to Zeta Potential

The electroosmosis apparatus shown in Figure 12.7a consists of two capillaries in parallel attached at either end to reservoirs of electrolyte solution. One of the capillaries – the working capillary – is arranged with reversible electrodes at either end, while the measuring capillary contains an air bubble to indicate fluid displacement. It is the glass-solution interface in the working capillary at which the electroosmosis phenomenon originates. Substances other than glass may also be investigated by this method, a particularly useful variation being the replacement of the capillary by a plug of powdered material that cannot be fabricated into a cylindrical tube. For the purpose of discussion, we continue to refer to the capillary. The conditions under which the same analysis applies to a plug will be clear from the following discussion.

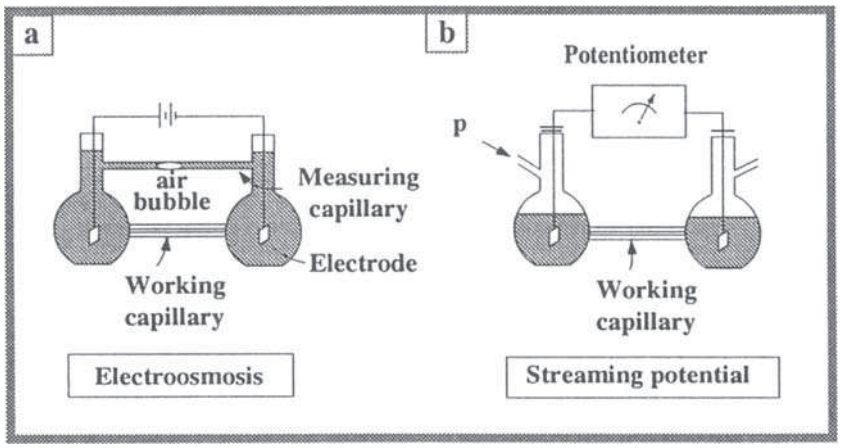


FIG. 12.7 Schematic illustrations of the apparatus used to measure (a) electroosmosis and (b) streaming potential.

When an electric field is applied across the working capillary, the double-layer ions begin to migrate and soon reach the steady-state velocity. In the steady state, electrical and viscous forces balance one another. The forces exerted on the ions by the medium are equal and opposite to the forces exerted on the medium by the ions; consequently, the liquid also attains a stationary-state velocity. The tangential displacement of the fluid relative to the wall defines a surface of shear at which the potential equals ζ.

Although the Helmholtz-Smoluchowski equation was derived in reference to electrophoretic mobility, it clearly applies to electroosmosis as well since the displacement of one part of the double layer relative to another part is common to both. Figure 12.3, for example, may be taken as an illustration of either electrophoresis or electroosmosis. The condition of the Helmholtz-Smoluchowski equation—that R_s is large compared to κ^{-1}—is clearly applicable to capillaries of macroscopic dimensions. We noted above that the Helmholtz-Smoluchowski equation applies to the electrophoresis of nonspherical particles as long as κR^* is large (with R^* the radius of the curvature); the same logic permits Equation (39) to be applied to cylindrical capillaries, as well as pores of irregular shape. It is this latter application that allows the replacement of a well-defined capillary by a porous plug of material in an apparatus such as that shown in Figure 12.7a.

Equation (38) may therefore be used to describe the relationship between the potential at the capillary wall and at the velocity of electroosmotic flow. The volume of liquid V displaced per unit time is given by multiplying both sides of Equation (38) by the cross-sectional area of the capillary:

$$V = vA = \varepsilon\zeta EA/\eta \tag{48}$$

Now suppose we apply Ohm's law to the capillary. The electric field is related to the current I and the conductivity k of the electrolyte solution as follows:

$$E = I/(Ak) \tag{49}$$

This result may be substituted into Equation (48) to yield

$$V = \varepsilon\zeta I/(\eta k) \tag{50}$$

This equation permits ζ to be evaluated from measurements of the rate of volume flow through the capillary; the measurements are made by observing the rate of displacement of the air bubble in the measuring capillary of Figure 12.7a.

12.6c Effect of Surface Conductivity on Electroosmosis

The last three equations are the first we have encountered in which conductivity plays a role. What is troublesome about this quantity is the fact that it is a property of bulk solutions, and we are considering here an effect that arises precisely as a result of the uneven distribution of ions near a charged wall. It is essential, therefore, to examine the current carried by the ions in the double layer. Toward this end, current may be written as the sum of two contributions:

$$I = I_b + I_s \tag{51}$$

where the subscripts b and s refer to bulk and surface contributions, respectively. Equation (49) may be used as a substitution for I_b, with πR_c^2 as the area of a cylindrical capillary of radius R_c. An analogous expression may be written for the current carried by the surface layer. In this case the bulk conductivity is replaced by surface conductivity, and the cross-sectional area is replaced by the perimeter of the capillary. With these substitutions, Equation (51) becomes

$$I = E(\pi R_c^2 k_b + 2\pi R_c k_s) = EA[k_b + (2k_s/R_c)] \tag{52}$$

According to this relationship, the product EA in Equation (48) should be replaced by

$$EA = I/[k_b + (2k_s/R_c)] \tag{53}$$

to give

$$V = \varepsilon\zeta I/\{\eta[k_b + (2k_s/R_c)]\} \tag{54}$$

It will be noted that the importance of the correction for surface conductivity increases as R_c decreases and vanishes as $R_c \to \infty$. Equation (54) also suggests that the numerical evaluation of k_s may be accomplished by studying electroosmosis in a set of capillaries identical in all respects except for variability in R_c. Finally, the expansion of Equation (50) to Equation (54) in correcting for surface conductivity explicitly assumes a cylindrical capillary. Experiments made with porous plugs cannot be corrected for surface conductivity by Equation (54), but the qualitative conclusion that the effect of surface conductivity increases as the pore radius decreases is valid in this case also.

It has already been noted that there is a close similarity between electroosmosis and streaming potential. Therefore we consider this additional electrokinetic phenomenon next.

12.7 STREAMING POTENTIAL

The definition of streaming potential was presented in the previous section. Here, we derive the relation between the streaming potential and the zeta potential and discuss some of the issues that must be considered in comparing zeta potentials obtained by different electrokinetic measurements.

12.7a Relation Between Streaming Potential and Zeta Potential

Figure 12.7b is a sketch of an apparatus that may be used to measure streaming potential. As was the case with electroosmosis, the capillary can be replaced by a plug of powdered material between perforated electrodes. An applied pressure difference p across the capillary causes the solution to flow through the capillary, thereby tangentially displacing the part of the double layer in the mobile phase from the stationary part.

The relationships developed in Chapter 4 for fluid flow through a capillary can be applied to this situation as follows:

1. The velocity of the fluid at radius r in a capillary of radius R_c and length ℓ is given by Equation (4.18):

$$v = [p/(4\eta\ell)](R_c^2 - r^2) \tag{55}$$

2. The volume flow rate through an elemental area $2\pi r dr$ is given by (see Equation (4.19)):

$$dV_F/dt = [p/(4\eta\ell)](R_c^2 - r^2)2\pi r\, dr \tag{56}$$

where V_F denotes the volume flow.

3. The current associated with this flow rate is

$$dI = \rho^*(dV_F/dt) = [\rho^* p/(4\eta\ell)](R_c^2 - r^2)2\pi r\, dr \tag{57}$$

where ρ^* is the charge density.

4. Next a change of variable is helpful. We replace r by a distance measured from the surface of shear x, where

$$x = R_c - r \tag{58}$$

In terms of this substitution, Equation (57) becomes

$$dI = -[\rho^* p/(4\eta\ell)](2R_c x - x^2)2\pi(R_c - x)\, dx \tag{59}$$

Our specific interest is in the region near the walls of the capillary where $x \ll R_c$. In this region Equation (59) may be approximated as

$$dI \approx -\pi[\rho^* p/(\eta\ell)]R_c^2 x\, dx \tag{60}$$

5. Substituting Equation (11.26) for ρ^* yields

$$dI = \frac{\pi \varepsilon p R_c^2}{\eta \ell} \frac{d^2\psi}{dx^2} x\, dx \tag{61}$$

6. The total current carried by the capillary is obtained by integrating the above equation. Integration by parts yields

$$I = \frac{\pi \varepsilon p R_c^2}{\eta \ell} \left[\left(x \frac{d\psi}{dx} \right)_0^{R_c} - \int_0^{R_c} \frac{d\psi}{dx} dx \right] = \frac{\pi \varepsilon p R_c^2 \zeta}{\eta \ell} \tag{62}$$

since $\psi = \zeta$ at $x = 0$ and $\psi = d\psi/dx = 0$ at $x = R_c$.

The quantity calculated by Equation (62) is known as the *streaming current*. It is specifically due to the net displacement of the mobile part of the double layer relative to the stationary part of the double layer. The field associated with this current is given by combining Equations (52) and (62):

$$E = \frac{\varepsilon \zeta}{\eta} \left(\frac{1}{k_b + 2k_s/R_c} \right) \frac{p}{\ell} \tag{63}$$

If both sides of Equation (63) are multiplied by the length of the capillary ℓ, the potential difference between the measuring electrodes—the *streaming potential* E_{str}—is obtained:

$$E_{str} = \frac{\varepsilon \zeta p}{\eta (k_b + 2k_s/R_c)} \tag{64}$$

The conditions under which Equation (64) for streaming potential and Equation (54) for electroosmosis were derived are comparable inasmuch as each applies to the case of large κR_c. Comparison of Equations (54) and (64) in the limit of large R_c shows that

$$(E_{str}/p) = (V/I) = \varepsilon\zeta/(\eta k) \tag{65}$$

The coupling of two different electrokinetic ratios (E_{str}/p and V/I) through Equation (65) is an illustration of a very general law of reciprocity due to L. Onsager (Nobel Prize, 1968). The general theory of the Onsager relations, of which Equation (65) is an example, is an important topic in nonequilibrium thermodynamics.

If the relationships shown in Equation (65) are to be used in computations, it is essential that proper units be used. Example 12.3 considers some numerical substitutions into Equation (65).

* * *

EXAMPLE 12.3 *Units of Electrokinetic Parameters.* Show that E_{str}/p, V/I, and $\varepsilon_0\zeta/\eta k$ all have units $m^3\ C^{-1}$. For water at 25°C, $\eta = 8.937 \cdot 10^{-4}$ kg $m^{-1}\ s^{-1}$ and $\varepsilon_r = 78.54$. Evaluate the proportionality factor between V/I and ζ/k if V is expressed in $cm^3\ s^{-1}$ and I is expressed in milliamperes with all other quantities in SI units. Evaluate the proportionality factor between E_{str}/p and ζ/k if p is expressed in torr with all other quantities in SI units.

Solution: Examine the SI units of each term in Equation (65). The units of (V/I) are $(m^3 s^{-1})/(C s^{-1}) = m^3\ C^{-1}$. The units of E_{str}/p are $V/(N\ m^{-2})$; when multiplied by the conversion factor $(J\ C^{-1})/V$, this becomes $m^3\ C^{-1}$. The units of $\varepsilon_0\zeta/\pi k$ are $(C^2\ J^{-1}\ m^{-1})(V)/(kg\ m^{-1}\ s^{-1})(ohm^{-1}\ m^{-1})$; when multiplied by the conversion factor $V\ (C\ s)^{-1}/ohm$, this becomes $J\ C^{-1}\ s/kg\ m^{-1} = m^3\ C^{-1}$.

Substituting the SI values for all quantities, we obtain the following for $\varepsilon\zeta/\pi k$

$$(78.54)(8.85 \cdot 10^{-12})\zeta/(8.937 \cdot 10^{-4})k = 7.777 \cdot 10^{-7}\zeta/k\ m^3\ C^{-1}$$

from which

$$V/I = 7.777 \cdot 10^{-7}\ \zeta/k\ m^3\ C^{-1} \cdot (10^2\ cm/m)^3 \cdot 1\ C\ s^{-1}/10^3\ mA$$
$$= 7.777 \cdot 10^{-4}\ \zeta/k\ cm^3\ s^{-1}/mA$$

and

$$E_{str}/p = [(7.777 \cdot 10^{-7}\ \zeta/k)\ m^3\ C^{-1}] \cdot (10^3\ liter/m^3) \cdot (1\ C\ V/1\ J)$$
$$\cdot (8.314\ J/0.08205\ liter\ atm) \cdot (1\ atm/760\ torr)$$
$$= (1.037 \cdot 10^{-4}\ \zeta/k)\ V\ torr^{-1}$$ ■

* * *

For 10^{-3} M NaCl, $k = 1.26 \cdot 10^{-2}$ ohm^{-1} m^{-1} and a surface with a ζ potential of 50 mV will displace about 11 cm^3 h^{-1} if a current of 1.0 mA flows through an electroosmosis apparatus. With the same electrolyte and the same value of ζ, an applied pressure of 760 mm Hg would produce a streaming potential of 313 mV.

In hydrocarbons the specific conductivity may be lower than that of aqueous solutions by many orders of magnitude, so the streaming potentials generated by the high-pressure pumping of these materials may be quite spectacular. The danger of sparking at such voltages plus the flammability of these substances makes the petroleum industry an area in which streaming potential finds important applications. For example, gasoline (for which the specific conductivity would be as low as 10^{-12} ohm^{-1} m^{-1} if untreated) pumping equipment must be grounded. In addition, a variety of organic-soluble electrolytes have been developed as antistatic additives for petroleum. Examples of two such compounds are tetraisoamyl ammonium picrate and calcium diisopropyl salicylate. Crude petroleum is less troublesome in this regard than refined products since the crude contains oxidation products, asphaltenes, and so on, which impart a natural conductivity to this material.

12.7b Comparison of Zeta Potentials from Different Methods

The objective of comparing values of ζ determined from electrophoresis with those determined by other electrokinetic methods was stated at the beginning of Section 12.6. Enough experiments have been conducted in which at least two of the electrokinetic methods we have discussed are compared to leave no doubt as to the self-consistency of ζ as determined by these different methods. There is no guarantee, however, that self-consistent ζ potentials are correct. Consistency means only that ζ has been extracted from experimental quantities by a self-consistent set of approximations. It should be emphasized, however, that the existence of a potential at the surface of shear—which is the common component in all the electrokinetic analyses we have discussed—is more than amply confirmed by these observations.

Two conditions must be met to justify comparisons between ζ values determined by different electrokinetic measurements: (a) the effects of relaxation and surface conductivity must be either negligible or taken into account and (b) the surface of shear must divide comparable double layers in all cases being compared. This second limitation is really no problem when electroosmosis and streaming potential are compared since, in principle, the same capillary can be used for both experiments. However, obtaining a capillary and a migrating particle with identical surfaces may not be as readily accomplished. One means by which particles and capillaries may be compared is to coat both with a layer of adsorbed protein. It is an experimental fact that this procedure levels off differences between substrates: The surface characteristics of each are totally determined by the adsorbed protein. This technique also permits the use of microelectrophoresis for proteins since adsorbed and dissolved proteins have been shown to have nearly identical mobilities.

12.8 THE SURFACE OF SHEAR AND VISCOELECTRIC EFFECT

The surface of shear is the location within the electrical double layer at which the various electrokinetic phenomena measure the potential. We saw in Chapter 11 how the double layer extends outward from a charged wall. The potential at any particular distance from the wall can, in principle, be expressed in terms of the potential at the wall and the electrolyte content of the solution. In terms of electrokinetic phenomena, the question is: How far from the interface is the surface of shear situated and what implications does this have on the relation between measured zeta potential and the surface potential?

First, the very existence of a surface of shear implies some interesting behavior within the fluid phase of the system under consideration. In our discussion of all electrokinetic phenom-

ena until now, we have assumed that the viscosity of the medium has its bulk value right up to the surface of shear. In addition, it has been implicitly assumed that the viscosity abruptly becomes infinite at the surface of shear.

At this point, it is convenient to recall Figure 7.13 and the discussion of it. In that context we observed that there is generally a variation of properties in the vicinity of an interface from the values that characterize one of the adjoining phases to those that characterize the other. This variation occurs over a distance τ measured perpendicular to the interface. In the present discussion viscosity is the property of interest and the surface of shear—rather than the interface per se—is the boundary of interest. The model we have considered until now has implied an infinite jump in viscosity, occurring so sharply that τ is essentially zero. From a molecular point of view such an abrupt transition is highly unrealistic. A gradual variation in η over a distance comparable to molecular dimensions is a far more realistic model.

With these ideas in mind, it is evident that we would do better to think of a *zone* of shear rather than a surface of shear. Although we continue to speak of the shear "surface," the term is not used in the mathematical sense of possessing zero thickness, but rather in the broader sense of Chapter 7. Moreover, under certain circumstances, the viscosity has a strong dependence on the electric field. This is known as *viscoelectric effect* and must be taken into account since the electric field changes sharply within the electrical double layer. We examine how the viscoelectric effect affects the Helmholtz-Smoluchowski results obtained above for the relation between the electrophoretic mobility and the zeta potential. Following this, we look at what conditions make the zeta potential obtained from the Helholtz-Smoluchowski result a good measure of the surface potential.

12.8a Viscoelectric Effect and Its Influence on Electrophoretic Mobility and Zeta Potential

How must the expressions derived in the sections above be modified to take into account the variation in η and the finite distance over which it increases? The answer is that η—the viscosity within the double layer—must be written as a function of location. Our objective in discussing this variation is not to examine in detail the efforts that have been directed along these lines. Instead, it is to arrive at a better understanding of the relationship between ζ and the potential at the inner limit of the diffuse double layer and a better appreciation of the physical significance of the surface of shear.

Measurements of the viscosity of organic liquids in the presence of an electric field reveal that there is an increase in viscosity in high electric fields that is described by the expression

$$(\eta_E - \eta_0)/\eta_0 = fE^2 \tag{66}$$

where the subscripts indicate the presence (E) or absence (0) of a field. The factor f is called the *viscoelectric constant* and has a value of about $2 \cdot 10^{-16}$ V^{-2} m^2 for several organic liquids. Thus a 10% increase in viscosity may be anticipated for a field strength of about $2 \cdot 10^7$ V m^{-1}.

An expression such as Equation (11.56) may be used to estimate E ($= d\psi/dx$) in the double layer. Table 12.1 shows values of E evaluated by means of this equation for a variety of ψ_0 values and 1 : 1 electrolyte concentrations. It will be noted that for high values of ψ_0 and high ionic strengths, the field in the double layer may be large enough to produce a very significant viscoelectric effect.

Now suppose we reexamine the derivation of the Helmholtz-Smoluchowski equation as given in Section 12.4. Returning to Equation (37), we note that the relationship between u and ζ is given by

$$u = \varepsilon \int_0^{\zeta} \frac{d\psi}{\eta} \tag{67}$$

where η has been left inside the integral this time since its value is assumed to vary with ψ. We continue to assume that ε is a constant since the effect of the field is known to be less for this quantity than for η.

TABLE 12.1 Values of the Electric Field (V m^{-1}) Calculated in the Double Layer by Equation (11.56) for Various ψ_0 Values and Concentrations of 1 : 1 Electrolyte

	c (mole $liter^{-1}$)		
ψ_0, mV	10^{-3}	10^{-2}	10^{-1}
50	$6.36 \cdot 10^6$	$2.01 \cdot 10^7$	$6.36 \cdot 10^7$
100	$1.98 \cdot 10^7$	$6.24 \cdot 10^7$	$1.98 \cdot 10^8$
150	$5.49 \cdot 10^7$	$1.74 \cdot 10^8$	$5.49 \cdot 10^8$
200	$1.51 \cdot 10^8$	$4.77 \cdot 10^8$	$1.51 \cdot 10^9$

Now we substitute η_E from Equation (66) for the viscosity in the double layer in Equation (67) to obtain

$$u = \frac{\varepsilon}{\eta_0} \int_0^{\zeta} \frac{d\psi}{1 + f(d\psi/dx)^2} \tag{68}$$

Finally, Equations (11.40) and (11.56) may be used to evaluate $d\psi/dx$ in the double layer:

$$u = \frac{\varepsilon}{\eta_0} \int_0^{\zeta} \frac{d\psi}{1 + [f(8000\, c\, R\, T/\varepsilon)] \sinh^2 (ze\psi/2k_B T)} \tag{69}$$

where c is in mole $liter^{-1}$ and 2 sinh x has been substituted for $e^x - e^{-x}$. If we define $A = (8000 fcRT/\varepsilon)$ and $B = ze/2k_B T$, this result is more concisely written as

$$u = \frac{\varepsilon}{\eta_0} \int_0^{\zeta} \frac{d\psi}{1 + A \sinh^2 (B\psi)} \tag{70}$$

If c (and therefore A) and ψ are small, Equation (70) becomes approximately

$$u \approx \frac{\varepsilon}{\eta_0} \int_0^{\zeta} [1 + A \sinh^2 (B\psi)]\, d\psi \tag{71}$$

Under the same conditions the sinh function may be expanded (see Appendix A), with only the leading term retained, to obtain

$$u \approx \frac{\varepsilon}{\eta_0} \int_0^{\zeta} [1 - A\, (B\psi)^2]\, d\psi \tag{72}$$

This equation is readily integrated to yield

$$u \approx \frac{\varepsilon}{\eta_0} \left(\zeta - \frac{AB^2}{3} \zeta^3 \right) = \frac{\varepsilon \zeta}{\eta_0} \left(1 - \frac{AB^2}{3} \zeta^2 \right) \tag{73}$$

Under conditions in which the second term is negligibly small, Equation (73) becomes identical to Equation (39), the Helmholtz-Smoluchowski result. On the other hand, when the concentration and ζ increase, the value of ζ that would be associated with an observed mobility is larger than the Helmholtz-Smoluchowski equation would indicate.

12.8b Deviation from Helmholtz-Smoluchowski Predictions

Equation (69) may also be integrated analytically. Although we do not consider the actual solutions, which are rather complex, Figure 12.8 shows graphically the results of these integrations for water at 25°C, assuming $f = 10^{-15}$ V^{-2} m^2. The abscissa shows values of ψ_0, the potential at the inner limit of the diffuse double layer, with $\eta u/\varepsilon$ plotted on the ordinate. It must be remembered that this last quantity equals ζ according to Equation (39)—which we

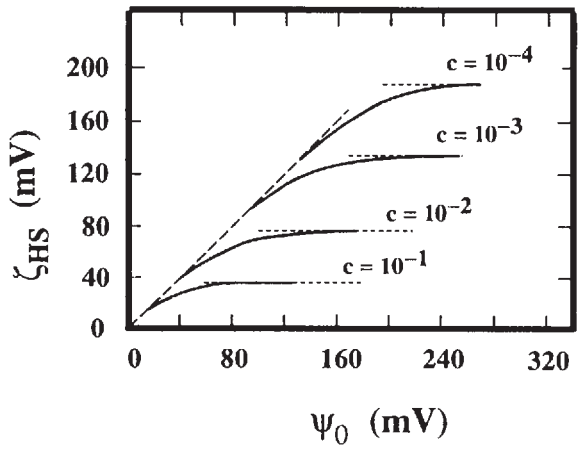


FIG. 12.8 Plot of $\eta u/\varepsilon$ versus ψ_0, that is, the zeta potential according to the Helmholtz-Smoluchowski equation, Equation (39), versus the potential at the inner limit of the diffuse part of the double layer. Curves are drawn for various concentrations of 1 : 1 electrolyte with $f = 10^{-15}$ V^{-2} m^2. (Redrawn with permission from J. Lyklema and J. Th. G. Overbeek, *J. Colloid Sci.*, **16**, 501 (1961).)

designate ζ_{HS}—when the viscosity is assumed to be the bulk value throughout the double layer. The figure shows that $\zeta_{HS} = \psi_0$ at low values of the potential. As the potential increases, however, ζ_{HS} begins lagging behind ψ_0, the effect indicated by Equation (73) in a limiting approximation. At still higher potentials, ζ_{HS} eventually reaches a constant value that is independent of the actual value of ψ_0.

Note, further, that this leveling off occurs at progressively lower potentials as the concentration of electrolyte increases. Increasing both the potential and the electrolyte concentration tends to increase the field in the double layer (see Table 12.1), which in turn increases the viscosity of solvent in the double layer. As the effective viscosity of the medium increases, the surface of shear occurs progressively further from the surface. This accounts for the fact that ζ_{HS} falls behind ψ_0 as ψ_0 increases. These conclusions are consistent with the experimental observation that ζ_{HS} for AgI becomes independent of the concentration of the potential-determining Ag^+ and I^- ions once the concentrations of these ions are well removed from the conditions at which the particles are uncharged.

The results shown in Figure 12.8 illustrate quite clearly the relationship between ζ and ψ_0 and in this way reveal the dependence of the location of the surface of shear on the structure of the double layer. It might appear that one could consult curves such as those shown in Figure 12.8 to read from the appropriate plot the value of ψ_0 that corresponds to a particular ζ, at least for values of ζ less than the limiting value. Although semiquantitative interpretations based on this figure may be trusted, some caution must be expressed about the numerous assumptions and approximations inherent in Figure 12.8. In summary, the following may be cited as examples of such constraints:

1. The possible immobilization of solvent near the surface due to either chemical or mechanical (as opposed to viscoelectric) interaction with the solid phase has not been considered.
2. Use of the Gouy-Chapman theory (Equation (69)) overlooks any specific effects arising from differences between ions, especially with regard to hydration.
3. The validity of Equation (66) in electrolyte solutions, especially the dependence of f on concentration, has not been investigated as fully as might be desired.

12.9 EXPERIMENTAL ASPECTS OF ELECTROPHORESIS

Of the electrokinetic phenomena we have considered, electrophoresis is by far the most important. Until now our discussion of experimental techniques of electrophoresis has been limited to a brief description of microelectrophoresis, which is easily visualized and has provided sufficient background for our considerations to this point. Microelectrophoresis itself is subject to some complications that can be discussed now that we have some background in the general area of electrical transport phenomena. In addition, the methods of *moving-boundary electrophoresis* and *zone electrophoresis* are sufficiently important to warrant at least brief summaries.

12.9a Microelectrophoresis

Microelectrophoresis depends on the visibility of the migrating particles under the microscope. As such, it is inapplicable to molecular colloids such as proteins. By adsorbing the protein molecules on suitable carrier particles, however, the range of utility for microelectrophoresis can be extended. Dark-field illumination (see Section 1.6a.1c) can sometimes be used to advantage to extend microelectrophoresis observations to small, high-contrast particles.

The migrating particles are observed in a cell that may be either cylindrical or rectangular. The walls must be optically uniform for observation and fewer optical corrections, and thermostating difficulties are encountered if the walls are thin. The working part of the apparatus is thus fragile, and auxiliary connecting rods are generally incorporated into the design to increase the mechanical strength of the cell. Figure 12.9 is a sketch of an electrophoresis apparatus with a rectangular working compartment.

The electric field in the cell is best established by means of reversible electrodes such as Ag-AgCl or Cu-$CuSO_4$. Care must be taken to prevent the electrolyte of the electrode from contaminating the dispersion. Platinized electrodes behave reversibly with low currents, but gas evolution causes troubles at higher currents.

The field strength is best obtained by including an accurate ammeter in the circuit to

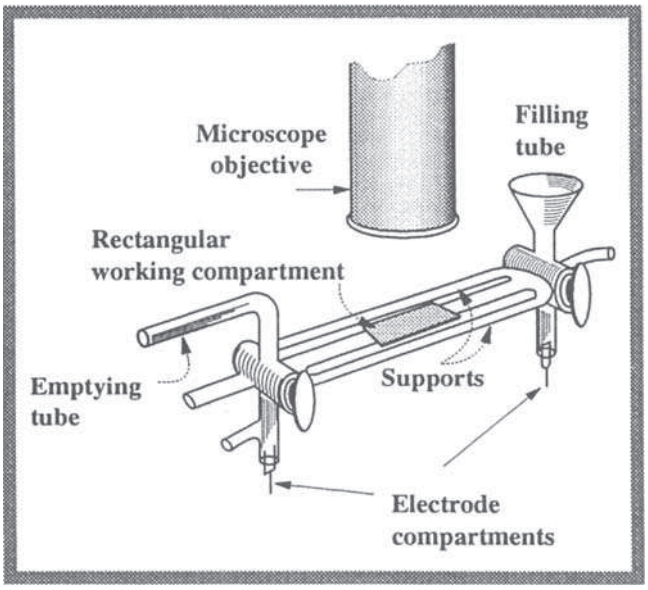


FIG. 12.9 Schematic illustration of a microelectrophoresis cell with a rectangular working compartment.

determine the current. Independent conductivity measurements in the cell with standard solutions permit the determination of the field through Equation (49).

The rate of particle migration is determined by measuring with a stopwatch the time required for a particle to travel between the marks of a calibrated graticule in the microscope eyepiece. If the objective of the microscope is immersed during the electrophoresis measurement, the calibration of the graticule should be made with the same immersion liquid.

Electrophoretic migrations are always superimposed on other displacements, which must either be eliminated or corrected to give accurate values for mobility. Examples of these other kinds of movement are Brownian motion, sedimentation, convection, and electroosmotic flow. Brownian motion, being random, is eliminated by averaging a series of individual observations. Sedimentation and convection, on the other hand, are systematic effects. Corrections for the former may be made by observing a particle with and without the electric field, and the latter may be minimized by effective thermostating and working at low current densities.

Even in the absence of a colloid, an electrolyte solution will display electroosmotic flow through a chamber of small dimensions. Therefore the observed particle velocity is the sum of two superimposed effects, namely, the true electrophoretic velocity relative to the stationary liquid and the velocity of the liquid relative to the stationary chamber. Figure 12.10a shows the results of this superpositioning for particles tracked at different depths in the cell. The particles used in this study are cells of the bacterium *Klebsiella aerogenes* in phosphate buffer. Rather than calculated velocities or mobilities, Figure 12.10a shows the reciprocal of the time

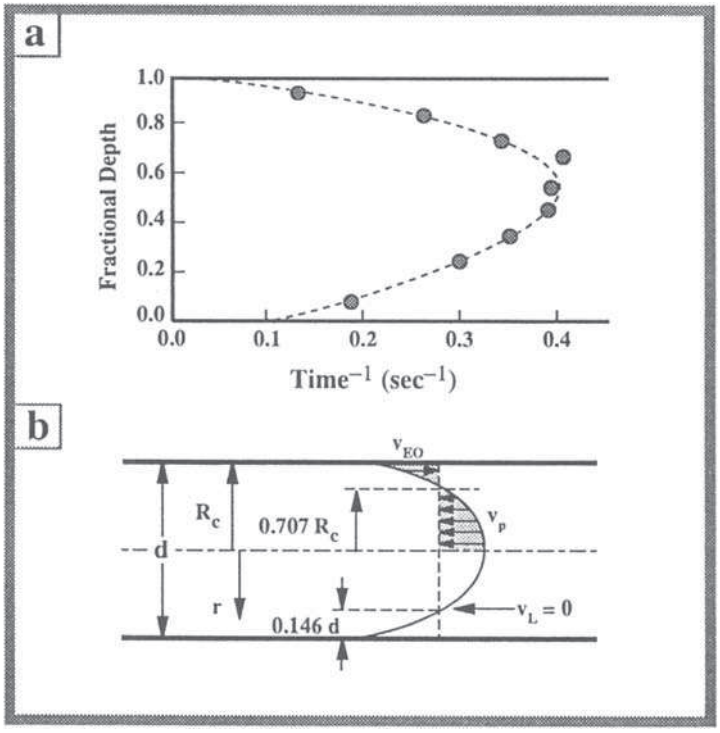


FIG. 12.10 Velocity profiles in electrophoresis cells: (a) velocity (as time^{-1}) of *Klebsiella aerogenes* particles as a function of their location in a rectangular electrophoresis cell (redrawn with permission from A. M. James, in *Surface and Colloid Science*, Vol. 11 (R. J. Good, and R. R. Stromberg, Eds.), Plenum, New York, 1979); (b) location of the surface of zero liquid velocity in a cylindrical capillary.

required for the particles to travel a fixed distance. Since the electrophoretic velocity is a single-valued property of the (uniform) particles under consideration, Figure 12.10a raises the question of which, if any, of these "velocities" represents the true mobility of these particles. Example 12.4 considers a possible interpretation of these results.

* * *

EXAMPLE 12.4 *Electrophoretic Mobility of Bacteria.* It is proposed to evaluate the electrophoretic mobility of the bacteria cells shown in Figure 12.10a by multiplying the appropriate value of time^{-1} by the distance of particle displacement and then dividing by E. Criticize or defend the following proposition: It is appropriate to use the maximum apparent velocity since this is measured at the center of the cell and is therefore subject to the least interference by wall effects.

Solution: The observed effect is the sum of two contributions, one of which is the electroosmotic flow of the medium through the cell. The latter has its maximum value at the center since the layer of fluid adjacent to the walls is stationary. The particles tracked at the center of the cell therefore possess the maximum increment in velocity due to electroosmotic flow. Since the cell is a closed compartment, the liquid displaced by electroosmosis along the walls must circulate by a backflow down the center of the tube. Since the total liquid flow in a closed cell must be zero, the appropriate value from Figure 12.10a to use for the velocity is the average of observations made at all depths. ■

* * *

Since the liquid circulates, there must be certain locations in the cell at which the forward and backward flows of the liquid are equal. An alternative to the averaging procedure suggested in the example is to do the particle tracking at a location at which the medium experiences no net flow.

The analysis of this effect in a closed cylindrical cell is obtained by subtracting from the electroosmotic velocity v_{EO} the velocity of flow v_P through a capillary given by Poiseuille's equation (Equation (4.18)):

$$v_L = v_{EO} - v_P = v_{EO} - C(r^2 - R_c^2) \tag{74}$$

where v_L is the velocity of the liquid and C is a constant. The requirement of no net displacement of liquid is incorporated by integrating Equation (74) over the cross section of the cylinder and setting the result equal to zero:

$$\int_0^{R_c} v_L \, (2\pi r) \, dr = 0 \tag{75}$$

In this expression R_c is the radius of the capillary and r is the radial distance from the capillary axis as shown in Figure 12.10b. Substitution of Equation (74) into Equation (75) and integration gives

$$C = -2v_{EO}/R_c^2 \tag{76}$$

This result may be substituted back into Equation (74) to evaluate that location in the cylinder at which the net liquid displacement is zero:

$$v_L = 0 = v_{EO}\left(1 + \frac{2}{R_c^2}(r^2 - R_c^2)\right) = v_{EO}\left(\frac{2r^2}{R_c^2} - 1\right) \tag{77}$$

This result shows that electroosmotic flow and backflow in the capillary cancel when the factor $(2r^2/R_c^2 - 1)$ equals zero. This condition corresponds to $r/R_c = 0.707$. Thus at 70.7% of the radial distance from the center of the capillary lies a circular surface of zero liquid flow. Any particle tracked at this position in the capillary will display its mobility uncomplicated by the effects of electroosmosis. This location may also be described as lying 14.6% of the cell diameter inside the surface of the capillary. Experimentally, then, one establishes the inside diameter of the capillary and focuses the microscope 14.6% of this distance inside the walls of the capillary. Corrections for the effect of the refractive index must also be included. Additional details of this correction can be found in the book by Shaw (1969).

The location of the surface of zero liquid flow in cells of rectangular cross section has also been worked out. For a cell in which the direction of migration is very long compared to the

width of the cell, the surface where $v = 0$ lies 21.1% of the cell depth above the bottom and below the top of the working compartment.

12.9b Moving-Boundary Electrophoresis

In addition to microelectrophoresis, another important method for the determination of mobility is the *moving-boundary method* (Longsworth 1959). In essence, this is no different from the moving-boundary method as applied to simple ions. The apparatus most commonly used is that of Arne Tiselius (Nobel Prize, 1948), which is illustrated schematically in Figure 12.11. The Tiselius cell consists of a U tube of rectangular cross section that is segmented in such a way that the sections between the lines AA′ and BB′ in the figure can be laterally displaced with respect to the rest of the apparatus. The offset segments of the U tube are filled with the colloidal dispersion and, after thermal equilibration with the buffer solution contained in other parts of the apparatus, the various sections are aligned so that sharp boundaries are obtained. The location of the boundaries is usually observed by schlieren optics that identify refractive index gradients (see Section 2.4). As the macroions migrate in the electric field, the schlieren peak becomes displaced and the mobility of a colloidal component may be determined by measuring the rate of boundary movement per unit electric field. Relatively longer times are required for accurate mobility experiments than for microelectrophoresis since the particles must migrate over macroscopic distances rather than microscopic ones. To avoid contamination of the electrolyte in the U tube with electrode products, the electrodes are generally located near the bottom of large reservoirs as shown in Figure 12.11. Relatively concentrated salt solution is used to cover the electrodes, with the buffer solution layered on top.

Under optimum conditions the dimensions of the cross section of the cell are such that the effects of electroosmosis are minimal. The rectangular profile of the cross section allows for both good thermal equilibration (because one dimension is short) and good optical precision (because the other dimension is longer).

Moving-boundary electrophoresis is most widely applied to protein mixtures. In such a case each molecular species travels with a characteristic velocity. After sufficient time the various components in a mixture become effectively separated, and the percentage of each may be determined by measuring the areas under the schlieren peaks. Figure 12.12a shows a

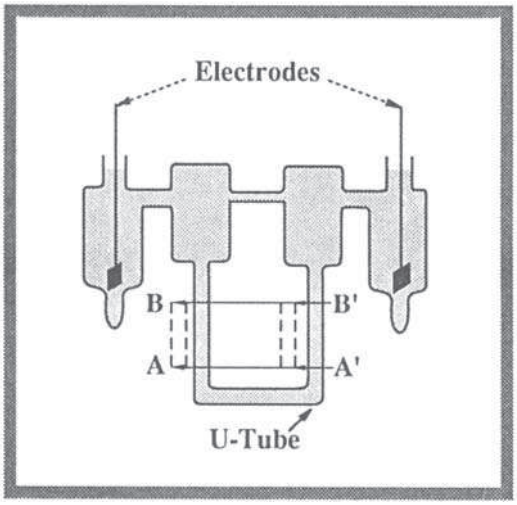
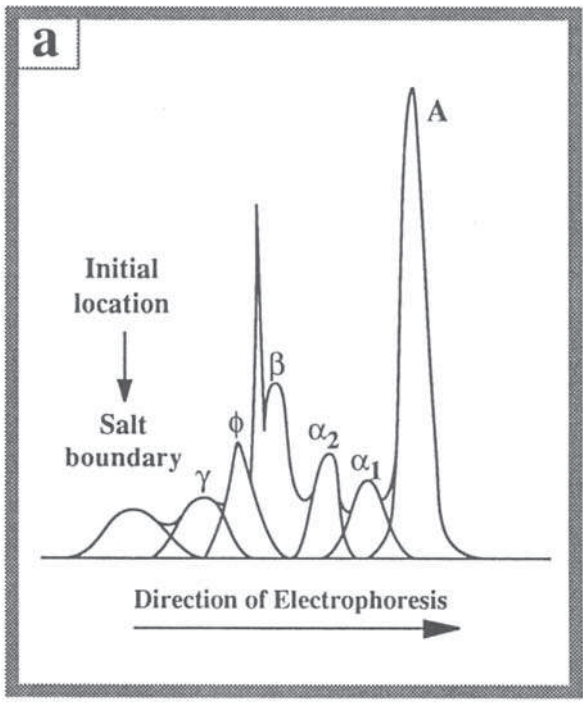


FIG. 12.11 Schematic illustration of a Tiselius-type moving boundary electrophoresis apparatus.



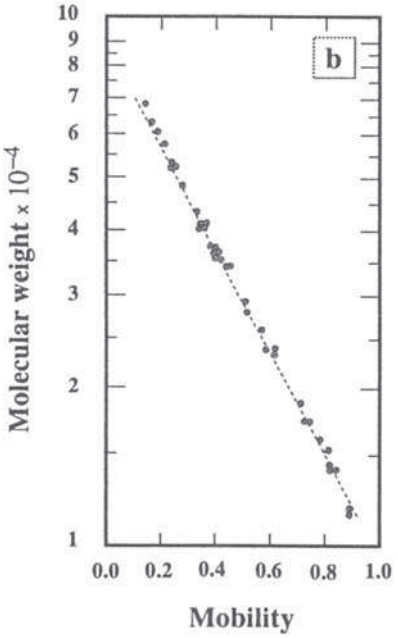


FIG. 12.12 Electrophoresis patterns for human serum: (a) schematic of schlieren profiles; and (b) semilog plot of protein molecular weight versus electrophoretic mobility for particles electrophoresed on cross-linked polyacrylamide. (Reprinted with permission from K. Weber and M. Osborn, *J. Biol. Chem.*, **244**, 4404 (1969).)

typical electrophoresis pattern for human blood serum. In this figure the protein albumin (A), α_1-, α_2-, β-, and γ-globulin, and fibrinogen (ϕ) are fairly clearly resolved. The remaining peak in the figure is the boundary between the original buffer and the colloid. This "false boundary" moves little in an electrophoresis experiment and is obviously not considered in determining the percentages of different proteins in a mixture. Some additional details on moving-boundary electrophoresis are available in Longsworth (1959) and Probstein (1994).

12.9c Zone Electrophoresis

When separation rather than determination of mobility is the primary objective of an electrophoresis experiment, a technique called *zone electrophoresis* is quite widely employed. In zone electrophoresis, a supporting medium such as moist filter paper or a gel such as polyacrylamide is the location of the particle migration. The method thus resembles solid-liquid chromatography, and many of the substrates and analytical methods of solid-liquid chromatography are used in this electrophoretic procedure as well. As with chromatography, a spot or band of a mixture is applied to one end of the support medium. As the electrophoresis proceeds, spots or bands of the individual components appear at different locations along the axis of the voltage gradient. Sometimes the resolution is improved by following the electrophoresis by a chromatographic separation at right angles to the direction of the initial separation.

Zone electrophoresis is influenced by adsorption and capillarity, as well as by electroosmosis. Therefore evaluation of mobility (and ζ) from this type of measurement is considerably more complex than from either microelectrophoresis or moving-boundary electrophoresis. Nevertheless, zone electrophoresis is an important technique that is widely used in biochemistry and clinical chemistry. One particularly important area of application is the field of immunoelectrophoresis, which is described briefly in Section 12.11. Additional information on zone electrophoresis may be obtained from Probstein (1994) and Hunter (1981) and the references given there. Variants of zone electrophoresis also exist; see, for example, Gordon et al. (1988) for information on a variant known as *capillary zone electrophoresis* and Righetti (1983) for information on what is known as *isoelectric focusing*.

Figure 12.12b illustrates the application of gel electrophoresis to protein characterization. In this illustration a cross-linked polyacrylamide gel is the site of the electrophoretic migration of proteins that have been treated with sodium dodecyl sulfate. The surfactant dissociates the protein molecules into their constituent polypeptide chains. The results shown in Figure 12.12b were determined with well-characterized polypeptide standards and serve as a calibration curve in terms of which the mobility of an unknown may be interpreted to yield the molecular weight of the protein. As with any experiment that relies on prior calibration, the successful application of this method requires that the unknown and the standard be treated in the same way. This includes such considerations as the degree of cross-linking in the gel, the pH of the medium, and the sodium dodecyl sulfate concentration. The last two factors affect the charge of the protein molecules by dissociation and adsorption, respectively. Example 12.5 considers a similar application of electrophoresis.

* * *

EXAMPLE 12.5 *Estimation of Number of Nucleotides in Glycine tRNA Using Electrophoresis.* Synthetic DNA standards and RNA molecules were electrophoresed in 7 M urea solution on cross-linked polyacrylamide gels (Maniatis et al. 1975). A semilog plot of the number of nucleotides versus the mobility relative to xylene cyanol FF dye is linear and includes the points (N = 100, u_{rel} = 0.33) and (N = 50, u_{rel} = 0.55). Estimate the number of nucleotides in the glycine tRNA molecule of *Staphylococcus epidermidis* if it shows a relative mobility of 0.16.

Solution: The linear semilog plot means that these data follow the equation $\ln N = b + mu_{rel}$. Since we know two points from this plot, we can evaluate the constants m and b by simultaneous equations. This procedure yields b = 5.63 and m = −3.09. Combining these constants with the observed mobility allows the number of nucleotides in the unknown to be calculated by the formula $\ln N = 5.63 + (-3.09)(0.16) = 170$. ■

* * *

12.10 DETERMINING THE SURFACE CHARGE FROM ELECTROKINETIC MEASUREMENTS

In the quantitative sections of this chapter the primary emphasis has been on establishing the relationship between the electrophoretic properties of the system and the zeta potential. We saw in Chapter 11 that potential is a particularly useful quantity for the characterization of lyophobic colloids. In this context, then, the ζ potential is a valuable property to measure for a lyophobic colloid. For lyophilic colloids such as proteins, on the other hand, the charge of the particle is a more useful way to describe the molecule. In this section we consider briefly what information may be obtained about the charge of a particle from electrophoresis measurements.

12.10a Relation Between Surface Charge and Zeta Potential

We have lamented the fact that electrokinetic potentials cannot be evaluated independently to check the correctness of various theories. However, the charge of a protein can be evaluated from its titration curve. Therefore, if we can find a way to evaluate particle charge from electrokinetic data, the long-sought independent verification will be established. The net charge q of a particle is equal and opposite to the total charge in the double layer. The increment of charge in a spherical shell of radius r and thickness dr in the double layer is given by the area of the shell times its thickness times the charge density:

$$dq = 4\pi r^2 \rho^* dr \tag{78}$$

Integrating this expression over the entire double layer gives

$$q = -\int_{R_s}^{\infty} 4\pi r^2 \rho^* \, dr = \int_{R_s}^{\infty} \varepsilon \nabla^2 \psi \, 4\pi r^2 \, dr = 4\pi\varepsilon \int_{R_s}^{\infty} \frac{d}{dr}\left(r^2 \frac{d\psi}{dr}\right) dr \tag{79}$$

where the Poisson equation (11.24) has been substituted for ρ^*. Integration yields

$$q = 4\pi\varepsilon \left(r^2 \frac{d\psi}{dr}\right)_{R_s}^{\infty} = -4\pi\varepsilon R_s^2 \left(\frac{d\psi}{dr}\right)_{R_s} \tag{80}$$

where the derivative is evaluated at $r = R_s$.

Now Equation (46) is used to evaluate the derivative in Equation (80):

$$\left(\frac{d\psi}{dr}\right)_{R_s} = -\frac{\zeta}{R_s}(1 + \kappa R_s) \tag{81}$$

Substituting this result into Equation (80) gives

$$q = 4\pi\varepsilon\zeta R_s(1 + \kappa R_s) \tag{82}$$

for the charge enclosed by the surface of shear. (Contrast this with Equation (11.50).)

This discussion shows that the evaluation of charge from electrokinetic measurements involves all the complications inherent in the evaluation of ζ plus the additional restrictions of low potentials and spherical particles. Additional relationships have been developed that permit these restrictions to be relaxed, but we do not discuss these here.

12.10b Charge of Protein Molecules

We conclude this section by comparing briefly the charge on protein molecules as determined by electrophoresis measurements through Equation (82) and as determined by titration. Protein molecules carry acid and base functions in side groups along the macromolecule. In a strongly acidic solution amine groups will be protonated, and the protein will carry a positive charge. Addition of a known number of equivalents of strong base to a measured volume of

protein solution results in a change of pH and a change in the state of charge of the protein. From the volume of the solution, the change of pH, and a knowledge of activity coefficients, the number of added equivalents of base that react with the protein may be determined. It should be noted that the added base may remove protons from either neutral groups or cationic groups.

Thus in acid solution a protein may have a charge corresponding to the binding of z H^+ ions: $+z$. After z OH^- ions have reacted with it, the molecule will have a *net* charge of *zero*. If the reactions consist exclusively of the removal of bound H^+ ions, the net charge (zero) would correspond to the actual charge of the particle. If all the reacting OH^- ions remove H^+ ions from neutral groups on the other hand, the molecule would be twice as highly charged as the initial species, with an equal number of positive and negative charges. In reality, both processes occur together, so it cannot be inferred that the point of equivalency—called the *isoionic point*—corresponds to an uncharged state. All that can be said is that the net charge is zero at the isoionic point. Addition of more base beyond this point will increase (still by both processes) the negative charge of the molecule even further. The isoionic point corresponds to a point at which the polyelectrolyte changes sign. This discussion shows that the net charge relative to the initial condition of the colloid is readily determined from titration curves.

The electrophoretic mobility of a protein solution may also be measured as a function of pH. By this technique it may also be observed that the colloid passes through a point of zero net charge at which its mobility is zero. The point at which charge reversal is observed electrophoretically is called the *isoelectric point*.

Figure 12.13 shows the relationship between the charge of egg albumin as determined by titration and by electrophoresis. The points were determined electrophoretically, and the solid line was determined by titration. The titration curve has been shifted so that the isoionic point and the isoelectric point match. It will be observed that the two independent charge determinations led to slightly different values. The charges determined electrophoretically are 60% of those determined analytically. If the titration results are multiplied by 0.60, the dashed line in Figure 12.13 is obtained. This shows clearly that the two determinations are identical in pH dependence, but raises the question as to the origin of the constant percentage difference.

There are several minor corrections that tend to reduce the discrepancy between the two curves, for example, corrections for relaxation and finite ion size. It should also be remembered that electrophoresis measures the net charge inside the surface of shear. To the extent that this diverges from the "surface" of the molecule, the two techniques may very properly

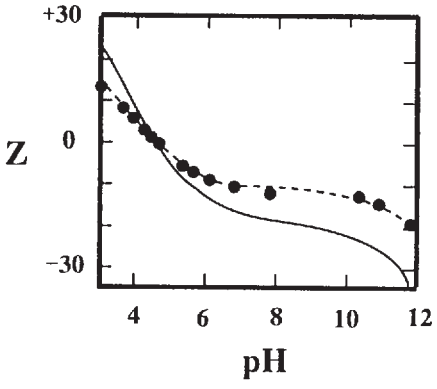


FIG. 12.13 Net charge of egg albumin versus pH. The points were determined by electrophoresis, and the solid line by titration; the broken line represents 60% of charge from titration. (Data from L. G. Longsworth, *Ann. NY Acad. Sci.*, **41**, 267 (1941). (Redrawn with permission from J. Th. G. Overbeek, Quantitative Interpretation of the Electrophoretic Velocity of Colloids. In *Advances in Colloid Science*, Vol. 3 (H. Mark and E. J. W. Verwey, Eds.), Wiley, New York 1950.)

"see" different charges for the colloid. Additional studies in this area, therefore, might help to clarify the relationship between the actual surface and the surface of shear.

We noted above that proteins display essentially the same mobility both as free molecules and when adsorbed on carrier particles. Adsorption clearly increases the radius of the kinetic unit appreciably, so this effect on mobility is unexpected. One way to rationalize this result is to assume that the protein adsorbs on the surface with very little alteration of the shape it has in free solution. Next assume that it is the radius of these molecular protuberances rather than the overall radius of curvature of the carrier that governs the mobility.

12.11 APPLICATIONS OF ELECTROKINETIC PHENOMENA

Throughout most of this chapter the emphasis has been on the evaluation of zeta potentials from electrokinetic measurements. This emphasis is entirely fitting in view of the important role played by the potential in the Derjaguin-Landau-Verwey-Overbeek (DLVO) theory of colloidal stability. From a theoretical point of view, a fairly complete picture of the stability of dilute dispersions can be built up from a knowledge of potential, electrolyte content, Hamaker constants, and particle geometry, as we discuss in Chapter 13. From this perspective the fundamental importance of the ζ potential is evident. Below we present a brief list of some of the applications of electrokinetic measurements.

12.11a Colloid Stability

As we have emphasized in some of the previous chapters, there are many practical situations in which coagulation is a process of considerable importance. Often all that is desired in these cases is either to maximize or minimize coagulation in some experimental system. Systems of practical interest are frequently so complex that theoretical models apply to them only qualitatively at best. In this context the concept of zeta potential emerges as a valuable practical parameter. If two systems of different ζ are compared—all other factors being equal—the one that has the higher ζ potential is expected to be more stable with respect to coagulation and the one with the lower potential less stable. The second case is particularly important. At the isoelectric point electrophoretic mobility is zero, ζ is zero, and the potential energy of repulsion between particles is minimal. Thus electrophoresis measurements can be used as an indicator for optimum conditions for coagulation. In this type of application the technique is used as a null detector; hence it is independent of any model or equation for interpretation.

12.11b Sewage Treatment

One important—if not so appealing—example of the above application is in sewage treatment. Industrial wastewater and domestic sewage contain an enormous assortment of hydrophilic and hydrophobic debris of technological and biological origin. The concentration of surface-active materials in sewage from household detergents alone is about 10 ppm. In addition, sewage abounds in amphipathic materials of natural and biological origin. These substances tend to adsorb on and impart a charge to the suspended solid and liquid particles in the polluted water. Negative zeta potentials in the range of 10 to 40 mV are fairly typical for the suspended particles in sewage.

A typical purification scheme consists of adding $NaHCO_3$ and $Al_2(SO_4)_3$ (alum) to water with agitation. The aluminum ion undergoes hydrolysis and precipitates as a gelatinous, polymeric hydrated oxide. Suspended material is enmeshed in this amorphous precipitate, which produces *flocs* by bridging the particles together. The polymeric nature of the "$Al(OH)_3$" precipitate permits us to compare it with protein in its ability to coat particles and impart to the carrier particles its own characteristic potential. Like proteins, $Al(OH)_3$ is also capable of reacting with both H^+ and OH^- so that these ions determine the charge of the suspended units, whether these are flocs formed by the $Al(OH)_3$ network or individual particles with an adsorbed layer of $Al(OH)_3$. In either case the charge is pH sensitive, the isoelectric point occurring near pH 6. It is under these pH conditions, then, that the flocculating effec-

tiveness of the precipitate is optimum. In fact, the pH is often adjusted so that the hydrous aluminum oxide surface has a slightly positive value of ζ (about 5 mV). This promotes further interaction with slightly anionic polymeric materials that are also added to further build up and strengthen flocs. Once adequate flocculation has been accomplished, the dispersed particles are removed by sedimentation, centrifugation, or filtration.

Numerous other applications could be listed in which electrokinetic characterization provides a convenient experimental way of judging the relative stability of a system to coagulation. Paints, printing inks, drilling muds, and soils are examples of additional systems with properties that are extensively studied and controlled by means of the ζ potential.

12.11c Environmental Remediation

Contamination in low-permeability soil is a problem of major importance in environmental remediation. Traditional treatments of contaminated soils include bioremediation methods, vapor extraction, and what are known as "pump-and-treat" methods. However, poor accessibility to the contaminants and difficulties in delivering reagents used for treatment make these current *in situ* methods very ineffective. Electroosmosis (combined possibly with one or more of the traditional techniques) can potentially serve as an alternative *in situ* treatment process, as shown in Figure 12.14.

Electroosmosis has been used for dewatering fine sands, clays, and silts since the 1930s, and its application in environmental remediation is somewhat similar to its earlier uses. For example, as illustrated in Figure 12.14, an electrical potential difference is set up between two embedded granular electrodes on either side of the contaminated zone. Water injected into the soil at the anode is made to flow through the contaminated zone under the action of electroosmosis, thus bringing the contaminants (e.g., metals and organics) to the surface at the cathode region for further treatment and disposal. Advantages of such a technique include a relatively uniform flow through heterogeneous regions, a high degree of control of the flow direction, and very low power consumption.

Figure 12.14 illustrates a vertical flow arrangement, but other configurations are also possible. The process as illustrated in Figure 12.14 is being developed by Monsanto Company and is known as the "lasagna process" because of the layered structure of the treatment zones (Ho et al. 1993).

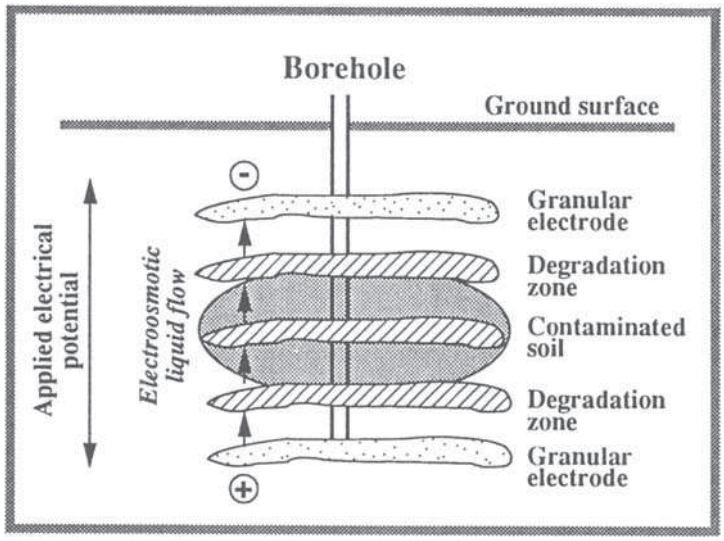


FIG. 12.14 The use of electroosmosis in environmental remediation (known as the lasagna process). (Redrawn with permission of Ho et al. 1993.)

The use of electroosmosis in groundwater remediation is not a well-established technology, and a number of technical issues are currently being investigated. However, it illustrates the types of large-scale practical applications of charge-induced phenomena in technology. Another interesting application of electroosmosis, for extracting bitumen from oil sands, is described by Masliyah (1994).

12.11d Immunoelectrophoresis

In addition to these applications in which ζ is used to monitor for optimum coagulation conditions, there are applications of electrophoresis that explicitly depend on mobility or differences in mobility for their usefulness. We have already noted that zone electrophoresis is similar in many ways to chromatography. One important application of the ability of electrophoresis to segregate materials by mobility is *immunoelectrophoresis*. This technique uses known immunochemical reactions between antigen and antibody for the identification of proteins separated electrophoretically. Experimentally, an antigen mixture is subjected to electrophoresis on a suitable medium (usually agar gel). Next the antibody mixture is introduced into a slit cut in the gel parallel to the axis of the separation. The antigen and antibody components then diffuse toward one another, producing an arc-shaped precipitate where the two fronts meet.

Tests of this sort are particularly useful for comparing either two antigen preparations (against a single antibody) or two antibody preparations (against a single antigen). In such a comparison one of the samples serves as a control, and differences between the two are revealed by an unpaired arc of precipitate at a particular location along the path of separation.

Alternatively, electrophoretic separation in one direction may be followed by a second electrophoresis in a perpendicular direction, the latter into a gel containing antibodies. This technique is called *crossed immunoelectrophoresis* and combines high resolution with the possibility of quantification by measuring the area of the precipitate formed. Figure 12.15 is a

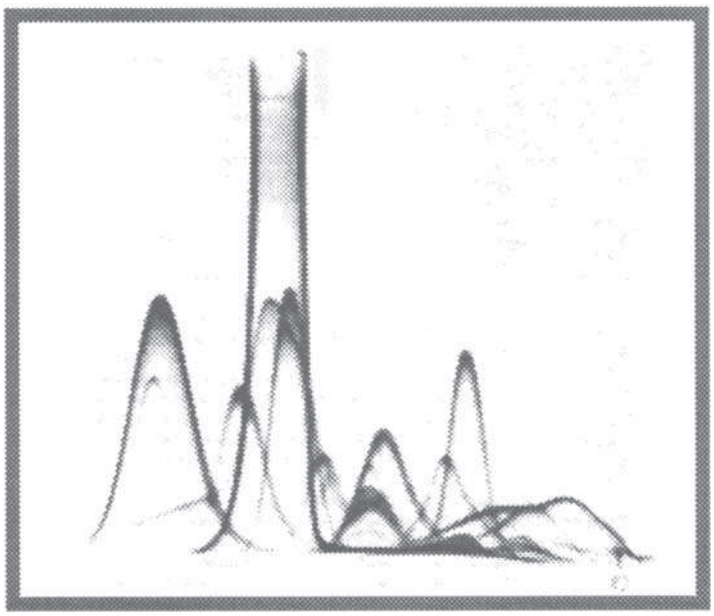


FIG. 12.15 Crossed immunoelectrophoresis of human serum with rabbit antihuman serum. (Redrawn with permission from B. Weeke, in *A Manual of Quantitative Immunoelectrophoresis: Methods and Applications* (N. H. Axelsen, J. Krøll, and B. Weeke, Eds.), Universitetsforlaget, Oslo, Norway, 1973.)

photograph of the peaks of antigen-antibody precipitates formed by crossed immunoelectrophoresis of human serum interacting with rabbit antihuman serum.

12.11e Electrodeposition

Electrodeposition is another direct application of electrophoretic mobility. In this process, as in electroplating with metals, the substance to be coated is made into an electrode of opposite charge from the particles to be deposited. At one time, natural rubber latex was extensively fabricated in this way. Paint coatings that are quite dense and coherent with little tendency to sag or run can be prepared by electrodeposition. If the deposited layer has insulating properties, this technique is also self-regulating, producing a uniform thin covering of very good quality.

12.11f Applications of Other Electrokinetic Phenomena

Although electrophoresis is the most important of the electrokinetic methods, it is not the only one with practical applications. We already noted in Section 12.7 that streaming potentials could be quite hazardous in low-conductivity, highly flammable substances such as purified hydrocarbons. In this case our knowledge of the effect enables us to minimize it. Dewatering fine suspensions that are not amenable to filtration is an application of electroosmosis, as mentioned in Section 12.1b. Peat, clay, and other minerals have been dewatered this way, and water may be removed from moist soil prior to excavation by electroosmosis. Electrodes are driven into the ground, with the cathode in the form of a perforated pipe. The surface of the soil particles carries a negative charge; therefore the diffuse part of the double layer is positive, and the solution moves toward the cathode. The water that collects in the cathode is subsequently removed by pumping. Similar ideas have been suggested in studies of salt rejection characteristics of reverse osmosis membranes (Jacazio et al. 1972; Sonin 1976).

REVIEW QUESTIONS

1. List the different electrokinetic phenomena and discuss their similarities and differences.
2. Why are these electrokinetic phenomena important?
3. What is the *mobility* of a particle? How is *electrophoretic mobility* defined?
4. What is *zeta potential*, and how is it related to the electrophoretic mobility? What properties of the dispersion influence such a relation?
5. What is the relation between the zeta potential and the *surface potential*?
6. What is the relation between the zeta potential and the charge on a particle? How is this relation determined?
7. What is the *Hückel equation*, and what approximations are made in its derivation?
8. What is the *Helmholtz-Smoluchowski* equation? How is it different from the Hückel equation?
9. What is *Henry's equation*, and what are the assumptions implicit in its derivation?
10. What is *electroosmosis*? How is it used to measure the zeta potential?
11. Give an example of the use of electroosmosis.
12. What is *surface conductivity*, and when and why is it important?
13. Define *streaming potential* and explain how it is measured. What is its relation to the zeta potential?
14. What is the *viscoelectric effect*? How does it affect electrokinetic phenomena?
15. What is *surface of shear*?
16. What are *moving-boundary electrophoresis* and *zone electrophoresis*? Where are they used?

REFERENCES

General References (with Annotations)

Crow, D. R., *Principles and Applications of Electrochemistry*, 4th ed., Blackie A and P, London, 1994. (Undergraduate level. An introduction to electrochemistry; requires only basic physical chemistry as prerequisite.)

Hunter, R. J., *Zeta Potentials in Colloid Science: Principles and Applications*, Academic Press, London, 1981. (Advanced. This is a research-level monograph on electrokinetic phenomena and electroviscous and viscoelectric effects and contains extensive details on the subject.)

Masliyah, J. H., *Electrokinetic Transport Phenomena*, Alberta Oil Sands Technology and Research Authority, Edmonton, Alberta, Canada, 1994. (Graduate and undergraduate levels. An excellent introduction to transport processes relevant to applications of electrokinetic phenomena. Most of the material is accessible to undergraduate students. Chapter 12 presents some very practical applications of electrokinetic phenomena of interest to engineers.)

Overbeek, J. Th. G., Electrokinetic phenomena. In *Colloid Science*, Vol. 1 (H. R. Kruyt, Ed.), Elsevier, Amsterdam, Netherlands, 1952.

Overbeek, J. Th. G., and Lyklema, J., Electric Potentials in Colloidal Systems. In *Electrophoresis*, Vol. 1 (M. Bier, Ed.), Academic Press, New York, 1959.

Overbeek, J. Th. G., and Wiersma, P. H., The Interpretation of Electrophoretic Mobilities. In *Electrophoresis*, Vol. 2 (M. Bier, Ed.), Academic Press, New York 1967. (Graduate and undergraduate levels. The above three articles, by three of the pioneers in colloid science, are some of the classical references on electrophoresis.)

Probstein, R. F., *Physicochemical Hydrodynamics*, 2d ed., Wiley-Interscience, New York, 1994. (A primarily first-year-graduate-level textbook on colloidal and hydrodynamic phenomena of interest in practice. Has good discussions on electrokinetic phenomena.)

Other References

Abramson, H. A., Moyer, L. S., and Gorin, M. H., *Electrophoresis of Proteins*, Hafner, New York, 1964.

Atkins, P. W., *Physical Chemistry*, 5th ed., W. H. Freeman, New York, 1994.

Carlson, C. F., U.S. Patent No. 2,221,776 (1938; 1940).

Gordon, M. J., Huang, X., Pentoney, S. L., Jr., and Zare, R. N., *Science*, **242**, 224 (1988).

Ho, S. V., Sheridan, P. W., Athmer, C. J., Brodsky, P. H., Heitkamp, M. A., and Brackin, J. M., Integrated *In Situ* Remediation Technology—The Lasagna Process, paper presented at the American Chemical Society meeting, Atlanta, GA, September 1993 (Paper 279, Session 43).

Jacazio, G., Probstein, R. F., Sonin, A. A., and Yung, D., *J. Phys. Chem.*, **76**, 4015 (1972).

Kitahara, A., and Watanabe, A. (Eds.), *Electrical Phenomena at Interfaces: Fundamentals, Measurements, and Applications*, Marcel Dekker, New York, 1984.

Kurita, T., *Electrophotography*, **3**, 16 (1961).

Loeb, A. L., Overbeek, J. Th. G., and Wiersema, P. H., *The Electrical Double Layer Around a Spherical Colloid Particle*, Massachusetts Institute of Technology Press, Cambridge, MA, 1960.

Longsworth, L. G., Moving Boundary Electrophoresis—Practice. In *Electrophoresis*, Vol. 1 (M. Bier, Ed.), Academic Press, New York, 1959.

Lyne, M. B., and Aspler, J. S., Ink-Paper Interactions in Printing—A Review. In *Colloids and Surfaces in Reprographic Technology* (M. Hair and M. D. Croucher, Eds.), American Chemical Society, Washington, DC, 1982.

Maniatis, T., Jeffrey, A., and van de Sande, H., *Biochemistry*, **14**, 3787 (1975).

Metcalfe, K. A., *J. Sci. Instrum.*, **32**, 74 (1955).

Metcalfe, K. A., *J. Sci. Instrum.*, **33**, 194 (1956).

Ohyama, Y., Kurita, T., and Takahashi, Y., *Electrophotography*, **3**, 26 (1961).

Righetti, P. G., *Isoelectric Focusing: Theory, Methodology and Applications*, Elsevier Biomedical, Amsterdam, Netherlands, 1983.

Shaw, D. J., *Electrophoresis*, Academic Press, New York, 1969.

Sonin, A. A., Osmosis and Ion Transport in Charged Porous Membranes: A Macroscopic Mechanistic Model. In *Charged Gels and Membranes I* (E. Sélégny, Ed.) D. Reidel, Dordrecht, Holland, 1976.

PROBLEMS

1. Particles of Fe_2O_3 with an average diameter of 1 μm were dispersed in xylene containing 5×10^{-3} mole liter^{-1} of copper(I) oleate. These showed an electrophoretic mobility of 0.110 μm s^{-1} V^{-1} cm. The conductivity of the solution was 4.7×10^{-10} ohm^{-1} cm^{-1}, indicating an ion

concentration about 10^{-11} M.* Calculate κ^{-1} for this concentration. Which limiting form of Equation (40) is most applicable in this system? Would the same conclusion be true for a 5×10^{-3} M aqueous solution of a 1 : 1 electrolyte? What is ζ for these particles? For xylene, $\varepsilon_r = 2.3$ and $\eta = 0.0065$ P.

2. Criticize or defend the following proposition: Zeta potentials for three different polystyrene latex preparations were calculated by the Helmholtz-Smoluchowski equation from electrophoresis measurements made in different concentrations of KCl.†

Latex designation	$R_s \times 10^8$ (cm)	ζ (mV) 10^{-1} M KCl	10^{-2} M KCl	10^{-3} M KCl
L	475	21	29	40
M	610	29	39	53
N	665	34	47	64

These zeta potentials are inaccurate because the range of κR_s values exceeds the range of validity for the Helmholtz-Smoluchowski equation. The nature of the error is such as to make the estimated values of ζ too low.

3. The electrophoretic mobility of sodium dodecyl sulfate micelles was determined by the moving-boundary method after the micelles were made visible by solubilizing dye in them. This quantity was measured at the critical micelle concentration (CMC) in the presence of various concentrations of NaCl. The radius of the micelles was determined by light scattering‡

Moles of NaCl liter^{-1}	$u \times 10^4$ (cm^2 s^{-1} V^{-1})	κR_s
0.00	4.55	0.61
0.05	3.63	1.69

Estimate from Figure 12.5a the appropriate value of C to be used in Equation (40) according to Henry's equation. Calculate ζ using these estimated C values. Figure 12.5b shows that Henry's equation overestimates C (and therefore underestimates ζ). Estimate C from Figure 12.5b using the curve for the ζ value that is nearest—on the high side—to the values obtained by using Henry's equation. Reevaluate ζ on the basis of these "constants." For this system, $\varepsilon_r = 78.5$ and $\eta = 0.0089$ P.

4. The accompanying mobility data for colloidal SiO_2 at a constant ionic strength of 10^{-3} M reveal the superpositioning of specific chemical effects on general electrostatic phenomena. Adjustment of pH was made by addition of HNO_3 or KOH, maintaining the ionic strength. The following results were obtained:§

	$u \times 10^4$ (cm^2 s^{-1} V^{-1})								
pH of solution:	2.0	3.0	4.0	5.0	6.0	7.0	8.0	9.0	10.0
SiO_2	0	−1.4	−1.7	−2.0	−2.3	−2.5	−2.6	−2.8	−3.0
SiO_2 + 10^{-4} M $La(NO_3)_3$	0	−1.1	−1.2	−1.2	−1.1	−0.1	+2.2	+0.5	−1.2

Criticize or defend the following propositions: H^+ and OH^- are potential determining for SiO_2—in the absence of a hydrolyzable cation—with an isoelectric point of 2.0. For solid $La(OH)_3$ the zero point of charge is known (by independent studies) to be 10.4. The solid

*Koelmans, H., and Overbeek, J. Th. G., *Discuss. Faraday Soc.*, **18**, 52 (1954).
†Kitahara, A., and Ushiyama, H., *J. Colloid Interface Sci.*, **43**, 73 (1973).
‡Stigter, D., and Mysels, K. J., *J. Phys. Chem.*, **59**, 45 (1955).
§James, R. O., and Healy, R. W., *J. Colloid Interface Sci.*, **40**, 42 (1972).

surface apparently becomes coated by $La(OH)_3$ at higher pH levels and goes through a transition from one character to another at intermediate pH values.

5. In their study of the effects of hydrolyzable cations on electrokinetic phenomena (see Problem 4), James and Healy compared the electrophoretic behavior of colloidal silica with the streaming potential through a silica capillary. In both sets of experiments the solution was 10^{-3} M KNO_3 and 10^{-4} M $Co(NO_3)_2$. The following results were obtained:

pH	6.0	7.0	7.5	8.0	9.0	10.0
ζ (mV) from streaming potential	−65	−55	−30	+10	+25	+20
$u \times 10^4$ ($cm^2\ s^{-1}\ V^{-1}$)	−2.5	−2.5	−2.2	−1.8	+0.5	+0.3

The silica surface area-to-solution volume ratio was 2×10^{-3} m^2 $liter^{-1}$ for the streaming potential experiment and 1.0 m^2 $liter^{-1}$ for the electrophoresis experiment. Calculate ζ_{HS} at each pH from the electrophoresis data ($\eta = 0.00894$ P, $\varepsilon_r = 78.5$). Propose an explanation for the charge reversal behavior of the silica. Discuss the origin of the difference between ζ_{HS} and $\zeta_{St\ Pot}$ in terms of this model.

6. Somasundaran and Kulkarni* measured the streaming potential of 10^{-3} N KNO_3 against quartz at 25°C, obtaining the following results:

E_{str} (mV)	−9.0	−18.0	−26.0	−35.0
p (mm Hg)	50	100	150	200

Use these data to evaluate ζ/k. What would be the value of the ratio V/I for this system? What would be the rate of volume displacement if a current of 1.0 mA flowed through the apparatus? Evaluate ζ for the quartz-solution interface, assuming $\Lambda \simeq 145$ $cm^2\ eq^{-1}\ ohm^{-1}$ for 10^{-3} N KNO_3.

7. It has been estimated† that a specific conductivity of 10^3 picomho m^{-1} would provide an ample margin of safety against electrokinetic explosions for the handling of refined petroleum products. These authors also measured the concentrations of various additives needed to reach this level of conductivity:

Solvent	Additive	Concentration (kmol m^{-3})
Benzene	Tetraisoamyl ammonium picrate	1×10^{-4}
Benzene	Calcium diisopropylsalicylate	5×10^{-3}
Gasoline	Ca salt of di-(2-ethylhexyl)sulfosuccinic acid	1×10^{-3}
Gasoline	Cr salt of mono- and dialkyl (C_{14}-C_{18}) salicylic acid	2.5×10^{-6}

Calculate the apparent value of the equivalent conductance Λ for each of these electrolytes in the conventional units $cm^2\ eq^{-1}\ ohm^{-1}$. How do the Λ values of these compounds compare with Λ_0 for simple electrolytes in aqueous solutions?

8. The pH variation of the electrophoretic mobility of solid $Th(OH)_4$ in 10^{-2} M HNO_3-KOH electrolyte is as follows:‡

pH	7.6	8.0	9.0	9.6	10.0	10.3	10.6	11.3
$u \times 10^4$ ($cm^2\ s^{-1}\ V^{-1}$)	+2.4	+2.2	+1.3	+1.0	−0.1	−1.1	−1.5	−1.8

Use these data to evaluate the isoelectric point for $Th(OH)_4$. Since H^+ and OH^- appear to be potential determining, ψ may be estimated at various pH levels according to Equation (11.1) if we identify the isoelectric point with the true point of zero charge. Compare these values

*Somasundaran, P., and Kulkarni, R. D., *J. Colloid Interface Sci.*, **45**, 591 (1973).
†Klinkenberg, A., and Poulston, B. V., *J. Inst. Pet.*, **44**, 379 (1958).
‡James, R. O., and Healy, T. W., *J. Colloid Interface Sci.*, **40**, 42 (1972).

with values of ζ calculated by means of the Helmholtz-Smoluchowski equation (η = 0.0089 P, ε_r = 78.5). Are the results qualitatively (quantitatively?) consistent with Figure 12.8?

9. The aggregation number n and radius of sodium dodecyl sulfate micelles (by light scattering) and the zeta potential (from electrophoresis, by an accurate formula) were determined in the presence of various concentrations of NaCl.*

Moles of NaCl liter^{-1}	ζ (mV)	$R_s \times 10^8$ (cm)	κR_s	n
0.01	92.3	22.1	0.86	89
0.03	80.9	23.0	1.32	100
0.10	68.3	24.0	2.40	112

Use Equation (82) to estimate the charge of the micelles. What approximation(s) in the derivation of Equation (82) prevents this expression from applying exactly to this system? On the basis of the charges evaluated by Equation (82), calculate the ratio of charge to aggregation number, the effective degree of dissociation, of these micelles. How do these results compare with the numbers given in Table 8.1?

10. An electrophoretic technique that is especially interesting for the study of proteins is called "isoelectric focusing." In this method electrophoresis is carried out across a medium that supports a pH gradient. The pH gradient and cell polarity are such that the cathode end of the column is relatively basic. Thus a positively charged protein gradually loses its charge as it migrates, finally coming to rest at a pH corresponding to its isoelectric point. Carlstrom and Vesterberg† used this method to study the heterogeneity of peroxidase from cow's milk. After focusing was achieved, the column was drained and the pH and absorbance (at 280 nm) of successive fractions of eluent were measured:

Fraction number	Absorbance	pH	Fraction number	Absorbance	pH
12	0.9	9.830	28	1.4	9.49
14	3.0	9.800	30	0.9	9.45
16	2.1	9.750	32	0.6	9.38
18	1.2	9.700	34	0.8	9.31
20	2.7	9.690	36	0.5	9.30
21	2.2	9.685	38	0.3	9.28
22	2.8	9.680	40	0.4	9.23
24	1.6	9.600	41	0.5	9.16
26	1.2	9.550	42	0.4	9.10

How many components does this sample apparently contain? What are the values of the isoelectric points for each?

*Stigter, D., and Mysels, K. J., *J. Phys. Chem.*, **59**, 45 (1955).

†Carlstrom, A., and Vesterberg, D., *Acta Chem. Scand.*, **21**, 271 (1967).

13

Electrostatic and Polymer-Induced Colloid Stability

You, who are blessed with shade as well as light, you who are gifted with two eyes, endowed with a knowledge of perspective, and charmed with the enjoyment of various colours, you, who can actually see an angle, and contemplate the complete circumference of a Circle in the happy region of Three Dimensions—how shall I make clear to you the extreme difficulty which we in Flatland experience in recognizing one another's configuration?

From Abbott's *Flatland*

13.1 INTRODUCTION

13.1a What Is Colloid Stability?

The term *colloid stability* stands for the ability of a dispersion to resist coagulation. The stability of dispersions may be either *kinetic* or *thermodynamic* and has been traditionally the primary focus of colloid science at least dating back to the ancient Egyptians. Kinetic stability is a consequence of a force barrier against collisions between the particles and possible coagulation subsequently. As we saw in Section 10.2, in such cases, coagulation is preferred because of the resulting reduction in thermodynamic "free" energy, but the interaction energy barrier in the interparticle energy is larger than the thermal energy and any other applied energy of the particles. Dispersions of charged latex particles in low-electrolyte environments provide examples of kinetically stabilized colloids. In the case of thermodynamic stability, coagulated states correspond to an *increase* in free energy and, therefore, are thermodynamically unfavorable.

We saw in Chapter 10 that the van der Waals force between particles in a dispersion is usually attractive and is strong at short interparticle separations. Therefore, if there are no repulsive interactions between particles, the dispersion will be unstable and coagulate. The protection against van der Waals attraction is usually provided in one of two ways:

1. As we saw in Chapter 11, surfaces of colloidal particles typically acquire charges for a number of reasons. The electrostatic force that results when the electrical double layers of two particles overlap, if repulsive, serves to counteract the attraction due to van der Waals force. The stability in this case is known as *electrostatic stability*, and our task is to understand how it depends on the relevant parameters.

2. In many practical instances (see Vignette I.5), electrostatic repulsion is not a convenient option. In such cases, a suitable polymer that adsorbs on the particle surfaces may be added to the dispersion. The resulting polymer layer masks the attraction and may also provide a repulsive force, partly due to pure steric effect, when the polymer layers on two interacting particles attempt to overlap with each other. This is what is known as *polymer-induced stability*. Polymer-induced stability is often referred to as *steric stability* for the above

reason, but the role of polymers in a colloidal dispersion is actually much more complex than this, and we try to get a feel for this below.

Our primary focus in this chapter is on kinetic stability of dispersions arising due to either electrostatic forces or polymer-mediated forces.

13.1b Why Is Colloid Stability Important?

Colloid stability enters our daily life in many different ways. A visit to the kitchen provides numerous examples of food colloids with microstructure and stability that are, in no small measure, an important aspect of their appeal to the palate! For example, mayonnaise—a mixture of vegetable oil, egg yolk, and vinegar or lemon juice—is an emulsion of oil in water and is stable because the lecithin molecules in the egg yolk provide the needed stability. Milk is another example. We have seen others in the vignettes in Chapters 1 and 4.

Electrostatic stability plays a dominant role in many separation processes, such as filtration of industrial wastewaters. Coagulation aids (known as *coagulants*) are routinely used to improve the effectiveness of separation processes in such cases. Polymer-induced stability is often the method of choice, particularly in the case of concentrated dispersions; for example, many pharmaceutical preparations, paints, inks, and liquid toners depend on surfactants or polymer additives for ensuring stable preparations. We see in Section 13.2 that in the case of concentrated dispersions both thermodynamic and kinetic issues often become very important.

Colloid stability plays a role in many processing operations as well. Vignette XIII provides an example of current interest.

VIGNETTE XIII DISPERSION-BASED PROCESSING: Steric Stabilization and Environmentally Friendly Polymerization Processing

Perhaps the term *steric stabilization* normally brings to mind dispersions such as paints and food colloids, which are usually stabilized against coagulation by a layer (sometimes a "brush") of polymer chains that mask the van der Waals attraction at short interparticle separations. However, there are other applications in which steric stabilization (and the steric effect, in general) provides interesting and exciting possibilities. We have already come across the role of the steric effect in the case of the so-called *stealth liposomes* as drug delivery vehicles in Vignette I.3 in Chapter 1. Here, let us look at another, the use of specially designed polymeric surfactants (*designer* surfactants?) for manufacturing polymer particles in an *environmentally friendly* fashion!

First, let us look at the classical manufacturing route to the large-scale production of many polymers of commercial importance (e.g., polystyrene, poly(vinyl chloride), poly(acrylic acid), etc.). These polymers are synthesized typically with water or an organic solvent as the dispersing medium (depending on whether the polymer is water insoluble or water soluble, respectively). This is a heterogeneous polymerization process that has two or more phases with the monomer or the polymer (or both) in a finely divided form (see Section 8.10b). The final product, in the form of a powder or a dispersion, is then used in subsequent fabrication steps to produce the end products in desired shapes through compaction, pressing, and so on. The particle sizes in the polymerization step are usually controlled by the addition of suitable surfactants that stabilize the particles against coagulation to prevent a large size distribution. To begin, this is already an example of steric stabilization in action! But what is wrong with it? The problem is that this processing route produces a large amount of hazardous waste, namely, either contaminated water or organic solvents (like chlorinated hydrocarbons and toluene), or both.

How can we minimize the damage to the environment? Common sense says that prevention is better than cure. If one can use an environmentally friendly solvent in the processing step, the discharge of hazardous chemicals and the need for environmental post-treatment can be avoided. This is an approach that is currently being explored in polymer processing as well as in other manufacturing technologies (DeSimone et al. 1994). In the case of the

polymerization operations, one possibility is to use supercritical CO_2, which resembles a liquid but has low viscosity, as the solvent. However, most polymers, with the exception of fluoropolymers, do not dissolve in CO_2. Here is the point at which specially designed surfactants enter the picture. What one needs is a molecularly engineered polymer surfactant with a backbone that can adsorb on the growing polymer particle, but with side chains or "tentacles" that are CO_2 loving so that the growing polymer particles can stay dispersed in the solvent (see Figure 13.1). In addition, adsorption of the surfactant backbone anchors the polymer on the surface of the particles, and the loops and the tails of the polymer provide a steric barrier against coagulation as desired. Recent research shows that such an approach is feasible.

We are not concerned with molecular engineering of surfactants in this chapter; our objective is to introduce the basic concepts concerning colloid stability, including the role of polymer (adsorbed or grafted on the particles or simply dispersed in the solvent along with the particles) in imparting stability to colloidal dispersions. In addition to highlighting the role of polymeric stabilization in a novel (and *politically correct*!) context, the application described in this vignette brings to the forefront a number of topics of interest in colloid and surface chemistry we have discussed in previous chapters.

13.1b Focus of This Chapter

The stability and the structure of dispersions (*structure* here means the spatial organization of the colloidal particles) are topics of considerable research activity currently; there is a lot that we do not know despite the long-standing focus on these topics in colloid science. The first step in approaching problems in this area is to study the origin and the nature of the interparticle forces and how they affect coagulation in dilute dispersions. This is what we focus on in this chapter.

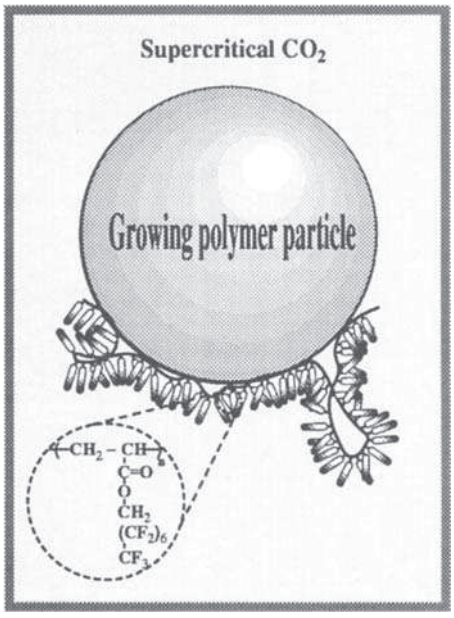


FIG. 13.1 A polymer particle in supercritical CO_2 is protected against coagulation by the steric action of specially designed polymer chains with fluorine-containing tails on the polymer backbone. (Redrawn with permission from K. C. Fox, *Science*, **265**, 321 (1994), and DeSimone et al. 1994.)

1. In Section 13.2, we begin with a closer look at one of the applications we alluded to in Vignette I.5 in Chapter 1 (colloidal processing of ceramics) in order to gain some perspective on how interparticle forces influence the structure of a dispersion.

2. The influence of interparticle interaction energies and how the energies vary with solution chemistry is the first key in understanding colloid stability. Since we have already developed a fairly detailed understanding of van der Waals and electrostatic forces in Chapters 10 and 11, we are already in a position to look at the role of interparticle energies on electrostatic stability. In Section 13.3, we investigate this and discuss the threshold value of electrolyte concentration, known as the *critical coagulation concentration* (CCC), beyond which a colloid coagulates rapidly. We also explore the role of ionic valences and a rule known as the Schulze-Hardy rule in this section.

3. A more quantitative measure of stability, known as the *stability ratio*, can be obtained by setting up and solving the equation for diffusive collisions between the particles. Quantitative formulations of stability, known as the *Smoluchowski and Fuchs theories of colloid stability*, are the centerpieces of classical colloid science. These and related issues are covered in Section 13.4.

4. Theoretical studies of the role of polymer additives lag behind their analogs in electrostatic stability since polymer molecules have considerably more configurational freedom and since the interaction of the polymer molecules with the solvent is an inseparable part of phenomena in polymer-colloid mixtures. We begin with some of the general issues and a thermodynamic analysis of the role of polymer on stability in Section 13.5.

5. In contrast to the situation in the case of van der Waals and electrostatic forces, very little is known about polymer-induced forces. The development of the surface force apparatus and scanning tunneling and atomic force microscopies have begun to shed light on this very difficult topic. In Section 13.6, we take a brief look at some of the polymer-induced forces of interest in colloid stability and structure.

6. In the final section, we build on the thermodynamic theories of polymer solutions developed in Chapter 3, Section 3.4, to provide an illustration of how a thermodynamic picture of steric stabilization can be built when excluded-volume and elastic contributions determine the interaction between polymer layers.

Despite the fact that there is much that is unknown about colloid stability, the topics covered in the chapter are sufficient to solve many routine problems of industrial interest, particularly in the case of electrostatic stability. More advanced information on polymer-induced forces is available in specialized monographs (Napper 1983; Israelachvili 1991; Sato and Ruch 1980) and in other texts on colloid science (Hunter 1987).

13.2 INTERPARTICLE FORCES AND THE STRUCTURE AND STABILITY OF DISPERSIONS

Our objective in this chapter is to establish the quantitative connections between interparticle forces and colloid stability. Before we consider this it is instructive to look at the role of interaction forces in a larger context, that is, the relation between interparticle forces and the microstructure of dispersions and the factors that determine such a relation. These aid us in appreciating the underlying theme of this chapter, namely, the manipulation of interparticle forces to control the properties of dispersions.

13.2a Competition Between Thermodynamics and Kinetics

Before we proceed, however, it is important to review briefly the roles thermodynamic and kinetic considerations play in determining the structure. In some cases, the distinction is easy to establish. In the case of the association colloids we discussed in Chapter 8, thermodynamics determined the formation and the structure of the colloidal particles and their subsequent transformations to more complex structures at higher concentrations of the particles. In

contrast, lyophobic colloids, such as the silica dispersion we saw in Example 5.4, are usually thermodynamically unstable, but are stable kinetically if the surface charges or potentials are sufficiently large. This is what we saw in Section 10.2 in our discussion of the relation between interparticle forces and colloid stability. In fact, arguments presented there form the backbone of the classical theory of electrostatic stability of colloids known as the *Derjaguin-Landau-Verwey-Overbeek* (DLVO) theory, based on kinetic arguments. We discuss this further in Sections 13.3 and 13.4.

Frequently, however, the stability and, more generally, the microstructure and the macroscopic states of dispersions are determined by kinetic *and* thermodynamic considerations. Thermodynamics dictates what the equilibrium state will be, but it is often the kinetics that determines if that equilibrium state will be reached and how fast. This becomes a consideration of special importance in practice since most processing operations involve dynamic variables such as flow, sedimentation, buoyancy, and the like. Although a detailed discussion of this is beyond our scope here, it is important that we consider at least one example so that we can place some of the topics we discuss in this chapter in proper context.

For this, let us consider the subject of Vignette I.5 on ultrastructural processing of ceramics, highlighted in Chapter 1.

13.2b Interplay Between Interparticle Forces and Structure

We have already seen in previous chapters and in a number of vignettes (for example, Vignette I.4 on *electrophoretic imaging devices* in Chapter 1 and Vignette IV on the rheology of chocolate in Chapter 4) that the microstructure and stability of dispersions determine the quality, processability, and properties of many products and devices. The colloidal processing of ceramics is a particularly interesting example since our goal in such a processing route is to optimize the colloidal forces so that we can minimize the competition between thermodynamics and kinetics.

First, let us begin with a consideration of how interparticle forces and the concentration of the particles work together to determine the structure of dispersions. Figure 13.2 is a schematic representation of the microstructure (i.e., the local arrangement of the particles) in a monodisperse colloid in terms of the particle concentration as the relative magnitude of attractive and repulsive forces varies between the extremes. The figure is like a "phase" diagram and shows roughly three regions that differ from each other in terms of the expected microstructure of the dispersion:

1. *Overall interparticle forces dominated by strong repulsion*: When the particles have large enough surface charges, the overall interaction force becomes strongly repulsive and could extend over large distances (of the order of particle dimensions or larger; i.e., the Debye-Hückel thickness, κ^{-1}, is very large). As we saw in Section 10.2, for all practical purposes this corresponds to a *thermodynamically* stable dispersion; in fact, because of the large repulsion, the particles can organize themselves in crystalline structures even at volume fractions of the order of 0.001 or lower, depending on the magnitude and the range of repulsion.

The type of crystalline structure that is formed depends on the concentration of the particles as well as the magnitude of the Debye-Hückel thickness. For large Debye-Hückel thicknesses a body-centered cubic crystal is formed, whereas for smaller values a face-centered cubic crystal is preferred. An example of the latter observed experimentally in a dispersion of latex spheres is shown in Figure 13.3. Note that this crystallization phenomenon is analogous to crystallization of simple atomic fluids, as is evident from Figure 13.3a, which shows the coexistence of a crystal with a "liquidlike" structure.

Because of the low volume fractions at which such transitions can occur, the typical interparticle spacing in these cases can be quite large. Therefore charged colloids can be used as model systems to study visually the influence of charge effects on phase transitions in colloidal as well as atomic systems (see Murray and Grier 1995 for another example).

The structure of the dispersion can be quite sensitive to the parameters that influence the

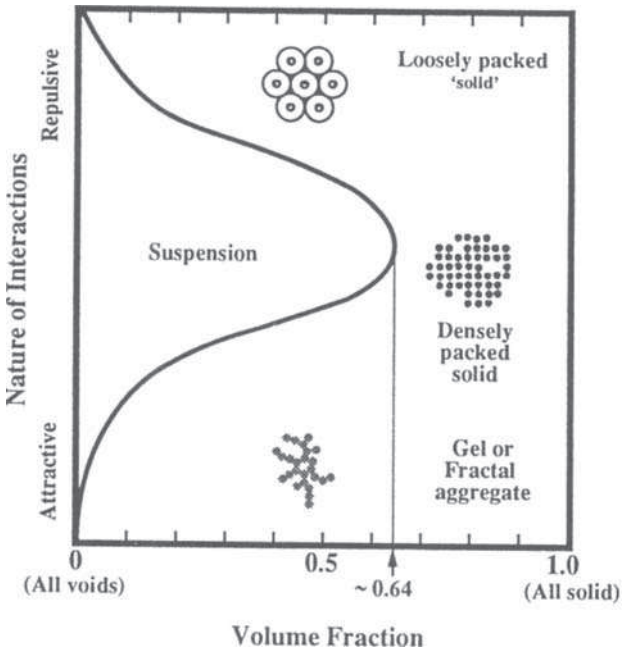


FIG. 13.2 Schematic illustration of the relation between the interparticle forces and the corresponding microstructure observed in dense, monodisperse colloids. (Adapted with permission from D. R. Ulrich, *Chem. and Eng. News*, 28–35, January 1, 1990.)

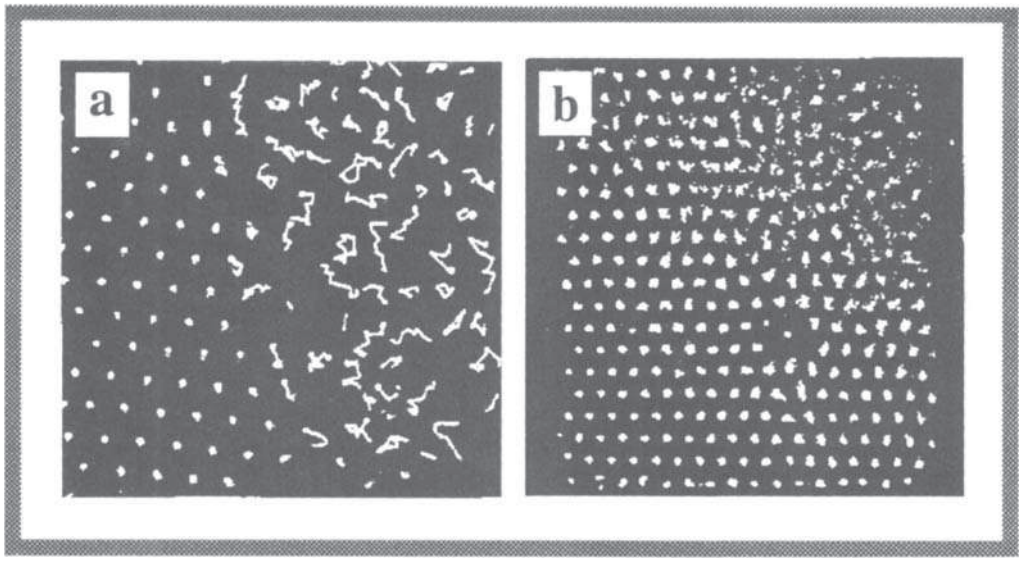


FIG. 13.3 Micrographs of local structure in a charged dispersion: (a) an ordered region coexisting with a liquidlike region; (b) an ordered crystalline structure, with a two-dimensional slice of the crystal shown. (Photographs courtesy of Dr. Norio Ise, Fukui Laboratory, Rengo Co., Fukui, Japan.)

interparticle forces near the liquid-crystal transition. This is illustrated in Figure 13.4, which presents stereograms based on computer simulations of a dispersion. The liquidlike isotropic structure seen in Figure 13.4a transforms to a crystalline (face-centered cubic) structure with a small change in the surface potential (Figure 13.4b).

2. *Overall interaction forces dominated by strong attraction*: At the other extreme, in Figure 13.2, attraction dominates the overall forces. Then the dispersion becomes thermodynamically and kinetically unstable and forms aggregates and an interconnected network known as colloidal "gels" as the particle concentration is increased. The aggregates in this case generally have a loose, fractal structure, similar to the one we saw in Example 5.4. Increases in the particle concentration do not eliminate the microvoids in the structure of the aggregates since strong van der Waals attraction leads to strong interparticle "bonds" that are difficult to break.

3. *Intermediate situations*: The situation in the intermediate region is much more complicated, but is very important in practice. When repulsion and attraction are comparable, the resulting microstructure depends on the details of the interaction forces more sensitively and can be manipulated by adjusting the relative magnitudes of the two forces. We already saw in Section 10.2 that—depending on the details of the interaction energy profile—aggregation in secondary or primary minima can occur in this case. More importantly, in contrast to cases 1 and 2 above, which do not permit closely packed structures, the intermediate situation can allow the formation of dense packing (see Fig. 13.2), and the solution chemistry and surface chemistry serve as important tools to achieve this goal.

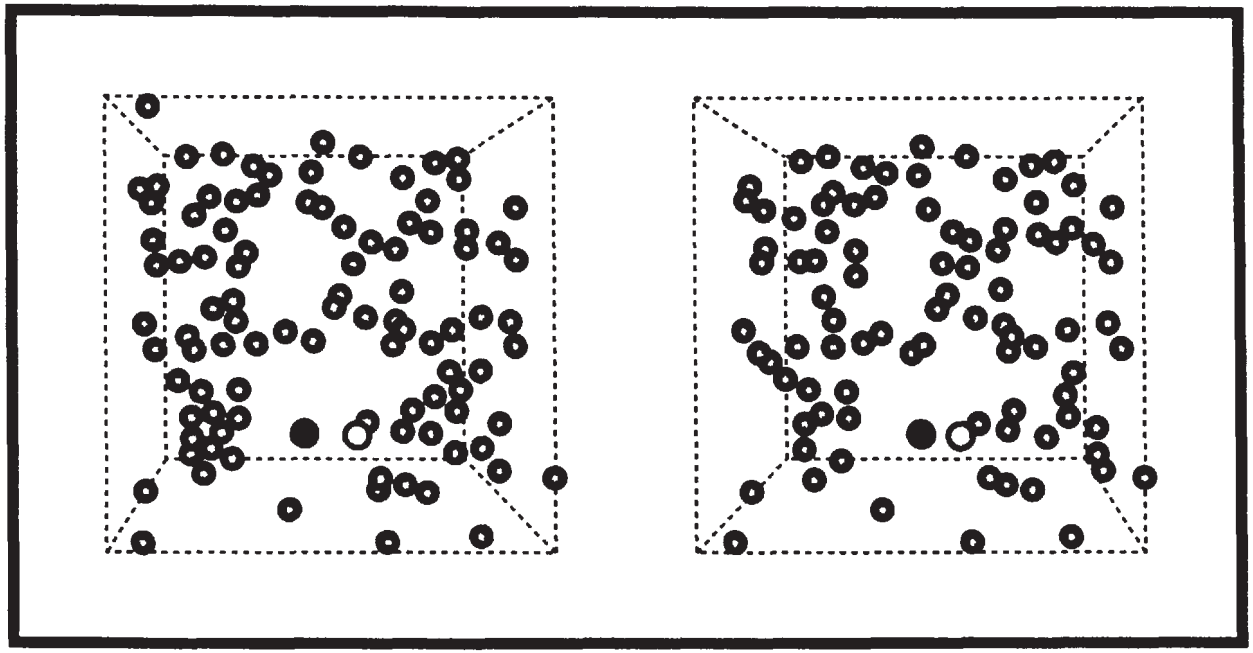
In general, "soft" repulsion at short interparticle separation distances and mild attraction at larger distances promote better packing, and this can be used profitably in colloidal processing of ceramics (see Vignette I.5 in Chapter 1). In fact, this provides one of the strong incentives for studying the effects of polymer additives (discussed in Sections 13.5–13.7) since polymers adsorbed on (or end-grafted onto) particles can be tailored to provide the needed "soft" repulsive cushion and to mask out the strong van der Waals attraction, which, as we saw above, promotes the formation of fractal aggregates. Intuitively, one expects the weak "bonds" resulting from weak attraction to permit a particle in a cluster to break loose and, perhaps, reattach itself repeatedly until it finds a site with a larger number of neighbors (hence a stronger bond).

The picture gets even more complicated when we include other variables. For example, if minimizing microstructural voids (or, "defects") is our goal, the logical choice is to use a mixture of particle sizes since the smaller particles (in principle) can fill the voids created by the larger ones. However, the particle size also has a strong influence on the structure and stability of dispersions. As an illustration, Figure 13.5 shows the interaction energy profiles (calculated from the expressions we have developed in Chapters 10 and 11) for spherical particles of two different diameters d_1 and d_2. This figure illustrates two very important points of interest. First, it shows that, for otherwise identical conditions, the repulsive barrier is greater for larger particles than for smaller ones because of the different dependence of repulsion and attraction on particle size. Therefore, even if the small particles are unstable because of low barriers, once the resulting aggregates reach a large size the dispersion may become stable against further coagulation. The structure that develops with increasing particle concentration in this case is a complicated function of the kinetic stability of the dispersion. Second, in dispersions with a distribution of particle sizes, the smaller particles may aggregate with the larger ones, although a monodisperse system of small particles may be stable by itself.

13.2c Modeling Equilibrium Structures and Time Evolution of Structures

The discussions above highlight the following: (a) the structure of a dispersion is a complicated function of interaction forces; (b) equilibrium thermodynamics dictates what is possible and what is not, but (c) for lyophobic colloids, ultimately it is kinetics that determines whether the structures predicted by thermodynamics can be realized in practice. One of the major objectives of thermodynamic and kinetic studies of colloidal systems is to be able to predict and

a



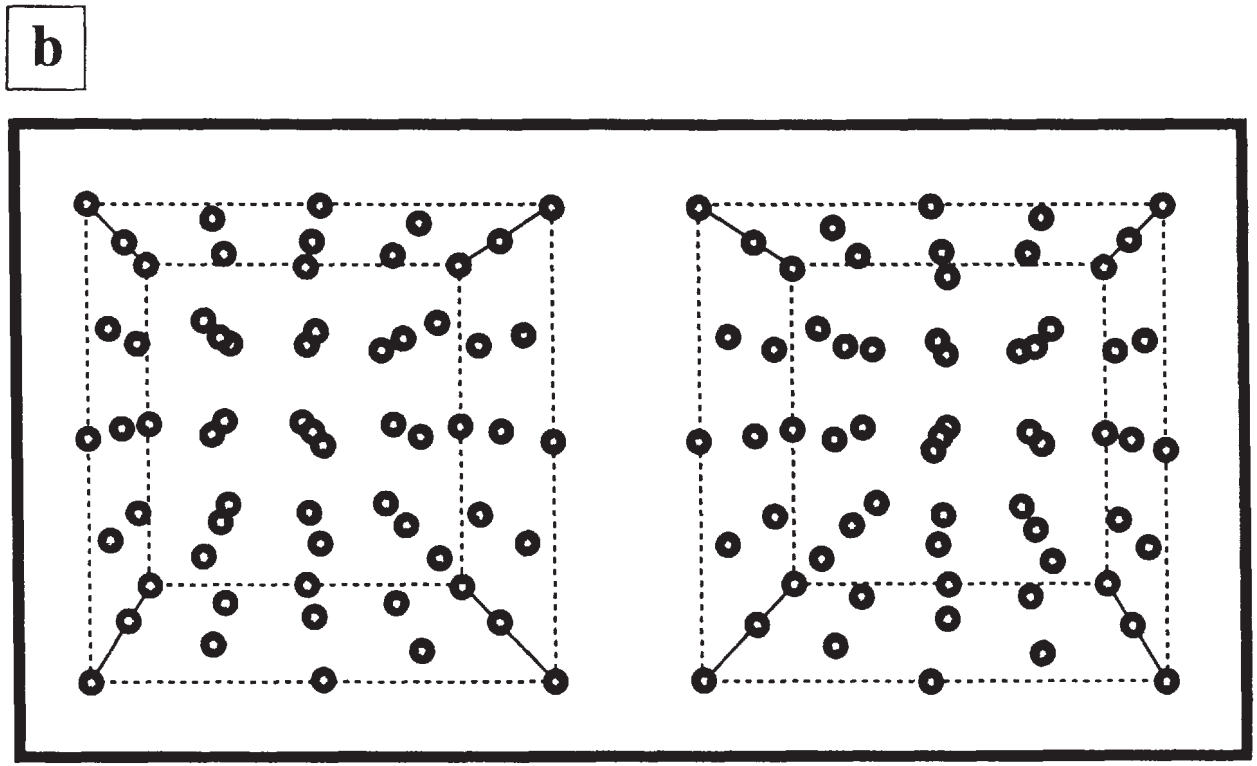


FIG. 13.4 Stereo pairs of colloidal dispersions generated using computer simulations. (a) Polystyrene latex particles at a volume fraction of 0.13 with a surface potential of 50 mV. The 1 : 1 electrolyte concentration is 10^{-7} mol/cm^3. The structure shown is near crystallization. (The solid-black and solid-gray particles are in the back and in the front, respectively, in the three-dimensional view.) (b) A small increase in the surface potential changes the structure to face-centered cubic crystals. (Redrawn with permission from Hunter 1989.)

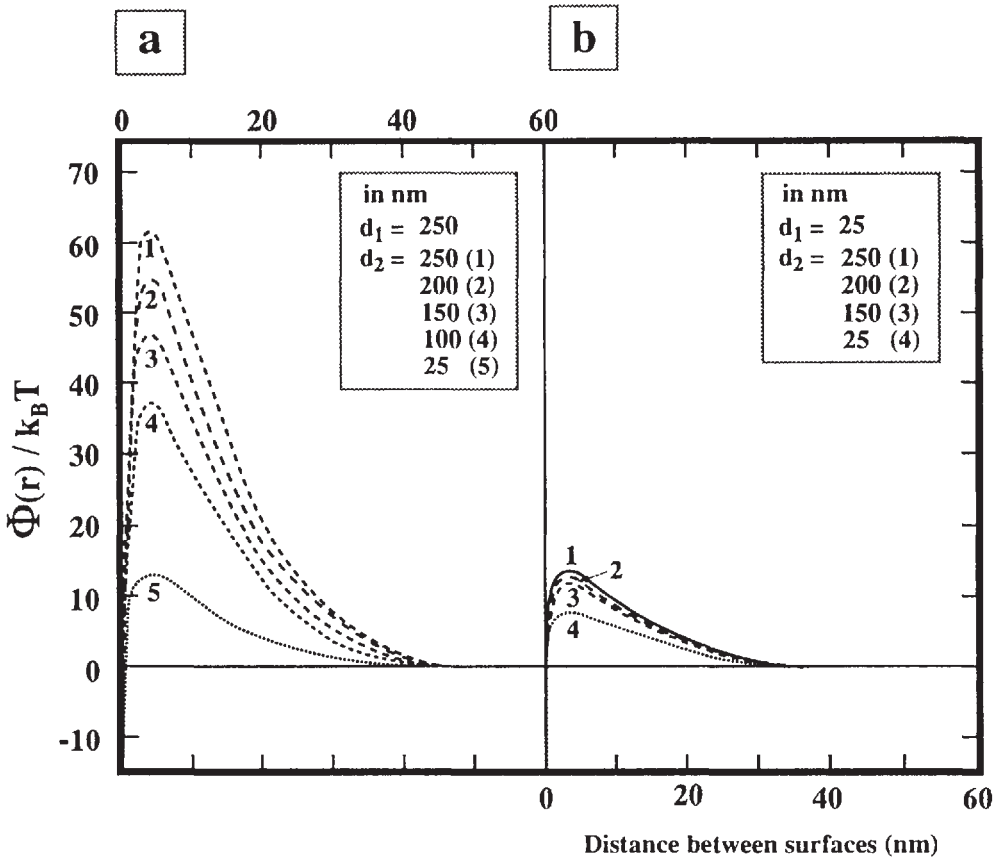


FIG. 13.5 Interaction energy between two spheres of diameters d_1 and d_2. (Redrawn with permission from C. J. Brinker G. and Scherer, *Sol-Gel Science: The Physics and Chemistry of Sol-Gel Processing*, Wiley, New York, 1990.)

control the structure of the dispersions. In a thermodynamic formulation the initial and final states must be clearly understood, and the transition between them is immaterial. In kinetics the path and any energy barriers along the way are important. In contrast to dilute dispersions, meeting the above objectives is considerably more difficult in the case of concentrated dispersions (especially the ones with additional complications such as variations in charges, sizes, and additives). This is an area of intense research activity currently, and radiation scattering techniques (Chapter 5), rheological behavior (Chapter 4), computer simulations (Figure 13.4 above), and statistical mechanical methods find considerable use in this context. The task is relatively more manageable in the case of dilute systems, and this forms the focus of this chapter. In the following sections we examine the classical approach to colloid stability and then consider the influence of polymers on stability.

13.3 THE DERJAGUIN-LANDAU-VERWEY-OVERBEEK THEORY OF COLLOID STABILITY

The interaction energy curves of the type shown in Figure 13.5 (and in Figure 10.1) are useful constructs for developing quantitative measures of kinetic stability. Such a study of stability is known as the *Derjaguin-Landau-Verwey-Overbeek* (DLVO) *theory*, in honor of the Russian physicists B. Derjaguin and L. Landau and the Dutch pioneers in colloid chemistry, E. Verwey and J. Th. G. Overbeek, who independently formulated theories of interaction forces between colloidal particles in the 1940s. In this section, we use the DLVO theory to examine, more quantitatively than we have done so far, the dependence of colloid stability on the various parameters that determine the shapes and the magnitudes of interaction energies between particles. A more elaborate formulation follows in Section 13.4.

13.3a Interaction Energy Curves and Their Dependence on the Properties of the Dispersion

The exact shape of potential energy curves depends on the physical factors responsible for the interaction and also on the assumed geometry of the particles. We are mainly concerned with the case of two interacting planes since the expressions describing the various interactions are simpler in this case than for the more realistic case of interacting spheres. The more complicated spherical geometry contains no major fundamental insights beyond those already obtained from considering interactions between two planar surfaces.

A quantitative expression for the net interaction of two blocks of material separated by a distance d between their surfaces is obtained by combining Equations (10.63) and (11.86) to give

$$\Phi_{net} = 64k_BTn_\infty\kappa^{-1}\Upsilon_0^2\exp(-\kappa d) - (A/12\pi)d^{-2} \tag{1}$$

where A is the Hamaker constant. In the next few paragraphs the effects of the Hamaker constant, the surface potential, and the electrolyte content—considered separately and in this order—on the net potential energy curves are examined.

13.3a.1 Effect of the Hamaker Constant A

It is understood that A in Equation (1) is the effective Hamaker constant A_{212} for the system. Of the variable parameters in this equation, it is the one over which we have least control; its value is determined by the chemical nature of the dispersed and continuous phases. The presence of small amounts of solute in the continuous phase leads to a negligible alteration of the value of A for the solvent.

The effect of variations in the value of A_{212} on the net potential energy is shown in Figure 13.6. Each of the curves in the figure is drawn for a different value of A, but at identical values of κ (10^9 m^{-1} or 0.093 M for 1 : 1 electrolyte) and ψ_0 (103 mV). As might be expected, the height of the potential energy barrier decreases and the depth of the secondary minimum increases with increasing values of A. If the cross-sectional area of interaction is 4.0 nm^2, each unit on the ordinate scale corresponds to k_BT at 25°C. This is the unit of thermal energy against which all interactions are judged to be large or small. Thus for the curves shown in Figure 13.6, the depth of the secondary minimum is slight, and only for the smallest A value is the barrier height significant for particles with this interaction cross section.

13.3a.2 Effect of the Surface Potential ψ_0

The potential at the inner limit of the diffuse part of the double layer enters Equation (1) through Υ_0, defined by Equation (11.65) with ψ_0 in place of ψ. For large values of ψ_0, $\Upsilon_0 \approx 1$, so sensitivity to the value of ψ_0 decreases as ψ_0 increases. Figure 13.7 shows the effect of variations in the value of ψ_0 on the total interaction potential energy with κ (10^9 m^{-1} or 0.093 M for a 1 : 1 electrolyte) and A ($2 \cdot 10^{-19}$ J) constant. The height of the potential energy barrier is seen to increase with increasing values of ψ_0, as would be expected in view of the

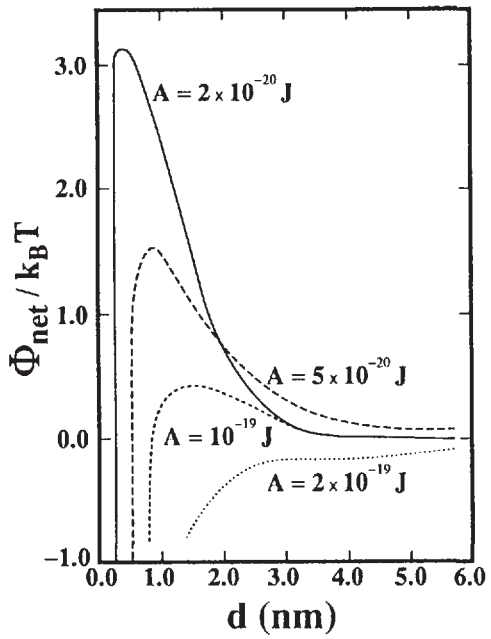


FIG. 13.6 Plot of Φ_{net} versus d according to Equation (1) for flat blocks. Curves are drawn for different values of A_{212} with constant values of κ (10^9 m^{-1}) and ψ_0 (103 mV). Units of ordinate are multiples of k_BT at 25°C for an interaction area of 4.0 nm^2.

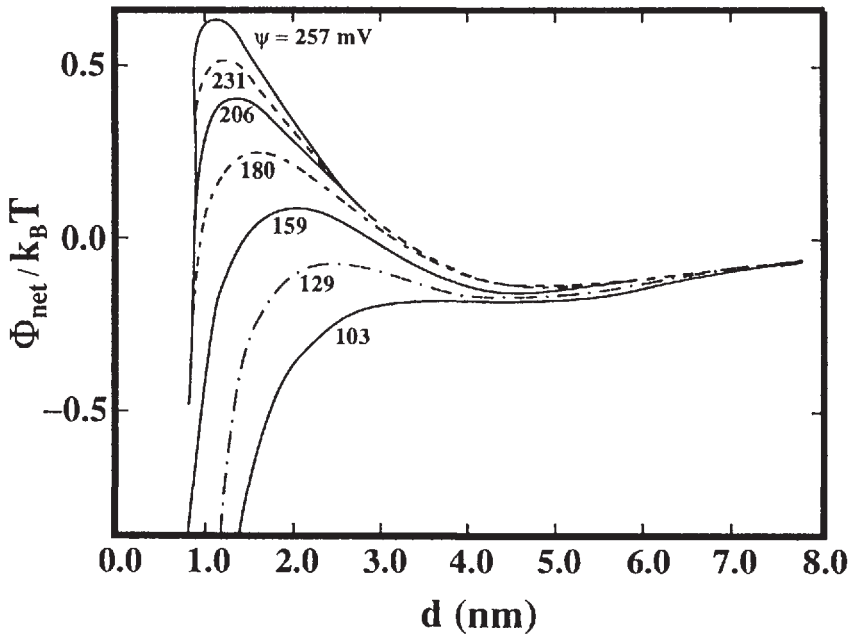


FIG. 13.7 Plot of Φ_{net} versus d according to Equation (1) for flat blocks. Curves are drawn for different values of ψ_0 with constant values of κ (10^9 m^{-1}) and A ($2 \cdot 10^{-19}$ J). Units of ordinate are multiples of k_BT at 25°C for an interaction area of 4.0 nm^2.

increase of repulsion with this quantity. For some systems, ψ_0 is adjustable by varying the concentration of potential-determining ions, as described in Section 11.2 for the AgI surface. We have already seen in Section 11.8 that this quantity can be complicated by other adsorption phenomena; this is why we described it above as the potential at the "inner limit of the diffuse part of the double layer" rather than simply "at the wall." As we saw in Chapter 12, electrokinetic experiments measure a potential within the double layer—the ζ potential—but it is not entirely clear at which location within the double layer this potential applies. However, the experimental ζ potential does establish a lower limit for ψ_0.

13.3a.3 Effect of Electrolyte Concentration

Of the various quantities that affect the shape of the net interaction potential curve, none is as accessible to empirical adjustment as κ. This quantity depends on both the concentration and valence of the indifferent electrolyte, as shown by Equation (11.41). For the present we examine only the consequences of concentration changes on the total potential energy curve. We consider the valence of electrolytes in the following section. To consider the effect of electrolyte concentration on the potential energy of interaction, it is best to use the more elaborate expressions for interacting spheres. Figure 13.8 is a plot of Φ_{net} for this situation as a function of separation of surfaces with κ as the parameter that varies from one curve to another.

Figure 13.8 has been drawn for spheres with radius $R_s = 100$ nm, $A = 10^{-19}$ J, and $\psi_0 = 25.7$ mV. The ordinate in this figure has been labeled both in joules and in multiples of k_BT at 25°C. For the system described by these curves a significant energy barrier is present at all

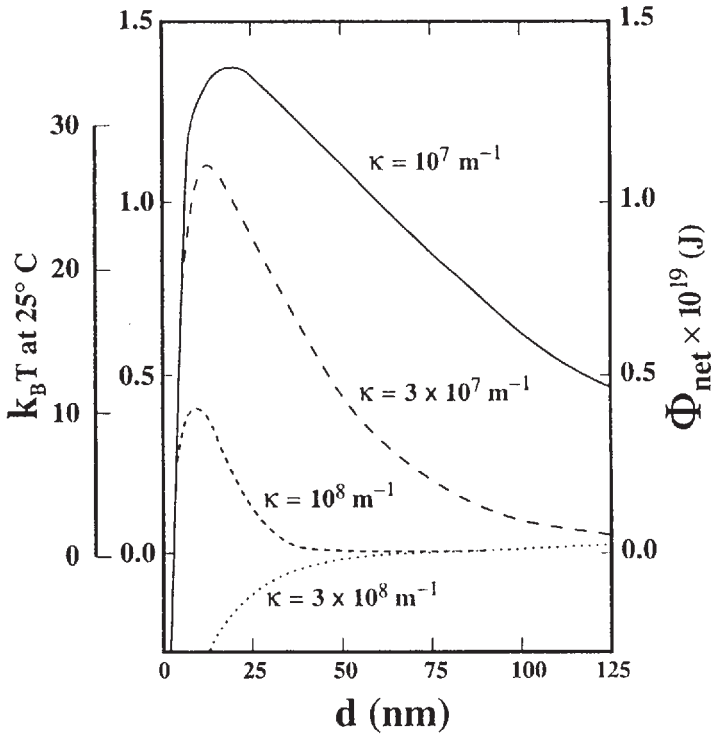


FIG. 13.8 Plot of Φ_{net} versus d, the minimum separation between surfaces, for two spheres of equal radius (100 nm). Curves are drawn for different values of κ with constant values of A ($2 \cdot 10^{-19}$ J) and ψ_0 (25.7 mV). (Redrawn with permission from E. J. W. Verwey and J. Th. G. Overbeek, *Theory of the Stability of Lyophobic Colloids*, Elsevier, Amsterdam, Netherlands, 1948.)

concentrations of a 1 : 1 electrolyte less than about 10^{-3} M. For concentrations between 10^{-3} and 10^{-2} M, however, the barrier vanishes. This particular colloid is thus expected to undergo a transition from a stable dispersion to a coagulated one with additions of an indifferent 1 : 1 electrolyte to a concentration in this range.

13.3b Implications for Colloid Stability

13.3b.1 Critical Coagulation Concentration

It has long been known that the addition of an indifferent electrolyte can cause a lyophobic colloid to undergo coagulation. The DLVO theory provides a quantitative explanation for this fact. Furthermore, it is known that, for a particular salt, a fairly sharply defined concentration is needed to induce coagulation. This concentration may be called the *critical coagulation concentration*. The DLVO theory in general and Figures 13.6–13.8 in particular can be summarized by the following statements:

1. The higher the potential at the surface of a particle—and therefore throughout the double layer—the larger the repulsion between the particles will be.
2. The lower the concentration of indifferent electrolyte, the longer is the distance from the surface before the repulsion drops significantly.
3. The larger the Hamaker constant, the larger is the attraction between macroscopic bodies.

Remember, the point of these figures is to see the effect on the potential energy curves of systematically varying one parameter at a time. It is the trends of behavior rather than the parameters themselves that are of greatest interest. In the following section we discuss the critical coagulation concentration as a simple quantitative test of the theory. In Section 13.4 we see how studies of the *rate* of coagulation provide still more stringent tests of the theory and the means for evaluating parameters of interest.

One of the easiest tests that can be performed on an aqueous colloid is to determine the critical concentration of electrolyte required to coagulate the colloid. We use the notation CCC (for critical coagulation concentration) to indicate this quantity. This experiment is conducted by introducing the dispersion into a series of test tubes and adding to each various proportions of water and electrolyte solution. In this way the total dilution of the dispersed particles is held constant while different amounts of salt are added to each. After mixing and waiting an arbitrary but consistent length of time, we visually inspect the tubes for evidence of the effect of the added salt. There will generally be clear evidence of coagulation (e.g., the settling out of the dispersed phase) in some of the tubes, whereas other tubes appear unchanged. Thus the highest concentration of salt that leaves the colloid unchanged and the lowest concentration that causes coagulation bracket the CCC. A second series of experiments may be conducted within this range to narrow the range of the CCC still further.

The actual concentration of electrolyte at the CCC depends on the following: (a) the time allowed to elapse before the evaluation is made, (b) the uniformity or, more likely, the polydispersity of the sample, (c) the potential at the surface, (d) the value of A, and (e) the valence of the ions. In a series of tests on any particular system, items (a)–(d) remain constant, so the CCC is a quantitative measure of the effect of the valence of the added ions. Table 13.1 summarizes some experimental results of this sort.

13.3b.2 Schulze-Hardy Rule

The results in Table 13.1 have been collected for colloids bearing both positive and negative surface charges. One of the earliest (1900) generalizations about the effect of added electrolyte is a result known as the *Schulze-Hardy rule*. This rule states that it is the valence of the ion of opposite charge to the colloid that has the principal effect on the stability of the colloid. The CCC value for a particular electrolyte is essentially determined by the valence of the counterion regardless of the nature of the ion with the same charge as the surface. The numbers listed in parentheses in Table 13.1 are the CCC values in moles per liter for counterions of the

TABLE 13.1 Critical Coagulation Concentration Values (in Moles Liter^{-1}) for Mono-, Di-, Tri-, and Tetravalent Ions Acting on Both Positive and Negative Colloids (Numbers in Parentheses) and CCC Values Relative to the Value for Monovalent Electrolytes in the Same System (Numbers Outside Parentheses)[a]

Valence of counterion	Negatively charged colloids			Positively charged colloids		Theory
	As_2S_3	Au	AgI	Fe_2O_3	Al_2O_3	
1	(5.5×10^{-2})	(2.4×10^{-2})	(1.42×10^{-1})	(1.18×10^{-2})	(5.2×10^{-2})	
	1	1	1	1	1	1
2	(6.9×10^{-4})	(3.8×10^{-4})	(2.43×10^{-3})	(2.1×10^{-4})	(6.3×10^{-4})	
	1.3×10^{-2}	1.6×10^{-2}	1.7×10^{-2}	1.8×10^{-2}	1.2×10^{-2}	1.56×10^{-2}
3	(9.1×10^{-5})	(6.0×10^{-6})	(6.8×10^{-5})	–	(8×10^{-5})	
	1.7×10^{-3}	0.3×10^{-3}	0.5×10^{-3}	–	1.5×10^{-3}	1.37×10^{-3}
4	(9.0×10^{-5})	(9.0×10^{-7})	(1.3×10^{-5})	–	(5.3×10^{-5})	
	17×10^{-4}	0.4×10^{-4}	1×10^{-4}	–	10×10^{-4}	2.44×10^{-4}
Potential-determining ion	S^{2-}	Cl^-	I^-	H^+	H^+	

Source: J. Th. G. Overbeek, in *Colloid Science*, Vol. I (H. R. Kruyt, Ed.), Elsevier, Amsterdam, Netherlands, 1952.

[a]Theoretical values are given by Equation (10).

indicated valence. That is, about $7 \cdot 10^{-4}$ M of divalent cation is needed to coagulate the negative As_2S_3 sols, whereas about $6 \cdot 10^{-4}$ M of divalent anion is required to coagulate positive Al_2O_3 sols.

The actual values of these concentrations depend on a whole array of unknown parameters, but their relative values depend only on the valence of the counterions. The entries outside parentheses in Table 13.1 are the values of the CCC relative to the value for the monovalent electrolyte in the same set of experiments. These are seen to be remarkably consistent for the divalent ions and acceptably close together for trivalent and tetravalent counterions.

Now let us see how this result is to be understood in terms of the DLVO theory. At first glance, it seems remarkable that any consistency at all can be found in tests as arbitrary as the CCC determination. It is not difficult, however, to show that these results are quite close to the values predicted in terms of the DLVO model for interacting blocks with flat faces. From an inspection of Figure 13.8, we concluded that the system at $\kappa = 10^8$ m^{-1} would be stable with respect to coagulation, whereas the one at $\kappa = 3 \cdot 10^8$ m^{-1} would coagulate. Furthermore, we examined the energy barrier to draw these conclusions. Next we must ask how the qualitative criteria we used in discussing the curves can be translated into an analytical expression.

One way of doing this is to assume that the demarcation between stable and unstable colloids occurs at the value of κ for which the height of the "barrier" is zero. Physically, this is a somewhat arbitrary choice: Thermal energy is sufficient to allow particles to overcome a barrier of low but nonzero height. Mathematically, however, the assumption that the maximum in the potential energy curve occurs at zero permits us to write

$$\Phi_{net} = 0 \qquad \text{at } d = d_m \tag{2}$$

and

$$d\Phi_{net}/dd = 0 \qquad \text{at } d = d_m \tag{3}$$

as the conditions for stability, where $d = d_m$ is the location of the maximum in the potential.

Applying Equations (2) and (3) to Equation (1) gives

$$64\, k_B T n_\infty \kappa^{-1} \Upsilon_0^2 \exp(-\kappa d_m) = (A/12\pi) d_m^{-2} \tag{4}$$

and

$$64 k_B T n_\infty \Upsilon_0^2 \exp(-\kappa d_m) = 2(A/12\pi) d_m^{-3} \tag{5}$$

where the subscript m reminds us that this describes the maximum. From these equations it is readily apparent that

$$\kappa d_m = 2 \tag{6}$$

is the criterion for stability according to this model. This may also be written as

$$d_m = 2\kappa^{-1} \tag{7}$$

in terms of the "thickness" of the double layer. Again we see an important distance measured in terms of κ^{-1}. If we had used the interaction energy expression corresponding to Equation (1) for *spherical* particles of the same radii, the above result would have been $d_m = \kappa^{-1}$. The difference is thus only a numerical factor; the functional relationship does not change.

It is the dependence of the CCC values on the valence of the electrolyte that we seek to obtain rather than the absolute value of the CCC. Therefore it is sufficient to proceed from this point by merely retaining those factors that involve either the concentration ($n_\infty \propto c$, where c is the molar concentration) or the valence z. A more detailed expression can be obtained easily (see Problem 1 at the end of the chapter), but we shall not consider it here.

Substituting Equation (6) back into Equation (5) yields

$$n_\infty \propto \kappa^3 \tag{8}$$

The dependence of Υ_0 on z has been neglected in writing this result, a procedure that is entirely justified for the level of approximation involved here (recall that $\Upsilon_0 \approx 1$). From the definition of κ (Equation (11.41)), we obtain

$$n_\infty \propto z^3 n_\infty^{3/2} \tag{9}$$

or

$$c \propto z^{-6} \tag{10}$$

which is the desired result. According to Equation (10), the CCC value varies inversely with the sixth power of the valence of the ions in solution. The column of numbers in Table 13.1 labeled "theory" follows the progression z^{-6}: $1, 2^{-6}, 3^{-6}, 4^{-6}$. The actual CCC values are seen to be in quite reasonable accord with these predictions.

Note that if ψ_0 is not assumed to be large, Υ_0 depends on both z and ψ_0. In this case the CCC is found to show a less sensitive dependence on the counterion valence than predicted by Equation (10). Example 13.1 examines this point.

* * *

EXAMPLE 13.1 *Critical Coagulation Concentration and ψ_0.* Use the accompanying data given below to criticize or defend the following proposition: Since the CCC for positively charged AgBr is less (regardless of counterion valence) than that for poly(vinyl chloride) (PVC) latex, ψ_0 must be less for AgBr.

	CCC (mole liter^{-1}) of ions opposite in charge to ψ_0	
Colloid	$z = 1$	$z = 2$
PVC latex	$2.3 \cdot 10^{-1}$	$1.2 \cdot 10^{-2}$
AgBr	$1.6 \cdot 10^{-2}$	$2.3 \cdot 10^{-4}$

Solution: Because of the arbitrary time of observation in CCC experiments, the absolute values of the CCCs have no significance. In this regard the proposition is wrong. It may be possible to rank the two colloids with respect to surface potential, however, by examining the order of the dependence of CCC on ion charge for each of the colloids:

For AgBr: $1.6 \cdot 10^{-2}/2.3 \cdot 10^{-4} = 69.6 = (1/2)^{-n}$ so $n = 6.12$

For PVC: $2.3 \cdot 10^{-1}/1.2 \cdot 10^{-2} = 19.2 = (1/2)^{-n}$ so $n = 4.26$

The fact that AgBr agrees with the prediction of Equation (10), which applies at high potentials, suggests that ψ_0 is greater for this colloid than for PVC. ■

* * *

Although this test of the DLVO theory itself introduces some additional approximations, it is a workable unification of experimental and theoretical points of view. The threshold of stability in terms of the concentration and valence of indifferent electrolyte is easily measured. Theoretical models describe the interaction between a pair of particles in terms of potential energy diagrams. The reconciliation of these two approaches constitutes an important step toward obtaining still more quantitative information from the study of coagulation. This is discussed in the following sections, which are concerned with the kinetics of coagulation. First, however, a few remaining comments about the critical coagulation concentrations must be made.

In Chapter 11 (Sections 11.4 and 11.6) we implicitly anticipated that the ion opposite in charge from the wall plays the predominant role in the double layer, the central observation of the Schulze-Hardy rule. This enters the mathematical formalism of the Gouy-Chapman theory in Equation (11.52), in which a Boltzmann factor is used to describe the relative concentration of the ions in the double layer compared to the bulk solution. For those ions that have the same charge as the surface (positive), the exponent in the Boltzmann factor is negative. This reflects the Coulombic repulsion of these ions from the wall. Ions with the same charge as the surface are thus present at lower concentration in the double layer than in the bulk solution.

The signs are reversed for oppositely charged ions; therefore the concentration of the latter is increased in the double layer. It may be shown—at least for high ψ_0 values—that the result of these considerations is essentially equivalent to emptying a region $2\kappa^{-1}$ thick of ions having the same charge as the wall (see Problem 11.5). Thus, in terms of the model for coagulation just presented, it is essentially only the counterions that contribute to the diffuse double layer at the critical separation for coagulation.

The CCC values reported in Table 13.1 in many cases are average values for several compounds of similar valence. The use of averages to compare CCC values is justified since the valence primarily determines the CCC for an electrolyte.

However, a closer inspection of the data reveals that there are second-order differences between different ions. For example, 0.058 and 0.051 M are the Li^+ and Na^+ concentrations required to coagulate As_2S_3 sols, and 0.165 and 0.140 M are the concentrations required to coagulate AgI sols. Although both sets of values are acceptably close to the mean (which includes a number of other compounds), it is also clear that Li^+ is consistently slightly less effective than Na^+ in inducing coagulation. A more complete sequence of these variations in effectiveness is as follows:

1. For monovalent cations,

$$Cs^+ > Rb^+ > NH_4^+ > K^+ > Na^+ > Li^+$$

2. For monovalent anions,

$$F^- > Cl^- > Br^- > NO_3^- > I^- > SCN^-$$

It is apparent from the correlation between the rankings of monatomic ions and their placement in the periodic table that some systematic effect is responsible for this ordering. This was the focus of Section 11.8 on Stern adsorption.

13.4 THEORY OF COAGULATION IN DILUTE DISPERSIONS

In this section we formulate the theory of kinetic stability of colloids. Our ultimate goal is to derive expressions for what is known as the stability ratio, defined in the following section, in terms of the interaction potential. The classical approach to this problem divides the process of coagulation into two steps. The first is the transport of particles toward each other, and the second is the eventual attachment on contact, for which we will assume that the particles stick to each other with a probability of unity on contact. The transport step can be driven by a number of mechanisms depending on the situation considered (e.g., externally imposed flow of fluids that carries the particles toward each other, differential sedimentation, and transport due to other forces such as magnetic or externally imposed electric fields), but for simplicity we consider only diffusion and attraction or repulsion due to interparticle forces. When the primary transport mechanism is diffusion, the coagulation is known as *perikinetic* coagulation. When velocity gradient is the dominant transport mechanism, the process is called *orthokinetic coagulation.*

13.4a Stability Ratio *W*

The stability of a dispersion against coagulation is expressed quantitatively by what is known as the *stability ratio*, usually denoted by W. The stability ratio is defined as

$$W = \frac{\text{Rate of diffusion-controlled interparticle collision}}{\text{Rate of interaction-force-controlled interparticle collision}} \tag{11}$$

If one assumes that a collision between two particles leads to permanent contact between the colliding particles, the diffusion-controlled collision rate in the numerator of the definition of W corresponds to "rapid" coagulation since the ever-present diffusion (i.e., the random Brownian motion) of the particles is unhindered by any energy barrier against contact. The denominator, the rate of collisions controlled by interaction forces (presumed to act against coagulation), then corresponds to "slow" coagulation. Thus large values of W imply that the

dispersion is slow to coagulate (and is "stable"), whereas W of the order of unity implies that the dispersion coagulates rapidly.

Clearly, W is a function of any property of the dispersion that affects the strength of the interparticle forces and the energy barrier that slows down (or prevents) coagulation. A classical goal of colloid science has been to develop the equations necessary to predict the extent of stability of dispersions so that the results could be used in combination with the theories of interaction forces developed in previous chapters to promote or prevent the stability of dispersions.

We focus on the above goal in the following sections. First, we develop the equations for describing the mutual transport and collision of particles in the case of "rapid" coagulation. Then we modify the transport equation to reflect appropriately the influence of interparticle forces; the solution of this equation leads to the collision rate for "slow" coagulation. From these we then develop the equation for W in terms of the expressions for interparticle energies. Finally, the resulting expression for W is used, with a set of simplified electrostatic and van der Waals interaction energies, to show how colloidal stability can be predicted for known physicochemical conditions.

13.4b Theory of Rapid Coagulation

Let us now consider coagulation of particles in the absence of any repulsive barrier. In addition, we assume that, although there are no interparticle forces that contribute to the transport of particles toward each other, there is sufficient attraction between the particles on contact for them to form a permanent bond. As early as 1917, Smoluchowski formulated the equations for the collision rate for particles transported by diffusion alone (Smoluchowski 1917), and we develop the same idea here.

We begin by considering an array of spherical particles with motion that is totally governed by Brownian movement. Let us assume that there are particles of two different radii, $R_{s,1}$ and $R_{s,2}$. We assume the spheres interact on contact, in which case they adhere, forming a doublet. Although this is a highly oversimplified picture, it provides a model from which more realistic models can be developed in subsequent stages of the presentation.

Figure 13.9 shows a schematic illustration of the formation of a doublet. We have fixed the origin of the coordinate system (i.e., $r = 0$, with r the center-to-center distance between two particles) at the center of a particle of type 2, that is, a particle with radius $R_{s,2}$. Since the particles adhere on contact, the rate at which these particles disappear equals the rate at which they diffuse across the dashed surface in the figure. This surface corresponds to a spherical

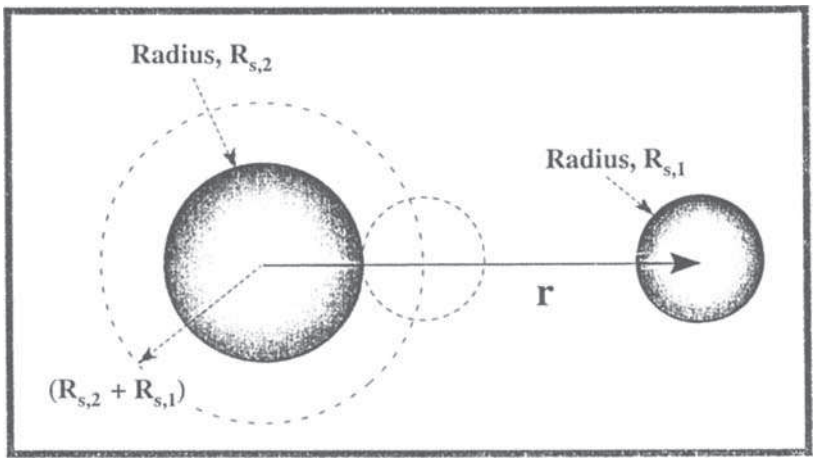


FIG. 13.9 Coagulation of two spherical particles of radii $R_{s,1}$ and $R_{s,2}$ to form a doublet.

surface of radius $(R_{s,1} + R_{s,2})$ inscribed around one of the spheres, which, for the present, is assumed to be stationary. After coagulation the number of independent kinetic units is locally decreased in the neighborhood of this coagulation site. Therefore we may imagine a concentration gradient around the fixed particle as responsible for the diffusion toward it.

As mentioned above, in 1917 M. Smoluchowski applied the theory of diffusion to this situation to evaluate the rate of doublet formation. According to Fick's first law (Equation (2.22)) J, the number of particles crossing a unit area toward the reference particle per unit of time is given by

$$J = -D_1(dN_1/dr) \tag{12}$$

where D_1 is the diffusion coefficient of the spheres of radius $R_{s,1}$, and N_1 is their total number of particles of type 1 per unit volume. This flux can be combined with a number or mass balance equation on a thin spherical shell to obtain the unsteady-state diffusion for the particles:

$$\frac{\partial N_1}{\partial t} = D_1 \frac{1}{r^2} \frac{\partial}{\partial r}\left(r^2 \frac{\partial N_1}{\partial r}\right) \tag{13}$$

where N_1 is the number concentration at position r and at time t. Note that this equation is the analog, in spherical coordinates, of Fick's second law of diffusion we derived in Chapter 2 (Equation (2.26)). The diffusion coefficient D_1 is given by the *Stokes-Einstein relation* (Equation (2.32)).

$$D = k_B T/6\pi\eta R_{s,1} \tag{14}$$

where T is the temperature of the dispersion (in K), η is the viscosity of the fluid (mass/(length · time)), and k_B is the Boltzmann constant. The diffusion equation for N_1 given above assumes that the spatial variation N_1 is spherically symmetric and depends on the radial distance only.

We restrict our attention to steady-state diffusion, for which the left-hand side of Equation (13) is zero. The resulting equation can be integrated easily, and one gets

$$N_1(r) = -B\frac{1}{r} + C \tag{15}$$

where B and C are integration constants that we determine shortly.

The flux at any distance r is obtained simply from the above solution using the Fick's law for flux:

$$J(r) = \text{Flux} = \text{Number of particles arriving at r per unit area per unit time}$$
$$= -D_1 \frac{dN_1}{dr} \tag{16}$$

which, for our solution, is

$$J(r) = -BD_1 \frac{1}{r^2} \tag{17}$$

Now, let us evaluate the constants B and C; for this we use the usual boundary conditions

$$\text{(i) As } r \to \infty, \quad N_1(r) \to N_{b1}, \quad \text{the bulk concentration of particles (of type 1)} \tag{18}$$

$$\text{(ii) At } r = R_{s,1} + R_{s,2}, \quad N_1(r) = 0 \tag{19}$$

where we have assumed that particles of radius $R_{s,1}$ are diffusing relative to particles of radius $R_{s,2}$. The reference point $r = 0$ is fixed at the center of a particle of radius $R_{s,2}$ (see Fig. 13.9). The second boundary condition states that the "concentration" of particles of radius $R_{s,1}$ at the contact point $r = R_{s,1} + R_{s,2}$ is zero.

From the above conditions one sees that $C = N_{b1}$ and $B = N_{b1}(R_{s,1} + R_{s,2})$. Therefore, the flux at the contact point $r = (R_{s,1} + R_{s,2})$ becomes

$$J(\text{at } r = R_{s,1} + R_{s,2}) = -D_1 N_{b1}(R_{s,1} + R_{s,2})^{-1} \tag{20}$$

The negative sign indicates that the particles of radius $R_{s,1}$ are transported toward the particle of radius $R_{s,2}$ (which has been assumed to be fixed in its position at $r = 0$). The magnitude of the collision rate Z_1, that is, the number of collisions of type 1 particles with a stationary particle of type 2 per unit time, is then

$$Z_1 = |J|4\pi(R_{s,1} + R_{s,2})^2 = 4\pi(R_{s,1} + R_{s,2})D_1N_{b1} \tag{21}$$

In general, particles of radius $R_{s,2}$ will also be executing random Brownian motion (i.e., diffusion). In such a case, D_1 should be replaced by $D_{12} = (D_1 + D_2)$. The collision rate Z_{12} (where the second subscript now reminds us that particle 2 is also executing diffusive motion) is then

$$Z_{12} = 4\pi(R_{s,1} + R_{s,2})D_{12}N_{b1} \tag{22}$$

The above result implies that the collision rate is of the form

$$Z_{12} = \alpha_r N_{b1} \tag{23}$$

where

$$\alpha_r = 4\pi(R_{s,1} + R_{s,2})D_{12} \tag{24}$$

with the subscript r indicating that the result is for rapid coagulation. One can now use this result to determine the reduction in N_{b1} as a result of the formation of 1-2 pairs (doublets). In particular, the rate of reduction of the bulk concentration N_{b1} with time t can be written as

$$dN_{b1}/dt = -\alpha_r N_{b1}N_{b2} \tag{25}$$

where we have multiplied Equation (23) by (a) N_{b2} since there are N_{b2} number of type 2 particles (used as reference particles in solving the diffusive collisions by particles of type 1) per unit volume of the dispersion and (b) -1 to indicate the reduction in the particles of type 1 due to coagulation. Note that the same equation with subscript 1 in place of 2 and vice versa describes the reduction in concentration N_{b2}.

For particles of identical radius R_s, one has

$$Z = 16\pi DR_s N_b = \alpha_r N_b \tag{26}$$

with

$$\alpha_r = 16\pi DR_s \tag{27}$$

Note that we no longer need the subscripts 1 and 2 on Z and N_b.

The coagulation rate for identical particles is then given by

$$\frac{dN_b}{dt} = -\frac{\alpha_r}{2}N_b^2 = -k_r N_b^2 \tag{28}$$

with $(\alpha_r/2)$ written as k_r, the *rate constant for rapid coagulation*. Notice that the factor (1/2) appears in this case to avoid counting the same particle twice in the total collision rate; that is, collision of particle i with particle j accounts also for collision of j with i. Equations (25) and (28) correspond to the rate expressions for bimolecular "reactions" and, in this sense, the above description of coagulation is analogous to two reactant particles forming a doublet as the product of the reaction.

Equation (28) can be solved easily to obtain the concentration N_b as a function of time. If N_{b0} is the overall (bulk) concentration at $t = 0$, one gets from the above equation

$$N_b(t)/N_{b0} = (1 + t/t_{1/2})^{-1} \tag{29}$$

where

$$t_{1/2} = \frac{2}{\alpha_r N_{b0}} = \frac{1}{k_r N_{b0}} \tag{30}$$

is the so-called *half-life* for coagulation, that is, the time it takes for the overall concentration to reduce to half the initial concentration N_{b0}. Equation (29) can also be written as

$$\frac{1}{N(t)} - \frac{1}{N_{b0}} = k_r t \tag{31}$$

One should keep in mind the restrictions or limitations implicit in this development. It has been assumed, in effect, that only binary collisions occur. The result obtained is therefore strictly applicable to dilute dispersions, for which the probability of the formation of triplets, quadruplets, and so on, is negligible. We touch on the generalization of Equation (25) in Section 13.4f.

The most reliable way to evaluate a rate constant for coagulation, therefore, is to measure N_b as a function of time. Although this is an easy statement to make, it is not an easy thing to do experimentally. One technique for doing this is literally to count the particles microscopically. In addition to particle size limitations, this is an extraordinarily tedious procedure. Light scattering (Chapter 5) is particularly well suited to kinetic studies since, in principle, experimental turbidities can be interpreted in terms of the number and size of the scattering centers. A variety of additional techniques for following the rate of particle disappearance has been developed for specific systems. We do not pursue these, but merely note that experimental rate constants for coagulation can be determined.

Now, substituting the Stokes-Einstein equation (Equation (14)) for the diffusion coefficient in the expression for k_r leads to

$$k_r = 4k_B T/3\eta \tag{32}$$

Note that the size of the particles drops out of the final expression for k_r; therefore the expression is equally valid for small molecules or colloidal particles so long as the various assumptions of the model apply. This constant describes the rate of diffusion-controlled reactions between molecules of the same size. In Example 13.2 we examine the numerical magnitude of the rate for the process we have been discussing.

* * *

EXAMPLE 13.2 *Variation of Particle Concentration Due to Rapid Coagulation.* An aqueous dispersion initially contains 10^9 particles cm^{-3}. Assuming rapid coagulation, calculate the time required for the concentration of the dispersed units to drop to 90% of the initial value. The viscosity of water is 0.010 P at 20°C, which may be used for the temperature of the experiment.

Solution: First we evaluate k_r, using Equation (32). It is convenient to use cgs units for this calculation; therefore we write $k_r = 4 \cdot (1.38 \cdot 10^{-16}) \cdot (293)/(3)(0.010) = 0.54 \cdot 10^{-11}$ cm^3 s^{-1}. Recall that the coefficient of viscosity has units (mass length^{-1} time^{-1}), so the cgs unit, the poise, is the same as (g cm^{-1} s^{-1}). As a second-order rate constant, k_r has units (concentration^{-1} time^{-1}), so we recognize that the value calculated for k_r gives this quantity per particle, or $k_r = 0.54 \cdot 10^{-11}$ cm^3 particle^{-1} s^{-1}. Note that multiplication by Avogadro's number of particles per mole and dividing by 10^3 cm^3 per liter gives $k_r = 3.25 \cdot 10^9$ liter $mole^{-1}$ s^{-1} for the more familiar diffusion-controlled rate constant.

The 90% time is analogous to the half-life of the reaction. By considering a smaller extent of reaction, the assumptions of the model are more apt to remain valid. Substituting $N_b = 0.90\ N_{b0}$ into Equation (31), we obtain $(0.90\ N_{b0})^{-1} - (N_{b0})^{-1} = k_r t_{0.90}$ or $t_{0.90} = (1.00 - 0.90)/0.90\ k_r N_{b0} = 0.10/(0.90)(109)(0.54 \cdot 10^{-11}) = 20.6$ s. Note the cancellation of concentration units in this last step. ■

* * *

Examples are readily found in which the observed rate constant for coagulation is several orders of magnitude smaller than the rate constant we have been discussing. These are cases of slow coagulation and imply a component of net repulsion between the dispersed particles. We continue with the analysis of the kinetics of slow coagulation at this point. This is the topic of the next section.

13.4c Theory of Slow Coagulation

Attractive interparticle forces can enhance collision rates (although only moderately) and can cause more rapid coagulation; however, in most practical cases of interest we are concerned with the *reduction* in collision rates (and the consequent increase in stability) caused by

energy barriers introduced through net interparticle repulsive forces (hence the name *slow* coagulation). The diffusion equation used in the last section can be modified to account for the presence of interparticle interaction forces, and a closed form expression can be developed for the collision rate. The corresponding analysis in this case is known as the *Fuchs theory of slow coagulation*, after Fuchs (1934), who addressed this problem first.

We saw above, from Fick's first law of diffusion, that the flux at a distance r from the central particle is given by

$$J(r) = -D_1 \frac{dN_1}{dr} \tag{33}$$

at steady state (when only diffusion is the transport mechanism). We must now add the flux due to the interparticle interaction energy $\Phi_{12}(r)$ between particles of type 1 and type 2 to the above expression. The interaction energy exerts a force given by $(-d\Phi_{12}/dr)$ on the diffusing particle. This force imposes on the particle an effective *drift velocity* v_{eff}, given by

$$v_{eff} = -\frac{1}{f}\frac{d\Phi_{12}}{dr} \tag{34}$$

where f is the *friction factor* (and $1/f$ is the *mobility* of the particle; see Atkins 1994). Note that for a spherical particle of radius $R_{s,1}$ in Stokes flow, $f = 6\pi\eta R_{s,1}$ as we introduced in Chapter 2 and used in the last section. The velocity v_{eff} can therefore be written as

$$v_{eff} = -D_1 \frac{d(\Phi_{12}/k_BT)}{dr} \tag{35}$$

by using the Stokes-Einstein relation. Equation (33) for the diffusive flux can now be modified to include the flux $v_{eff} N_1$ caused by the drift velocity of the particles in the direction of the force due to interparticle energy:

$$J(r) = -D_1\left[\frac{dN_1}{dr} + N_1 \frac{d(\Phi_{12}/k_BT)}{dr}\right] \tag{36}$$

The magnitude of the number of particles transported through the spherical cross section of area $4\pi r^2$ is then equal to the collision rate Z_1, which at steady state becomes

$$Z_1 = -4\pi D_1 r^2\left[\frac{dN_1}{dr} + N_1\frac{d(\Phi_{12}/k_BT)}{dr}\right] = \text{Constant} \tag{37}$$

This equation can be simplified by defining

$$y(r) = \exp\left[\Phi_{12}(r)/k_BT\right]N_1(r) \tag{38}$$

to

$$\frac{Z_1}{4\pi D_1}\exp\left[-\Phi_{12}(r)/k_BT\right]\frac{dr}{r^2} = dy \tag{39}$$

On integration one has

$$N_1(r) = e^{-\Phi_{12}(r)/k_BT}\left[N_{b1} - \frac{Z_1}{4\pi D_1}\int_r^\infty e^{\Phi_{12}(r)/k_BT}\frac{dr}{r^2}\right] \tag{40}$$

where the conditions that $N = N_{b1}$ and $\Phi_{12} \to 0$ as $r \to \infty$ have been used.

The second boundary condition (i.e., $N_1 = 0$ at $r = R_{s,1} + R_{s,2}$, which also implies that $\{\exp[\Phi_{12}(r)/k_BT]N_1(r)\}$ is also equal to zero at $r = R_{s,1} + R_{s,2}$) can now be used to get the collision rate Z_1 (with a stationary reference particle of radius $R_{s,2}$):

$$Z_1 = 4\pi D_1 N_{b1} \div \int_{R_{s,1}+R_{s,2}}^\infty e^{\Phi_{12}(r)/k_BT}\frac{dr}{r^2} \tag{41}$$

As discussed in the previous section, D_1 will have to be replaced with D_{12} for two mutually diffusing particles of radii $R_{s,1}$ and $R_{s,2}$:

$$Z_{12} = 4\pi D_{12} N_{b1} \div \int_{R_{s,1}+R_{s,2}}^{\infty} e^{\Phi_{12}(r)/k_B T} \frac{dr}{r^2} \tag{42}$$

The total rate of collision (and, hence, the coagulation rate) is now given by

$$\frac{dN_{b1}}{dt} = -Z_{12} N_{b2} = -\left\{4\pi D_{12} N_{b1} \div \int_{R_{s,1}+R_{s,2}}^{\infty} e^{\Phi_{12}(r)/k_B T} \frac{dr}{r^2}\right\} N_{b2} \tag{43}$$

in analogy with Equation (25).

Equation (43) can be written as

$$dN_{b1}/dt = -\alpha_s N_{b1} N_{b2} \tag{44}$$

analogous to the case of rapid coagulation. The subscript s on the rate coefficient α_s draws attention to the fact that our focus here is slow coagulation:

$$\alpha_s = \left\{4\pi D_{12} \div \int_{R_{s,1}+R_{s,2}}^{\infty} e^{\Phi_{12}(r)/k_B T} \frac{dr}{r^2}\right\} \tag{45}$$

For identical particles of radius R_s, with $D_{12} = D_1 + D_2 = 2D$, one gets from Equation (42)

$$Z = 8\pi D R_s N_b \div \int_0^{\infty} e^{\Phi(s)/k_B T} \frac{ds}{(s+2)^2} \tag{46}$$

where s is the dimensionless surface-to-surface distance defined by $s = [(r/R_s) - 2]$. The corresponding coefficients α_s and k_s become

$$\alpha_s = 8\pi D R_s \div \int_0^{\infty} e^{\Phi(s)/k_B T} \frac{ds}{(s+2)^2} = 2k_s \tag{47}$$

where the fact that $k_s = (\alpha_s/2)$ has been used.

When there is no interaction force between the particles (i.e., $\Phi(r) \equiv 0$), the above result reduces to α_r, corresponding to the rapid coagulation rate given by Equation (27) in the previous section. When there is a strong repulsive barrier, the integral in Equation (47) leads to a large value, thereby reducing the rate of coagulation.

13.4d Stability Ratio *W* and Its Dependence on $\Phi(r)$

Equations (27) and (47) show that

$$k_s = k_r/W \tag{48}$$

where W is the stability ratio defined in Equation (11). Thus

$$W = 2\int_0^{\infty} e^{\Phi(s)/k_B T} \frac{ds}{(s+2)^2} \tag{49}$$

As we noted above, the evaluation of W for given values of dispersion properties such as surface potential, Hamaker constant, pH, electrolyte concentration, and so on, forms the goal of classical colloid stability analysis. Because of the complicated form of the expressions for electrostatic and van der Waals (and other relevant) energies of interactions, the above task is not a simple one and requires numerical evaluations of Equation (49). Under certain conditions, however, one can obtain a somewhat easier to use expression for W. This expression can be used to understand the qualitative (and, to some extent, quantitative) behavior of W with respect to the barrier against coagulation and the properties of the dispersion. We examine this in some detail below.

When the repulsion barrier is large (i.e., Φ_{max} is about 10 k_BT or larger), one can evaluate the integral in the expression for W using what are known as asymptotic techniques and obtain the following expression (Derjaguin 1989, p. 162):

$$W \approx 2\left(\frac{2\pi k_B T}{-\Phi''(s_m)}\right)^{1/2} \frac{e^{\Phi(s_m)/k_B T}}{(s_m + 2)^2} \tag{50}$$

where s_m is the value of s corresponding to the maximum in Φ [i.e., $\Phi(s_m) = \Phi_{max}$] and $\Phi''(s_m) = d^2\Phi/ds^2$ evaluated at $s = s_m$. Note that because $\Phi(s_m)$ is the maximum in the potential, the second derivative of Φ at $s = s_m$ is negative and $[-\Phi''(s_m)]$ is positive. Typically, the location of the maximum in $\Phi(s)$ occurs at distances of the order of a few nanometers. Therefore, for particle radii of the order of 100 nm or larger, $s_m \ll 1$, and the above equation simplifies to

$$W \approx \frac{1}{2}\left(\frac{2\pi k_B T}{-\Phi''(s_m)}\right)^{1/2} e^{\Phi_{max}/k_B T} \tag{51}$$

Equation (51) shows that W is a sensitive function of Φ_{max}, the maximum in the interaction potential, which in turn is a very sensitive function of properties such as ψ_0, electrolyte concentration, and so on. As a consequence, the stability ratio decreases rapidly with, for example, added electrolyte, and the dispersion coagulates beyond a threshold value of electrolyte concentration known as the critical coagulation concentration, as we saw in Section 13.3b.1.

Example 13.3 shows another way of deriving the above equation.

* * *

EXAMPLE 13.3 *Expression for Stability Ratio in Terms of* Φ_{max}. By replacing r by r_m, the center-to-center distance of separation at the maximum in the potential energy curve and using a truncated Taylor series about the maximum to estimate $\Phi(r)$, show that $W \propto \exp(\Phi_m/k_BT)$, with Φ_m the height of the potential energy barrier at the maximum. Comment briefly on these and any other assumptions or approximations involved.

Solution: The function $(r^{-2})\exp(\Phi/k_BT)$ has its maximum at Φ_m and drops off rapidly for $\Phi < \Phi_m$. This justifies focusing attention on the maximum. Furthermore, the exponential term is more important than the r^{-2} factor; hence the latter is replaced by r_m^{-2}.

The Taylor series expansion of Φ can be written

$$\Phi \approx \Phi_m + (r - r_m)(\partial\Phi/\partial r)_m + [(r - r_m)^2/2](\partial^2\Phi/\partial r^2)_m + \ldots$$

according to Appendix A. The subscript m reminds us that the derivatives are evaluated at the maximum, and for this reason the term $(\partial\Phi/\partial r)_m$ equals zero. With these substitutions Equation (49) may be written as (in terms of the center-to-center distance r instead of the dimensionless surface-to-surface distance s)

$$W = \frac{2R_s}{r_m^2} e^{\Phi_m/k_B T} \int_{2R_s}^{\infty} \exp\left(\frac{(\partial^2\Phi/\partial r^2)(r - r_m)^2}{2k_B T}\right) dr$$

$$= \frac{2R_s}{r_m^2} e^{\Phi_m/k_B T} \int_{2R_s - r_m}^{\infty} \exp(-p^2(\Delta r)^2) d(\Delta r)$$

with $p^2 = -(\partial^2\Phi/\partial r^2)_m/2k_BT$. In the second part of the above equation, the variable has been changed to $\Delta r\,(= r - r_m)$ with the limits adjusted accordingly. We can rewrite the above result in terms of two integrals, one going from $\Delta r = (2R_s - r_m)$ to $\Delta r = 0$ (i.e., r going from $2R_s$ to r_m) and the second from $\Delta r = 0$ to $\Delta r = \infty$:

$$W = \frac{2R_s}{r_m^2} e^{\Phi_m/k_B T}\left\{\int_{2R_s - r_m}^{0} \exp(-p^2(\Delta r)^2) d(\Delta r) + \int_0^{\infty} \exp(-p^2(\Delta r)^2) d(\Delta r)\right\}$$

The second integral is one of those shown in Table 2.2 and is equal to $(1/2)(\pi/p^2)^{1/2}$. As noted above, $(\partial^2\Phi/\partial r^2)_m$ is negative since the point of evaluation is a maximum; therefore (p^2) is positive, and there is no sign problem with the square root. The fact that the function in question drops off sharply with distance from the maximum implies that the first integral can be written as

$$\int_0^{r_m - 2R_s} \exp\left(-p^2(\delta r)^2\right) d(\delta r) \approx \int_0^{\infty} \exp\left(-p^2(\delta r)^2\right) d(\delta r)$$

where δr is now $(r_m - r)$. Therefore, we again have the same result as above, that is, the first integral is also equal to $(1/2)(\pi/p^2)^{1/2}$. The final expression for W is thus

$$W = \frac{2\pi^{1/2} R_s}{r_m^2 p} e^{\Phi_m/k_B T}$$

It is a simple exercise to show that the above result is identical to Equation (50). If p can be regarded as a constant, then W plays a role in Equation (51) that converts the latter to the form of the Arrhenius expression for ordinary chemical rate constants.

Let us consider some variations of the above approximation.

Case 1. The location of the maximum r_m is approximately $2R_s$ and the potential drops off relatively slowly.

In this case, the lower limit of the integral in

$$W = \frac{2R_s}{r_m^2} e^{\Phi_m/k_B T} \int_{2R_s - r_m}^{\infty} \exp\left(-p^2(\Delta r)^2\right) d(\Delta r)$$

can be replaced with zero and, using the arguments presented above, we obtain

$$W = \frac{\pi^{1/2} R_s}{r_m^2 p} e^{\Phi_m/k_B T} \approx \frac{\pi^{1/2}}{4R_s p} e^{\Phi_m/k_B T}$$

This expression can be used for arriving at the stability ratio for charged particles in nonaqueous media in which the repulsion can be modeled using a simple Coulombic expression (see Problem 3 at the end of the chapter).

Case 2. Step function barrier.

A useful approximation for the interaction energy is a step function of the form

$$\begin{aligned} \Phi(r) &= -\infty && \text{for } r < 2R_s \\ &= \Phi_m && \text{for } 2R_s < r < 2R_s + \kappa^{-1} \\ &= 0 && \text{for } r > 2R_s + \kappa^{-1} \end{aligned}$$

where κ^{-1} represents the range of the potential. In this case, the integral for the stability ratio can be evaluated easily to obtain

$$W = \frac{1}{2\kappa R_s} e^{\Phi_m/k_B T}$$

Although highly simplified, the above expression provides a simple way to get an estimate of W. ■

* * *

The development sketched in Example 13.3 is not valid under all circumstances, but when it applies, it allows Equations (48) and (49) to be approximated by

$$k_s \propto k_r e^{-\Phi_m/k_B T} \tag{52}$$

This is the Arrhenius form to which the example refers. In it, the height of the maximum in a net potential energy curve plays the role of the activation energy. In the next chapter we see how this method has been used to evaluate W for systems in which the overlapping ion atmospheres of approaching colloidal particles provides the repulsion needed to give slow coagulation.

13.4e Stability Ratio and Critical Coagulation Concentration

Using the approach developed in Example 13.3 and interaction energy expressions for spherical particles, it has been possible to predict how the stability ratio W varies with electrolyte concentration according to the DLVO theory. Since W can be measured by experimental studies of the rate of coagulation, this approach allows an even more stringent test of the DLVO theory than CCC values permit. We shall not bother with algebraic details, but instead go directly to the final result:

$$\log W = K_1 \log c + K_2 \tag{53}$$

where K_1 and K_2 are constants and c is the concentration of the ions in moles per liter. For water at 25°C the value of K_1 has been calculated as $[-2.15 \cdot 10^9 \Upsilon_0^2 R_s/z^2]$ where Υ_0 is given by Equation (11.65) with ψ_0 in place of ψ, z is the valence of the counterions, and R_s (in m) is the radius of the particles. Notice that because of the way Equation (53) has been written, the value of K_2 depends on the units used for c, although taken together the right-hand side is dimensionless since log W is dimensionless. We shall not go into this further since our primary objective here is to use Equation (53) to examine the dependence of W on c and its agreement with experimental results.

Figure 13.10 is a plot of log W versus log c for AgI sols of several different particle sizes. The experimental W values in this figure were determined from absorbance measurements. According to the preceding section, data of this sort not only test the DLVO theory but also permit the evaluation of several important colloidal parameters. From the data in Figure 13.10 the following conclusions can be drawn:

1. A plot of log W versus log c is linear as required by Equation (53).
2. The concentrations at which $W = 1$ (where the breaks in the curves appear) measure the CCC values for the electrolyte involved. The CCC values for mono-, di-, and trivalent ions are about 0.199, $2.82 \cdot 10^{-3}$, and $1.3 \cdot 10^{-4}$ mole liter^{-1}, respectively. These are in the ratio $1 : 1.42 \cdot 10^{-2} : 0.7 \cdot 10^{-3}$. These figures compare very favorably with the other experimental data for AgI and the theoretical values presented in Table 13.1.
3. Slow coagulation is observed for log $W < 4$ or $W \approx 10^4$. For a typical potential energy curve, this corresponds to a value of Φ_m of about 15 $k_B T$. From this we may conclude that the height of an energy barrier must be at least 15 $k_B T$ if the colloid is to have any appreciable stability. Likewise, we may assume that unless the secondary minimum is approximately this deep, particles will be able to "escape" from it. In view of the general shape of the potential energy curves, the retardation effect, and this assessment of what constitutes a "high" barrier or a "deep" well, it seems likely that *rigid* aggregates are not formed in the secondary minimum.
4. Equation (53) can be used to analyze the slopes of the curves in Figure 13.10 since the mean size of the AgI particles is known. In this way, Reerink and Overbeek (1954) found ψ_0 values in the range 12 to 53 mV and A values in the range $0.2 \cdot 10^{-20}$ to 10^{-19} J. Both of these

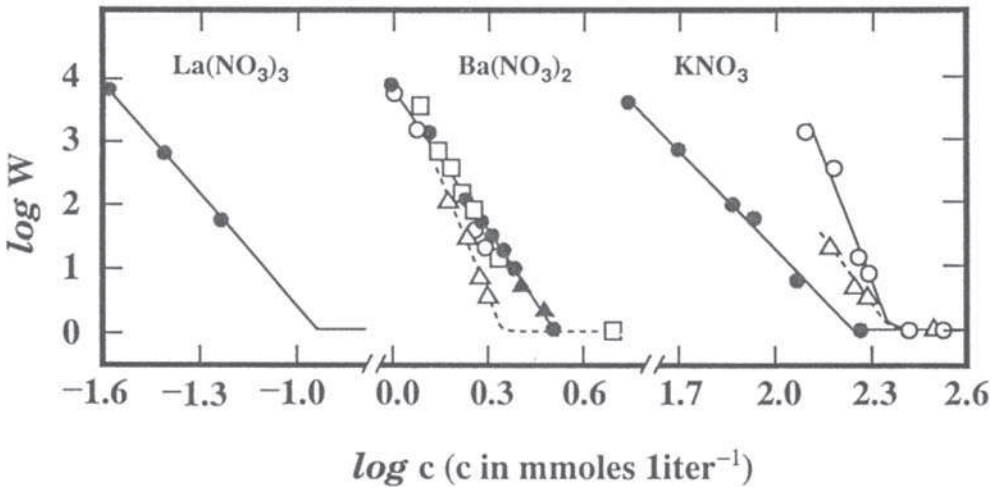


FIG. 13.10 Plot of log W versus log c for AgI sols of five different particle sizes coagulated with the electrolytes shown. The mean particle radii in the different sols are filled circles, 52.0 nm; open circles, 22.5 nm; squares, 53.5 nm; filled triangles, 65.0 nm; and open triangles, 158.0 nm. (Redrawn with permission from H. Reerink and J. Th. G. Overbeek, *Discuss. Faraday Soc.*, **18**, 74 (1954).)

are of the proper order of magnitude—no minor accomplishment in itself in light of the diverse assumptions required to get to this point.

5. The values of A and ψ_0 obtained from this analysis are slightly less satisfying in detail: The values of A show a lot of scatter and ψ_0 appears to be too low. Recall that the variation of the CCC with z^{-6} implies large values of ψ_0 (see Section 13.3b.2); for lower ψ_0 values a different dependence on z is expected.

6. Least satisfactory of all is the correlation with particle size. The results shown in Figure 13.10 were determined for AgI sols covering a 10-fold range of particle sizes.

It is evident from Figure 13.10 that the slopes do not vary over a similar range, as required by Equation (53). As a matter of fact, there are examples for which the steepest slope is associated with the coarsest particles (as required by theory) and others for which it occurs with the smallest particles. The quantitative predictions fail on this particular point, but, as we see below, there are some discrepancies between the theoretical model and the actual experimental system that may account for this apparent insensitivity to particle size. Example 13.4 considers another application of Equation (53) to an experimental system.

* * *

EXAMPLE 13.4 *Change of Stability Ratio with Ionic Concentration.* Colloidal gold stabilized by citrate ions and having a mean particle radius of 103 Å was coagulated by the addition of $NaClO_4$. The kinetics of coagulation were studied colorimetrically and the stability ratio W for different $NaClO_4$ concentrations was determined (Enüstün and Turkevich 1963):

$c \cdot 10^3$ (mole liter^{-1})	2	3	5	8	10.5
W	48	31	17	8.9	0.84

When these data are plotted in the manner suggested by Equation (53), a straight line is obtained up to about 10^{-2} M, at which point a precipitous deviation from linearity sets in. The slope of the linear portion is about -1.20; estimate Υ_0 from this slope. Verify that this value of Υ_0 corresponds to a value of ψ_0 equal to about 25 mV. Estimate what the CCC value would be for this system if W continued to vary according to the same function of c both above and below 10^{-2} M. Suggest an explanation for the abrupt decrease in W near 10^{-2} M.

Solution: The slope of the linear portion equals K_1, the theoretical value of which is given above. Since R_s is known for these particles, Υ_0 may be calculated as follows:

$$\Upsilon_0^2 = 1.20/[(2.15 \cdot 10^9)(103 \cdot 10^{-10})] = 0.054$$

or

$$\Upsilon_0 = 0.23$$

Table 11.4 shows that this value of Υ_0 corresponds to a value of ψ_0 between 20 and 40 mV. For $\psi_0 = 25$ mV, Equation (11.65) shows that $\Upsilon_0 = \exp\{[25/2(25.7)] - 1\}/\{\exp[25/2(25.7)] + 1\} = 0.24$, which is very close to the experimental value. If the linear portion of the plot is extrapolated to log $W = 0$, the value for log CCC is found to be -1.25, from which CCC = 0.055 M. Apparently significant Na^+ adsorption begins to occur at about 10^{-2} M, and W begins to decrease rapidly above this concentration. ■

* * *

Before concluding this section, it seems desirable to comment a bit more fully on some possible sources of the discrepancy between the predictions of Equation (53) and the data shown in Figure 13.10. It is convenient to divide these remarks into those that involve the interaction energy explicitly and those that pertain to the kinetic part of the discussion.

In the context of the interaction energy the following considerations are relevant:

1. It may not be adequate to describe the interaction between AgI particles—especially at relatively close range—in terms of the radii of the dispersed units. In fact, the radii of surface protuberances rather than the dimensions of the particle as a whole may affect the short-range interaction.

2. Throughout this discussion only nonspecific effects have been considered; that is, we have totally neglected to consider ion adsorption and the contribution of the Stern layer to the overall picture. This can be a serious source of complication, at least in some systems. This is

evident from the fact that some dispersions show a reversal of charge (from negative to positive) with the addition of La^{3+} and Th^{4+}, indicating the adsorption of these ions.

Several aspects of the kinetic part of the discussion above also warrant additional comments. These and a few other items are discussed in the following section.

13.4f Other Factors Affecting Coagulation Kinetics

There are a number of issues related to kinetics of coagulation that are not discussed in the previous sections. For example,

1. For highly asymmetrical particles, the probability of collision is greater than that predicted for identical particles. This may be understood by noting that the diffusion coefficient is most influenced by the smaller dimensions of the particles (therefore increased), and the "target radius" is most influenced by the longer dimension (also increased, relative to the case of symmetrical particles); see Equations (24) and (42).
2. The frequency of collisions is also expected to be greater in a polydisperse system than in a monodisperse system by the same logic as presented in item 1.
3. The presence of velocity gradients in the system may also increase the rate of coagulation above the value given by Equation (24) or (42).

The ratio of the probability of a collision induced by a fluid velocity gradient (dv/dx) (i.e., orthokinetic coagulation) to the collision probability under the influence of Brownian motion (perikinetic coagulation—what we have considered so far) has been shown to be (Probstein 1994)

$$k_{r,\,Flow}/k_{r,\,Diff.} = [\eta(2R_s)^3(dv/dx)]/(2k_BT) \tag{54}$$

(For particles of different sizes, $2R_s$ should be replaced with $R_{s,1} + R_{s,2}$.) Since this increases with the cube of particle size, it may be the dominant mechanism for the coagulation of larger particles. Note that all the kinetic complications—items 1 through 3—tend to cancel out of the evaluation of the stability ratio since the rates of both rapid and slow coagulation are determined on the same colloid. In spite of these complications, the value of the kinetic approach over, say, using Equation (11.1) or electrophoresis results (see Chapter 12) to determine ψ_0 is that the potential is evaluated in the actual coagulating system and hence includes any contribution from Stern adsorption. Once a suitable value for ψ_0 is known, potential energy curves for that value of ψ_0 and a measured concentration of electrolyte (i.e., κ) can be constructed for different values of A_{212}. That plot of Φ_{net} versus d that is most consistent with W (e.g., by the method of Example 13.3) may be used to identify A_{212} for the system under consideration.

For a polydisperse colloid (or for a monodisperse colloid that has evolved to a polydisperse suspension of aggregates of various sizes), we can develop an equation to calculate the concentrations of the aggregates as a function of time. For example, Equation (25) can be generalized to

$$\frac{dN_{bm}}{dt} = \frac{1}{2}\sum_{i=1}^{m-1} k_{i,(m-i)}N_{bi}N_{b(m-i)} - \sum_{i=1}^{\infty} k_{i,m}N_{bi}N_{bm} \qquad m > 1 \tag{55}$$

where N_{bj} is the concentration of particles of size j in the bulk and $k_{i,j}$ is the rate coefficient for collisions between particles of size i and size j. The first term on the right-hand side has been multiplied by (1/2) to avoid double counting the same collisions (i.e., $i \leftrightarrow (m - i)$ collisions are the same as $(m - i) \leftrightarrow i$ collisions). The terms in the first summation on the right are known as the "birth" term since they represent the formation of particles of size m from the collisions of i and $(m - i)$. Similarly, the terms in the second summation are known as the "death" terms since they represent the disappearance of size m because of the formation of larger particles through $m \leftrightarrow i$ collisions. The above equation is therefore known as the *birth-death equation* or *population balance equation* (since it describes the populations of particles of various sizes). One can show that this equation reduces to the simpler ones we have used in the previous sections under appropriate conditions.

Although Equation (55) is formally correct, in practice one needs to make a number of assumptions to be able to use it for calculating the aggregate concentrations. For example, one usual assumption is that the radius of an aggregate of size m is simply the radius of a sphere with a volume that is equal to the volume of all the particles in the aggregate; that is, the likely nonspherical shape of the aggregate and the porosity are ignored. The use of the birth-death equation in the case of slow coagulation is complicated further by the fact that the rate coefficients are functions of the stability ratio W, which, in turn, is a complicated function of the interaction potential Φ_{ij} between particles of sizes i and j (see the discussion in Section 13.2b in the context of Fig. 13.5). The use of birth-death population balance equations is more common in aerosol science since some of the approximations needed (such as equating the volume of an aggregate to the volumes of all the particles in the aggregate and approximating the aggregates as spheres) are more easily met, particularly for liquid aerosol droplets. We shall not discuss these here further; more information on the above is available in Sonntag and Strenge (1987) and standard books on aerosols (e.g., Hidy and Brock 1970).

We shall now turn our attention to polymer-induced forces and their influence on colloid stability.

13.5 POLYMER-COLLOID MIXTURES: A PHENOMENOLOGICAL PERSPECTIVE

As mentioned in Section 13.1, polymers have been used since antiquity to stabilize dispersions of solids in liquids against coagulation. Paints and inks used by ancient civilizations were prepared by dispersing suitable pigments in water and "protecting" the resulting system by additives such as gum arabic, egg albumin, or casein. Gelatin has also been used extensively as a stabilizing agent. In molecular terms, these substances are charged polymers (polyelectrolytes) and their stabilizing influence is traceable to both electrostatic and polymeric effects. Each of these contributions is complicated in its own right, so we have divided the discussion into two parts. Charge effects have been discussed in Chapter 11 in terms of low molecular weight electrolytes. In this chapter, we consider the stabilizing effects of nonionic polymers. The advantages of polymer-induced stability over electrostatic stability imparted through low molecular weight electrolytes is summarized in Table 13.2.

13.5a General Considerations

The role of polymers on colloid stability is considerably more complicated than electrostatic stability due to low molecular weight electrolytes considered in Chapter 11. First, if the added polymer moieties are polyelectrolytes, then we clearly have a combination of electrostatic effects as well as effects that arise solely from the polymeric nature of the additive; this combined effect is referred to as *electrosteric* stabilization. Even in the case of nonionic

TABLE 13.2 Electrostatic and Steric Stabilization: A Comparison

Electrostatic stabilization	Steric stabilization
Addition of electrolytes causes coagulation.	Insensitive to electrolytes in the case of nonionic polymers.
Usually effective in aqueous systems.	Equally effective for both aqueous and nonaqueous dispersions.
More effective at low concentrations of the dispersion.	Effective at both low and high concentrations.
Coagulation is not always possible.	Reversible coagulation is more common.
Freezing of the dispersion induces irreversible coagulation.	Good freeze-thaw stability.

Source: Hunter, 1987.

polymers, addition of the polymer to a dispersion can promote stability or destabilize the dispersion, depending on the nature of interactions between the polymer and the solvent and between the polymer and the dispersed particles. As a result, both polymer solution thermodynamics and the thermodynamics of polymer-colloid interactions play important roles.

The importance of polymer solution thermodynamics in the present context will become evident when we discuss polymer-induced forces in Section 13.6. For the present, in order to illustrate the above point, we may consider a very highly simplified picture of *some* of the possible effects of polymer chains on a dispersion, as depicted in Figure 13.11.

1. In the case of very low polymer concentrations, *bridging flocculation* may occur as a polymer chain forms bridges by adsorbing on more than one particle (see also Fig. 13.12f).
2. At higher concentrations of the polymer, "brushlike" layers can form on the particles. These brushes can extend over sufficiently large distances to mask out the influence of van der Waals attraction between the particles, thereby imparting stability to the dispersion. This mechanism, already mentioned in Section 13.2, is known as *steric stabilization*. For steric stabilization, the polymer molecules must be adsorbed or anchored on the particle surfaces.
3. At moderate to high polymer concentrations, the "free" polymer chains in the solution may begin to exercise an influence. One such effect is the so-called *depletion flocculation* caused by the exclusion of polymer chains in the region between two particles when the latter are very close to each other (i.e., at surface-to-surface distances less than or equal to approximately the radius of gyration of the polymer chains). The depletion effect is an osmotic effect and is discussed further in Section 13.6.
4. At high polymer concentrations, one may also have what is known as *depletion stabilization*. The polymer-depleted regions between the particles can only be created by demixing the polymer chains and solvent. In good solvents the demixing process is thermodynamically unfavorable, and under such conditions one can have depletion stabilization.

We are concerned primarily with steric stabilization in this chapter.

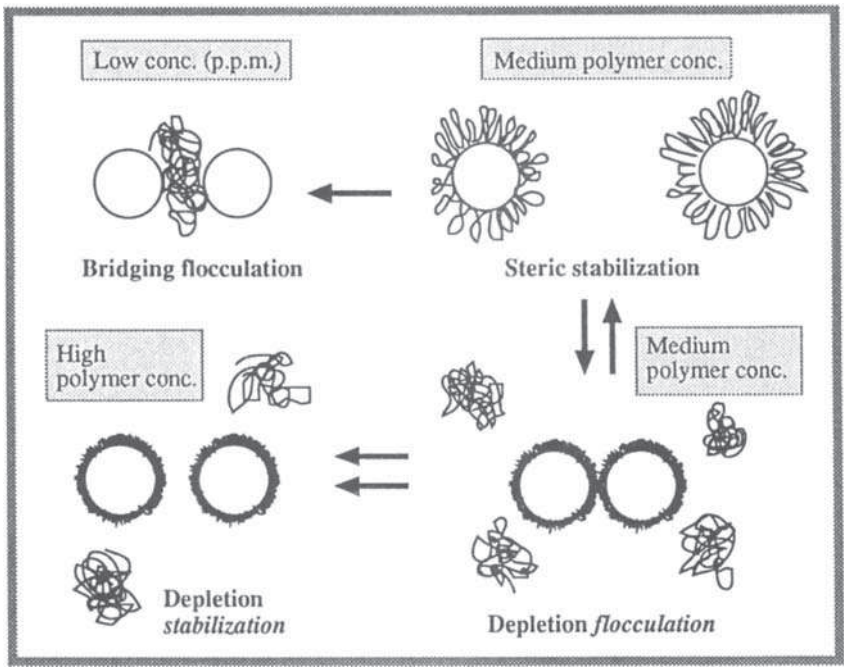


FIG. 13.11 A simplified representation of the effects of polymer additives on the stability of dispersions. See the text for explanation. (Redrawn with permission from Hunter 1987.)

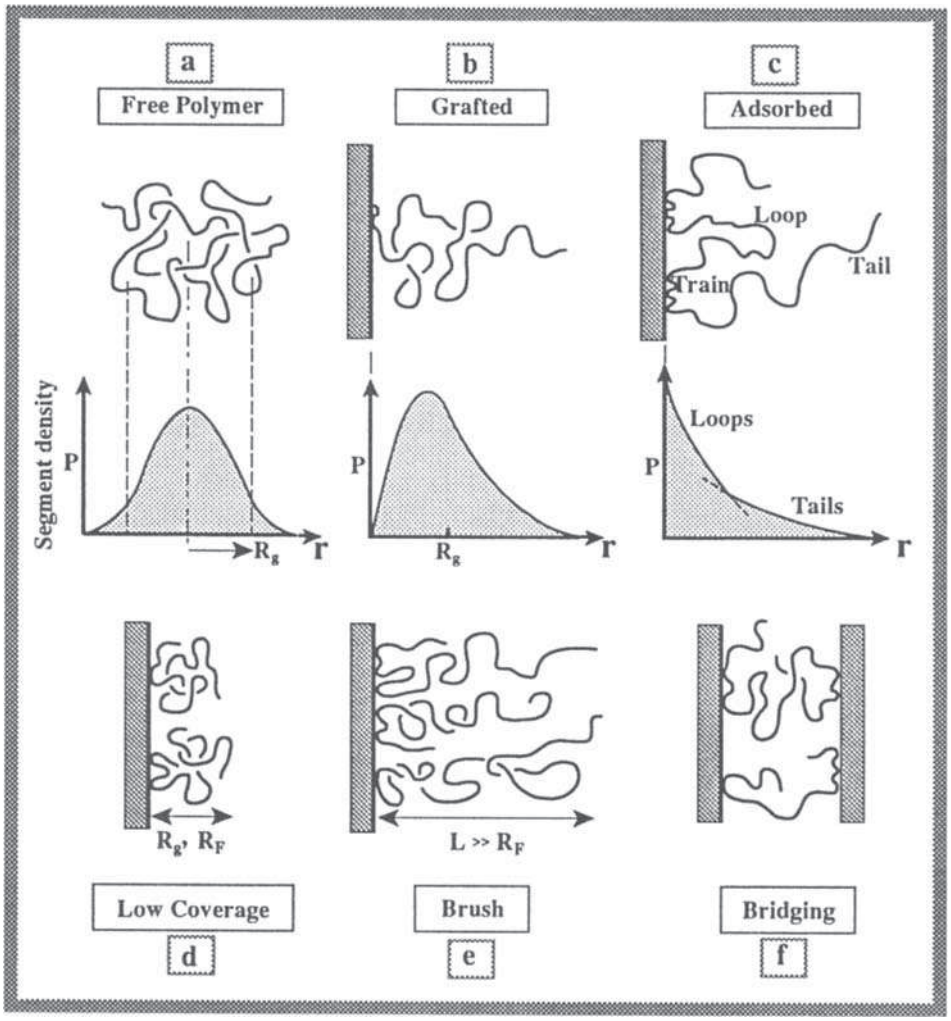


FIG. 13.12 The structure of polymer chains in bulk solution and near a solid interface: (a) configuration of a chain in bulk solution and the corresponding segment-density distribution with R_g the radius of gyration of the polymer chain; (b) an end-grafted chain; (c) an adsorbed chain; (d) configurations of chains adsorbed on a surface at low surface coverage (i.e., there is no nearest-neighbor overlap) and R_F is the so-called Flory radius of the polymer chain ($R_F = \alpha R_g$, with α known as the intramolecular expansion factor; α is unity in ideal solutions, larger than unity in good solvents and less than unity in poor solvents [see Equation (4.90)]); (e) adsorption at high coverage, leading to a polymer brush; (f) bridging. (Redrawn with permission from Israelachvili 1991.)

The above discussion also points out why homopolymers (i.e., polymers containing only one kind of repeat unit) are not usually a good choice as steric stabilizers. The first requirement for stabilization by polymers is that the polymer adsorb at the solid-solution interface since it is the resulting "fringe" on the solid particles that produces the desired result. In general, the adsorbed polymer is considered to reside partially at surface sites and partially in loops or tails in the adjoining solution. The distribution of polymer segments between these two states depends on the relative strength of the interactions between the polymer and the solid compared to those between the polymer and the solvent. Figure 13.12 illustrates some of the possible configurations of the polymer chains (including polymer brushes and bridging

mentioned above) and the corresponding segment densities (i.e., number of monomer segments per unit area parallel to the surface). Synthetic polymers designed specifically as stabilizers are often block copolymers that contain two different kinds of repeat units, clustered in long sequences of one kind. In this type of polymer, one sequence is designed to optimize the adsorption, while the other gives maximum extension from the surface. In polymers made of a single kind of repeat unit, these two considerations tend to work in opposition.

Attachment of a single segment of the polymer chain is sufficient to confine the molecule to the layer of solution adjacent to the adsorbing surface. The solid exerts very little influence on the polymer molecule as a whole in such a case. In fact, the overall spatial extension of the polymer chain is expected to be about the same as that of an isolated molecule in this situation. The polymer-solvent interaction plays a more important role than the polymer-surface interaction in determining the thickness of the adsorbed layer in this case. This is only one of the relative interaction combinations possible, but it is the one that we consider in the greatest detail. As the number of polymer segments actually attached to the surface increases, the influence of the surface causes the spatial extension of the adsorbed chains to decrease.

The picture that emerges from the above discussion visualizes the layer adjacent to the solid surface as a polymer solution characterized by some average volume fraction of polymer ϕ^* and having an average thickness δR_s. If the interaction with the surface is not too strong, δR_s may be on the order of $2R_g$, twice the radius of gyration of the polymer in the solution under consideration. Example 13.5 considers how the thickness of such a layer can be determined experimentally.

* * *

EXAMPLE 13.5 *Determination of the Thickness of Adsorbed Polymer Layer from the Intrinsic Viscosity of the Dispersion.* An adsorbed layer of thickness δR_s on the surface of spherical particles of radius R_s increases the volume fraction occupied by the spheres and therefore makes the intrinsic viscosity of the dispersion greater than predicted by the Einstein theory. Derive an expression that allows the thickness of the adsorbed layer to be calculated from experimental values of intrinsic viscosity.

Solution: Equation (4.41) gives the Einstein relationship between $[\eta]$ and ϕ, the volume fraction occupied by the dispersed spheres. The volume fraction that should be used in this relationship is the value that describes the particles as they actually exist in the dispersion. In this case this includes the volume of the adsorbed layer. For spherical particles of radius R_s covered by a layer of thickness δR_s, the total volume of the particles is $(4/3) + 4\pi R_s^2 \delta R_s$. Factoring out the volume of the "dry" particle gives $V_{dry}(1 + 3\delta R_s/R_s)$, which shows by the second term how the volume is increased above the core volume by the adsorbed layer. Since it is the "dry" volume fraction that is used to describe the concentration of the dispersion and hence to evaluate $[\eta]$, the Einstein coefficient is increased above 2.5 by the factor $(1 + 3\delta R_s/R_s)$ by the adsorbed layer. The thickness of adsorbed layers can be extracted from experimental $[\eta]$ values by this formula. ■

* * *

There are several additional points to be noted about this adsorbed layer:

1. The polymer concentration ϕ^* in the adsorbed layer is different from that in the bulk solution. The two are related through the adsorption isotherm of the polymer.
2. As illustrated in Figure 13.12, the concentration ϕ^* is not expected to be uniform at all distances outward from the wall, although we use some average value of this quantity as if it was uniform.
3. For steric stabilization, the surface layer rather than the bulk solution is the region of interest (see Fig. 13.13).

13.5b Thermodynamic Considerations

As the distance of separation between the core particles decreases in the coagulation step, the adsorbed layers begin to overlap as shown in Figure 13.13. Ultimately, it is the crowding of the polymer chains within this overlap volume that produces any stabilizing effect observed. Consequently, this mechanism for protecting against coagulation is called *steric stabilization*.

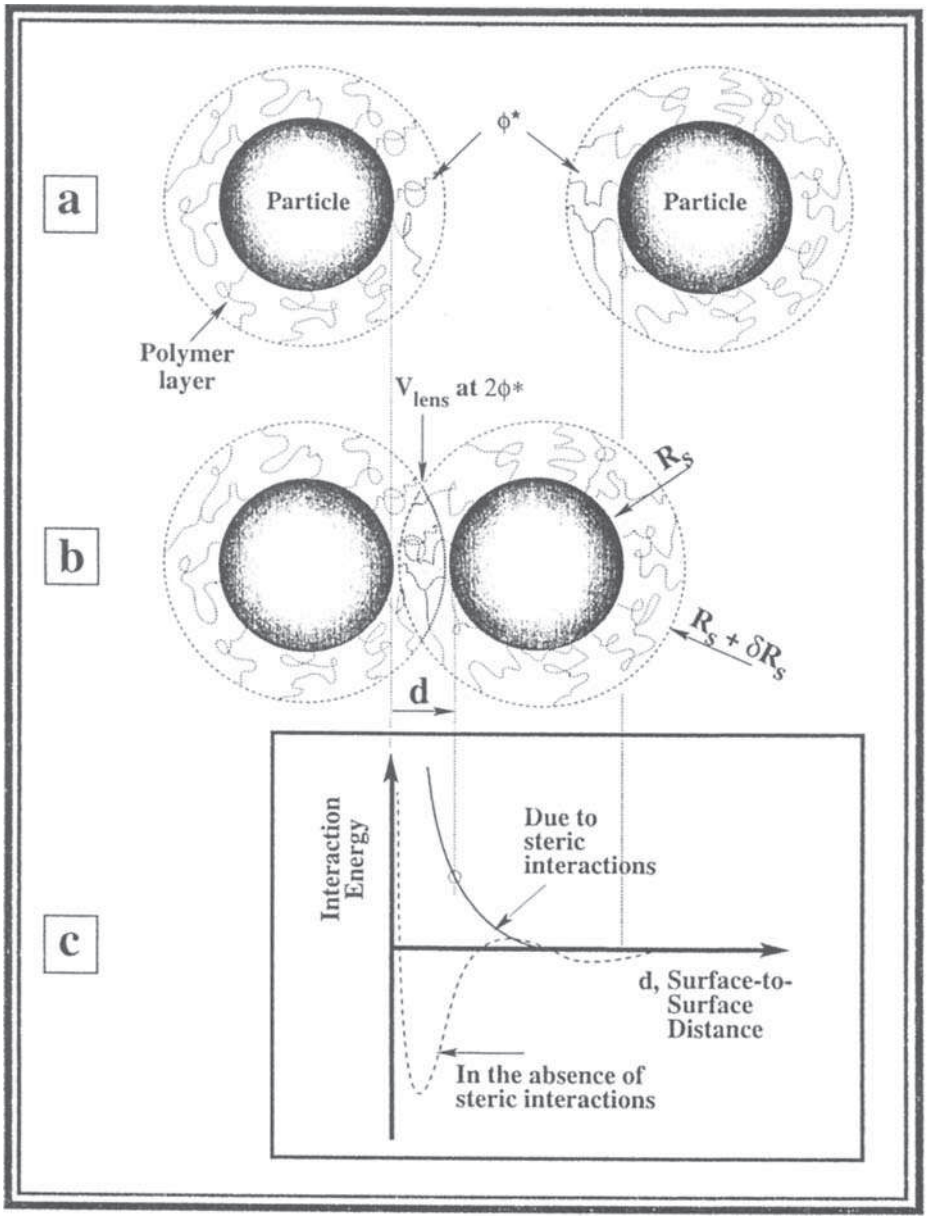


FIG. 13.13 Interaction between polymer-coated particles. Overlap of adsorbed polymer layers on close approach of dispersed solid particles (parts a and b). The figure also illustrates the repulsive interaction energy due to the overlap of the polymer layers (dark line in part c). Depending on the nature of the particles, a strong van der Waals attraction and perhaps electrostatic repulsion may exist between the particles in the absence of polymer layers (dashed line in part c), and the steric repulsion stabilizes the dispersion against coagulation in the primary minimum in the interaction potential.

In Section 13.7 we consider a specific model by which this can be accomplished. For now we take a more phenomenological point of view. It is an experimental fact that, at least under some circumstances, an adsorbed polymer layer stabilizes a dispersion against aggregation. This implies that the approaching particles in an aggregation step experience an increase in free energy ΔG_R (subscript R for repulsion) that prevents the completion of the step. Although the details of this repulsion are irrelevant for now, we associate ΔG_R with the overlap shown in Figure 13.13; that is, ΔG_R is zero when the overlap is zero and increases as the volume of the lens-shaped overlap region increases. As a free energy change, ΔG_R can be either positive or negative. In keeping with the usual sign conventions, a positive value for this quantity indicates repulsion (i.e., protection against aggregation), while a negative value contributes (along with van der Waals forces) to spontaneous aggregation.

As usual, ΔG_R can be broken into enthalpy and entropy contributions:

$$\Delta G_R = \Delta H_R - T\Delta S_R \tag{56}$$

where the individual terms describe changes in the respective property arising from the overlap. In principle, ΔH_R and ΔS_R can both be either positive or negative; therefore the possibility exists for ΔG_R to change sign with changes in temperature. In fact, it is observed experimentally that some sterically stabilized dispersions are caused to aggregate by increases in temperature and others by decreasing T. The threshold temperature for the onset of flocculation in these systems is called the *critical flocculation temperature* (CFT). Thermodynamics offers a formalism for interpreting these observations. With this in mind, let us consider some different sign combinations for ΔH_R and ΔS_R:

1. Suppose ΔH_R and ΔS_R are both positive. In this case the enthalpy change arising from the close approach of particles with adsorbed layers opposes aggregation while ΔS_R favors it. Since ΔS_R is weighted by T in ΔG_R, it follows that increasing T causes the entropy effect to become more important. The situation described here is one in which increasing temperature is expected to cause aggregation. Polyisobutylene adsorbed from 2-methyl butane and polyoxyethylene adsorbed from aqueous electrolyte are examples of systems that show a CFT with increasing temperature. Since it is the positive ΔH_R that is responsible for the stability in this case, such a system is said to display *enthalpic* stabilization.

2. Suppose ΔH_R and ΔS_R are both negative. In this case ΔS_R opposes aggregation while ΔH_R favors it. Since the resistance to aggregation decreases with decreasing temperature, aggregation is expected as T is lowered. Poly(12-hydroxystearic acid) adsorbed from *n*-heptane and polyoxyethylene adsorbed from methanol are examples of systems that display a CFT with decreasing temperature. Since ΔS_R is the source of the stabilization in these cases, this mechanism is called *entropic* stabilization.

3. If ΔH_R is positive and ΔS_R is negative, ΔG_R is positive at all temperatures, and the system is not subject to aggregation by changes in temperature.

Several things should be noted about the above discussion. First, both ΔH_R and ΔS_R are generally functions of temperature and may change signs themselves as T varies. Second, a given polymer may be governed by ΔH_R in one solvent and by ΔS_R in another. Finally, the addition of a second solvent to a dispersion can also induce aggregation in a polymer-stabilized system. We saw in Chapter 3 that changes of solvent goodness (as seen by the properties of polymer solutions) could be brought about by both temperature changes and addition of diluents.

Figure 13.14 illustrates the sort of data that can be used to determine the CFT for a dispersion. The absorbance of the system is measured as a function of temperature. A discontinuity in absorbance is observed to develop over a relatively narrow range of temperatures. The system shown in Figure 13.14 is an aqueous latex dispersion stabilized by polyoxyethylene. The threshold for aggregation is about 291 K. One characteristic of steric stabilization is that aggregated systems usually redisperse spontaneously if the goodness of the solvent is subsequently improved. In terms of the potential energy diagrams of Figure 10.1, this shows that aggregation in these systems does not occur by particles dropping into a deep primary minimum, but rather occurs in a shallow minimum at a larger distance from the surface.

Before we turn to a more detailed look at the origin of steric stabilization, it is informative

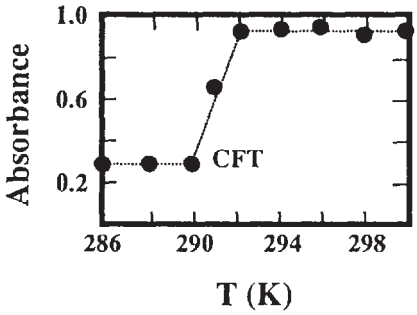


FIG. 13.14 Critical flocculation temperature of aqueous poly(vinyl acetate) dispersion stabilized by poly(oxyethylene) indicated by a sharp change in absorbance with temperature. (Redrawn with permission from D. H. Napper, in *Colloid and Interface Science* (M. Kerker, R. L. Rowell, and A. C. Zettlemoyer, Eds.), Academic Press, New York, 1977.)

to review the assortment of observations that are encountered if the polymer content of the continuous phase is varied from almost pure solvent to pure liquid polymer. As we have already seen, at very low polymer concentrations the solute can induce aggregation in a dispersion; at somewhat higher concentrations it can stabilize the dispersion against aggregation. At still higher concentrations there is a wide range of polymer concentrations in which the dispersion aggregates. Dispersions that are stable against aggregation have been prepared in polymer melts. This variety of behaviors with increasing polymer concentration suggests that the process under consideration is too complicated for explanation by a single model. In Section 13.7 we examine a mechanism for the stabilization that is observed at relatively low polymer concentrations. In such a case one can assume the adsorbed polymer molecule is not very different from an isolated molecule of the same polymer in solution. This assumption limits the applicability of our discussion but permits us to invoke some of the concepts of Chapter 3 for the problem at hand.

However, before we consider the above model, let us review briefly the types of interparticle forces that can result from the presence of polymer chains at particle-solvent interfaces.

13.6 POLYMER-INDUCED FORCES

In developing the expressions for van der Waals and electrical double-layer forces in Chapters 10 and 11 we have assumed that the surfaces involved are atomically smooth. Of course, in practice this is very seldom the case. One can divide "surface roughness" into two categories: *static roughness* and *dynamic roughness*. The former denotes surface roughness resulting from surface imperfections, as in the case of a solid surface. What is of interest to us, however, is the latter, which refers to thermally mobile surface molecules (usually adsorbed or grafted onto the surface) that may rearrange their positions and orientations in response to temperature, interactions with the solvent molecules, rearrangements of neighboring surface-bound molecules, proximity to another surface, and so on. The surface-bound molecules may be low molecular weight species or macromolecules such as neutral polymers or polyelectrolytes. The magnitude of the fluctuations depends on the size and the nature of the molecules. What is important is that, even if the scale of the fluctuations of these molecules is less than a nanometer (as one might expect in the case of simple molecules), the effects of such fluctuations on the roughness of the surface and the forces of interactions between two surfaces are not inconsequential. In fact, in many cases they play a very important role.

Our focus in this section is on the effects of polymer molecules adsorbed or grafted onto surfaces, but before we examine them in some depth it is good to get an idea of what phenomena cause the above molecular fluctuations to manifest themselves as forces (of attraction or repulsion). Even in the case of small molecules adsorbed strongly on a surface, the

presence of another surface in proximity restricts the orientational freedom the molecules otherwise enjoy. This loss of entropy manifests itself as a repulsive force in the absence of any other interactions. The interaction force is then said to be *entropically driven*. The same principle applies in the case of polymer molecules adsorbed or grafted on a surface when another such surface is close by. When the second surface, with or without a polymer layer, is close enough to restrict the configurational freedom of the polymer chains dangling from the first surface, the net effect is to create an entropically driven repulsive or steric force between the surfaces.

What makes the understanding of such forces particularly difficult, especially in the case of polymer layers, is that the overall effect may be influenced by other factors such as the affinity of the polymer segments to each other and the affinity to solvent molecules. As a consequence the net force may be *enthalpically* (i.e., energetically) *driven* or entropically driven and may vary with other factors such as temperature (since, for example, temperature may change the nature of solvent-polymer-segment interactions; see Chapter 3) or depending on whether the polymer chains are physically *adsorbed* on the surfaces or *grafted* firmly to the surfaces (see Figure 13.12 for an illustration of the differences between the structures of adsorbed and grafted layers). The resulting net interaction can be attractive or repulsive, and the polymer additives may, therefore, serve as stabilizers or destabilizers.

Ideally, it would be desirable to be able to develop quantitative expressions for the interaction energies so that we can deal with coagulation or flocculation, at least in the case of fairly dilute dispersions, the way we did in Sections 13.3–13.4 for electrostatic stabilization. It is possible to develop approximate expressions for interaction energy due to various individual effects such as osmotic repulsion, attraction or repulsion due to the overlap of the tails of the adsorbed (or grafted) polymer layers, interaction of the loops in the layers, and so on (see Fig. 13.15). However, the complicated nature of polymer-induced interactions makes these tasks very difficult. In this section, we merely illustrate some of the issues that need to be considered in developing a fundamental quantitative understanding of polymer-induced forces. In Section

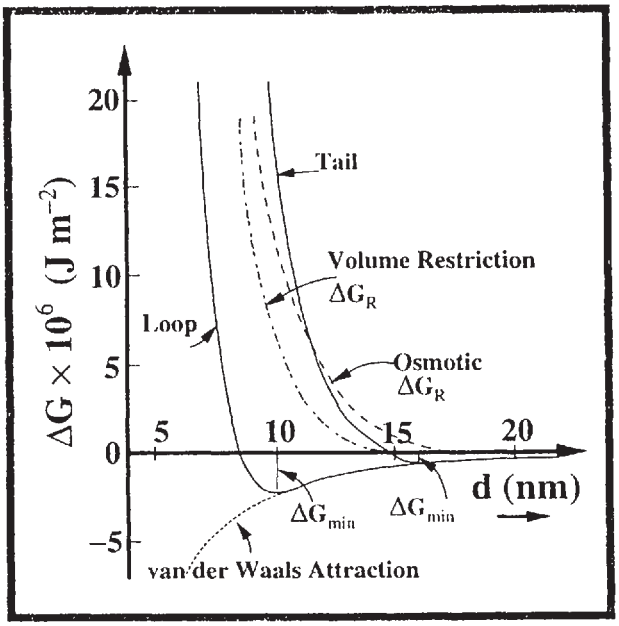


FIG. 13.15 Examples of the various contributions to the interaction energies between two polymer-coated particles. The curves shown illustrate qualitatively the change in Gibbs free energy due to the overlap of the tails, loops, and so on. (Redrawn with permission from Sato and Ruch 1980.)

13.7 we return to a thermodynamic analysis of stability along the lines of the discussion presented in Section 13.5 for a simple case to illustrate one of the approaches.

13.6a Repulsive Forces Due to Polymers

As mentioned above, there are a number of factors that affect the repulsive forces arising from the loss of configurational entropy of polymer chains.

1. The number of polymer chains per unit surface area (i.e., the density of surface coverage) determines whether or not interactions between the neighboring chains will have an influence on the extension of the chains from the surfaces. The affinity or the lack of affinity between the neighboring chains also affect the interaction forces.
2. Whether a polymer is grafted on the surface or simply adsorbed on the surface has a bearing on the force between two polymer-coated surfaces. Adsorption is a *reversible* process and can be affected by temperature, compression of the polymer layer, and the like.
3. The quality of solvent (i.e., solvent-polymer interactions) can also clearly affect the interaction forces. In a good solvent, polymer segments favor contacts with the solvent. Since the compression of the polymer layer by an approaching surface tends to squeeze out the solvent and force segment-segment interactions, the net result is a repulsion. In contrast, poor solvents produce an opposite effect, and a net attraction is possible for certain range of compression (see Section 13.6b).

A full theoretical treatment is therefore very difficult, and we restrict ourselves to two cases, primarily to illustrate some of the above points.

For example, consider a surface with a low coverage of end-grafted polymer chains under theta conditions (see Chapter 3). If the density of polymer ends per unit area of the surface is denoted by n_s (number per unit area), the typical magnitude of the distance between the grafted ends on the surface is equal to $n_s^{-1/2}$. If the density is low enough so that $n_s^{-1/2} > R_g$, the radius of gyration of the polymer chain, we may assume that the neighboring chains do not interfere with each other and that their configurations in the solution are essentially the same as what one would expect in a dilute solution of the polymer in the same solvent (see Fig. 13.12d). The repulsive energy of interaction between two such surfaces can be obtained theoretically (Dolan and Edwards 1974) and is a power series of (d/R_g), with d the distance between the interacting surfaces. In a certain range of distances, however, one can approximate the energy by an exponential function as below:

$$\Phi(r) \approx 36\, n_s k_B T \exp(-d/R_g) \qquad 2 < (d/R_g) < 8 \tag{57}$$

As one moves away from low to high surface coverages, however, interactions between neighboring chains begin to influence how far the chain extends into the solution. At high coverages, the surface layer is commonly referred to as a *brush* (see Fig. 13.12e), and the polymer chains tend to extend farther into the solvent. In a theta solvent, the distance of extension L increases as N^{ν}, with N the number of segments of monomer units in the polymer chain and ν roughly unity for high coverages (it is 0.5 for low coverages since R_g is of the order of $N^{0.5}$ for low coverages; see Equation (2.77)). In this case also it has been possible to obtain a quantitative expression, which again is exponential in (d/L) for a restricted range of (d/L). The length L itself is a function of the surface density, length of the monomer units, the degree of polymerization (i.e., the number of monomers N per chain), and the nature of the solvent. We shall not go into the theoretical and quantitative details since our purpose here is merely to point out the general issues that are important.

The repulsive force between surfaces with end-grafted polymer chains has been fairly well studied both theoretically and experimentally and more details can be obtained from advanced and specialized textbooks such as Israelachvili (1991) and Napper (1983). The situation is much more complicated in the case of chains adsorbed on surfaces. In this case, the segments adsorbed on the surfaces are held on the surfaces by relatively weaker forces (in contrast to

end-grafted chains), and the adsorbed segments may continually detach from and reattach to the surfaces, especially as a second surface approaches the first. The calculation of the repulsive force is difficult because of this and because different segments of a polymer chain may adhere to both surfaces causing polymer "bridges" (see Fig. 13.12f). Moreover, the force between two surfaces at a given distance of separation may be time dependent since the time for equilibration between two surfaces can be rather large.

13.6b Attractive Forces Due to Polymers

As mentioned in the previous section, conditions corresponding to poor solvents give rise to attractive forces between polymer layer. At short enough distances, however, steric repulsion takes over, and the overall force has regions of repulsion as well as attraction. The attractive forces can come about for at least three reasons; we consider each briefly.

13.6b.1 Segment-Segment Attraction in Poor Solvents

In poor solvents, polymer segments prefer each other over the solvent. As polymer layers overlap with each other, segment-segment attraction occurs and draws the particles together. This occurs both in adsorbed layers and in grafted layers as the temperature is taken below the theta temperature (Θ) at low and high coverages and is illustrated in Figure 13.16. As illustrated in this figure, at close enough separations steric repulsion due to the overlap of the segments begins to dominate eventually, and one sees a net repulsion. As the temperature is taken above the theta temperature (i.e., as one goes from poor solvent to good solvent), the segment-segment attraction vanishes, and the force becomes repulsive at all separations (see Fig. 13.16).

13.6b.2 Bridging Attraction

Any polymer chain that has an affinity with a surface has the potential to form a bridge between the surfaces; this may give rise to an attraction known as *bridging attraction*. However, just as segment-segment forces, the segment-surface interaction can be attractive or repulsive depending on the affinity between the segments and the surfaces and the availability of free surface sites for adsorption. Strong bridging attraction is favored when a polymer is attracted to a surface that is not too highly or too sparsely covered with other polymer

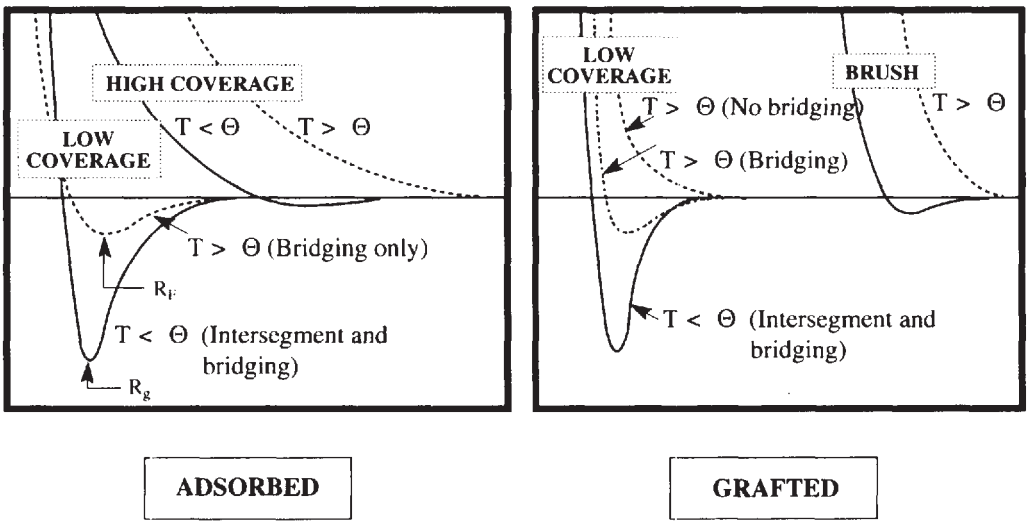


FIG. 13.16 Interaction forces between polymer-coated surfaces and their dependence on the type of layers and quality of the solvents. (Redrawn with permission from Israelachvili 1991.)

segments. In the case of densely covered surfaces, the availability of vacant surface sites is limited and bridging is unlikely. In the case of low coverages, the density of bridges will also be low. Although bridging attraction may exist in the last cases, the net attraction is relatively low because of the low number of bridges.

These are illustrated in Figure 13.16 for low and high surface coverages and for temperatures below and above the theta temperature. For instance, for adsorbed polymer layers at low coverage, the attraction is due to the formation of bridges for the temperature above the theta temperature. For $T < T_\theta$, both bridging and segment-segment attraction join together to increase the total attraction.

13.6b.3 Depletion Forces

Another source of attraction between two surfaces is possible when the surfaces are immersed in a solution of a nonadsorbing polymer (e.g., a polymer that does not adsorb on, or is repelled by, the surfaces). Although this force is generally weak, it can play a significant role in destabilization of colloidal particles under certain circumstances.

In order to understand the source of this force, consider two particles separated by a distance d as shown in Figure 13.17. The dispersed polymer molecules exert an osmotic pressure force on all sides of the particles when the particles are far apart, that is, when $d > R_g$. Then, there is no net force between the two particles. However, when $d < R_g$, there is a depletion of polymer molecules in the region between the particles since otherwise the polymer coils in that region lose configurational entropy. As a consequence, the osmotic pressure forces exerted by the molecules on the "external" sides of the particles exceed those on the interior (see Fig. 13.17), and there is a net force of attraction between the two particles. The range of this attraction is equal to R_g in our highly simplified model.

The depletion forces are relatively weak compared to the dispersion force and solvation forces but become significant with increases in the concentration and molecular weight of the polymer. In practice, however, the presence of strong depletion interaction requires a high polymer concentration (and therefore low molecular weights and R_g's). The existence of depletion forces has been predicted using computer simulations and has been verified experimentally using the surface force apparatus (SFA; see Section 1.6c.2) for surfaces immersed in a micellar solution, in which the spherical micelles play the same role as polymer molecules. However, theoretical treatments of depletion forces (and the bridging forces discussed above) are not as advanced as those for other polymer-induced forces.

The complexities of the polymer-mediated forces evident from the above discussions make it difficult to formulate theories of coagulation and phase separation for such interactions. Nevertheless, it is instructive to consider in detail an example of how the effects of polymer chains are incorporated in quantitative prediction of dispersion stability. In the following section we discuss such an example, although we restrict ourselves to a discussion of a thermodynamic analysis of stability.

13.7 STERIC STABILIZATION: A MODEL FOR THE INITIAL ENCOUNTER

We discussed in Section 13.5 how thermodynamic considerations determine the effects of polymer layers on stabilization. In this section we consider a simple case of interaction between two polymer layers to illustrate the ideas introduced above. It will become evident that some, but not all, of the polymer-induced forces discussed in Section 13.6 are encompassed by the arguments presented in this section. Even with some factors omitted, detailed determination of forces is considerably involved, as is evident from the following discussion.

Consider two particles with adsorbed layers approaching each other. The adsorbed layers on the core particles first begin to overlap at the outermost extreme of the "fringe," at which the surface exerts the least influence. As a first approximation, then, the initial encounter between two approaching core particles is comparable to the approach of two polymer coils in solution. In Chapter 3, Section 3.4a, we saw that the concept of excluded volume could be

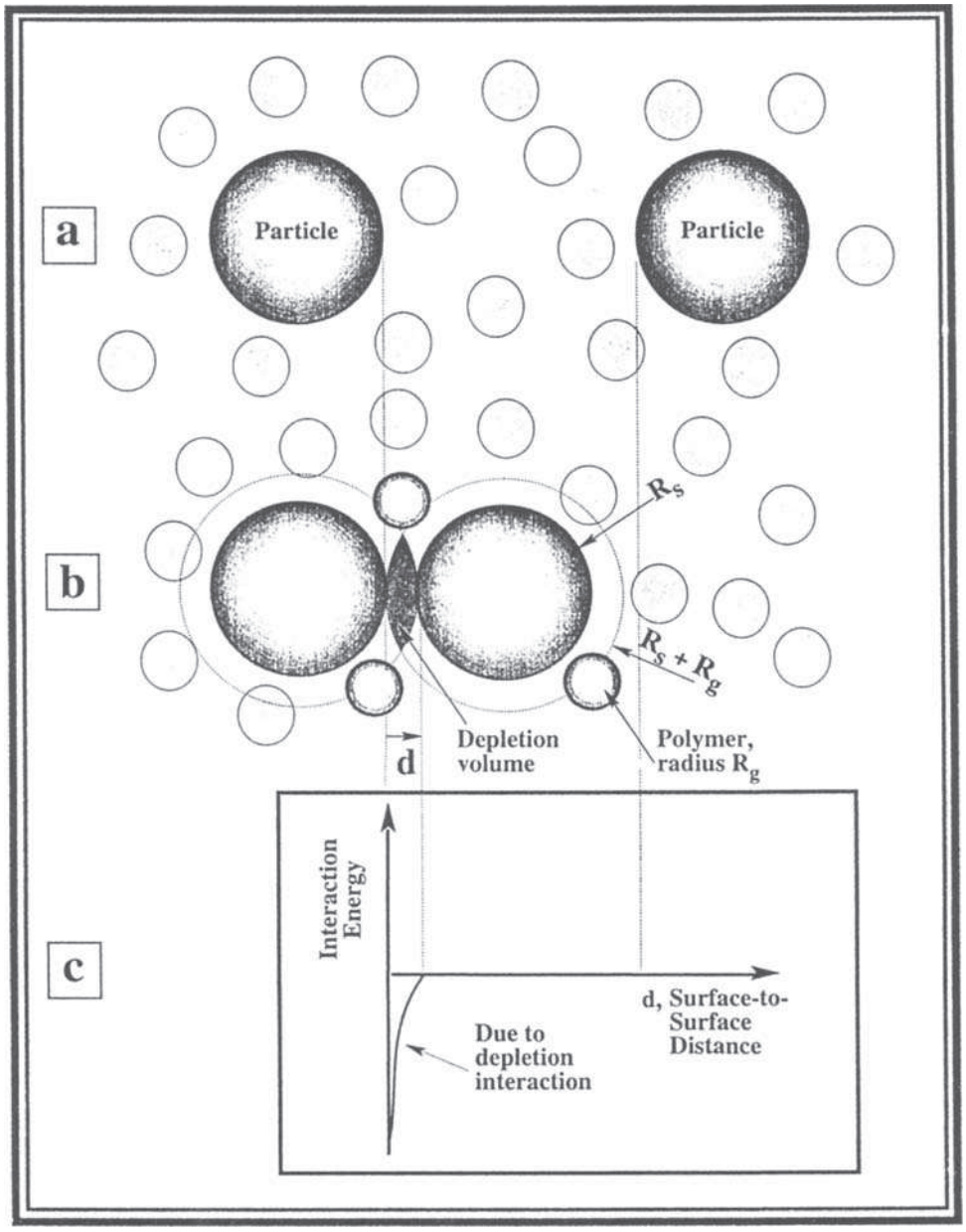


FIG. 13.17 Depletion attraction between two surfaces immersed in a polymer solution.

used to account for the initial nonideality in a polymer solution. Remember that the excluded volume is that region of space from which one molecule is denied access because of the presence of a second molecule. This also describes what happens as the adsorbed layers on two interacting particles approach one another. To quantify this idea, we are interested in an expression for ΔG_R as a function of the distance of separation between core particles as shown in Figure 13.13.

13.7a Free-Energy Change Due to Excluded-Volume Interactions: The Flory-Krigbaum Approach

It is important to remember that the overlapping layers in which we are interested are solutions of pendant or looped polymer chains surrounded by solvent. There is room for interpenetration of the two domains, but the process is uphill thermodynamically.

This can be illustrated through the following arguments against the overlap of coil domains using some pertinent results from previous chapters:

1. If we treat the domain of the chain as a random coil, Equation (2.73) or (2.77) shows that the radius of this domain is proportional to the square root of the degree of polymerization n. This means the volume of the domain varies with $n^{3/2}$.
2. Since n is the number of chain segments in this volume, the volume fraction ϕ^* of the domain that is actually occupied by polymer is proportional to $n/n^{3/2} = n^{-1/2}$.
3. The fraction of the domain that is *not* occupied by polymer is $(1 - \phi^*) = (1 - n^{-1/2})$. For large n this fraction is close to unity, which shows that there is plenty of space within the domain for additional polymer segments.
4. Those sites that are not occupied by chain segments are potential placement sites for the segments of a second polymer molecule.
5. Following the kind of statistical argument used in Section 3.4, we argue that there are $(1 - n^{-1/2})^n$ ways of placing a second molecule of n segments within the domain of the first.
6. This last expression is approximately equal to $\exp(-n^{1/2})$, which shows that the probability of a second molecule entering the domain of the first decreases rapidly with increasing n.

Flory and Krigbaum developed these ideas into a theory of solution nonideality that is useful in the present context. As the two coil domains overlap as shown in Figure 13.13, the concentration of chain segments in the lens-shaped volume of overlap doubles compared to its value in the separate layers: $\phi^* \rightarrow 2\phi^*$. Solutions tend to dilute spontaneously and not become more concentrated; therefore we expect ΔG in the lens to be positive for this process. The total free energy change associated with the overlap depends on both ΔG_{ov} and the volume of the lens; that is,

$$\Delta G_R = (\Delta G_{ov})(V_{lens}) = (\text{Concentration effect}) \cdot (\text{Geometrical effect}) \tag{58}$$

Next we consider these two contributions separately.

The Flory-Huggins theory of Section 3.4b provides the components from which we can assemble expressions for $\Delta G_{m,\phi^*}$ and $\Delta G_{m,2\phi^*}$, the weighted difference of which gives ΔG_{ov}. The strategy is to apply these expressions to the domain of the individual polymer coil, which we define as V_d. If it was necessary to arrive at a numerical estimate for this volume, we could treat the domain as a sphere of radius R_g and write $V_d = (4/3)\pi R_g^3$. Within such a domain, the following applies:

1. The volume fraction of polymer is ϕ^* and the volume fraction of solvent is $(1 - \phi^*)$.
2. The number of polymer molecules N_2 is unity, and the number of solvent molecules is $[(1 - \phi^*)V_d/(\bar{V}_1/N_A)]$, with $\bar{V}_1$ the partial molar volume of the solvent. Therefore, $N_1 = (1 - \phi^*)V_d N_A/\bar{V}_1$.
3. The Flory-Huggins expression for the enthalpy of mixing is given by Equation (3.71). In the present notation it becomes

$$\Delta H_m = (1/2)zN_1\phi_2\Delta w = \chi RTN_1\phi^*$$

4. The Flory-Huggins expression for the entropy of mixing is given by Equation (3.65). In the present notation it becomes

$$-T\Delta S_m = RT(N_1 \ln \phi_1 + N_2 \ln \phi_2) = RT[N_1 \ln (1 - \phi^*) + N_2 \ln \phi^*]$$

Since $N_2 \ll N_1$, the second term can be neglected compared to the first to give

$$-T\Delta S_m \approx RTN_1 \ln(1 - \phi^*)$$

5. Within the volume of the coil domain we can write

$$\Delta G_m = \Delta H_m - T\Delta S_m = RTN_1[\chi\phi^* + \ln(1 - \phi^*)]$$

Substituting for N_1 from item 2, we then have

$$\Delta G_m = (RTV_d N_A/\overline{V}_1)(1 - \phi^*)[\chi\phi^* + \ln(1 - \phi^*)]$$

which may be approximated as

$$\Delta G_m = (RTV_d N_A/\overline{V}_1)[(\chi - 1)\phi^* + (1/2 - \chi)\phi^{*2}]$$

by expanding the logarithm (see Appendix A) and retaining no terms higher than second order in ϕ^*.

6. For the process $\phi^* \rightarrow 2\phi^*$, $\Delta G_{ov} = (\Delta G_{m,2\phi^*} - 2\Delta G_{m,\phi^*})$. Therefore

$$\begin{aligned}\Delta G_{ov} &= (RTV_d N_A/\overline{V}_1)\{[(\chi - 1)(2\phi^*) + (1/2 - \chi)(2\phi^*)^2] \\ &\quad - 2[(\chi - 1)\phi^* + (1/2 - \chi)\phi^{*2}]\} \\ &= (2RTV_d N_A/\overline{V}_1)(1/2 - \chi)\phi^{*2}\end{aligned}$$

7. We can write $\phi^* = \overline{V}_2/N_A V_d$, with $\overline{V}_2$ the partial molar volume of the polymer. With this substitution

$$\Delta G_{ov} = 2k_B T(\overline{V}_2^2/V_d\overline{V}_1)(1/2 - \chi)$$

8. Finally, we give without proof the expression for the volume of the lens that experiences the free energy change given by item 7 (see Figure 13.13b):

$$V_{lens}^* = \frac{V_{lens}}{V_d} = \frac{2\pi}{3}\left(\delta R_s - \frac{d}{2}\right)^2\left(3R_s + 2\delta R_s + \frac{d}{2}\right)V_d^{-1}$$

Substituting the results in items 7 and 8 into Equation (58) gives

$$\Delta G_R = \frac{4\pi}{3}k_B T(\overline{V}_2^2/V_d^2\overline{V}_1)(1/2 - \chi)\left(\delta R_s - \frac{d}{2}\right)^2\left(3R_s + 2\delta R_s + \frac{d}{2}\right) \tag{59}$$

which is the result toward which we have been working.

Two of the terms in Equation (59) are easy to interpret in relation to dispersion stability. Although it is not the entire geometrical effect, the term containing $(\delta R_s - d/2)$—which is half the maximum width of the lens—shows that the repulsion increases with the square of this quantity. This shows how the repulsion develops as the overlap increases.

The term $[(1/2) - \chi]$ is the only factor in Equation (59) that can have either positive or negative values, depending on whether χ is less than or greater than 1/2. Again, we review some ideas from Section 3.4b pertaining to the Flory-Huggins interaction parameter χ:

1. In units of $k_B T$, χ measures the energy change per pair for the process (1,1) + (2,2) $\rightarrow$ 2(1,2) in which the indices refer to different pairwise interactions.
2. $\chi = 1/2$ corresponds to the critical point on a miscibility diagram for a polymer of infinite molecular weight.
3. $\chi < 1/2$ corresponds to a good solvent, and $\chi > 1/2$ corresponds to a poor solvent.
4. According to Equation (3.81),

$$\frac{1}{2} - \chi = \psi\left(1 - \frac{\Theta}{T}\right)$$

so $T = \Theta$ divides the temperature range into good ($T > \Theta$) and poor ($T < \Theta$) regions.

This review indicates that good solvent conditions (in terms of either χ or Θ) result in a positive value for ΔG_R. This is what would be expected from a model that assumes that the first encounter between particles with adsorbed layers is dominated by the polymers. Conversely, in a poor solvent ΔG_R is negative and amounts to a contribution to the attraction between the core particles as far as flocculation is concerned. Under these conditions the polymer itself is at the threshold of phase separation. Van der Waals attraction between the core particles further promotes aggregation, but it is possible that coagulation could be induced in a poor solvent even if the medium decreases the effective Hamaker constant to zero.

Replacing $[(1/2) - \chi]$ by $[1 - \Theta/T]$ offers an opportunity to test the ideas of the Flory-Krigbaum theory against experimental observations of the CFT. It is apparent from the material presented here that the CFT and the Θ temperature correspond to the same condition. Table 13.3 lists CFT values and independently determined Θ temperatures for several systems. The agreement between the two is quite satisfactory for these systems. Incidentally, electrolytes are added to the aqueous media in Table 13.3 to suppress the ion atmosphere mechanism for stabilization.

13.7b Inclusion of Elastic Contributions

There is another type of free energy change that can be considered within the overlap volume in addition to the concentration effect considered by the Flory-Krigbaum theory. This additional contribution to ΔG_{lens} is likely to be more important for $d < \delta R_s$ and should be considered when the outcome of the encounter is not determined by the initial approach of the colliding particles. This contribution arises from an elastic response by the adsorbed polymer, effectively pushing the approaching particles apart.

The elasticity of polymer coils is a well-known phenomenon and is involved in many important mechanical properties of bulk polymers. Stated briefly, it arises from a difference in conformational entropy between stretched and randomly jumbled chains. A statistical theory that counts the number of ways the two conformations can come about can be combined with the Boltzmann entropy equation (Equation (3.45)) to give an expression for the

TABLE 13.3 Critical Flocculation Temperatures for Various Polymer-Solvent Systems, with Θ Temperatures Included for Comparison

Stabilizer	Molecular weight	Dispersion medium	CFT (in K)	Θ (in K)
Poly(ethylene oxide)	10,000	0.39 M $MgSO_4$	318	315
	96,000		316	315
	1,000,000		317	315
Poly(acrylic acid)	9,800	0.2 M HCl	287	287
	51,900		283	287
	89,700		281	287
Poly(vinyl alcohol)	26,000	2 M NaCl	302	300
	57,000		301	300
	270,000		312	300
Polyacrylamide	18,000	2.1 M $(NH4)_2SO_4$	292	–
	60,000		295	–
	180,000		280	–
Polyisobutylene	23,000	2-Methylbutane	325	325
	150,000		325	325

Source: Reprinted with permission of D. H. Napper, in *Colloid and Interface Science*, Vol. 1 (M. Kerker, R. L. Rowell, and A. C. Zettlemoyer, Eds.), Academic Press, New York, 1977.

entropy change associated with stretching a chain or its "snapping" back to equilibrium. At small deformations, individual chains obey Hooke's law with the force constant

$$k_H = 3k_BT/(n\ell_0^2) \tag{60}$$

where n is the degree of polymerization and ℓ_0 is the step length in the random walk analysis of Section 2.7. By Equation (2.77), the denominator in this expression can be replaced with $6R_g^2$. In the context of steric stabilization, we can readily picture the close approach of two core particles as compressing a layer of polymeric "springs." According to Hooke's law, these springs will oppose compression with a restoring force that is proportional to the extent of compression with a force constant given by Equation (60). This is the origin of the elastic mechanism for interparticle repulsion from adsorbed polymers.

One of the first theoretical attempts to understand steric stabilization of dispersions was based on an entropic mechanism that resembles the elastic contribution to ΔG_R. We consider this mechanism in Example 13.3.

* * *

EXAMPLE 13.6 *An Entropic Model for Steric Stabilization Due to Adsorbed Polymer Layers.* Picture a flat surface to which rigid rods are attached by ball-and-socket-type joints. The free ends of the rods can lie anywhere on the surface of a hemisphere. The approach of a second surface blocks access to some of the sites on the cap of the hemisphere. Outline the qualitative argument that converts this physical picture to a theory for stabilization. What are some of the shortcomings of the model?

Solution: When the two solid surfaces are far apart ($d = \infty$), the free end of each adsorbed rod has access to Ω_∞ sites, with $\Omega_\infty = 2\pi L^2$ and L the length of the rod. When the separation is such that the second surface cuts off access to some of these sites, the number of accessible sites becomes Ω_d. The subscript here indicates a separation less than some critical distance that is the threshold for interaction. The exact form of Ω_d and the critical separation at which it begins to apply depends on whether one or both surfaces carry the adsorbed rods. The fraction of the area of the hemisphere that remains accessible to the free ends of the rods could be calculated from geometrical considerations. Using these Ω values as substitutions in Equation (3.46), we obtain $\Delta S_R = k_B \ln (\Omega_d/\Omega_\infty)$. Since $\Omega_d < \Omega_\infty$, ΔS_R is negative. This gives the effect per rod; if there are N such rods per unit area and if $\Delta H_R = 0$, then we obtain $\Delta G_R = -Nk_BT \ln (\Omega_d/\Omega_\infty)$, which gives a positive repulsion as required. This model has several deficiencies:

1. It is unrealistic for polymers, although it may be a reasonable approximation for linear amphipathic molecules.
2. It assumes very low surface coverage so that the individual rods do not interfere laterally.
3. It is a purely entropic mechanism and makes no provision for enthalpy effects. ■

* * *

What we have covered in this chapter barely scratches the surface of a vast area of applications of colloidal phenomena in chemical and materials processing industries and in environmental and other operations. There are many fundamental, as well as practical, problems in the above topics (especially ones involving polymers, polyelectrolytes, and polymer-colloid and polymer-surfactant mixtures) that are currently areas of active research in engineering, chemistry, physics, and biology. Some of the references cited at the end of this chapter contain good reviews of topics that are extensions of what we have covered in this chapter (see, e.g., Elimelech et al. 1995, Hirtzel and Rajagopalan 1985, Israelachvili 1991, Gregory 1989, and O'Melia 1990).

REVIEW QUESTIONS

1. What is meant by the *microstructure* of a dispersion?
2. What is meant by the *stability* of a dispersion? Why is it important? Give a few examples for which stability is important and a few for which it is not desirable.
3. Discuss the differences between the *thermodynamic* and *kinetic* factors that determine the structure and stability of dispersions. Give examples of dispersions with stability that are

controlled by thermodynamic factors. Give a few examples for which kinetic considerations determine stability.

4. How does the interparticle interaction energy influence thermodynamic or kinetic stability? Discuss how variations in dispersion properties influence thermodynamic or kinetic stability.
5. What is the *critical coagulation concentration*? How does it vary with interaction energies?
6. What is the *Derjaguin-Landau-Verwey-Overbeek theory*?
7. Explain the *Schulze-Hardy rule*. Is it empirical or based on theory?
8. What are *perikinetic* and *orthokinetic* coagulation?
9. What is the *stability ratio W*? What values of W correspond to a stable dispersion? Why?
10. What is meant by *rapid coagulation*? What is the basic principle behind the *Smoluchowski theory of rapid coagulation*? What is the rate coefficient for rapid coagulation? How is it defined, and what properties of the dispersion determine its magnitude? What are the limitations of this theory as presented in the text?
11. What is meant by *slow coagulation*? What is the basic principle behind the *Fuchs theory* of slow coagulation? What is the rate coefficient for slow coagulation? How is it defined, and what properties of the dispersion determine its magnitude? What are the limitations of this theory as presented in the text?
12. How is the stability ratio related to the interparticle interaction energy? Under what conditions can it be written in *Arrhenius form*?
13. What is the relation between the stability ratio and the DLVO theory? How would you use the DLVO theory to predict the stability ratio of a dispersion?
14. Discuss how the stability ratio varies with dispersion properties such as electrolyte concentration, pH, surface potential, Hamaker constant, particle size, and so on.
15. Discuss the agreements and disagreements between the theoretical predictions for the stability ratio with what is observed experimentally.
16. What is a *birth-death* (or *population balance*) equation?
17. What are the factors that are relevant for extending the theories of coagulation presented here to (a) polydisperse colloids, (b) nonspherical colloids, and (c) conditions for which fluid flow is important?
18. Discuss how polymers influence colloid stability.
19. For polymer-induced stability, would you recommend the use of a homopolymer or a block copolymer? Why?
20. Discuss polymer-colloid interactions and steric stability from a thermodynamic perspective. What is *enthalpic* stabilization? What is *entropic* stabilization? What is the *critical flocculation temperature* (CFT)?
21. Does the adjective *steric* fully justify the role of polymers in imparting stability to a dispersion? Discuss.
22. List the types of polymer-induced forces one can expect when two particles with polymer coatings interact with each other. Discuss what factors influence the existence and the magnitude of such forces.
23. Why can polymer-induced forces be functions of solution temperature?
24. Why does polymer solution thermodynamics play an important role in polymer-colloid mixtures?
25. What is the *depletion force*? What is the *bridging force*?

REFERENCES

General References (with Annotations)

Elimelech, M., Gregory, J., Jia, X., and Williams, R., *Particle Deposition and Aggregation: Measurement, Modelling and Simulation*, Butterworth-Heinemann, Oxford, England, 1995. (Graduate and research levels. A state-of-the-art treatment of deposition of colloidal particles and their dependence on colloidal forces. Includes theoretical, computational, and experimental approaches.)

Hirtzel, C. S., and Rajagopalan, R., *Colloidal Phenomena: Advanced Topics*, Noyes, Park Ridge, NJ, 1985. (Research monograph. A broad, qualitative review of colloidal phenomena. Discusses colloid stability as well as deposition phenomena and structural evolution in concentrated dispersions. Contains an extensive collection of references prior to 1985.)

Hunter, R. J., *Foundations of Colloid Science*, Vol. 1, Clarendon Press, Oxford, England, 1987.

Hunter, R. J., *Foundations of Colloid Science*, Vol. 2, Clarendon Press, Oxford, England, 1989. (Undergraduate and graduate levels. Along with Volume 1, these two volumes cover almost all the topics covered in the present chapter at a more advanced level. Volume 1 discusses DLVO theory and thermodynamic approaches to polymer-induced stability or instability and is at the undergraduate level. Volume 2 presents advanced topics (e.g., statistical mechanics of concentrated dispersions, rheology of dispersions, etc.).)

Israelachvili, J. N., *Intermolecular and Surface Forces*, 2d ed., Academic Press, London, 1991. (Graduate and undergraduate levels. An excellent and intuitive introduction to polymer-induced forces is given in this volume, which also discusses direct measurement of such forces using the surface force apparatus.)

Kruyt, H. R. (Ed.), *Colloid Science. Vol. 1. Irreversible Systems*, Elsevier, Amsterdam, Netherlands, 1952. (Graduate and undergraduate levels. A classic reference on colloids. Chapters 6–8, by Professor J. Th. G. Overbeek, present the classical DLVO theory of colloidal forces and their application to kinetics of coagulation.)

Murray, C. A., and Grier, D. G., Colloidal Crystals, *American Scientist*, **83**, 238 (1995). (Graduate-level concepts, but some of the general ideas presented are accessible to undergraduates. This is a moderately technical, but qualitative, overview of the use of charged latex particles for studying phase transitions in atomic solids and alloys. The color illustrations presented provide a glimpse of the numerous possibilities made possible by "model colloids' for studying structure of materials.)

Napper, D. H., *Polymeric Stabilization of Colloidal Dispersions*, Academic Press, London, 1983. (Graduate-level monograph. An advanced and in-depth treatment of the role of polymers in colloid stability.)

Sato, T., and Ruch, R., *Stabilization of Colloidal Dispersions by Polymer Adsorption*, Marcel Dekker, New York, 1980. (Research monograph. An advanced treatment of polymer-induced forces.)

Sonntag, H., and Strenge, K., *Coagulation Kinetics and Structure Formation*, Plenum Press, New York, 1987. (Undergraduate level. A concise volume devoted to classical theories of coagulation kinetics. Contains more details than given in this book. Accessible to advanced undergraduates.)

Other References

Atkins, P. W., *Physical Chemistry*, 5th ed., W. H. Freeman, New York, 1994.

Derjaguin, B. V., *Theory of Stability of Colloids and Thin Films*, Consultants Bureau, New York, 1989.

DeSimone, J. M., Maury, E. E., Menceloglu, Y. Z., McClain, J. B., Romack, T. J., and Combes, J. R., *Science*, **265**, 356 (1994).

Dolan, A. K., and Edwards, S. F., *Proc. Roy. Soc. London*, **A337**, 509 (1974).

Enüstün, B. V., and Turkevich, J., *J. Am. Chem. Soc.*, **85**, 3317 (1963).

Fuchs, N. A., *Z. Phys.*, **89**, 736 (1934).

Gregory, J., *CRC Critical Reviews in Environmental Control*, **19**, 185 (1989).

Hidy, G. M., and Brock, J. R., *The Dynamics of Aerocolloidal Systems*, Pergamon Press, Oxford, England, 1970.

Matijevic, E., *J. Colloid Interface Sci.*, **43**, 217 (1973).

O'Melia, C. R., Kinetics of Colloidal Chemical Processes in Aquatic Systems. In *Aquatic Chemical Kinetics: Reaction Rates of Processes in Natural Water* (W. Stumm, Ed.), Wiley-Interscience, New York, 1990

Probstein, R. F., *Physicochemical Hydrodynamics: An Introduction*, 2d ed., Wiley-Interscience, New York, 1994.

Reerink, H., and Overbeek, J. Th. G., *Discuss. Faraday Soc.*, **18**, 74 (1954).

Smoluchowski, M., *Z. Phys. Chem.*, **92**, 129 (1917).

Tien, C., *Granular Filtration of Aerosols and Hydrosols*, Butterworth, Stoneham, MA, 1989.

PROBLEMS

1. Analogous to the planar case considered in Section 13.3, using the Derjaguin approximation, the interaction energy between two spherical particles of radius R_s can be written as

$$\Phi(d) = \pi R_s\{-(A/12\pi)d^{-1} + 64\, k_B T\, n_\infty\, \kappa^{-2}\, \Upsilon_0^2 \exp(-\kappa d)\}$$

Show that the location d_m of the maximum in the potential in this case is given by

$d_m = \kappa^{-1}$ if $\Phi(d_m)$ is also zero.

Substitute this in Equation (2) or (3) and solve for the critical coagulation concentration (CCC):

$$CCC \sim 10^5 [(k_B T)^5 (\varepsilon_r \varepsilon_0)^3 \Upsilon_0^4] / [(ze)^6 A^2]$$

2. Draw a sketch of the integral for the stability ratio W in Example 13.3 and verify that the assumptions made there to evaluate the integral are correct when the maximum in the interaction energy is large.

3. Morrison* uses the following simple Coulombic form of repulsion and the Hamaker expression for attraction for spherical particles of radius R_s for interaction between the particles in nonaqueous dispersions:

$$\Phi(r) = -\frac{A R_s}{12 d} + \frac{4\pi\varepsilon_r \varepsilon_0 R_s^2 \psi_0^2}{r}$$

where A is the Hamaker constant for interaction between two particles through the fluid, d is the shortest surface-to-surface distance between the particles, r is the center-to-center separation, and ψ_0 is the surface potential. The location of the maximum in the interaction energy may be assumed to be approximately $2R_s$.

a. Show that the stability ratio in this case may be approximated by

$$W \approx \left(\frac{A k_B^2 T^2}{3072\pi (\varepsilon_r \varepsilon_0 R_s \psi_0^2)^3}\right)^{1/4} \exp\left(\frac{2\pi \varepsilon_r \varepsilon_0 R_s \psi_0^2}{k_B T}\right)$$

b. For $A = 10^{-20}$ J and $T = 295$ K, show that the criterion for stability can be written as

$$\varepsilon_r R_s \psi_0^2 > 10^3$$

(with R_s in μm and ψ_0 in mV) if we assume that the dispersion is stable for $W > 10^5$.

4. Obtain the result for the stability ratio

$$W \approx \frac{1}{2\kappa R_s} e^{\Phi_m / k_B T}$$

given in Example 13.3 for the step function energy barrier given by

$$\begin{aligned} \Phi(r) &= -\infty && \text{for } r < 2R_s \\ &= \Phi_m && \text{for } 2R_s < r < 2R_s + \kappa^{-1} \\ &= 0 && \text{for } r > 2R_s + \kappa^{-1} \end{aligned}$$

where κ^{-1} represents the range of the potential.

5. It has been observed† that AgI sols at pH 3.5 are coagulated by 4.5×10^{-5} M $Al(NO_3)_3$ in the absence of a second salt and by 1.7×10^{-4} M $Al(NO_3)_3$ in the presence of 0.009 M K_2SO_4. Calculate the value of κ for each of these solutions. Is the threshold of instability consistent with your expectations in terms of the value of κ for these two systems? The authors of this research suggest that $K = 370$ for the equilibrium $Al^{3+} + SO_4^{2-} \rightleftharpoons AlSO_4^+$. Calculate the concentration of Al^{3+} in the system containing K_2SO_4. Does the behavior of the AgI appear to be correlated with the concentration of "free" Al^{3+}? Is the specific adsorption of Al^{3+} expected on AgI in the presence of 4×10^{-4} M excess KI? Discuss in terms of ψ_0 and Φ.

6. Verify that combining Eqs. (5) and (6) with the definition of κ [Eq. (11.35)] leads to the following expression (purely numerical factors may be omitted):

$$CCC \propto n_\infty \propto \frac{\varepsilon^3 (k_B T)^5 \Upsilon_0^4}{e^6 A^2 z^6}$$

By the series expansion of Υ_0 verify that $\Upsilon_0^4 \propto (ze\psi_0/k_B T)^4$ if ψ_0 is low. Use these two results to predict the dependence of the CCC on the ionic valence if ψ_0 is small. Compare this result with the same quantity in the limit of large ψ_0.

---

*Morrison, I. D., *Langmuir*, 7, 1920 (1991); Morrison, I. D., The Influence of Electric Charges in Nonaqueous Dispersions, in *Dispersion and Aggregation: Fundamentals and Applications* (B. M. Moudgil and P. Somasundaran, Eds.) Engineering Foundation, New York, NY 1994.

†Stryker, L. J., and Matijević, E., *J. Phys. Chem.*, 73, 1484 (1969).

7. Arachidic acid sols were studied with different concentrations of La^{3+} added. The stability ratio W and the direction of particle migration in an electric field (i.e., particle charge) were observed* and the following results obtained:

c (mole La^{3+} liter^{-1})	10^{-5}	3×10^{-5}	10^{-4}	3×10^{-3}	10^{-3}
W	7.9	4.5	~1	1.6	15.8
Particle charge	−	−	~0	+	+

Taking 10^{-4} M as the CCC value for La^{3+}, CCC values of 7.29×10^{-2} M and 1.1×10^{-3} M would be predicted for monovalent and divalent cations, respectively, according to Equation (10). In view of the observed behavior of La^{3+}, would you expect these calculated CCC values to be correct or too low or too high? Explain briefly.

8. Kitahara and Ushiyama† flocculated a polystyrene latex of radius 665 Å with KCl. The stability ratio W was found to vary with the KCl concentration as follows:

log c (c in mole liter^{-1})	0	−0.13	−0.33	−0.44	−0.60
log W	0	0	0.30, 0.46	0.73	1.20

From a plot of log W versus log c determine the CCC value and Υ_0 [by means of Eq. (53)]. Use the approximation for Υ_0 given in Problem 6 to estimate ψ_0 for this colloid. Use the values of the CCC and Υ_0 determined in Eqs. (5) and (6) to estimate the effective Hamaker constant A_{212} for polystyrene dispersed in water. Describe how A might be estimated using a more realistic model than that used in the derivation of Eqs. (5) and (6).

9. Müller‡ studied by dark-field microscopy the flocculation of colloidal gold upon the addition of NaCl to the aqueous sol. For a sample in which the gold particles have a 36.9-Å radius, the following particle counts were observed at different times after the colloid was made about 0.2 M with NaCl:

t(s)	120	195	270	390	450	570
$N \times 10^{-8}$ (cm^{-3})	11.2	7.3	5.4	4.5	3.7	2.7

Determine the second-order rate constant k_{exp} which describes this flocculation process. How does k_{exp} compare with k_r as given by Eq. (32)?

10. Polystyrene latex particles were coagulated by the addition of $Ba(NO_3)_2$. The number of dispersed particles deposited onto a planar polystyrene surface was determined 15 min after the addition of salt by optical microscopy. The light microscope does not permit the aggregation of the deposited particles to be determined; subsequent examination by the electron microscope gives this information. Clint et al.§ obtained the following results:

$Ba(NO_3)_2$ concentration $\times 10^3$ (mole liter^{-1})	Total deposition cm$^{-2} \times 10^{-5}$ (after 15 min)	Percent deposit		
		Single	Double	Triple
9.1	8.04	94.7	3.3	0.3
15.4	14.25	95.0	4.3	0.4
22.7	14.43	82.9	11.3	3.5
57.0	11.25	75.0	15.8	5.6

Discuss these data in terms of the following points:

(a) For all salt concentrations the order of particle abundance in the deposit is single > double > triple.

(b) The decrease in total deposition with increasing concentration is not offset by the higher aggregation state of the deposit, but arises from the slower diffusion of more highly aggregated kinetic units.

---

*Ottewill, R. H., and Wilkins, D. J., *Trans. Faraday Soc.*, **58**, 608 (1962).

†Kitahara, A., and Ushiyama, H., *J. Colloid Interface Sci.*, **43**, 73 (1973).

‡Müller, H., *Kolloid Z.*, **38**, 1 (1926).

§Clint, G. E., Clint, J. H., Corkil, J. M., and Walker, T., *J. Colloid Interface Sci.*, **44**, 121 (1973).

11. If ccoagulation involves two noninteracting spheres of different radii R_i and R_j, Equations (24) and (28) predict

$$k_r = \frac{2}{3}\frac{k_B T}{\eta}(R_i + R_j)\left(\frac{1}{R_i} + \frac{1}{R_j}\right)$$

Show that this expression is identical to

$$k_r = \frac{2}{3}\frac{k_B T}{\eta}\left|4 + \left(\sqrt{\frac{R_i}{R_j}} - \sqrt{\frac{R_j}{R_i}}\right)^2\right|$$

Estimate the ratio R_i/R_j needed to account for a k_r value of 2.9×10^{-11} cm^3 s^{-1} as observed for arachidic acid sols.* Does this expression reduce to the proper limit when $R_i = R_j$?

12. Verify (a) that Equation (40) is a solution to Equation (37), (b) that Equation (41) reduces to Equation (21) if $\Phi = 0$, and (c) that Equation (46) leads to a rate constant larger than k_r if $\Phi = 0$ for $r > \Delta$ and $\Phi = -\infty$ for $r < \Delta$, where $\Delta > 2R_s$. Show that the experimental k_r value cited in Problem 11 is consistent with a value of Δ equaling 5.4 R_s for an aqueous colloid at 20°C ($\eta = 0.01$ P). Discuss the relevancy of this last result to the rapid flocculation of particles between which van der Waals attraction exists.

13. Ahmed et al.† measured η_{red}/ϕ for polystyrene latexes with adsorbed layers of commercial poly(vinyl alcohol) (PVA) samples of different molecular weights. The latex particles were 190 nm in diameter and the limiting values of η_{red}/ϕ as $\phi \to 0$ had the following values for PVA samples of the indicated molecular weight:

M_{PVA} (g mole^{-1}):	None	26,400	23,000	80,000	79,100
R_g (nm)	–	6.5	7.4	13.2	13.0
$[\eta]$	3.0	5.0	5.5	8.2	9.1

Use the experimental value of $[\eta]$ for the bare particles and the relationship given in Example 13.5 to estimates δR_s for these particles. How do the layer thicknesses compare with $2R_g$, for which the given radii of gyration were determined for the polymers in bulk solution?

14. The parameter χ is proportional to the energy of interaction per 1-2 pair. To allow for solvent molecules of various sizes, we can write $\chi \propto n_1^* \Delta w$, where n_1^* is the number of segments in a solvent molecule, or $\bar{V}_1/V_1^*$, where V_1^* is the molar volume of a segment. The ratio $(1/2 - \chi)/\bar{V}_1$ that appears in the expression for ΔG_R in Equation (59) can be written $(1/2\bar{V}_1) - (\text{const.}\ \Delta w/V_1^*)$. Criticize or defend the following proposition: For a specific polymer in a homologous series of solvent molecules of different sizes, the second term in this expression should remain constant while the first decreases with increasing $\bar{V}_1$. When the "solvent" is the melt of the polymer under consideration, the first term is negligible because $\bar{V}_1$ becomes the partial molar volume of the polymer and is very large. Therefore ΔG_R becomes negative for such a system, and flocculation is predicted. Since this contradicts experimental evidence, the Flory-Krigbaum model is seen to break down at this limit.

15. Mackor‡ used the model outlined in Example 13.6 to derive the expression $\Delta G_R = Nk_B T(1 - d/L)$ for the repulsion per unit area of particles carrying N rods of length L when the surfaces are separated by a distance d. Assuming this repulsion equals the van der Waals attraction when the particle separation is 1.5 nm, calculate the effective Hamaker constant in this system if $L = 2.5$ nm. Select a reasonable value for N in this calculation and justify your choice.

16. In view of the model used in Problem 15, criticize or defend the following proposition: If one surface carries adsorbed rods and the other is bare, the system could be stabilized against flocculation by dispersing the particles in a medium of intermediate γ. Such a system would remain dispersed indefinitely since both steric considerations and a negative Hamaker constant oppose flocculation.

---

*Ottewill, R. H., and Wilkins, D. J., *Trans. Faraday Soc.*, **58**, 608 (1962).

†Ahmed, M. S., El-Aasser, M. S., and Vanderhoff, J. W., in *Polymer Adsorption and Dispersion Stability* (E. D. Goddard and B. Vincent, Eds.), American Chemical Society, Washington, DC, 1964.

‡Mackor, E. L., *J. Colloid Sci.*, **6**, 492 (1951).

Appendix A

Examples of Expansions Encountered in This Book

1. Inverse of $(1 - x)$:

$$1/(1 - x) = 1 + x + x^2 + x^3 + \ldots$$

2. Logarithm:

$$\ln(1 + x) = x - (1/2)x^2 + (1/3)x^3 - \ldots \qquad (-1 < x < +1)$$

3. Binomial:

$$(1 \pm x)^n = 1 \pm nx + [n(n - 1)/2!]x^2 \pm [n(n - 1)(n - 2)/3!]x^3 + \ldots \qquad (x^2 < 1)$$

4. Taylor's series for $f(x)$ around $x = x_0$:

$$f(x) = f(x_0) + (x - x_0)f'(x_0) + [(x - x_0)^2/2!]f''(x_0) + \ldots$$

where each prime on f indicates a differentiation with respect to x.

5. Sine function:

$$\sin x = x - x^3/3! + x^5/5! - \ldots$$

6. Hyperbolic sine function:

$$\sinh x = x + x^3/3! + x^5/5! + \ldots$$

7. Hyperbolic cosine function:

$$\cosh x = 1 + x^2/2! + x^4/4! + \ldots$$

8. Exponential function:

$$e^x = 1 + x + x^2/2! + x^3/3! + \ldots$$

REFERENCE

Gradshteyn, I. S., and Ryzhik, I. M., *Table of Integrals, Series, and Products*, 5th ed., Academic Press, New York, 1993. (There are numerous excellent reference books available on mathematical formulas. This book has a reasonably large collection, far more than what is needed for the present book. A CD-ROM version of this book is also available: CD-ROM Version 1, Alan Jeffrey, Ed.)

Appendix B

Units: CGS-SI Interconversions

From time to time, probably all science students find themselves entangled in a problem of units. For those who have advanced through physical chemistry to the level of this book, these problems have obviously not been insurmountable. It is likely, however, that—along with feelings of frustration—these students have been left with the wish that everyone used the same units, specifically those units with which they are most comfortable. In response to the recognized need for uniformity, IUPAC recommends the use of *Système international d'unités (International System of Units, SI)* units, which are essentially standardized mks units.

The SI system is based on mutually consistent units assigned to the nine physical quantities listed in Table B.1. In addition to the SI units for these nine quantities, the table also lists cgs or other commonly encountered units, as well as the conversion factors between the two. In this table the headings at the top of the table indicate how the conversion factors are to be used in going from SI to cgs/common units, whereas the bottom headings indicate the use of these factors for calculations in the reverse direction.

From these nine basic quantities, numerous other SI units may be derived. Table B.2 lists a number of these derived units, particularly those relevant to colloid and surface chemistry. The table is arranged alphabetically according to the name of the physical quantity involved. Note that instructions for the use of the conversion factors—depending on the direction of the conversion—are given in the top and bottom headings of the columns. Table B.2 is by no means an exhaustive list of the various derived SI units; Hopkins (1973) reports on many additional conversions, as do most handbooks and numerous other references.

One reason for the great diversity of units in existence is the fact that quantities of such diverse magnitudes are measured. A general rule is that the unit should be appropriate in magnitude to the quantity being measured. To obtain a dimension of convenient size in SI units, the SI unit is multiplied by a power of 10 and the prefixes listed in Table B.3 are affixed to the unit.

REFERENCES

Hopkins, R. A., *The International (SI) Metric System and How It Works*, Polymeric Services, Reseda, CA, 1973.

McGlashan, M. L., *Pure Appl. Chem.*, **21**, 577 (1970).

Page, C. H., and Vigoureux, P. (Eds.), *The International System of Units (SI)*, National Bureau of Standards, Special Publication 330, Washington, DC, 1974.

Paul, M. A., *J. Chem. Educ.*, **48**, 569 (1971).

TABLE B.1 Basic SI Units and Their Relation to cgs or Other Common Units[a]

	SI unit ×		Conversion factor	→ cgs/common unit	
Physical quantity	Name	Symbol		Name	Symbol
Length	Meter	m	10^2	Centimeter	cm
Mass	Kilogram	kg	10^3	Gram	g
Time	Second	s	1	Second	s
Electric current	Ampere	A	2.998×10^9	Statampere	statamp
Thermodynamic temperature	Kelvin	K	1	Kelvin	K
Luminous intensity	Candela	cd	π	Lambert	(cm^2)
Amount of substance	Mole	mole	1	Mole	mole
Plane angle	Radian	rad	$180/\pi$	Degree (angle)	°
Solid angle	Steradian	sr	1	Steradian	sr
	SI unit ←		Conversion factor	÷ cgs/common unit	

[a]Note that different column headings are given at the top and bottom of the table to facilitate conversions from SI to cgs and from cgs to SI, respectively.

TABLE B.2 Derived SI Units and Their Relation to cgs or Other Common Units[a]

Physical quantity	SI unit	×	Conversion factor	→	cgs/common unit
Acceleration	$m\ s^{-2}$		10^2		$cm\ s^{-2}$
Acceleration, angular	$rad\ s^{-1}$		1		$rad\ s^{-1}$
Area	m^2		10^4		cm^2
			10^{20}		$Å^2$
Capacitance (farad)	$F = m^{-2}\ kg^{-1}\ s^4\ A^2 = C\ V^{-1}$		8.99×10^{11}		statfarad
Charge (Coulomb)	$C = A\ s = J\ V^{-1}$		3.00×10^9		statcoulomb (esu)
Charge density, surface	$C\ m^{-2}$		3.00×10^5		$statcoul\ cm^{-2}$
Charge density, volume	$C\ m^{-3}$		3.00×10^3		$statcoul\ cm^{-3}$
Conductance (siemens)	$S = m^{-2}\ kg^{-1}\ s^3\ A^2 = ohm^{-1}$		8.99×10^{11}		$statmho\ (statohm^{-1})$
Conductivity	$ohm^{-1}\ m^{-1}$		8.99×10^9		$statmho\ cm^{-1}$
			10^{-2}		$mho\ cm^{-1}\ (ohm^{-1}\ cm^{-1})$
Density	$kg\ m^{-3}$		10^{-3}		$g\ cm^{-3}$
Diffusion coefficient	$m^2\ s^{-1}$		10^4		$cm^2\ s^{-1}$
Dipole moment	C m		3.00×10^{11}		statcoul cm
Electric field	$V\ m^{-1}$		3.34×10^{-5}		$statvolt\ cm^{-1}$
			10^{-2}		$V\ cm^{-1}$
Electric potential (volt)	$V = m^2\ kg\ s^{-3}\ A^{-1} = J\ C^{-1}$		3.34×10^{-3}		statvolt
Energy (joule)	$J = m^2\ kg\ s^{-2} = N\ m$		10^7		erg
			0.2390		calorie
Entropy	$J\ K^{-1}$		0.2390		$cal\ K^{-1}$
Force (newton)	$N = m\ kg\ s^{-2}$		10^5		dyne
Frequency (hertz)	$Hz = s^{-1}$		1		s^{-1}
Friction factor	$kg\ s^{-1}$		10^3		$g\ s^{-1}$
Heat capacity	$J\ K^{-1}$		0.2390		$cal\ K^{-1}$
Molarity	$mole\ dm^{-3}$		1		$mole\ liter^{-1}$
Moment, dipole	C m		3.00×10^{11}		statcoul cm

Moment, force	$N\ m$	10^7	dyne cm
Moment, inertia	$kg\ m^2$	10^7	$g\ cm^2$
Momentum	$N\ s$	10^5	dyne s
Momentum, angular	$J\ s$	10^7	erg s
Period	s	1	s
Permitivity	$F\ m^{-1}$	8.99×10^9	statfarad cm^{-1}
Polarization, electric	$C\ m^{-2}$	3.00×10^5	statcoul cm^{-2}
Potential (volt)	V	3.34×10^{-3}	statvolt
Power (watt)	$W = m^2\ kg\ s^{-3} = J\ s^{-1}$	10^7	$erg\ s^{-1}$
Pressure (pascal)	$Pa = m^{-1}\ kg\ s^{-2} = N\ m^{-2}$	10	dyne cm^{-2}
		9.87×10^{-6}	atm
Radius of gyration	m	10^2	cm
Resistance (ohm)	$ohm = m^2\ kg\ s^{-3}\ A^{-2} = VA^{-1}$	1.11×10^{-12}	statohm
Specific heat capacity	$J\ kg^{-1}\ K^{-1}$	2.39×10^{-4}	cal $g^{-1}\ K^{-1}$
Stress	$N\ m^{-2}$	10	dyne cm^{-2}
Surface energy	$J\ m^{-2}$	10^3	erg cm^{-2}
Surface tension	$N\ m^{-1}$	10^3	dyne cm^{-1}
Torque	N m	10^7	dyne cm
Velocity	$m\ s^{-1}$	10^2	$cm\ s^{-1}$
Velocity, angular	$rad\ s^{-1}$	1	$rad\ s^{-1}$
Viscosity	$N\ s\ m^{-2}$	10	dyne s cm^{-2} (P)
Volume	m^3	10^6	cm^3
		10^3	dm^3 (liter)
Wave number	m^{-1}	10^{-2}	cm^{-1}
Weight	N	10^5	dyne

SI unit	←	Conversion factor	÷ cgs/common unit

[a]Note that different column headings are given at the top and bottom of the table to facilitate conversions from SI to cgs and from cgs to SI, respectively. The cgs units must be divided *by* the conversion factor to get the SI units.

TABLE B.3 Multiples of Units, Their Names, and Symbols

Multiple	Prefix	Symbol
10^{12}	tera	T
10^{9}	giga	G
10^{6}	mega	M
10^{3}	kilo	k
10^{2}	hecto	h
10	deca	da
10^{-1}	deci	d
10^{-2}	centi	c
10^{-3}	milli	m
10^{-6}	micro	μ
10^{-9}	nano	n
10^{-12}	pico	p
10^{-15}	femto	f
10^{-18}	atto	a

Appendix C

Statistics of Discrete and Continuous Distributions of Data

C.1 INTRODUCTION

Students of the physical sciences generally encounter statistics in two different places. One of these deals with the treatment of experimental data. From this viewpoint, all measured quantities contain some error, which raises questions concerning the best way to report the results of multiple measurements. This is obviously related to our problem of describing, for example, the "characteristic dimension" of the particles discussed in Chapter 1 (Figure 1.10). Another place in which the science student encounters statistics is in the theoretical description of large populations or populations that change through a large number of states, as, for example, in the kinetic molecular theory of gases. We are concerned with this aspect of statistics also. For example, the randomly coiled piece of string we considered in Chapter 1 (Section 1.5a.2) changes size and shape continually while it is being shaken.

These two applications of statistics, from our point of view, will differ primarily in the kind of information we have available about our system. Sometimes, as when measuring micrographs, we have individual information on a large number of particles. Our question under these circumstances is how to condense these data into a few key parameters. In other circumstances, the experimental quantity itself will be an "average" quantity. Our question, then, is what kind of distribution is consistent with this average. In both cases, the underlying fact is the existence of a distribution of values for the quantity in question. We consider some aspects of these statistical topics here; references in statistics should be consulted if additional information is needed.

C.2 DISCRETE DISTRIBUTIONS

Suppose we have just measured the diameters of a field of polydisperse spheres in an electron micrograph. The data in such cases consist of sets of numbers such as the ones we saw in Table 1.5. Our objective is to devise reasonable ways of presenting a description of the system in terms of the measured data. A fairly large number of observations is required for any statistical approach to be valid; therefore merely to tabulate the measurements is inadequate. Some condensation of the data is clearly required. Generally, the first step along these lines is a device known as *classification* of the data. Classification consists of sorting the observed quantities into 10–20 categories called *classes*. Having fewer than 10 categories results in a loss of detail in the description of the distribution; having more than 20 categories does not improve the representation in proportion to the extra effort it requires. The frequency distribution of such a sample is a tabulation of the number of particles in each class. Table 1.5 in Chapter 1, for example, represents the frequency distribution for a hypothetical array of spheres; all the numerical examples of this section are based on this sample of 400 particles. Each class is represented by the midpoint of the interval, a quantity called the *class mark*, symbolized by d_i for class i. Similarly, we define the number of particles in each class as n_i.

We discussed in Chapter 1 how discrete data—such as the ones reported in Table 1.5—can be represented graphically as a histogram, that is, a bar graph in which the class marks are plotted as the abscissa and the height of the bar is proportional to the number of particles in the class (Fig. 1.18a). The corresponding cumulative curve, that is, the total number (or fraction) of particles $n_{T,i}$ having diameters less (sometimes more) than and including a particular d_i are plotted versus d_i. This was illustrated in Figure 1.18b.

In this appendix, we summarize how the discrete data sets can be represented in terms of averages, standard deviation, and moments in a concise way. In principle, under certain conditions, these quantities represent the same information represented through histograms.

C.2a Average and Standard Deviation

In Section 1.5c.1 we presented the following general definition of an average:

$$\text{Average} = \sum_i (\text{Weighting factor})_i (\text{Quantity being averaged})_i \tag{1}$$

where the weighting factor f_i and the quantity being averaged ϕ_i can both mean different things in different contexts. The most common definition of a weighting factor is the number fraction of the particles in each class i. We indicate this by the additional subscript n of f:

$$f_{n,i} = n_i / \sum_i n_i \tag{2}$$

Then the *mean* or the average of ϕ_i denoted by $\bar{\phi}$ is given by

$$\bar{\phi} = \sum_i f_{n,i}\phi_i = \frac{\Sigma_i n_i \phi_i}{\Sigma_i n_i} \tag{3}$$

and the *standard deviation* σ

$$\sigma = \left(\sum_i f_{n,i}(\phi_i - \bar{\phi})^2\right)^{1/2} = \left(\frac{\Sigma_i n_i (\phi_i - \bar{\phi})^2}{\Sigma_i n_i}\right)^{1/2} \tag{4}$$

of the distribution. The significance of the standard deviation should be noted. The quantity $[\phi_i - \bar{\phi}]$ is the deviation of a particular value from the mean, and the deviations can be positive or negative. Comparing Equation (1) with Equation (4), we see that σ^2 is actually the *number average of the square of the deviations* $[\phi_i - \bar{\phi}]$. The square root of this average, then, is a measure of the spread of the data in a particular sample. For this reason, σ is often called the *root mean square* (rms) deviation. From a computational point of view, the following formula, which is a different way of writing Equation (4), provides an easier means for evaluating σ:

$$\sigma = \left[\overline{\phi^2} - (\bar{\phi})^2\right]^{1/2} \tag{5}$$

This result was used in Section 1.5c.3b to relate $(\overline{M}_w/\overline{M}_n)$ to σ.

In general, the *number average* (i.e., based on number fraction $f_{n,i}$ as the weight function) of any property, say, ψ, of the particles is defined as

$$\bar{\psi} = \sum_i f_{n,i}\psi_i \tag{6}$$

where ψ_i is the value of the property in class i. If ψ is taken to be the area A of the particles, one then has for the average area, that is, area per particle $\bar{A}$:

$$\bar{A} = \frac{\pi \Sigma_i n_i d_i^2}{\Sigma_i n_i} = \pi \sum_i f_{n,i} d_i^2 \tag{7}$$

The diameter of a sphere having this "average" area is the surface area average diameter $\bar{d}_s$ and equals

$$\bar{d}_s = \left(\sum_i f_{n,i} d_i^2\right)^{1/2} \tag{8}$$

The surface average diameter is always larger than the direct average of the diameters for a polydisperse system since the larger diameters contribute relatively more to the sum of the squares than they would if totaled directly. Example C.1 illustrates such a calculation.

* * *

EXAMPLE C.1 *Average Surface Area Versus Surface Area Based on Average-Size Particles.* Using the distribution of spheres in Table 1.5, calculate the area of each size sphere in the distribution and average these areas, using the number of spheres in each class as weighting factors. How is this result related to $\bar{d}_s$ for this population?

Solution: To calculate the area of each size sphere, we apply the formula $A = \pi d^2$ to each class in Table 1.5:

d_i (μm)	A_i (μm^2)	$n_i A_i$ (μm^2)
0.05	$7.85 \cdot 10^{-3}$	$5.50 \cdot 10^{-2}$
0.15	$7.07 \cdot 10^{-2}$	1.06
0.25	$1.96 \cdot 10^{-1}$	3.53
0.35	$3.85 \cdot 10^{-1}$	$1.08 \cdot 10^{1}$
0.45	$6.36 \cdot 10^{-1}$	$2.04 \cdot 10^{1}$
0.55	$9.50 \cdot 10^{-1}$	$6.65 \cdot 10^{1}$
0.65	1.33	$8.63 \cdot 10^{1}$
0.75	1.77	$1.04 \cdot 10^{2}$
0.85	2.27	$1.02 \cdot 10^{2}$
0.95	2.84	$1.08 \cdot 10^{2}$
1.05	3.46	$6.58 \cdot 10^{1}$
1.15	4.15	$1.66 \cdot 10^{1}$
		Sum = $5.85 \cdot 10^{2}$

Therefore the "average" area is $5.85 \cdot 10^2/400 = 1.46\ \mu m^2$.

This is the value used in Section 1.5c.1. This average area divided by π gives $(\bar{d}_s)^2$. ■

* * *

The general formulas for calculating averages are given by Equations (1) and (2). Equation (2) represents the weighting factor in normalized form. A weighting factor is said to be *normalized* if the sum of weighting factors for the whole population equals unity, a consideration that must be introduced at some point in the calculation. When fractions of the whole are used as weighting factors, normalization is introduced through the definition of the weighting factor.

C.2b Higher-Order Moments of the Distribution

In general one can define the kth *moment* of the distribution about a point d_0 as

$$k\text{th moment} = \sum_i f_{n,i} (d_i - d_0)^k \tag{9}$$

Note that Equation (9) implies that the square of the standard deviation σ^2 is the *second moment* of d relative to the mean $\bar{d}$. Higher order moments can be used to represent additional information about the shape of a distribution. For example, the third moment is a measure of the "skewness" or lopsidedness of a distribution. It equals zero for symmetrical distributions and is positive or negative, depending on whether a distribution contains a higher proportion of particles larger or smaller, respectively, than the mean. The fourth moment (called *kurtosis*) purportedly measures peakedness, but this quantity is of questionable value.

In discussing the random walk and diffusion in Chapter 2, we use continuous functions as the weighting factors for calculating averages (e.g., Equation (2.63)). In the following section we discuss in greater detail the use of continuous weighting functions in statistics.

C.3 THEORETICAL DISTRIBUTION FUNCTIONS

We noted in Section 1.5c that histograms of distributions of quantities such as particle size approach smooth distribution curves as the number of classes is increased to a very large number. Sometimes it is desirable to represent a distribution function by an analytical expression that is a continuous function of the measured variable. We consider only a few examples of such distribution functions here.

C.3a Normal or Gaussian Distribution Function

The most familiar of such functions is the *normal*, or *Gaussian*, distribution function:

$$f(x)dx = \frac{1}{\sigma\sqrt{2\pi}} \exp\left[-\frac{1}{2}\left(\frac{x - \bar{x}}{\sigma}\right)^2\right]dx \tag{10}$$

In this equation, $f(x)dx$ expresses the fraction of particles having x values between x and $x + dx$; it replaces $f_{n,i}$, which plays a corresponding role in discrete distributions. Some characteristics of the normal distribution are the following:

1. The function $f(x)$ has its maximum value at $x = \bar{x}$ and drops off exponentially with the square of the deviation of x from the mean, when such deviations are measured as fractions or multiples of the standard deviation.
2. The preexponential factor accomplishes the normalization of the function; that is, the integral of the function over all possible values of x ($-\infty$ to ∞) equals unity. In a broad distribution σ is large, and the exponential does not drop off as rapidly as in a narrow distribution (recall that all deviations are measured relative to the standard deviation).
3. Since the area under the curve is always unity, a narrow distribution will show larger values of $f(x)$ at the maximum, whereas a broader distribution will have a smaller value for the function at the maximum. This is why the standard deviation appears in the denominator of the preexponential normalization factor.

The normal distribution is the "curve" over which students and teachers alike agonize in connection with course grades. We discuss this distribution function in greater detail in Chapter 2. For the present we are concerned only with its descriptive capabilities. For this purpose it is sufficient to note that tables are available (e.g., Beyer 1987; also see the other references at the end of this Appendix) that supply the value of this function in terms of the standard unit,

$$f(t)dt = \frac{1}{\sqrt{2\pi}} \exp\left(-\frac{t^2}{2}\right)dt \tag{11}$$

The normal distribution is commonly encountered in the cumulative form, that is, as the fraction of particles larger (oversized) or smaller (undersized) than a particular t_i value. Since the total area under the normal curve equals unity, the area under one "tail" of the curve from t_i to ∞ gives the fraction of the population having t values greater than the integration limit t_i:

$$f_{t>t_i} = \frac{1}{\sqrt{2\pi}} \int_{t_i}^{\infty} \exp\left(-\frac{t^2}{2}\right)dt \tag{12}$$

Likewise, the cumulative fraction of particles smaller than t_i equals

$$f_{t<t_i} = 1 - \frac{1}{\sqrt{2\pi}} \int_{t_i}^{\infty} \exp\left(-\frac{t^2}{2}\right)dt \tag{13}$$

Tables are also available (e.g., see Beyer 1987) for the area under the normal curve between $\bar{t}$ ($\bar{t} = 0$) and one value of t_i (i.e., they apply to one tail only). This area is known as the *error function* and is often symbolized as erf (t_i):

$$\text{erf}\,(t_i) = \frac{1}{\sqrt{2\pi}} \int_0^{t_i} \exp\left(-\frac{t^2}{2}\right) dt \tag{14}$$

In terms of the error function, Equation (12) becomes

$$f_{t>t_i} = \frac{1}{2} \pm \text{erf}\,(t_i) \tag{15}$$

where the positive value is used if t_i is negative and the negative value is used if t_i is positive. These signs are reversed if the cumulative fraction of undersized particles is to be determined. Consulting the tables, we see that in a normally distributed sample 15.87% of the particles will have t values greater than $+1.0$. This is the percentage of particles for which the deviation from the mean is greater than one standard deviation unit.

Example C.2 considers a numerical application of these ideas.

* * *

EXAMPLE C.2 *Polydispersity in Size: Gaussian Distribution.* A sample of 75 particles follows the normal distribution with respect to particle diameters, with $\bar{d} = 1.140$ μm and $\sigma = 0.311$ μm. Consult a table of the normal distribution to evaluate the fraction of particles in the population having diameters less than 1.0 μm. What is the probability that a particle picked at random from this population lies in the class for which $0.95 < d < 1.05$ in the histogram of this distribution?

Solution: Evaluate t for $d = 1.00$: $t = (d - \bar{d})/\sigma = (1.00 - 1.14)/0.311 = -0.450$. Tables of the normal distribution (see Beyer 1987) indicate that the area under the curve is 0.1736 at $t = 0.45$. To interpret this, picture the familiar bell-shaped curve centered at $t = 0$ ($d = \bar{d} = 1.14$ μm); we are interested in an abscissa value of $t = -0.45$ ($d = 1.0$). The figure 0.1736 gives the fraction of the area under the whole curve that lies between $t = -0.45$ and $t = 0.0$. This means that $(0.5 - 0.1736) = 0.3264$ is the fraction of the area that lies beyond $t = -0.45$. This means that about 33% of the particles have diameters less than 1.00 μm.

For $d = 0.95$, $(d - \bar{d})/\sigma = -0.61$; the area between $t = -0.61$ and $t = 0.0$ is 0.229 according to the tables. For $d = 1.05$, $(d - \bar{d})/\sigma = 0.29$; the area between $t = -0.29$ and $t = 0.0$ is 0.114. Therefore the probability of a particle falling between 0.95 and 1.05 is $(0.229 - 0.114) = 11.5\%$. ■

* * *

Suppose a polydisperse system is investigated experimentally by measuring the number of particles in a set of different classes of diameter or molecular weight. Suppose further that these data are believed to follow a normal distribution function. To test this hypothesis rigorously, the chi-squared test from statistics should be applied. A simple graphical examination of the hypothesis can be conducted by plotting the cumulative distribution data on probability paper as a rapid, preliminary way to evaluate whether the data conform to the requirements of the normal distribution.

Probability paper is a commercially available graph paper that has one coordinate subdivided in ordinary arithmetic units and the other coordinate subdivided into cumulative probability units. The latter are spaced in such a way that normally distributed data will produce a straight line graph when the cumulative percentage of undersize (or oversize) particles is plotted on the probability coordinate, and the size variable (diameters, weights, etc.) is plotted on the arithmetic scale. Figure C.1 shows schematically how (a) normally distributed data are transformed when replotted as (b) a cumulative distribution and, finally, when (c) graphed on probability paper. The x value corresponding to $y = 50\%$ on probability paper gives the mean value. The x value at $y = 15.87\%$ gives $(\bar{x} - \sigma)$, and the x value at $y = 84.13\%$ $(100 - 15.87)$ gives $(\bar{x} - \sigma)$ when the percentage of undersize particles is plotted (the signs are reversed when the percentage of oversize particles is plotted). From these values σ may be determined. Thus a linear plot on probability paper suggests conformity to the normal distribution and also permits the graphical evaluation of $\bar{x}$ and σ.

As we see in Chapter 2, the normal distribution comes about when a large number of purely random factors is responsible for the distribution. It is mainly applicable to particles

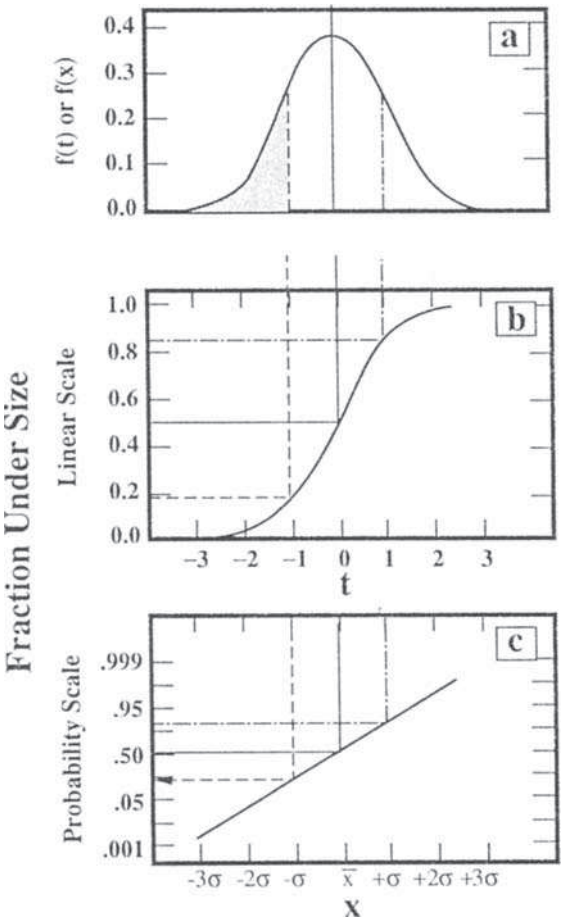


FIG. C.1 A normal, or Gaussian, distribution: (a) represented as a frequency function; (b) represented as a cumulative function; and (c) represented as a cumulative function linearized by plotting on probability paper.

that are produced by condensation, precipitation, or polymerization processes, which are purely random.

C.3b Log-Normal Distribution Function

Dispersions that are produced by comminution—the mechanical subdivision of larger chunks—are more likely to produce a linear graph on probability paper if the logarithm of the variable rather than the variable itself is plotted against the probability. Graph paper graduated this way is called *log-probability paper*. The logarithmic scale implies a much wider range of values for the variable, and also an asymmetrical distribution function may be written by analogy with Equation (10):

$$f(\ln x) = \frac{1}{\ln \sigma_g \sqrt{2\pi}} \exp\left[-\frac{1}{2}\left(\frac{\ln x_i - \ln \bar{x}_g}{\ln \sigma_g}\right)^2\right] \tag{16}$$

However, an important difference also emerges from this analogy. The quantities that are normally distributed are logarithms of variables, not the variables themselves. This means that the mean and standard deviation obtained from log-probability plots are geometric averages

rather than arithmetic averages. This is the significance of the subscript g in Equation (16). This is most easily understood by writing the expression for the number average value for the quantity $\ln x_i$:

$$\overline{\ln x} = \sum_i f_i \ln x_i = \sum_i \ln x_i^{f_i} \tag{17}$$

Taking the antilog of this quantity converts the summation into a product over all terms, indicated by Π:

$$\text{antiln } (\overline{\ln x}) = \prod_i x_i^{f_i} = \bar{x}_g \tag{18}$$

When the averaging is carried out in this way, the result is known as the geometric mean x_g. The coordinate corresponding to the 15.87% undersize y value equals $(\ln x_g - \ln \sigma_g)$. Because of the properties of logarithms, this is the same as the logarithm of the ratio (x_g/σ_g). From this, σ_g may be evaluated. We shall not concern ourselves further with these geometrical averages except to note that

$$\bar{x}_g < \bar{x}_n \tag{19}$$

for any polydisperse system. (The subscript n on the $\bar{x}$ on the right-hand side of Equation (19) stands for *arithmetic* average of the type in Equation (3).) The validity of this relationship is easily demonstrated by calculating the two averages for a hypothetical distribution.

REFERENCES

Beyer, W. H. (Ed.), *CRC Handbook of Mathematical Sciences*, 6th ed., CRC Press, Boca Raton, FL, 1987. (One of the standard references for tables of mathematical concepts and formulas.)

Crow, E. L., Davis, F. A., and Maxfield, M. W., *Statistics Manual*, Dover, New York, 1960. (There are numerous excellent books on statistics available in print. This book is a handy, affordable manual that is sufficient for most purposes.)

Meyer, S. L., *Data Analysis for Scientists and Engineers*, Wiley, New York, 1975. (This is a more detailed manual on statistics and contains very useful collections of tables, distribution functions, data analysis procedures, and graphical techniques.)

Appendix D

List of Worked-Out Examples

Example	Topic	Page
1.1	Variation of specific surface area with geometry	9
1.2	Surface area of fractal aggregates	27
1.3	Polydispersity of a synthetic polymer	37
2.1	Most probable settling velocity from sedimentation data	72
2.2	Particle-size determination from sedimentation equation	74
2.3	Sedimentation in an ultracentrifuge	78
2.4	Solvation and ellipticity from sedimentation data	83
2.5	Diffusion and Gaussian distribution	89
2.6	Temperature-dependence of diffusion coefficients	92
3.1	Molecular weight from osmotic pressure measurements	117
3.2	Degree of polymerization and molecular weight distribution	119
3.3	Excluded volume from osmotic pressure measurements	124
3.4	Theta temperature from second virial coefficient data	134
3.5	Evaluation of charges on macroions from osmotic pressures	138
4.1	Stress-strain relationship from a concentric-cylinder viscometer	152
4.2	Capillary viscometers versus concentric-cylinder viscometers	157
4.3	Inherent viscosity at low volume fractions	167
4.4	Extent of hydration from intrinsic viscosity measurements	170
4.5	Empirical determination of the Mark-Houwink coefficients	182
4.6	Variation of viscosity with polymer configuration	187
5.1	Polarizability of particles	201
5.2	Molecular weights from Rayleigh ratios	210
5.3	Use of Zimm plots	221
5.4	Structure of aggregates probed by small-angle scattering	226
5.5	Effective diameter of an enzyme from DLS	239
5.6	Cumulant analysis of DLS data	241
6.1	Laplace equation: A thermodynamic derivation	259
6.2	Determining surface tension from the Kelvin equation	262
6.3	Heat of immersion from surface tension and contact angle	268
6.4	Surface tension and the height of a meniscus at a wall	278
6.5	Interfacial tensions from the Girifalco-Good-Fowkes equation	289
7.1	Molecular weight of a solute from π versus A isotherms	313
7.2	Use of the van't Hoff equation for monolayers	315
7.3	Suppression of evaporation by monolayers	321
7.4	Surface excess concentration from surface tension data	329

7.5	Use of Langmuir adsorption isotherms	335
7.6	Interpretation of adsorption using electrocapillary curves	347
8.1	Reaction equilibrium and phase equilibrium models of micellization	361
8.2	Calculating the geometric parameters of the core of a micelle	364
8.3	Packing parameter for a spherical micelle	369
8.4	Gibbs energy and entropy changes due to micellization	373
8.5	Equilibrium and rate constants in micellar catalysis	383
8.6	An NMR study of solubilization in a reverse micelle	387
8.7	Interpreting phase diagrams of microemulsions	392
9.1	Construction of adsorption isotherms	411
9.2	Evaluating isotherms from equations of state	415
9.3	Analysis of adsorption data using the Langmuir isotherm	423
9.4	Kinetic-theory-based description of binary adsorption	425
9.5	Calculating adsorption energy from the BET isotherm	431
9.6	Rate of atomic collisions as a function of pressure	441
9.7	Comparing bulk and surface structures using LEED patterns	447
9.8	The lattice structures of adsorbate and adsorbed layers	451
10.1	Relative magnitudes of van der Waals forces and relation to heat of vaporization	476
10.2	Dispersion force and nonideality of gases	479
10.3	Strength of van der Waals forces and the structure of materials	481
10.4	Hamaker constant of liquid polystyrene	490
10.5	Particle engulfment by an advancing solidification front	494
11.1	Dependence of Debye-Hückel parameter on temperature and type of electrolytes	512
11.2	Relation between surface charge density and surface potential	519
11.3	Influence of electrostatic repulsion on the thickness of soap films	523
11.4	Interaction between spherical particles: The Derjaguin approximation	525
12.1	Debye-Hückel expression for ionic activity coefficients	539
12.2	Relation between electrophoretic mobility and zeta potential	543
12.3	Units of electrokinetic parameters	554
12.4	Electrophoretic mobility of bacteria	561
12.5	Estimation of number of nucleotides in Glycine tRNA using electrophoresis	564
13.1	Critical coagulation concentration and ψ_0	591
13.2	Variation of particle concentration due to rapid coagulation	596
13.3	Expression for stability ratio in terms of Φ_{max}	599
13.4	Change of stability ratio with ionic concentration	602
13.5	Thicknesses of adsorbed polymer layers from the intrinsic viscosity of the dispersion	607
13.6	An entropic model for steric stabilization	619
C.1	Average surface area and surface area based on average-size particles	633
C.2	Polydispersity in size: Gaussian distribution	635

This page intentionally left blank

Index

The notation *e*, *f*, *t* or *v* accompanying certain entries implies that the examples, figures, tables or vignettes, respectively, appearing on the indicated pages *also* contain relevant information.

Absorption cross section, 231
Absorption efficiency, 231
Adhesion, 270, 271*f*
  work of, 271
Admicelle, 342
Adsorbate, definition, 332
Adsorbent, definition, 331
Adsorption, 323, 405
  apparatus, 410*f*
  in applied potential, 343–348
  on crystal surfaces, 439–451
  energetics of, 433–436
  experimental treatment, 407–412
  hysteresis, 437–439
  polymer, 606*f*
  in porous solids, 436–439
  on solid surfaces, 331–338
  from solutions, 323, 331
    applications of, 338–343
  statistical thermodynamics, 420–424
  theoretical treatment, 412–419
  thermodynamics, 419–424
Adsorption isotherms, 302, 332, 308*f*, 407, 411*e*, 412*f*, 417*t*, 416*f*
  Harkin-Jura, 416, 417*t*
  Henry's law limit, 413
  Langmuir, 420–422, 423*e*
  relation to equations of state, 413, 415*e*
  and surface phases, 308*f*
  van der Waals, 416
Advancing contact angle, 272, 273*f*
Aggregation
  cluster-cluster, 29
  diffusion-limited, 29, 30*f*
  monomer-cluster, 29, 30
  reaction-limited, 29
Aggregation number of micelles, 358, 360*t*
Aggregates, 25
  fractal dimension of, 26, 27*e*, 225, 226*e*
[Aggregates]
  relation to growth mechanisms, 29, 30*f*
  surface area, 27*e*
Amphipathic molecules, 301
Analytical separations, 62
Anodic branch of electrocapillary curve, 345
Archibald method, 100
Ascending (rising) branch of electrocapillary curve, 344
Association colloids, 56, 355
Athermal mixing, 128
Atomic force microscope (AFM), 44*v*
Auger electron spectroscopy (AES), 406
Autocorrelation function, 238
Average, 32, 35*t*, 631, 632
  area, 34, 632
  arithmetic, 637
  geometric, 637
  number, 33, 632
  volume, 34

Barometric equation, 100
Bashforth-Adams equation, 279, 280
Bashforth-Adams tables, 281*t*, 281*f*
Beer-Lambert equation, 231
Beta-emitting surfactants, 331
Bilayer, 4*v*, 7*f*, 396, 397
Bingham plastics, 175
Binomial expansion, 625
Biological membranes, 395–398
Black lipid membrane (BLM), 397
Boltzmann distribution, 98
Boltzmann equation for entropy, 120
Bragg equation, 40, 443
Brownian motion, 85–90
Brunauer-Emmett-Teller (BET) adsorption isotherm, 425–433, 429*f*
  derivation using kinetic theory, 425–428

[Brunauer-Emmett-Teller (BET) adsorption isotherm]
parameters of, 428
test of, 428–433

Cabannes factor, 213
Calorimetric heat of adsorption, 433
Capacitor model, 504, 515
diffuse model, comparison with, 515
Capillary condensation, 437–439, 438*f*
Capillary constant, 254
Capillary viscometer, 154, 156, 157*f*, 157*e*
Capillary zone electrophoresis, 564
Casimir-Polder interaction, 482
Catalysis, 49*v*, 405, 407*v*
heterogeneous, 49*v*, 407*v*
metals, 451–455, 452*t*
micellar, 380–385
turnover number of catalysts, 454
Cathodic branch of electrocapillary curve, 345
Ceramics, colloidal processing of, 16*v*
cgs units, 626
conversion to SI units, 627*t*
Charge density, 506
Debye-Hückel theory, 515
from electrocapillary curve, 346
Gouy-Chapman theory, 518
surface potential, relation to, 515
Charged micelles, 358
Charged monolayers, 308
Charged proteins, 565
Chemical vapor deposition, 407*v*
Chemisorption, 405, 406, 408*f*
Chi-squared test, 635
Chromatography, 45, 62*v*
gel filtration, 48
gel permeation, 48
relation to electrophoresis, 564
size exclusion, 45, 48*f*, 50*f*
Clapeyron equation, 433
Class, 32, 631
Classification of data, 631
Class mark, 32, 631
Clausius-Mosotti equation, 203*t*
Cloud point, 377
Coagulants, 499
Coagulation, 463
Coagulation, theories of, 592–600
Fuchs (slow coagulation), 596
Smoluchowski (rapid coagulation), 593
Coalescence, 15
Coefficient
diffusion, 80–85, 92*e*
[Coefficient]
Mark-Houwink, 38, 182*e*, 182*t*
sedimentation, 77
spreading, 272, 300
of surface viscosity, 319, 320
virial, and osmotic pressure, 112, 113
of viscosity, 69, 145, 148
Cohesion, 270, 271*f*
work of, 70
Cohesive energy density (CED), 128
Coil expansion factor, 186
Coincident structures, 449
Colligative properties, 110, 119
Colloid crystals, 579, 580*f*, 583*f*
Colloid-enhanced transport, 2*v*, 3*f*
Colloids
applications, 6*t*
classification, 2
food, 31*v*
hydrophilic, 10
hydrophobic, 10
lyophilic, 10
lyophobic, 13
"model" colloids, 23
self-similar, 27
shapes, 20, 22*f*, 23*f*
Colloid stability, 463, 567, 575, 576
and interparticle forces, 578–581, 580*f*
and van der Waals forces, 464–467
and potential energy diagrams, 466*f*
Commercial surfactants, 332*t*
Complex refractive index (absorbing material), 229
Computer simulations, 29, 30*f*
Concentric-cylinder viscometer, 150, 51*f*, 152*e*, 157*e*
Condensation in capillaries, 437, 4439*f*
Condensed states, in monolayers, 309
Conductance, equivalent, ionic, 537
Conductivity
bulk solutions, 554
at critical micelle concentration, 359
surface, 554
Cone-and-plate viscometer, 153*f*
Consolidate, 17
Contact angle, 248, 252
advancing, 272, 273*f*
hysteresis, 272–276, 273*f*
measurement of, 253–255, 276–283
capillary rise technique, 254–255, 253*f*
tilted plate technique, 252*f*, 253
Wilhelmy plate technique, 253–254, 253*f*, 276
of powders and porous solids, 283–286

[Contact angle]
receding, 272, 273*f*
relationship to surface tension, 265
Continuous distribution functions, 631
Continuous phase, 10
Conversion, units, 627*t*
Coulomb's law, 197, 505
Critical chain length of hydrocarbon tail, 364*e*, 367*f*, 368
Critical coagulation concentration (CCC), 578, 588, 589*t*, 591*e*
and stability ratio, 600
Critical flocculation temperature, 609
Critical micelle concentration (CMC), 11, 357, 359*f*, 360*t*, 374
Crystalline structures, 17, 580*f*, 583*f*
Crystallization on surfaces, 408*f*
Frank-van der Merwe, 408*f*
Stranski-Krastanov, 408*f*
Volmer-Weber, 408*f*
Crystallography, basic principles, 443–445
Cumulative curve, 632
Curved interfaces
effect on phase equilibria, 261–263
effect on nucleation, 264–265 (*see also* Young equation)

Deborah number, 176
de Broglie equation, 42
Debye equation, 469, 472
Debye-Hückel model, 501, 508–516
Debye-Hückel parameter, 510
physical significance of, 512, 512*e*, 513*t*
Degree of aggregation, 358, 360*t*
Depletion
flocculation, 605*f*
interaction, 614, 615*f*
stabilization, 605*f*
volume, 615*f*
Derjaguin approximation, 525*e*
Derjaguin-Landau-Verwey-Overbeek (DLVO) theory, 585
Detergency, 338–339
Dialysis, 139
Diffuse double layer, 505, 508–520
Diffusion, 62, 78–85, 89*e*
apparatus, 90, 91*f*
and Brownian motion, 85–90
and chemical potential, 80, 81
coefficient, 80–85, 92*e*
cumulative, 242
from dynamic light scattering, 236–242
mutual, 241

[Diffusion]
effect of solvation, 82
and friction factor, 80–85
self, 241
equilibrium with sedimentation, 98–100
and Fick's laws, 79, 80
and random walk, 85–90
thermodynamic description, 80–82
Diffusing wave spectroscopy (DWS), 194*v*
Dilatant fluids, 175
Dispersed phase, 10
Dispersion force, 482
Dissymmetry ratio, 221–223
Distribution functions
continuous, 631
discrete, 631
statistics of, 631–637
Donnan equilibrium, 105, 106*v*, 133–136, 331
and biophysics, 106*v*
and osmotic pressure, 136
Double layer (*see* Electrical double layer)
Drug delivery systems, 11*v*
Dupré equation, 265
Dynamic scattering, 193, 236–242, 239*e*, 241*e*
effect of polydispersity, 240
measuring diffusion coefficients, 238, 239*e*
measuring particle size, 238, 239*e*
Dzyaloshinskii-Lifshitz-Pitaevskii theory, 486

Einstein's equation for viscosity of dispersions, 164
Elastic, 146
Electrical double layer, 499, 505
capacitor model, 504
and surface charges, 502
Electrical double layer interaction, 499, 520–527
Electrocapillarity, 344–345, 347*e*
Electrode, 503
reversible, 503
silver iodide, 503
Electrodeposition, 570
Electrokinetic phenomena, 534
applications, 567–570
Electroosmosis, 534, 550–553, 551*f*
effect of surface conductivity, 552–553
and streaming potential, 550
Electrophoresis, 534, 538
experimental aspects, 559–564
moving-boundary, 562
zone, 564
Electrophoretic image display (EPID), 13*v*

Electrophoretic mobility, 537, 561*e*
viscoelectric effect, influence of, 556
Electrophotography, 535*v*
Electrostatic interaction, 499, 500*v*, 501*f*
Electroviscous effects, 171–180
primary, 178
secondary, 179
tertiary, 179
Electrodialysis, 139
Ellipsoid
oblate, 22*f*
prolate, 22*f*
Ellipticity
and friction factor, 83
from sedimentation data, 72*e*, 84*t*
and viscosity, 171
Enthalpy
of adsorption, 336
of micellization, 373, 374*t*
of mixing, 120, 122, 126–127
surface, 257*t*
Environmental remediation, 568*f*
Environmental scanning electron microscopy (E-SEM), 44
Equation
barometric, 100
Bashforth and Adams, 279, 280
Beer-Lambert, 231
Boltzmann, for entropy, 120
Bragg, 40, 443
Brunauer, Emmett and Teller (BET), 428
Clapeyron, 433
Clausius-Mosotti, 203*t*
Coulomb, 505
de Broglie, 42
Debye for dipole interaction, 472
Einstein, viscosity, 164
Fick (I), 79
Fick (II), 80
Freundlich, 337
Gibbs, 325
Gibbs-Dühem, 324
Gibbs-Helmholtz, 373
Girifalco-Good, 287
Girifalco-Good-Fowkes, 288
Gouy-Chapman, 517
Harkins-Jura, 417
Helmholtz-Smoluchowski, 545
Henry, 548
Hückel, 543
Keesom, 472
Kelvin, 262
Krieger-Dougherty, 169
[Equation]
Langmuir
for gases, 422
for liquids, 333
Laplace, 251
Lippmann, 346
London, 474
Navier-Stokes, 160
Poiseuille, 156
Poisson, 508
Poisson-Boltzmann, 509
linearized, 510
Raoult, 108
Rayleigh, 202
sedimentation, 69
Simha, 171*f*
Staudinger-Mark-Houwink, 181
Stokes, 161
Stokes-Einstein, 81
van der Waals
three-dimensional, gases, 477
two-dimensional, gases, 416
Van't Hoff, 112
Washburn, 286
Young, 265
Young-Dupré, 266
Equilibrium film pressure, 267
Error function, 92, 634
Expansions for
binomial function, 625
exponential function, 625
hyperbolic cosine, 625
hyperbolic sine, 625
logarithmic function, 625
sine function, 625
Excluded volume, 120, 124*e*, 287
Experimental tools, 38

Faraday constant, 503, 537
Fick's law, 63, 78
first, 79
second, 80
Field Flow Fractionation (FFF), 62*v*
Film pressure, 304
experimental measurements, 304–308
versus area isotherms, 308*f*, 311–316, 315*e*
Floatation, 338
Flocculation
bridging, 605*f*
depletion, 605*f*
Flory-Huggins theory, 125–132
enthalpy of mixing, 127

[Flory-Huggins theory]
entropy of mixing, 126
interaction parameter, 129
Flory-Krigbaum theory, 616
Flory temperature (*see also* Theta temperature), 131
Fluid mosaic model of a membrane, 396
Force measurement, 50
direct methods, 53, 54*f*, 55*f*
indirect methods, 51, 52*f*
Form factor, 215–218, 223
expressions for, 216
Fowkes equation, 489
Fractal, 225, 226*e*, 227*f*
aggregate, 27*e*, 225
definition, 27
mass, 27
Fractal dimension, 26, 27*e*, 225, 226*e*
Frank-Van der Merwe growth, 408*f*
Freundlich isotherm, 337
Friction factor, 65–67
and axial ratio, 83
and diffusion coefficient, 80
and solvation, 82
and viscous force, 537
Fuchs theory of colloid stability, 578

Gamma functions, 87, 88*t*
Gasoline and streaming potential, 555
Gaussian distribution function, 89*e*, 90*f*, 634, 635*e*
Genetic engineering, 11*v*
Gibbs-Donnan equilibrium (*see* Donnan equilibrium)
Gibbs equation for adsorption, 323–325
experimental results, 327–331
Gibbs-Helmholtz equation, 373
Gibbs monolayer, 297
Girifalco-Good equation, 287
Girifalco-Good-Fowkes equation, 288
Gold sols, 232
Good solvent, 125
Gouy layer, 505
Gouy-Chapman layer, 505, 527
Gouy-Chapman model, 501, 516–520
Graticule, 22
Guinier region, 225

Hamaker constant, 484, 485*t*, 488*t*
from bulk properties, 486–490
combining relations for, 491–493
[Hamaker constant]
from corresponding state theory, 489, 490*e*
negative values of, 493–494
from surface tension, 487, 488*t*
Harkin-Jura equation, 417
Heat of adsorption, 433
integral, 435
isosteric, 434
Helmholtz-Smoluchowski equation, 546, 550
Helmholtz plane, 527–528
inner, 527
outer, 527
Henry's equation, 546–548
Hooke's law and polymers, 619
Hückel equation, 546, 550
Heterogeneous catalysis, 407*v*
on metal surfaces, 451–455, 452*t*
Histograms, 32, 33*f*, 632
Hydrophobic effect, 357, 375
Hyperfiltration, 140

Immunoelectrophoresis, 569
Incoherent structures, 449
Indifferent ions, 503
Interface, 2
Interfacial tension, 290
London component, 290*t*
Interparticle interaction forces and energies
due to depletion effect, 614, 615*f*
due to polymers, 610–613, 613*f*
effect of electrolyte concentration, 587*f*
effect of Hamaker constant, 585, 586*f*
effect of surface potential, 585, 586*f*
Isoelectric focusing, 564
Isoelectric point, 566
Isoionic point, 566
Isomorphic substitution of ions, 502
Isotherms
Brunauer-Emmett-Teller (BET), 428
Freundlich, 337
Harkin-Jura, 417
Langmuir, 333
Isotopic labeling of surfactants, 331

Keesom equation, 469, 472
Kelvin equation, 261, 262
Kinetic molecular theory, 99
Kirkwood-Riseman theory, 147, 186
Krieger-Dougherty equation, 169
Kurtosis, 633

Langmuir-Blodgett film, 297, 298*v*, 299*f*, 342, 343*f*
Langmuir film balance, 304, 305*f*, 306*f*
Langmuir adsorption isotherm, 333, 334*f*, 335*e*, 420, 424
  kinetic theory, 424–425
  limitations of, 336–338
  statistical thermodynamic derivation, 420–423
Langmuir layer, 297
Laplace equation, 251, 259*e*
  and capillary rise, 260–261
Lasagna process, 568*f*
Lennard-Jones potential, 469, 470*f*
Life sciences, 4*v*
Light scattering, 193, 360
  absorbance, 209
  experimental aspects, 207–213, 207*f*
  intensity measurements, 208
  turbidity, 209, 360
Lipid molecules, 7, 11*v*
Liposomes, 11*v*, 12*f*, 398
Lippmann equation, 345–346
Liquid-condensed (LC) phase, 310
Liquid-expanded (LE) phase, 309
Liquidlike structures, 17, 580*f*, 582*f*
Log-normal distribution, 636
London equation, 469, 473, 474
Low-Energy Electron Diffraction (LEED), 406, 440–451
  apparatus, 441*f*
  interpretation, 445–451

Macroions, 537
Mark-Houwink coefficients, 38, 182*e*, 182*t*
Mass action model, 357
Mean, 632 (*see also* Average)
Membrane potential, 136
Micellar encapsulation, 356*v*
Micellar-enhanced ultrafiltration, 356*v*
Micelle, 355, 358
  catalysis by, 380–385, 383*e*
  core of, 364*e*
  fjord structure, 365
  reef structure, 365
  solubilization in, 375–380
  structure of, 363–370, 365*f*
Micellization, 361
  chemical reaction model, 357–358, 370, 372
  enthalpy change due to, 373, 374*t*
  entropy change due to, 373*e*, 374*t*, 375
  Gibbs energy change due to, 373*e*, 374*t*
  and packing considerations, 367–370
[Micellization]
  phase equilibrium model, 361*e*, 372–375
  thermodynamics of, 370–375
Microelectrophoresis, 538, 559, 560*f*
Microemulsions, 389–395
  applications of, 392–395
  as "swollen micelles", 390*f*, 391
  phase diagrams of, 391*f*, 392*e*, 393*f*
Microscopy, 39, 42*f*
  optical, 39
    contrast, 39
    dark-field, 41
    resolving power, 39
    magnification, 39
  electron, 42, 42*f*
  scanning-probe, 43, 44*v*, 46*f*
Microstructured materials, 18*v*
Mie theory, 232–235
Miller indices, 443
Mimetic chemistry, 356
Mobility, 536–538
Molecular sieve, 49*v*, 50
Molecular weight, 36, 117, 118
  distribution, 118, 119*e*
    and degree of polymerization, 119*e*
  from light scattering, 210*e*
  number average, 36, 37*e*, 38*t*
  viscosity average, 38*t*, 183
  weight average, 36, 37*e*, 38*t*
Moments of a distribution, 633
Monolayers, 298
  gas phase, 308*f*, 311
  intermediate phase, 308*f*, 317
  insoluble, 300
  liquid-condensed (LC) phase, 308*f*, 310, 317
  liquid-expanded (LE) phase, 308*f*, 309, 316
  solid phase, 308*f*, 317
  spread, 300
  structure of, 309–318
  van der Waals equation, 314
Moving-boundary electrophoresis, 562
Multiple scattering, 194*v*, 196*f*

Navier-Stokes equation, 147, 158–161
Nerve cells and Donnan equilibrium, 106*v*
Newton's law of viscosity, 147, 148
Non-Newtonian behavior, 149*f*, 17
Normal distribution function, 89*e*, 90*f*, 634, 635*e*
Normalization, 633
"Not-quite-indifferent" electrolytes, 527
Numerical aperture, 40

Optimal head group area, 367*f*, 368
Orthokinetic coagulation, 592
Osmometry, 110, 114
  applications, 114
  and measurement of molecular weight, 116, 117*e*
  and polydispersity, 118
Osmosis, reverse, 140
Osmotic equilibrium, 106, 110, 132
  and charged systems, 132–139
Osmotic phenomena, applications of, 139
Osmotic pressure, 105, 106*v*, 108, 111, 129, 137*t*
  apparatus, 110*f*, 116*f*
  charged particles, 136–139
  and charges of macroions, 138*e*
  at critical micelle concentration, 359*f*
  definition, 111
  equilibrium time, 114, 117*f*
  experimental, 114
  ideal solutions, 114
  molecular weight measurements using, 117*e*
  nonideal solutions, 112
  reduced, 114
  thermodynamic foundations, 108–114
  two-dimensional, on liquids, 314

Packing parameter, 369*e*, 371*t*
Palisade layer, 365
Particle size distribution, 31
  histogram, 32, 33*f*, 632
Partition functions, 121, 419–423
  and adsorption isotherms, 422
Peclet number, 176
Perikinetic coagulation, 592, 603
Phase equilibrium model, 357, 361*e*
Phospholipid, 4*v*
Physisorption, 405, 406
Pigment particles, 13
Poiseuille equation, 154, 156
Poisson-Boltzmann equation, 509
  linearized, 510
Poisson equation, meaning of, 508
Polarizability of particles, 201*e*
Polydispersity, 31
Polymer
  adsorption of, 604, 606*f*
  coils, 94–98
    end-to-end distance, 94–96
    radius of gyration, 96–98
  forces induced by, 608*f*, 610–614, 611*f*, 613*f*, 615*f*
  radius of gyration of, 96–98
[Polymer]
  and random walk statistics, 94–96
  solutions, Flory-Huggins theory of, 125–132
  surfaces, organic, low energy, 267
Polymer/colloid mixtures, 604
Polymer-induced forces, 608*f*, 610–614, 611*f*, 613*f*, 615*f*
  attractive forces, 613*f*
  repulsive forces, 612
Poor solvent, 125
Porosimetry, 285
Potential determining ions, 503
Potential distribution
  around cylindrical surfaces, 511
  around spherical surfaces, 511
  near planar surfaces, 509–511
Primary minimum, 467

Radiation scattering, 193
Radius of gyration, 35*t*, 219, 222*t*
Random walk, 85
  and average displacement, 93–94
  and diffusion, 88–93
Random walk statistics, 85, 93
  diffusion coefficients from, 88, 90–93
  and random coil, 94–98
Raoult's law, 108
Rapid coagulation, 592–596
Rayleigh equation, 202, 203*t*
Rayleigh ratio, 206
Rayleigh scattering, 195, 214*t*
Repulsive interactions
  between planar double layers, 520–524
  between spherical double layers, 525–526
Reverse micelles, 386–389
  solubilization in, 387*e*
  uses of, 387–389
Reverse osmosis, 140
Rheology, 145, 146*v*
  of chocolate, 146*v*
Rheopectic, 175
Root-mean-square (RMS) value, 632

Scanning electron microscopy (SEM), 42, 43
Scanning probe microscopy (SPM), 44*v*
Scanning tunneling microscopy (STM), 44*v*, 45, 46*f*
Scattering
  dynamic, 193, 236
  Debye theory, 214, 215–223, 214*t*
  by gases, 202

[Scattering]
Guinier region, 225
intraparticle interference, 213–227
by large absorbing particles, 229–232
light, 193, 195, 229*t*
Mie theory, 232–235
multiple, 194
neutron, 202, 229*t*
Porod region, 225
Rayleigh equation, 202, 203*t*
by single molecules, 202
static, 193
X-ray, 228, 229*t*
Scattering vector, 217
physical significance, 223
Schulze-Hardy rule, 588
Secondary minimum, 467
Second virial coefficient, 107, 123, 129, 132*e*
Flory-Huggins, 130
light scattering, 212
osmotic pressure, 113, 124, 130
Sedimentation, 17, 62, 64–78
analysis of data, 72*e*, 73*f*
centrifugal, 74–78
coefficient, 77
effect of nonsphericity, 70
effect of solvation, 70
and ellipticity, 71*f*
equation, 69
and particle-size distribution, 73*f*, 74*e*
equilibrium with diffusion, 98*f*, 99, 100
field flow fractionation (FFF), 62*v*
gravitational, 67–74
measurements, 71–74
and polydispersity, 71
sensitivity to density differences, 67
sewage treatment, 568
and solvation, 67
Sedimentation potential, 534
Self-assembled monolayers, 249*v*, 250*f*
Self-assembly, 355
Semipermeable membrane, 110
Shear, 148, 151*t*
Shear thinning, 146
SI units, 626, 627*t*
Siegert relation, 237
Slow coagulation, 592, 593, 596–598
Smoluchowski theory of colloid stability, 578
Solution thermodynamics, statistical foundations, 120–125
Solvation
from sedimentation data, 83*e*, 84*t*
and surface excess, 327
and viscosity, 170
Solvent
adsorption of, 338
"goodness" of, 96, 125, 130–132
goodness and aggregation, 609
induced absorption band, 366
and theta temperature, 130–132
Specific surface area, 8
variation with geometry, 9*e*
Spectroscopic methods, 406
Spreading, 270, 271*f*, 272
Spreading coefficient, 272, 300
Spread monolayers, 300
applications of, 320–323
properties of, 301
Stability, 14–19, 16*v*, 19*v*, 465–467, 575
kinetic, 15, 16*f*
of dispersions, 14
thermodynamic, 17
of thin films, 463*v*
Stability ratio, 578, 592–604
and critical coagulation concentration, 600
equations for, 598, 599*e*
and ionic concentration, 602*e*
Stabilization
depletion, 605*f*
electrostatic, 604*t*
steric, 11, 604*t*, 605*f*
Standard deviation, 32, 37, 632
Static scattering, 193
Stationery settling velocity, 66
Statistical entropy, 120
and entropy of mixing, 122
Staudinger-Mark-Houwink equation, 181, 182*e*
Stealth effect, 11
Stealth liposomes, 11
Steric stabilization, 576*v*, 578, 614–619
model for initial encounter, 614–619
Sterling's approximation, 87, 421
Stern adsorption, 527–530
Stern surface, 527
Stern layer, 528*f*
Stokes
approximation, 161
equation, 161
law, 63, 69, 83, 537
Stokes-Einstein equation, 81, 196, 239, 242, 594
Stranski-Krastanov growth, 408*f*
Streaming current, 554
Streaming potential, 534, 551*f*, 553–555
relation to zeta potential, 553

Structure factor
dynamic, 228
interparticle, 227–228
intraparticle, 223–227
uses of, 228
Sulfur sols, 235
Supernet, 449
Surface area
importance of, 5, 7*t*, 8*t*
specific, 8
Surface charge density, 515
surface potential, relation to, 516, 519*e*
Surface charges, 502
from electrokinetic measurements, 565–567
origin, 502*t*
zeta potential, relation to, 565
Surface energy, 5
Surface excess charge, 499
Surface excess concentration, 327
ion dissociation, effect of, 330
measurement of, 331
surface tension, related to, 327, 329*e*
Surface excess properties, 325*f*, 325–327, 329*e*
Surface force apparatus (SFA), 53, 54*f*, 55*f*
Surface of shear, 528*f*, 555–558
Surface pressure, 301
and surface tension, 301
versus area isotherms, 302
Surface reconstruction, 449
Surfaces, thermodynamics of, 255–257
Surface tension, 248, 251, 276–283, 289*t*, 301, 327, 329*e*, 487–489
and cohesion, adhesion and spreading, 270–272
as force, 251
Girifalco-Good equation, 287
Girifalco-Good-Fowkes equation, 288
and Hamaker constant, 487–489
implications to curved surfaces, 257–265
implications to capillarity, 257–265
measurement of, 253–255, 278*e*
capillary rise technique, 254–255, 253*f*
drop-weight method, 255
maximum bubble-pressure method, 255
ring method, 255
sessile-drop technique, 279
tilted plate technique, 252*f*, 253
Wilhelmy plate technique, 253–254, 253*f*, 276, 302
molecular interpretation, 286–291
relationship to contact angle, 265
as surface free energy, 255
Surface viscosity, 318
Surfactants, 297, 302*t*
molecular architecture and shapes of micelles, 367–370
Swamping electrolyte, 137
Swollen micelles, 391

Taylor series, 625
Ternary phase diagrams, 378, 379*f*, 391, 393
Theta (Θ) temperature, 130–131, 132*e*, 186, 613
Thin-film growth, 407*v*
Thixotropy, 175, 181
Tortuosity, 284
Transmission electron microscopy (TEM), 42*f*
Tunneling current, 44*v*
Turbidity, 210, 211*f*, 360
Tyndall spectra, 235–236

Ultracentrifuge, 74, 75*f*, 78*e*, 100
optics of, 75*f*
Ultrafiltration, 140
Units conversion, 627*t*

van der Waals equation of state
three-dimensional (bulk gases), 477
two-dimensional (surface phases), 416
van der Waals forces, 482
calculation of, 483–485
Debye interaction, 469, 471–472, 477*t*
direct measurement of, 490, 491*f*
Dzyaloshinskii-Lifshitz-Pitaevskii (DLP) theory, 486
expressions for, 483–485, 486*t*
and heat of vaporization, 476*e*
Keesom interaction, 469, 472, 477*t*
for large particles, 479-482
London interaction, 469, 473-475, 477*t*
macroscopic implications, 477–479
molecular origins, 471–475
and nonideality of gases, 479*e*
over large distances, 479–483
retarded, 471, 482–483
from surface tension, 487, 488*t*
and structure of materials, 481*e*
Van't Hoff equation, 3.2c
Vesicles, 398
Vignettes, 4
adsorption, 407
bilayers, 4
biology, 4
biophysics, 4, 106

[Vignettes]
catalysis, 49
ceramic processing, 16
chemical vapor deposition, 407
chemisorption, 407
chocolate, 146
colloid-enhanced transport, 2
composites, polymer, 18
contact angle, 249
copolymers, 18
cosmetics, 11
crystal growth, 407
diffusing wave spectroscopy, 194
Donnan equilibrium, 106
drug delivery systems, 11
electrophoretic image display (EPID), 13
electrophotography, 535
electrostatic interactions, 500
epitaxial films, 407
field flow fractionation, 62
food colloids, 31
Langmuir-Blodgett films, 298
liposomes, 11
micellar encapsulation, 356
micellar enhanced ultrafiltration (MEUF), 356
molecular recognition, 500
nerve cells, 106
osmotic pressure, 106
physiology, 106
physisorption, 407
polymer adsorption, 576
polymer composites, 18
rheology, 146
scanning probe microscopy, 44
scanning tunneling microscopy, 44
sedimentation field flow fractionation, 62
separation processes, 49, 356
size exclusion, 49
spreading, 463
stability of thin films, 463
steric stability, 576
wettability, 249, 463
zeolites, 49
Virial coefficients, 108
and osmotic pressure, 112, 113
and van der Waals constants, 113
Viral expansion, 112
Viscoelastic, 146, 176
Viscoelectric effect, 171, 174, 555
Viscometers
capillary, 154, 156, 157*f*, 157*e*
concentric cylinder, 150, 151*f*, 152*e*, 157*e*
cone-and-plate, 153*f*
Viscosity, 145, 148, 150*t*
Newton's law, 147, 148
and polymer configuration, 187*e*
of polymer solutions, 181–187
Staudinger-Mark-Houwink equation, 181–183, 182*e*
Kirkwood-Riseman theory, 186
Viscosity of dispersions
effect of solvation and shapes, 169
electroviscous effects, 171–174
Einstein's equation, 164
Einstein's theory, 147, 161, 164*f*
Krieger-Dougherty equation, 169
viscoelastic effects, 171, 174
Volmer-Weber growth, 408*f*
Volume of hydrocarbon chain, 367*f*, 368

Washburn equation, 286
Wettability, 249*v*, 250*f*
Wood notation, 450

Xerography, 535
X-ray scattering, 228, 229*t*

Yield stress (or, value), 149*f*, 175*f*, 180
Young equation, 265*f*, 265
effect of solid surface, 266
effect of surface heterogeneities, 266
and equilibrium film pressure, 267
and heat of immersion, 268*e*, 269*f*
Young-Dupré, 266 (*see also* Young equation)

Zeolite, 49*v*, 50*f*, 285
Zero liquid flow in electrophoresis, 561
Zero point of charge, 503, 566
Zeta potential, 530, 534, 536
effect of double layer relaxation, 548–550
general theory, 546–550
Helmholtz-Smoluchowski limit, 546, 550
Henry's equation, 546–548
Hückel limit, 546, 550
retardation effect, 549
streaming potential, relation to, 553
thick electrical double layers, 538–544
thin electrical double layers, 544–546
viscoelectric effect, influence of, 556
Zimm plot, 218–221, 221*e*
Zone electrophoresis, 564